STRUCTURAL SYSTEMS RESEARCH PROJECT

Report No.
SSRP - 92/11

THE USE OF CROSS-SECTION WARPING FUNCTIONS IN COMPOSITE ROTOR BLADE ANALYSIS

Final Report

by

J.B. Kosmatka

Final report on a research project funded through
NASA Research Grant Number NAG-1-1151

Period of Performance
5/15/90–7/1/92

Department of Applied Mechanics
and Engineering Sciences
University of California, San Diego
La Jolla, California

University of California, San Diego
Structural Systems Research Project

Report No. SSRP-92/11

THE USE OF CROSS-SECTION WARPING FUNCTIONS IN COMPOSITE ROTOR BLADE ANALYSIS

by

J.B. Kosmatka
Associate Professor of Applied Mechanics

Final report on a research project funded through
NASA Research Grant Number NAG-1-1151

Period of Performance
5/15/90-7/1/92

Department of Applied Mechanics and Engineering Sciences
University of California, San Diego
La Jolla, California 92093-0411

Table of Contents

The Use of Cross-Section Warping Functions in Advanced Composite Rotor Blade Analysis

by

J. B. Kosmatka
Department of Applied Mechanics and Engineering Science
University of California, San Diego
La Jolla, California 92093

Introduction

Current helicopter rotor blade designs incorporate fiber composite materials as a means of controlling weight, deformation, and vibration (i.e., structural tailoring). Although fiber composites are orthotropic in material property classification, they can exhibit general anisotropic material behavior to applied loads (extension-bend-twist coupling) when the fiber orientations do not coincide with the structural coordinate system [1]. Exact analytical solutions of this problem based upon three-dimensional elasticity are intractable. Three dimensional finite-element modeling may be applied, however, this approach is too costly for the discretization necessary for accurate stress and deformation determination.

Instead one-dimensional beam-type models based upon standard or refined theories are used. Standard beam theories, which are derived by extending the Bernoulli-Euler theory to include extension-bend-twist coupling effects, have been developed for thin-wall rectangular cross-sections and general nonhomogeneous cross-sections [2,3]. In addition refined beam theories, which include the effects of transverse shear deformation, exist for thin-wall single cell cross-sections. All of the existing one-dimensional beam-type models yield only gross structural behavior such as force resultants, moments, extension, bending rotations, and twisting angles. Stress distributions may be calculated according to kinematic (Bernoulli-Euler and Saint-Venant torsion) hypotheses, but they do not reveal the inter-laminar shear states. Moreover, up to 48 unique constants must be known for each different cross-section. These cross-section constants provide important information concerning the beam axial, bending, torsion, and shear stiffnesses, as well as coupling stiffnesses. But these constants, which

are dependent upon the general warping of the cross-section, can very significantly with changes in cross-section geometry and/or material definition. Thus it becomes very difficult for an analyst to assess how minor changes in the cross-section definition will effect the overall blade behavior.

Alternatively, Saint-Venant's elasticity solutions for extension, bending, torsion, and flexure of a prismatic beam can be used to analyze the cross-section of advanced composite helicopter rotor blades. These elasticity solutions accurately describe the displacement, stress (including inter-laminar shear), and general cross-section warping distribution for a given applied tip-load condition. Thus, these solutions can be used to complement existing one-dimensional beam theories by providing a means for: (1.) determining the general three-dimensional warping of the cross-section, (2.) calculation of the warping-dependent cross-section constants, and (3.) accurate calculation of the stress distribution throughout the blade using the calculated shear and moment resultants that can be determined from an appropriate derived one dimensional beam theory. This beam theory must be derived using assumptions that insure that the kinematic and stress fields are fully compatible with the aforementioned Saint-Venant elasticity solutions.

Research Objectives

During the contracted period, our research was concentrated into three areas:

1.) The development of an accurate and a computationally efficient method for predicting the cross-section warping functions in an arbitrary cross-section composed of isotropic and/or anisotropic materials. This new method involved using a "power series" representation for the in-plane and out-of-plane warping functions and then solving for the power series coefficients using variational principles. Our work developed a theoretical approach and computational procedure for cross-sections composed of isotropic materials (Chapter 2) and generally anisotropic materials (Chapter 3). In addition, a separate research effort was undertaken to develop the "exact" cross-section warping functions and fully coupled three-dimensional displacement and stress field for a tip-loaded cantilevered beam having a solid elliptical cross-section and composed of generally anisotropic materials (Chapter 4). These exact solutions are extremely useful for

validating the computationally predicted warping functions and also for correlation of the stress and displacements distributions of a one-dimensional beam theory.

2.) The development of a general higher-order one-dimensional theory for anisotropic beams. This theory is used to study the behavior of beams having an arbitrary nonhomogeneous cross-section, where the effects of shear deformation and local cross-section deformation are included using the aforementioned cross-section warping functions. Thus, it is imperative that the beam theory is derived so that the kinematic and stress assumptions are fully compatible with those of the Saint-Venant elasticity solutions. Numerical results have proven that this new beam theory accurately predicts both the displacement and stress distribution (all six components). In our work, we first developed a linear dynamic one-dimensional theory for isotropic beams, where we studied the static and free vibrational behavior so as to assess the importance of the in-plane and out-of-plane warping functions (Chapter 5). Our results show that the in-plane functions are required for acquiring accurate shear stress distributions, whereas only the out-of-plane warping function is required for static and free vibration displacement information. Second, we developed a general nonlinear one-dimensional theory for spinning anisotropic beams (Chapter 6). Our preliminary results show the importance of including both the in-plane and out-of-plane warping functions for determining accurate stress information and coupled displacement behavior (i.e. static deformed shapes and mode shapes).

3.) The development of an analytical model for assessing the extension-bend-twist coupling behavior of nonhomogeneous anisotropic beams with initial twist (Chapter 7). A model was formulated, where the displacement solutions are defined with pretwist-dependent functions that represent the extension, bending and torsion and pretwist-dependent in-plane and out-of-plane cross-section warping functions. Numerical results illustrate the strong extension-torsion coupling behavior in thin-wall advanced-composite beams as a function of ply angle, initial twist level, and initial twist axis location.

In the remaining six chapters of this report, the three different research areas and associated sub-research areas are covered independently including separate introductions, theoretical developments, numerical results, and references. This was done because, first, each of the six topics are very independent in their focus and scope

and, second, each of the six chapters is a copy of an extended manuscript of an accepted and/or published Journal or Conference article. For example, the work of Chapter 2 has been published as a conference article [4] and has been extended and accepted to the AIAA Journal [5]. The results of Chapter 3, which has been recently completed, has been submitted to the International Journal of Solids and Structures [6]. The work of Chapter 4 has been submitted for publication by The Journal of Composite Materials [7]. The results of Chapter 5 have appeared in condensed form in a conference article [8] and will appear in extended form in the Journal of Sound and Vibration [9]. The model of Chapter 6 is being published as a conference article [10] and will be submitted to a Journal when additional numerical results are completed. Finally, the formulation of Chapter 7, was presented in a conference research article [11] and an AIAA Journal article [12]. In all 9 articles, the valuable assistance of R.C. Lake and the financial support of the NASA-Langley Research Center was acknowledged.

References

1.) Nixon, N. W.; "Extension-twist Coupling Behavior of Composite Circular Tubes with the Application to Tilt-Rotor Blade Design," Proceedings of the 28th AIAA/ASME/ASCE/AHS Structures, Structural Dynamics, and Materials Conference, Monterey, California, Part 1, pp. 295-303, 1987.

2.) Kosmatka, J. B., "Structural Dynamic Modeling of Advanced Composite Propellers by the Finite Element Method", Ph.D Dissertation, University of California at Los Angeles, 1986, pp. 1-308.

3.) Kosmatka, J. B., and P. P. Friedmann, "Vibration Analysis of Composite Turbo-propellers Using a Nonlinear Beam-Type Finite Element Approach," AIAA Journal, Vol. 27, November, 1989, pp. 1606-1614.

4.) Kosmatka, J. B.; "Flexure-Torsion Behavior of Shear-Deformable Beams with Applications to Aircraft Wing-Sections Proceedings of the 33rd AIAA/ASME/ASCE/AHS/ASC Structures, Structural Dynamics, and Materials Conference, Paper No. 92-2467, vol. 2, pp. 763-773, April, 1992.

5.) Kosmatka, J. B.; "Flexure-Torsion Behavior of Prismatic Beams, Part I: Warping and Section Properties via Power Series," AIAA Journal, accepted.

6.) Kosmatka, J. B.; "Behavior of a Prismatic Anisotropic Cantilever Beam via Power-Series" International Journal of Solids and Structures, accepted.

7.) Ie. C. A., and J. B. Kosmatka; "Elasticity Solutions, Shear Center Location, and Shear Deformation of a Tip-Loaded Anisotropic Cantilevered Beam With an Elliptical Cross-Section," The Journal of Composite Materials, submitted.

8.) Kosmatka, J. B. and C. Ie; "On the Vibration Behavior of Shear-Deformable Prismatic Beams Including In-Plane Cross-Section Deformations," Proceedings of the 32nd AIAA/ASME/ASCE/AHS/ASC Structures, Structural Dynamics, and Materials Conference, Paper No. 91-1201, vol. 2, pp. 1462-1474, April, 1991.

9.) Kosmatka, J. B.; "Transverse Vibrations of Shear-Deformable Beams Using a General Higher-Order Theory," The Journal of Sound and Vibration, (in press).

10.) Ie. C. and J. B. Kosmatka, "Formulation of a Nonlinear Theory for Spinning Anisotropic Beams," Proceedings of the 1992 ASME Winter Annual Meeting, Nov. 10-13, Anaheim, CA.

11.) Kosmatka, J. B.; "Extension-Bend-Twist Coupling Behavior of Thin-Walled Advanced Composite Beams with Initial Twist," Proceedings of the 32nd AIAA/ASME/ASCE/AHS/ASC Structures, Structural Dynamics, and Materials Conference, Paper No. 91-1023, vol. 2, pp. 1037-1049, April, 1991.

12.) Kosmatka, J. B., "Extension-Bend-Twist Coupling Behavior of Nonhomogeneous Anisotropic Beams with Initial Twist," AIAA Journal, vol. 30, no. 2, 1992, pp. 519-527.

Chapter 2: A Power Series Approach for Isotropic Beams with Arbitrary Cross-Sections

Abstract

The behavior of a tip-loaded cantilever beam with an arbitrary cross-section is studied using Saint-Venant's semi-inverse method along with a power series solution for the out-of-plane flexure and torsion warping functions. For complex cross-sections, the calculated power series coefficients represent a "best-fit approximation" to the exact warping function. The resulting warping functions are used to determine the cross-section properties. A new linear relation is developed for locating the shear center, where the twist rate is zero about the line of shear centers. Numerical results are presented to verify the approach and second provide section data on NACA four-series airfoils not currently found in the literature.

Introduction

Closed-form solutions for Saint-Venant's flexure and torsion problems (tip-loaded cantilever beam) exist for only a few simple cross-section shapes (ellipse, rectangle, equilateral triangle) [1-3]. For general cross-section shapes (i.e., cambered airfoils), the cross-section dependent flexure and torsion warping functions cannot be determined exactly and thus approximate techniques must be used. One proven approach for approximately determining the Saint-Venant torsion [4] and flexure [5] functions involves the application of the finite element method. In this approach, the general cross-section is discretized into triangular and/or quadrilateral subregions (elements) with out-of-plane nodal variables that represent the cross-section warping, where the warping distribution is determined by applying the principle of minimum potential energy. While the finite element approach is well behaved, it has two shortcomings. First a large number of elements are required for complex cross-sections, which leads to a large set of linear algebraic equations. Second, the resulting array of calculated nodal values provides very little physical insight into the warping definition and one typically resorts to graphical finite element post-processing techniques to understand the warping distribution. An alternative approach, which has been developed by Mindlin [6] for the solution of Saint-Venant's torsion problem (generalized plane strain), involves assuming a double power series for the warping function. The power series coefficients are determined by solving a set of linear algebraic equations, where the number of equations is equal to the number of unknown coefficients. Thus, the problem size is independent of the cross-

section complexity, and only dependent on the number of terms in the power series.

The objective of the current investigation is to study the flexure and torsion behavior of a tip-loaded cantilever beam with an arbitrary cross-section, where both the flexure and torsion warping functions are expressed as a double power series in terms of the cross-section coordinates. The coefficients associated with the power series terms are determined by solving a set of variationally derived linear algebraic equations, where the number of equations is equal to the number of unknown coefficients. For complex cross-sections, the calculated coefficients represent a "best-fit approximation" to the exact warping function which may be an infinite series of transcendental functions. To aid in the evaluation of the power series weighted area integrals, the cross-section is discretized into a series of triangular subregions, where the integration in each subregion is evaluated exactly using Guassian Qaudrature formulas for triangles [7,8]. The triangle aspect ratio is not critical as opposed to the finite element method, since the power series is a global cross-section function and not a local element function.

Once the flexure and torsion warping functions are known for a given cross-section and material definition (Poisson's ratio), then the resulting three-dimensional displacement and stress distributions can be used to: (1.) study the overall beam behavior, (2.) determine important beam-type section properties including; the torsion constant, shear deformation coefficients, shear center location, and shear correction factors (for Timoshenko's beam theory [9,10]), and (3.) develop a one-dimensional beam theory [11] that includes cross-section flexure and torsion warping effects and is fully compatible with the three-dimensional stress and displacements predictions of Saint-Venant.

The determination of the shear center location has been studied by numerous researchers [2,3,5,12-15], where the shear center is commonly defined as "*the load point where the mean value of the local cross-section twist is zero (i.e., local twist rate about the section centroid is zero)*". Applying this definition to Saint-Venant's flexure and torsion problems leads to a zero twist rate about the centroidal axis, but any other line parallel to the centroidal axis, including the line of shear centers, will have a nonzero twist rate. This nonzero twist rate for all lines except the centroidal axis occurs because the application of a transverse tip load produces a linearly increasing bending stress state normal to the cross-section and straining within the cross-section. This straining within the cross-section, which causes the particles of the cross-section to translate and rotate into an anticlastic surface, also increases linearly from the beam tip. Thus any line

that is composed of cross-section particles that are offset from the centroidal axis will undergo linearly varying twist (i.e. constant twist rate with zero twist at the beam-tip) as a result of an applied transverse tip load. Recently, in [16,17], an analytical approach was developed for locating the shear center in thin plate-like cross-sections, where the aforementioned definition was modified to be "*the load point where the twist rate about the line of shear centers is zero*". Although the two definitions appear to be very similar, this definition insures that the shear center is coincident with the center of twist. Moreover, numerical results for thin triangular cross-sections revealed profound differences (40-67% depending upon Poisson ratio) in the shear center locations. In my current paper, the shear center location is determined using both the classical definition and the more recent definition [16,17], where a linear relationship between the two locations is developed that is valid for any cross-section shape and material definition.

Numerical results are presented to verify the approach and provide new data for NACA four-series airfoils. The sensitivity of the section properties (especially the shear center location) with airfoil thickness and camber is of interest to aeroelasticians because of the profound effect these parameters have on divergence and flutter speed calculations. The current work significantly improves upon the fundamental studies of the shear center location for solid airfoils [15,18], where these analyses approximately treated cambered airfoils as cubic ovals.

Theoretical Background

General Beam Behavior

We begin by considering a cantilever prismatic beam of length L with an arbitrary cross-section of area A composed of a homogeneous, isotropic material. A Cartesian coordinate system (x,y,z) with corresponding displacement components (u,v,w) is defined with the origin at the centroid of the root end and the (x,y) axes coincide with the principal axes of the root cross-section. See Fig. 1. The beam is subjected to a force with flexure components (P_x, P_y) that act through the centroid of the tip cross-section ($z=L$) in the x- and y-directions, respectively, and an applied torque (M_z), where they satisfy the following three equations of stress equilibrium;

$$P_x = \int_A \tau_{xz}\, dA\,, \qquad P_y = \int_A \tau_{yz}\, dA\,, \qquad M_z = \int_A (x\tau_{yz} - y\tau_{xz})dA\,. \qquad (1.a\text{-}c)$$

Furthermore, the body forces are considered negligible so that the in-plane stresses (σ_{xx}, σ_{yy}, τ_{xy}) are equal to zero and the normal stress is defined as a linear function, following Saint-Venant's assumptions [1-3],

$$\sigma_{zz} = \left\{ \frac{P_x}{I_{yy}} x + \frac{P_y}{I_{xx}} y \right\} (z - L) \tag{2}$$

where I_{xx} and I_{yy} represent the principal moments of inertia about the x- and y-axes, respectively. Introducing these assumptions into the stress equilibrium equations and integrating yields the well-known form [1-3] of the displacement components and shear stresses

$$u = \frac{P_x}{EI_{yy}} \left\{ \frac{L}{2} z^2 - \frac{z^3}{6} + \frac{\nu}{2} \left\{ x^2 - y^2 \right\} (L - z) \right\} + \frac{P_y}{EI_{xx}} \{ \nu xy (L - z) \} - \theta yz + b_4 z - b_6 y + b_1 \tag{3.a}$$

$$v = \frac{P_y}{EI_{xx}} \left\{ \frac{L}{2} z^2 - \frac{z^3}{6} + \frac{\nu}{2} \left\{ y^2 - x^2 \right\} (L - z) \right\} + \frac{P_x}{EI_{yy}} \{ \nu xy (L - z) \} + \theta xz + b_5 z + b_6 x + b_2 \tag{3.b}$$

$$w = - \frac{P_x}{EI_{yy}} \left\{ x \left\{ Lz - \frac{z^2}{2} \right\} \right\} - \frac{P_y}{EI_{xx}} \left\{ y \left\{ Lz - \frac{z^2}{2} \right\} \right\} + \psi(x,y) - b_4 x - b_5 y + b_3 \tag{3.c}$$

$$\tau_{yz} = - \frac{GP_x}{EI_{yy}} \{ \nu xy \} - \frac{GP_y}{EI_{xx}} \left\{ \frac{\nu}{2} (y^2 - x^2) \right\} + G \left\{ \frac{\partial \psi}{\partial y} + x\theta \right\} \tag{3.d}$$

$$\tau_{xz} = - \frac{GP_x}{EI_{yy}} \left\{ \frac{\nu}{2} (x^2 - y^2) \right\} - \frac{GP_y}{EI_{xx}} \{ \nu xy \} + G \left\{ \frac{\partial \psi}{\partial x} - y\theta \right\} \tag{3.e}$$

where, E is the Young's modulus of the material, ν is the Poisson's ratio, G is the shear modulus that satisfies ($= E/(2(1+\nu))$), θ is the beam twist rate about the centroidal axis, $\psi(x,y)$ is a function that describes warping out of the cross-section plane, and b_1-b_6 are integration constants that are specified by defining the fixity of the beam root. In the current development, the geometric boundary conditions are prescribed by restraining the translational motion of the root centroid (x=y=z=0) and requiring that the slope and twist of the centroidal axis are zero at the beam root,

$$u = v = w = \frac{\partial u}{\partial z} = \frac{\partial v}{\partial z} = \frac{\partial u}{\partial y} - \frac{\partial v}{\partial x} = 0 . \tag{4.a-f}$$

This approach is identical to that of [2,3] and thus $b_i = 0$ (i = 1-6).

The determination of the warping function (ψ) is accomplished by applying the principle of minimum potential energy

$$\delta\Pi = \delta U - \delta W_\theta = 0 \tag{5.a}$$

where (δU) is the variation of the strain energy given by

$$\delta U = \int_0^L \int_A \delta\sigma_{zz}\varepsilon_{zz} + \delta\tau_{yz}\gamma_{yz} + \delta\tau_{xz}\gamma_{xz}\ dA\ dz\,, \tag{5.b}$$

since ($\sigma_{xx} = \sigma_{yy} = \tau_{xy} = 0$), and δW_θ is the variation of the work of external forces that results from the applied tractions on the beam ends;

$$\delta W_\theta = \int_A \left\{\sigma_{zz}\big|_{(z=L)} - \sigma_{zz}\big|_{(z=0)}\right\} \delta\psi dA = \frac{P_x L}{I_{yy}}\int_A x\,\delta\psi dA + \frac{P_y L}{I_{xx}}\int_A y\,\delta\psi dA\,. \tag{5.c}$$

Substituting Eqns. (2,3,5.*b*, 5.*c*) into (5.*a*) and carrying out the integration over the beam-length

$$\delta\Pi = 0 = GL\int_A \frac{\partial}{\partial x}(\delta\psi)\left\{\frac{\partial\psi}{\partial x} - y\theta - \frac{P_x}{EI_{yy}}\left\{\frac{\nu}{2}(x^2 - y^2)\right\} - \frac{P_y}{EI_{xx}}\{\nu xy\}\right\}$$

$$+\frac{\partial}{\partial y}(\delta\psi)\left\{\frac{\partial\psi}{\partial y} + x\theta - \frac{P_x}{EI_{yy}}\{\nu xy\} - \frac{P_y}{EI_{xx}}\left\{\frac{\nu}{2}(y^2 - x^2)\right\}\right\} dA \tag{6}$$

$$-\frac{P_x}{EI_{yy}}EL\int_A x\delta\psi\ dA - \frac{P_y}{EI_{xx}}EL\int_A y\delta\psi\ dA\ .$$

An examination of Eq. (6) reveals that (ψ) can be expressed as a linear combination of three cross-section dependent functions that are proportional to the rates of beam curvature and twist

$$\psi(x,y) = \psi_1(x,y)\frac{P_x}{EI_{yy}} + \psi_2(x,y)\frac{P_y}{EI_{xx}} + \psi_3(x,y)\theta \qquad (7)$$

where (ψ_1, ψ_2) represent the shear-dependent warping functions and (ψ_3) is the Saint-Venant torsion warping function.

The shear stress distributions of Eqns. (3.*d,e*) can be expressed in terms of the rates of bending curvature and twist by making use of Eq. (7),

$$\tau_{yz} = \tau_{yz(1)}\frac{P_x}{EI_{yy}} + \tau_{yz(2)}\frac{P_y}{EI_{xx}} + \tau_{yz(3)}\theta$$

$$\tau_{xz} = \tau_{xz(1)}\frac{P_x}{EI_{yy}} + \tau_{xz(2)}\frac{P_y}{EI_{xx}} + \tau_{xz(3)}\theta \qquad (8.a,b)$$

where

$$\tau_{yz(1)} = G\left\{\frac{\partial\psi_1}{\partial y} - \nu xy\right\}, \qquad \tau_{xz(1)} = G\left\{\frac{\partial\psi_1}{\partial x} - \frac{\nu}{2}\left(x^2 - y^2\right)\right\},$$

$$\tau_{yz(2)} = G\left\{\frac{\partial\psi_2}{\partial y} - \frac{\nu}{2}\left(y^2 - x^2\right)\right\}, \qquad \tau_{xz(2)} = G\left\{\frac{\partial\psi_2}{\partial x} - \nu xy\right\}, \qquad (8.c,h)$$

$$\tau_{yz(3)} = G\left\{\frac{\partial\psi_3}{\partial y} + x\right\}, \qquad \tau_{xz(3)} = G\left\{\frac{\partial\psi_3}{\partial x} - y\right\}.$$

The twist rate (θ) as a function of the applied loads (P_x, P_y, M_z) can now be determined by substituting Eq. (8) into (1.*c*), integrating and rearranging

$$\theta = \frac{1}{a_3}\left(M_z - a_1\frac{P_x}{EI_{yy}} - a_2\frac{P_y}{EI_{xx}}\right), \qquad (9.a)$$

where

$$a_i = \int_A x\tau_{yz_{(i)}} - y\tau_{xz_{(i)}}\, dA, \qquad (i = 1,3). \qquad (9.b)$$

Torsional Rigidity and Shear Center Location

The cross-section torsional rigidity (GJ) is commonly defined as the constant (a_3) in Eq. (9.*a*). The remaining two constants (a_1,a_2) in Eq. (9.*a*) can be used to locate the classical definition of the shear center (x_S,y_S); *'the load point that produces a zero mean value cross-section twist' (i.e., zero local twist about section centroid, $\theta = 0$)* [2,3,5,12-15]. This location can be determined by applying a general flexural force (P_{xS}, P_{yS}) through the unknown point (x_S,y_S), recognizing the equivalent centroidal forces and moments are

$$P_x = P_{xS}, \qquad P_y = P_{yS}, \qquad M_z = P_{yS}\,x_S - P_{xS}\,y_S, \qquad (10.a\text{-}c)$$

substituting these resultants into Eq. (9.*a*), rearranging, noting that ($\theta = 0$), and then:

$$x_S = \frac{a_2}{EI_{xx}}, \qquad y_S = -\frac{a_1}{EI_{yy}}. \qquad (10.d,e)$$

Although this definition leads to a zero twist rate about the line of centroids there will be a nonzero twist rate about every other line parallel to the centroidal axis as a result of the formation of the anticlastic surface. This is observed by calculating the micromolar twist rate as

$$\frac{\partial \omega_z}{\partial z} = \frac{1}{2}\left(\frac{\partial \gamma_{yz}}{\partial x} - \frac{\partial \gamma_{xz}}{\partial y}\right) = \theta - \frac{P_x}{EI_{yy}}\{\nu\, y\} + \frac{P_y}{EI_{xx}}\{\nu\, x\}. \qquad (11)$$

Applying a force (P_{xS}, P_{yS}) through the above shear center definition will produce a zero micromolar twist rate about the centroid axis (since x=y=θ =0), but a nonzero micromolar twist rate (θ_S) about the calculated line of shear centers (x_S,y_S) that is equal to:

$$\left.\frac{\partial \omega_z}{\partial z}\right|_{\substack{x = x_S \\ y = y_S}} = \theta_S = -\frac{P_{xS}}{EI_{yy}}\{\nu\, y_S\} + \frac{P_{yS}}{EI_{xx}}\{\nu\, x_S\}. \qquad (12)$$

This nonzero micromolar twist rate is illustrated in Fig. 2.*a*, where the deformed root (z=0) and tip (z=L) cross-sections of the loaded (P_{yS}) cantilever beam are superimposed.

An alternate shear center location (x_S^*,y_S^*) can also be determined so that the application of an applied flexure force (P_{xS}, P_{yS}) will produce a zero twist rate about the calculated line of shear centers and insure that the shear center is coincident with the

center of twist. The current model has advantages over the procedure of [16,17] in that it uses the Saint-Venant results directly and can be applied to any arbitrary cross-section, not just thin cross-sections. This calculation involves finding the load point in the cross-section plane that will produce a twist rate about the centroidal axis that is equal to the negative of the anticlastically produced micromolar twist rate, thus

$$\theta = -\theta_s^* = \frac{P_{xs}}{EI_{yy}}\left(\nu\, y_s^*\right) - \frac{P_{ys}}{EI_{xx}}\left(\nu\, x_s^*\right) . \tag{13}$$

where these twist rates offset each other to produce a zero twist rate about the line of shear centers. See Fig. 2.*b*. Substituting Eqns. (13) and (10.*a-c*) into (9.*a*), one can determine this shear center location as:

$$x_s^* = \frac{a_2}{(EI_{xx} + \nu GJ)}, \qquad y_s^* = -\frac{a_1}{(EI_{yy} + \nu GJ)}, \tag{14.a,b}$$

or in terms of the previous (classical) definition by making use of Eq. (10.*d,e*) and (G/E = 1/2(1+ν)):

$$x_s^* = \frac{x_s}{1 + \frac{\nu}{(1+\nu)}\frac{J}{2I_{xx}}}, \qquad y_s^* = \frac{y_s}{1 + \frac{\nu}{(1+\nu)}\frac{J}{2I_{yy}}}, \tag{14.c,d}$$

and the percent difference between the two locations can be expressed as:

$$\frac{x_s - x_s^*}{x_s^*} = \frac{\nu}{(1+\nu)}\frac{J}{2I_{xx}}, \qquad \frac{y_s - y_s^*}{y_s^*} = \frac{\nu}{(1+\nu)}\frac{J}{2I_{yy}}. \tag{14.e,f}$$

It is interesting to note that (x_S^*,y_S^*) will always be less than or equal to (x_S,y_S), where the two locations are equal when either the Poisson's ratio is zero, the shear center is coincident with the centroid (a_2=a_3=0), or the cross-section is very thick so that (J/I_{xx}) or (J/I_{yy}) is effectively zero. For most thin solid cross-sections (including NACA airfoils or triangles), $J/I_{xx} \approx 4$, and thus the percent difference when measured from the centroid will generally vary from 40% to 67% depending upon the Poisson ratio (assuming 0.25<ν<0.50), which is agreement with the work of [16,17].

Shear Deformation

An examination of the displacement components of Eq. (3.*a-c*) reveals that the calculated centroidal tip displacements ($u(x=y=0,z=L) = P_x L^3/3EI_{yy}$, $v(x=y=0,z=L) = P_y L^3/3EI_{xx}$) agree with the strength of materials solution, but the additional displacement associated with shear deformation does not appear as a result of our original assumption (Eq. 4.a-f) that the slope of the deformed centroidal axis at the beam root is zero ($b_4, b_5=0$). This additional displacement can be included by simply rotating the deformed beam so that the slope of the deformed cross-section at the centroid ($x=y=0$) is coincident with the *x-y* plane, and thus the deformed centroidal axis will have a nonzero slope (see [3] for additional details). The rotation angles are equal to the shear strains (γ_{xz}, γ_{yz}) at the centroid of the beam root ($x=y=z=0$) and thus by combining Eqns. (3,7,9.*a*,10) the shear angles defined in terms of the applied forces (P_x, P_y, M_z) are:

$$b_4 = \gamma_{xz(o)} = \left(\left.\frac{\partial \psi_1}{\partial x}\right|_{x=y=0} + y_s \frac{EI_{yy}}{GJ} \left.\frac{\partial \psi_3}{\partial x}\right|_{x=y=0} \right) \frac{P_x}{EI_{yy}} + \left(\left.\frac{\partial \psi_2}{\partial x}\right|_{x=y=0} - x_s \frac{EI_{xx}}{GJ} \left.\frac{\partial \psi_3}{\partial x}\right|_{x=y=0} \right) \frac{P_y}{EI_{xx}} + \left.\frac{\partial \psi_3}{\partial x}\right|_{x=y=0} \frac{M_z}{GJ} \tag{15.a}$$

$$b_5 = \gamma_{yz(o)} = \left(\left.\frac{\partial \psi_1}{\partial y}\right|_{x=y=0} + y_s \frac{EI_{yy}}{GJ} \left.\frac{\partial \psi_3}{\partial y}\right|_{x=y=0} \right) \frac{P_x}{EI_{yy}} + \left(\left.\frac{\partial \psi_2}{\partial y}\right|_{x=y=0} - x_s \frac{EI_{xx}}{GJ} \left.\frac{\partial \psi_3}{\partial y}\right|_{x=y=0} \right) \frac{P_y}{EI_{xx}} + \left.\frac{\partial \psi_3}{\partial y}\right|_{x=y=0} \frac{M_z}{GJ} \tag{15.b}$$

where the subscript (*o*) is introduced to symbolize the evaluation of the function at the centroid ($x=y=0$). The final form of the displacement components including shear deformation (from Eq. (3.*a-c*)) is:

$$u = \frac{P_x}{EI_{yy}}\left\{\frac{L}{2}z^2 - \frac{z^3}{6} + \frac{\nu}{2}\left\{x^2 - y^2\right\}(L - z)\right\} + \frac{P_y}{EI_{xx}}\{\nu xy(L - z)\} - \theta yz + b_4 z \tag{16.a}$$

$$v = \frac{P_y}{EI_{xx}}\left\{\frac{L}{2}z^2 - \frac{z^3}{6} + \frac{\nu}{2}\left\{y^2 - x^2\right\}(L - z)\right\} + \frac{P_x}{EI_{yy}}\{\nu xy(L - z)\} + \theta xz + b_5 z \tag{16.b}$$

$$w = -\frac{P_x}{EI_{yy}}\left\{x\left\{Lz - \frac{z^2}{2}\right\}\right\} - \frac{P_y}{EI_{xx}}\left\{y\left\{Lz - \frac{z^2}{2}\right\}\right\} + \psi(x,y) - b_4 x - b_5 y \tag{16.c}$$

where ψ, θ, b_4, and b_5 are defined in Eqns. (7), (9.*a*), (15.*a*), and (15.*b*), respectively.

Kinematics of a Compatible One-Dimensional Theory

A fully compatible one-dimensional beam theory can be developed using the following kinematic relations

$$\begin{aligned} u(x,y,z) &= U(z) - y\Theta(z) + \psi_x(x,y), \\ v(x,y,z) &= V(z) + x\Theta(z) + \psi_y(x,y), \\ w(x,y,z) &= W(z) - x\Phi_y(z) + y\Phi_x(z) + \psi_z(x,y), \end{aligned} \tag{17.a-c}$$

where (U,V,W) are z-dependent displacement functions that act along the x,y, and z directions, respectively, (Φ_x,Φ_y,Θ), are z-dependent rotations about the x,y, and z axes, respectively, and (ψ_x,ψ_y,ψ_z) represent cross-section dependent "residual" (or warping) displacements of the beam. The in-plane functions (ψ_x,ψ_y) which are associated with formation of the anticlastic surface, can be neglected by assuming $(\sigma_{xx}=\sigma_{yy}=\tau_{xy}=0)$ and thus using a one-dimensional constitutive model:

$$\sigma_{zz} = E\,\varepsilon_{zz} = E\left\{\frac{\partial W}{\partial z} - x\frac{\partial \Phi_y}{\partial z} + y\frac{\partial \Phi_x}{\partial z}\right\},$$

$$\tau_{yz} = G\,\gamma_{yz} = G\left\{x\frac{\partial \Theta}{\partial z} + \frac{\partial V}{\partial z} + \Phi_x + \frac{\partial \psi_z}{\partial y}\right\}, \tag{18.a-c}$$

$$\tau_{xz} = G\,\gamma_{xz} = G\left\{-y\frac{\partial \Theta}{\partial z} + \frac{\partial U}{\partial z} - \Phi_y + \frac{\partial \psi_z}{\partial x}\right\}.$$

If one assumes that (U,V,W) and (Φ_x, Φ_y,Θ) represent the displacements and rotations about the centroid [9], then the corresponding definition of the one-dimensional out-of-plane warping function (from Eq. (16.*c*)) is

$$\psi_z = \psi(x,y) - b_4 x - b_5 y\,. \tag{19}$$

where (ψ) is given in Eq. (7).

Alternatively, based upon the work of [10], one can assume that (U,V,W) and (Φ_x,Φ_y) are the mean displacements and the mean rotations of the cross-section

$$U, V, W = \frac{1}{A}\int_A (u, v, w)\, dA\ , \qquad \Phi_x = \frac{1}{I_{xx}}\int_A y\, w\, dA\ , \qquad \Phi_y = -\frac{1}{I_{yy}}\int_A x\, w\, dA\ , \quad (20.a\text{-}e)$$

and the correct form of the out-of-plane warping is obtained by substituting Eq. (16.c) into (20.*a-e*) and then into (17.*c*):

$$\psi_z = \psi - \frac{y}{I_{xx}}\int_A y\, \psi\, dA - \frac{x}{I_{yy}}\int_A x\, \psi\, dA - \frac{1}{A}\int_A \psi\, dA\ , \qquad (20.f)$$

where (ψ) is given in Eq. (7).

The development of the equations of motion and the corresponding boundary conditions using the kinematic relations of Eqns. (17.*a-c*) can be determined using Hamilton's principle, where the bending and torsion related section constants are dependent upon the one-dimensional out-of-plane warping function (ψ_z). The complete details of this refined model can be found in the second part of this paper [11].

Finally, a set of linear equations can be developed that relates the kinematic description of shear strain and twist rate to the shear (P_x,P_y) and torsion (M_z) resultants, which can be used to (1) transform the warping function definition (Eq. (7)) to a kinematically scaled function, and (2) provide valuable one-dimensional cross-section constants. Substituting Eqns. (18.*b,c*) into Eqns (1.*a-c*) and carrying out the integration over the cross-section results in

$$\begin{bmatrix} R_{11} & R_{12} & 0 \\ R_{21} & R_{22} & 0 \\ R_{31} & R_{32} & 1 \end{bmatrix} \begin{Bmatrix} P_x \\ P_y \\ M_z \end{Bmatrix} = \begin{bmatrix} S_{11} & 0 & S_{13} \\ 0 & S_{22} & S_{23} \\ 0 & 0 & S_{33} \end{bmatrix} \begin{Bmatrix} \frac{\partial U}{\partial z} - \Phi_y \\ \frac{\partial V}{\partial z} + \Phi_x \\ \frac{\partial \theta}{\partial z} \end{Bmatrix}\ , \qquad (21)$$

where the coefficients (R_{ij}) and (S_{ij}) are defined in the Appendix. Multiplying Eq. (21) by the inverse of [R] results in the following set of linear equations

$$\begin{Bmatrix} P_x \\ P_y \\ M_z \end{Bmatrix} = \begin{bmatrix} GA\,k_{11} & GA\,k_{12} & -GA\bar{y}\,k_{13} \\ GA\,k_{12} & GA\,k_{22} & GA\bar{x}\,k_{23} \\ -GA\bar{y}\,k_{13} & GA\bar{x}\,k_{23} & GJ \end{bmatrix} \begin{Bmatrix} \frac{\partial U}{\partial z} - \Phi_y \\ \frac{\partial V}{\partial z} + \Phi_x \\ \frac{\partial \theta}{\partial z} \end{Bmatrix}, \tag{22}$$

where (k_{11}, k_{12}, k_{22}) are the shear correction coefficients needed for Timoshenko's beam theory [9] and (k_{13}, k_{23}) are the shear correction coefficients for coupling between flexure and torsion. This approach for flexure-torsion behavior is an extension of the method developed in [10] for uncoupled bending only.

Solution Procedure

Warping Function Determination via Power Series

The warping function (ψ) of Eq. (7), which is dependent upon both the cross-section shape as well as the material properties, can be determined by solving a set of variationally derived algebraic equations based upon the principle of minimum potential energy. In this development the warping function is defined as a power series:

$$\psi(x,y) = \sum_{m=0}^{\infty} \sum_{n=0}^{\infty} c_{mn}\, x^m y^n - c_{00}\,, \tag{23}$$

where c_{mn} are the unknown coefficients and the rigid body translation coefficient (c_{00}) is not included since it was accounted for in Eq. (3.c) by (b_3). If one assumes a finite series, then the above equation can be written in matrix form as

$$\psi(x,y) = [N(x,y)]\{c\} \tag{24}$$

where [$N(x,y)$] is an array of the power terms, {c} is an array of unknown coefficients, and the array sizes are dependent upon the selected polynomial order. For example, if a

cubic polynomial was selected, then based upon Pascal's triangle there are nine terms, and the above arrays have the form:

$$[N(x,y)] = \left\{ x, \quad y, \quad x^2, \quad xy, \quad y^2, \quad x^3, \quad x^2y, \quad xy^2, \quad y^3 \right\},$$

$$\{c\}^T = \{ c_{10}, c_{01}, c_{20}, c_{11}, c_{02}, c_{30}, c_{21}, c_{12}, c_{03} \}. \tag{25.a,b}$$

A set of linear algebraic equations for determining the coefficients $\{c\}$ can be obtained by substituting Eq. (24), into Eq. (6) and taking the variation with respect to the unknown coefficients ($\delta\psi = [N(x,y)]\{\delta c\}$):

$$[K]\{c\} = [[F_w] - [F_c]]\{Q\}, \tag{26.a}$$

where the stiffness matrix is defined as

$$[K] = GL \int_A \frac{\partial}{\partial x}[N(x,y)]^T \frac{\partial}{\partial x}[N(x,y)] + \frac{\partial}{\partial y}[N(x,y)]^T \frac{\partial}{\partial y}[N(x,y)]\, dA \tag{26.b}$$

the force matrices are presented as

$$[F_w] = EL\left[\int_A x[N]^T dA, \quad \int_A y[N]^T dA, \quad 0 \right], \tag{26.c}$$

$$[F_c] = GL \int_A \left[\frac{\partial}{\partial y}[N(x,y)]^T, \frac{\partial}{\partial x}[N(x,y)]^T \right] \begin{bmatrix} -\nu xy & -\frac{\nu}{2}\left(y^2 - x^2\right) & x \\ -\frac{\nu}{2}\left(x^2 - y^2\right) & -\nu xy & -y \end{bmatrix} dA, \tag{26.d}$$

and

$$\{Q\}^T = \left\{ \frac{P_x}{EI_{yy}}, \frac{P_y}{EI_{xx}}, \theta \right\}. \tag{26.e}$$

The coefficients $\{c^{(1)}\}$ associated with the unit warping function (ψ_1) in Eq. (7) are determined by setting $\{Q\}^T = \{1,0,0\}$. Similarly, the coefficients $\{c^{(2)}\}$ for (ψ_2) and $\{c^{(3)}\}$

for (ψ_3) are determined by performing analyses with $\{Q\}^T = \{0,1,0\}$ and $\{Q\}^T = \{0,0,1\}$, respectively. Thus, the complete warping function distribution for the three cases can be written matrix form as;

$$\{\psi_1, \psi_2, \psi_3\} = [N(x,y)]\left\{\left\{c^{(1)}\right\}, \left\{c^{(2)}\right\}, \left\{c^{(3)}\right\}\right\} . \tag{27}$$

Computer Program

A computer program was written where, first, the boundary of a general cross-section is defined using (n) coordinate points with (n) straight line segments connecting the points. Second, the cross-section is discretized into (n) triangular subregions, where one edge of a triangle is a boundary line segment and the other two edges connect the end-points of a boundary line segment with the user-defined cross-section origin. Thus all of the subregions have one corner that is defined at the origin. See Fig. 3.*b* for an example of a rectangle defined using four triangular subregions. Third, the cross-section centroid and principal axes are calculated and then the cross-section coordinates and applied forces are transformed to the cross-section principal axes. Fourth, the area integrals (Eqns. 26.*b-d*) for each triangle subregion are evaluated using exact Gaussian Quadrature formulas [8], where the cross-section power series polynomial can be user-defined. Fifth, the complete cross-section stiffness and force matrices are formed by simply adding together (not finite element type assembling) all of the triangular subregion matrices. Sixth, the coefficients for each of the three cases of $\{Q\}$ are determined. Seventh, the calculated coefficients along with the power series polynomial definition are used to determine the shear stress distribution and the cross-section properties (shear center location, torsion constant, shear correction factors, etc.). Finally the calculated values are transformed from the cross-section principal axes back to the user defined coordinate system.

This approach strongly differs from previous finite element based approaches [4,5] in that the global matrix size is defined by the assumed polynomial order and not the complexity of the cross-section. Moreover, cross-section cavities can be easily treated by simply subtracting off the triangular subregions that define the cavity. The aspect ratio of a triangle subregion is not critical, since the power series is a global cross-section function and not a local subregion function (i.e., finite element method).

Numerical Results

Prismatic cantilever beams with three different cross-section types are studied to first verify the current approach (ellipse, rectangle), Fig. 3, and second illustrate important results not found in the literature (NACA 4-digit airfoils), Fig. 4. The beam material properties are defined as (E=1.0, ν=0.333).

Ellipse

Initially the current approach was verified by studying the behavior of cantilever beams with elliptical cross-sections having a wide range of aspect ratios ($0.01 \le b/a \le 100$), where (a) and (b) are the semi-axes length in the x and y directions, respectively. See Figure 3.*a*. Each elliptical cross-section was discretized using 90 points on the cross-section (i.e. 90 triangular subregions) and the warping functions were defined using a cubic polynomial (9 unknown coefficients) with a corresponding exact Gaussian Quadrature formula [8]. In Fig. 5, the variation of the nonzero nondimensionalized coefficients for an applied bending curvature rate (P_x/EI_{yy}) and twist rate (θ) are presented as a function of aspect ratio (b/a), where the circles are the current calculated power series solution and the bold solid lines are the exact solution from [2]. The flexure solution in the x direction is composed of only three nonzero terms ($\psi_1 = c_{10}x + c_{12}xy^2 + c_{30}x^3$), where the remaining 6 calculated coefficients are equal to zero. The c_{10} term is proportional to the shear strain at the beam root ($\gamma_{xz(o)}$) and thus is used as a measure of shear deformation in the x-direction (b_4), from Eq. (15.a):

$$\frac{c_{10}}{a^2} = \frac{1}{a^2}\left.\frac{\partial \psi_1}{\partial x}\right|_{x=y=0} = \frac{\gamma_{xz(o)} EI_{yy}}{a^2 P_x} = \frac{b_4 EI_{yy}}{a^2 P_x} . \qquad (28.a)$$

Applying a force in the y-direction (P_y), would produce only three nonzero coefficients; c_{01}, c_{21}, and c_{03}, where again the remaining 6 coefficients are equal to zero. The coefficient c_{01} is proportional to ($\gamma_{yz(o)}$) and represents a measure of shear deformation in the y-direction (b_5):

$$\frac{c_{01}}{b^2} = \frac{1}{b^2}\left.\frac{\partial \psi_2}{\partial y}\right|_{x=y=0} = \frac{\gamma_{yz(o)} EI_{xx}}{b^2 P_y} = \frac{b_5 EI_{xx}}{b^2 P_y} . \qquad (28.b)$$

The twist rate dependent warping function is composed of only the bi-linear term ($\psi_3 = c_{11}xy$), where the remaining 8 coefficients are equal to zero and c_{11} goes to zero as the cross-section becomes a circle (b/a=1). The torsion constant (GJ=a_3) was calculated for each aspect ratio and was found to be in exact agreement (identical to 8 decimal places) with the closed-form solution of [2]:

$$GJ = G\pi\frac{a^3b^3}{a^2+b^2}, \tag{29}$$

which was expected since the current torsion warping function is in agreement with the published solutions. The shear center was calculated and found to be coincident with the centroid for all aspect ratios (x_s^*=x_s=0, y_s^*=y_s=0). Finally, the shear correction factors (k_{11},k_{22}) were calculated and compared to the results of Cowper [10] (see Table 1). The current predictions are in near exact agreement over a broad range of aspect ratios, where it is interesting to note that for a force acting through a very thin ellipse (for example P_y with b/a≈0) the shear correction factor approaches zero while a force acting through a thick ellipse (P_x with b/a≈0) the shear correction factor approaches 0.917184.

Rectangle

The behavior of cantilever beams having rectangular cross-sections was also studied in order to further validate the current approach. A wide range of aspect ratios ($0.01 \le b/a \le 100$) were investigated, where each cross-section was discretized using the four corner points (four triangular subregions). See Fig. 3.*b*. From [2], the exact solution of the x-dependent bending curvature rate warping function (ψ_1) is defined as:

$$\psi_1 = a^2\left\{\frac{\nu}{3}\left(\frac{b}{a}\right)^2 - (1+\nu)\right\}x - \left\{\frac{\nu}{2}\right\}xy^2 + \frac{1}{6}\left\{2+\nu\right\}x^3 + \frac{4\nu b^3}{\pi^3}\sum_{n=1}^{\infty}\frac{(-1)^n}{n^3}\frac{\sinh(n\pi\frac{x}{b})}{\cosh(n\pi\frac{a}{b})}\cos(n\pi\frac{y}{b}). \tag{30}$$

In order to compare the current power series predictions with the above infinite series of transcendental functions, a Taylor series expansion was performed on Eq. (30) and the first three nonzero terms were found to be:

$$\psi_1 = a^2\left\{\frac{\nu}{3}\left(\frac{b}{a}\right)^2 - (1+\nu) + 4\nu S_{(-2)}\right\}x - \frac{\nu}{2}\left\{1 + 4S_{(0)}\right\}xy^2 + \frac{1}{6}\left\{2 + \nu + 4\nu S_{(0)}\right\}x^3 + \cdots \tag{31.a}$$

where

$$S_{(l)} = \sum_{n=1}^{\infty} \frac{(-1)^n \left(n\pi\frac{a}{b}\right)^l}{\cosh\left(n\pi\frac{a}{b}\right)} . \qquad (31.b)$$

The torsion rate warping function (ψ_3) is also described by an infinite transcendental series [2], but as (b/a) approaches either zero or infinity the series reduces to simply ($\psi_3=c_{11}xy$) with $c_{11}=-1$ or $c_{11}=1$, respectively. Moreover, the torsion warping function for a square cross-section ($b/a=1$) can be expressed using a Taylor series expansion as:

$$\psi_3 = 1.574\,xy\left(\left(\frac{x}{a}\right)^2 - \left(\frac{y}{b}\right)^2\right) - 0.9021\,xy\left(\left(\frac{x}{a}\right)^4 - \left(\frac{y}{b}\right)^4\right) + 0.4909\,xy\left(\left(\frac{x}{a}\right)^6 - \left(\frac{y}{b}\right)^6\right)$$
$$+ 9.794\,xy\left(\frac{x}{a}\right)^2\left(\frac{y}{b}\right)^2\left(\left(\frac{x}{a}\right)^2 - \left(\frac{y}{b}\right)^2\right) + \cdots \quad . \qquad (32)$$

The calculated torsion rate warping function (ψ_3) is used to determine the torsion rigidity

$$GJ = a_3 = G\,k_t\,(2a)^3(2b) \qquad (33)$$

where (k_t) is the torsion constant.

Two cross-section aspect ratios (b/a = 1, 100) were initially studied to assess the convergence of the calculated coefficients and the warping-dependent cross-section constants as a function of the polynomial order for the warping function. In Tables 2 and 3, the first three nonzero flexure coefficients, the first torsion coefficient, the shear correction factor, and the torsion constant are presented as a function of power series order and solution matrix size. In addition, reference values for the calculated values are presented, where the three flexure coefficients are determined using Eq. (31), the torsion coefficient is taken from Eq. (32), the shear correction factor (k_{11}) is taken from [10], and the torsion constant (k_t) is taken from [2,3]. From these tables, it is obvious that the integrated cross-section constants converge to the reference values much quicker than the actual power series coefficients. This occurs because the calculated coefficients represent a "best-fit" of the user-defined polynomial to the transcendental series, and changing the order of the polynomial will change the magnitude of the calculated

coefficients, but it will have virtually no effect on the integrals of these functions. Thus, if one is only interested in warping related cross-section constants, then a low-order power series polynomial can be used, but if one is interested in the details of the warping function, then a much higher-order polynomial is required.

In Fig. 6, the first three nonzero nondimensionalized power series flexure coefficients (symbols) are presented along with the Taylor series representation of Eq. (30) given by the bold solid lines. The power series solution produces near exact agreement over a broad range of aspect ratios ($0.01 \le b/a < 100$), where a ninth-order polynomial (54 unknowns) was used for the warping function. As (b/a) approaches 100 (transversely loaded plate-type cross-section), the power series predictions deviate from the Taylor series representation. This can be traced to the fact that the infinite transcendental series in Eq. (30) converges slowly for large (b/a) and the selected ninth-order polynomial can not accurately represent this behavior. Thus, one would need to go to an even higher-order polynomial for this severe aspect ratio. The shear center (x_S,y_S) and shear correction factors (k_{11}, k_{22}) were calculated for the entire range of aspect ratios and it was found that the shear center was always located at the centroid and the shear correction factors were always equal to 0.85105, which is in exact agreement with [10] using $\nu = 0.333$. The calculated torsion constant (k_t) is presented in Table 4 as a function of aspect ratio, where the current results are in near perfect agreement with [2].

NACA 4-Digit Airfoils

The final set of beam cross-sections that were investigated included six NACA 4-digit airfoils of different thickness (NACA 0006, 0012, 0018) and camber (NACA 2512, 4512, 6512). The numbering system for these airfoils is based upon section geometry [19], where the first digit indicates the maximum value of the mean-line ordinate in percent of chord (c), the second digit indicates the distance from the leading edge to the maximum camber location in tenths of chord, and the last two digits indicate the maximum thickness (t_{max}) in percent of chord. Two of the studied airfoils, NACA-0012 and NACA-4512, are presented in Fig. 4, where a second coordinate system ($\tilde{x}$,$\tilde{y}$) is introduced with the origin taken as the leading edge. Each airfoil was discretized using 95 points on the cross-section boundary (i.e. 95 triangular subregions), the warping functions were modeled using a 9th order power series polynomial (54 unknown coefficients), and the numerical integration was performed exactly using a 52-point Gaussian Qaudrature formula [8].

The calculated section properties for the six airfoils are presented in Table 5. The

first five parameters represent the chord normalized geometric section constants and the sixth parameter (β) is the rotation angle from (x,y) to the principal axes (x,y) with counter clockwise defined as positive. The remaining nine parameters represent the torsion- and flexure-dependent values. The torsion coefficient (k_t), which is nearly independent of airfoil thickness and camber, is found using the calculated torsion constant (GJ)

$$GJ = a_3 = G\,k_t(t_{max})^3 c\,. \tag{34}$$

The chord normalized flexure dependent coefficients (c_{10}, c_{01}) are also presented and are used to provide a measure of chord-wise and thickness-wise shear deformation (see Eqns. 28.a,b). From the coefficient (c_{10}), it is readily apparent that the application of a force in the chordwise direction (P_x) will produce nearly constant shear-deformation regardless of airfoil thickness or camber. Whereas the shear deformation associated with a thickness-wise force (P_y) is highly dependent upon the airfoil thickness but only slightly dependent upon camber. The shear center locations are also presented for the two definitions using the second coordinate system ($\tilde{x}$,$\tilde{y}$). Both definitions locate the shear center ahead of the centroid, where the difference between the two definitions is nearly 50% (measured from the centroid with ν=0.333) in the x-direction and a minimal amount in the y-direction (cambered airfoils). It is interesting to note that the shear center moves rearward (closer to the centroid) by either increasing the thickness or camber. The difference that these two shear center locations have on the torsional divergence speed of a straight uniform aircraft wing can be studied using (from [20]):

$$U_D = \frac{\pi}{2L}\sqrt{\frac{GJ}{c\,e\,a_0(\rho/2)}}\,, \tag{35}$$

where (ρ) is the air density, (a_0) is the lift curve slope, and (e) is the distance from the elastic axis (line of shear centers) to the quarter-chord. The ratio of the divergence speed (U_D^*) using the corrected shear center location (aligned with the center of twist) based upon [16,17] to the divergence speed (U_D) using the classical definition [12], while holding everything else constant, is equal to:

$$\frac{U_D^*}{U_D} = \sqrt{\frac{e}{e^*}}\,, \tag{36}$$

where the results for the six different airfoil sections are given in Table 5. Thus it is apparent that the new (corrected) shear center location will predict divergence speeds

that are significantly lower (6-12%) than those using the classic shear center definition and this reduction is larger for thin airfoils with little or no camber.

Lastly, the shear correction factors (k_{11},k_{22}) are presented. Increasing the airfoil thickness will produce a minor decrease in (k_{11}) but increase (k_{22}) significantly. This observation is in close agreement with the thin elliptical cross-section results (Table 1, $0.01<b/a<0.20$). Introducing camber will significantly reduce both shear correction factors (k_{11},k_{22}).

Conclusions

The flexure-torsion behavior of a tip-loaded cantilever beam with an arbitrary cross-section is studied using Saint-Venant's semi-inverse method along with a power series solution for the out-of-plane flexure and torsion warping functions. The power series coefficients are determined by solving a set of variationally derived linear algebraic equations. For complex cross-sections, the calculated coefficients represent a "best-fit approximation" to the exact warping function. A new linear relation is developed for locating the shear center using the Saint-Venant flexure and torsion solutions, where the twist rate is zero about the line of shear centers (not the centroidal axis). In addition the kinematic relations for a fully compatible one-dimensional beam theory are presented, where the calculated current flexure and torsion warping functions are fully integrated into the development (see part II [11]). Numerical results are presented for three different cross-sections (ellipse, rectangle, NACA four-digit airfoils). For elliptical cross-sections, it was shown that the calculated coefficients, as well as all of the section properties, were in exact agreement with existing elasticity solutions. For the rectangular cross-section, it was shown that the calculated power series coefficients represent a "best-fit" to the transcendental functions and a low-order polynomial can be used if only warping-related section properties are desired, whereas a higher-order polynomial is required if the warping function is to be studied in detail. Finally for NACA four-digit airfoils, the shear deformation and shear correction factor associated with a thickness-wise force (P_y) is highly dependent upon the airfoil thickness but only slightly dependent upon camber. The x-direction shear center location is ahead of the centroid with the difference in the two definitions being nearly 50% (for ν=0.333) when measured from the airfoil centroid, and increasing either the airfoil thickness or the camber will move the shear center closer to the centroid. These differences correspond to a 6-12% decrease in the divergence speed for the corrected shear center definition versus the classic definition.

Acknowledgements

The support of this research was provided by the NASA-Langley Research Center through grant NAG-1-1151-FDP, with R. C. Lake as project monitor. The discussions and encouragement provided by E. Reissner are gratefully acknowledged.

References

1.) Love, A. E. H., A Treatise on the Mathematical Theory of Elasticity, 4th ed., Dover Publications, 1944, pp. 310-348.

2.) Sokolnikoff, I. S., Mathematical Theory of Elasticity, 2nd ed., McGraw-Hill, New York, 1956, pp. 104-220.

3.) Timoshenko, S. P. and J. N. Goodier, Theory of Elasticity, 3rd ed., McGraw-Hill, New York, 1970, pp. 291-313 and pp. 354-374.

4.) Herrmann, L. R., "Elastic Torsional Analysis of Irregular Shapes," ASCE Journal of Engineering Mechanics Division, vol. 91, 1965, pp. 11-19.

5.) Mason, W. E., and L. R. Herrmann, "Elastic Shear Analysis of General Prismatic Beams," ASCE Journal of Engineering Mechanics Division, vol. 94, 1968, pp. 965-983.

6.) Mindlin, R. D., "Solution of St. Venant's Torsion Problem by Power Series," International Journal of Solids and Structures, vol. 11, 1975, pp. 321-328.

7.) Cowper, G. R., "Gaussian Quadrature Formulas for Triangles," International Journal for Numerical Methods in Engineering, vol. 7, 1973, pp. 405-408.

8.) Dunavant, D. A., "High Degree Efficient Symmetrical Gaussian Quadrature Rules for Triangle," International Journal for Numerical Methods in Engineering, vol. 21, 1985, pp. 1129-1148.

9.) Timoshenko, S. P., "On the Correction for Shear of the Differential Equations for

Transverse Vibrations of Prismatic Beams," Philosophical Magazine, vol. 41, 1921, pp. 744-746.

10.) Cowper, G. R., "The Shear Coefficient in Timoshenko's Beam Theory," ASME Journal of Applied Mechanics, vol. 33, 1966, pp. 335-340.

11.) Kosmatka, J. B., "Flexure-Torsion Behavior of Prismatic Beams, Part II: A Compatible Shear Deformable One-Dimensional Theory", AIAA Journal, (to be published).

12.) Griffith, A.A., and G. I. Taylor, "The Problem of Flexure and its Solution by the Soap-Film Method," Reports and Memoranda Adv. Comm. Aeronautics, No. 399, 1917.

13.) Stevenson, A. C., "Flexure with Shear and Associated Torsion," Philosophical Transactions of the Royal Society, vol. 237, 1939, pp. 161-229.

14.) Goodier, J. N., "A Theorem on the Shearing Stress in Beams, Journal of the Aeronautical Sciences, vol. 11, 1944, pp. 272-280.

15.) Duncan, W. J., "The Flexural Centre of Centre of Shear," Journal of the Royal Aeronautical Society, vol. 57, 1953, pp. 594-597.

16.) Reissner, E., "The Center of Shear as a Problem of the Theory of Plates of Variable Thickness," Ingenieur-Archiv, vol. 59, 1989, pp. 324-332.

17.) Reissner, E., "Approximate Determinations of the Center of Shear by Use of the Saint-Venant Solution for the Flexure Problem of Plates of Variable Thickness," Archive of Applied Mechanics-Ingenieur-Archiv, vol. 61, no. 8, 1991, pp. 555-566.

18.) Jacobs, J. A., "The Centre of Shear of Aerofoil Sections," Journal of the Royal Aeronautical Society, vol. 57, 1953, pp. 235-237.

19.) Abbott, I. R., and A. E. Von Doenhoff, Theory of Wing Sections, 1st ed., Dover Publications, New York, 1959, pp. 111-115.

20.) Bisplinghoff, R. L., H. Ashley, and R. L. Halfman, Aeroelasticity, 2nd ed., Addison-Wesley Publishing, Co. Inc., 1955, p. 432.

Appendix

$$S_{11} = S_{22} = GA, \tag{A.1,2}$$

$$S_{13} = G\int_A \left(\frac{\partial \psi_{z3}}{\partial x} - y\right) dA, \qquad S_{23} = G\int_A \left(\frac{\partial \psi_{z3}}{\partial y} + x\right) dA, \tag{A.3,4}$$

$$S_{33} = G\int_A x\left(x + \frac{\partial \psi_{z3}}{\partial y}\right) - y\left(\frac{\partial \psi_{z3}}{\partial x} - y\right) dA, \tag{A.5}$$

$$R_{11} = 1 - \frac{G}{EI_{yy}}\int_A \frac{\partial \psi_{z1}}{\partial x} dA, \qquad R_{12} = -\frac{G}{EI_{xx}}\int_A \frac{\partial \psi_{z2}}{\partial x} dA, \tag{A.6,7}$$

$$R_{21} = -\frac{G}{EI_{yy}}\int_A \frac{\partial \psi_{z1}}{\partial y} dA, \qquad R_{22} = 1 - \frac{G}{EI_{xx}}\int_A \frac{\partial \psi_{z2}}{\partial y} dA, \tag{A.8,9}$$

$$R_{31} = -\frac{G}{EI_{yy}}\int_A \left(x\frac{\partial \psi_{z1}}{\partial y} - y\frac{\partial \psi_{z1}}{\partial x}\right) dA, \quad R_{32} = -\frac{G}{EI_{xx}}\int_A \left(x\frac{\partial \psi_{z2}}{\partial y} - y\frac{\partial \psi_{z2}}{\partial x}\right) dA. \tag{A.10,11}$$

Table 1: Shear correction factors for elliptical cross-sections (ν=0.333).

b/a	k_{11}	k_{11} [11]	k_{22}
0.01	0.917181	0.917181	0.004777
0.10	0.916854	0.916854	0.309770
0.20	0.915869	0.915869	0.602246
0.50	0.909272	0.909272	0.829613
1.00	0.888864	0.888864	0.888864
2.00	0.829613	0.829613	0.909272
5.00	0.602246	0.602246	0.915869
10.0	0.309770	0.309970	0.916854
20.0	0.105567	0.105567	0.917102
100.0	0.004777	0.004777	0.917181

Table 2: Calculated nonzero flexure and torsion power series coefficients, shear correction factor, and torsion constant for a square cross-section (b/a=1.00) with (ν=0.333).

Polynomial Order	Matrix Size	Flexure - x direction				Torsion	
		c_{10}/a^2	c_{30}	c_{12}	k_{11}	c_{31} ($-c_{13}$)	k_t
2	5	0.8887	-	-	1.000	-	0.167
4	14	1.2405	-0.3888	0.1110	0.85105	1.556	0.141
6	27	1.2324	-0.3615	0.1018	0.85105	1.250	0.141
8	44	1.2340	-0.3690	0.1108	0.85105	1.574	0.141
Reference		1.2340	-0.3705	0.1114	0.85105	1.574	0.141

Table 3: Calculated nonzero flexure and torsion power series coefficients, shear correction factor, and torsion constant for a thin rectangular cross-section (b/a=100) with (ν=0.333).

Polynomial Order	Matrix Size	Flexure - x direction				Torsion	
		c_{10}/a^2	c_{30}	c_{12}	k_{11}	c_{11}	k_t
2	5	-554.0	-	-	1.000	1.00	0.333
4	14	0.7783	-0.3888	-0.1663	0.85105	1.00	0.333
6	27	1.2483	-0.1118	-0.1670	0.85105	1.00	0.333
8	44	1.1130	-0.2334	-0.1514	0.85105	1.00	0.333
Reference		0.9943	-0.2873	-0.1382	0.85105	1.00	0.333

Table 4: Torsion coefficients (k_t) for rectangular cross-sections (ν=0.333).

b/a	k_t	k_t [2]
1.00	0.14058	0.141
1.20	0.16613	0.166
1.50	0.19578	0.196
2.00	0.22871	0.229
2.50	0.24940	0.249
3.00	0.26336	0.263
4.00	0.28086	0.281
5.00	0.29137	0.291
10.00	0.31297	0.312
∞	0.33333	0.333

Table 5: Section properties of NACA four-digit airfoils (ν=0.333).

	NACA-0006	NACA-0012	NACA-0018	NACA-2512	NACA-4512	NACA-6512
centroid						
$\tilde{x}/c$:	0.42067	0.42067	0.42067	0.42061	0.42039	0.42006
$\tilde{y}/c$:	0.00000	0.00000	0.00000	0.01520	0.03037	0.04550
A/c^2	0.04106	0.08213	0.12319	0.08219	0.08238	0.08270
I_{xx}/c^4 (10^{-5})	0.84944	6.79550	22.9350	6.97050	7.49940	8.39180
I_{yy}/c^4 (10^{-3})	2.26500	4.52990	6.79490	4.53690	4.55840	4.59370
β (degrees)	0.00000	0.00000	0.00000	0.41351	0.82850	1.24740
k_t	0.15642	0.15386	0.14986	0.15396	0.15427	0.15479
c_{10}/c^2 (10^{-1})	1.89102	1.89302	1.89633	1.89609	1.90553	1.92117
c_{01}/c^2 (10^{-4})	8.15829	32.5947	73.1685	32.5100	32.2590	31.8141
$\tilde{x}_s/c$:	0.33935	0.34093	0.34350	0.34399	0.35233	0.36402
$\tilde{y}_s/c$:	0.00000	0.00000	0.00000	0.02183	0.04378	0.06595
$\tilde{x}_s^*/c$:	0.36634	0.36711	0.36838	0.36871	0.37319	0.37985
$\tilde{y}_s^*/c$:	0.00000	0.00000	0.00000	0.02196	0.04398	0.06614
k_{11}	0.91545	0.91462	0.91323	0.90181	0.86340	0.80324
k_{22}	0.07740	0.24212	0.40041	0.22576	0.19355	0.16671
U_D^*/U_D	0.87640	0.88120	0.89350	0.89100	0.91140	0.93710

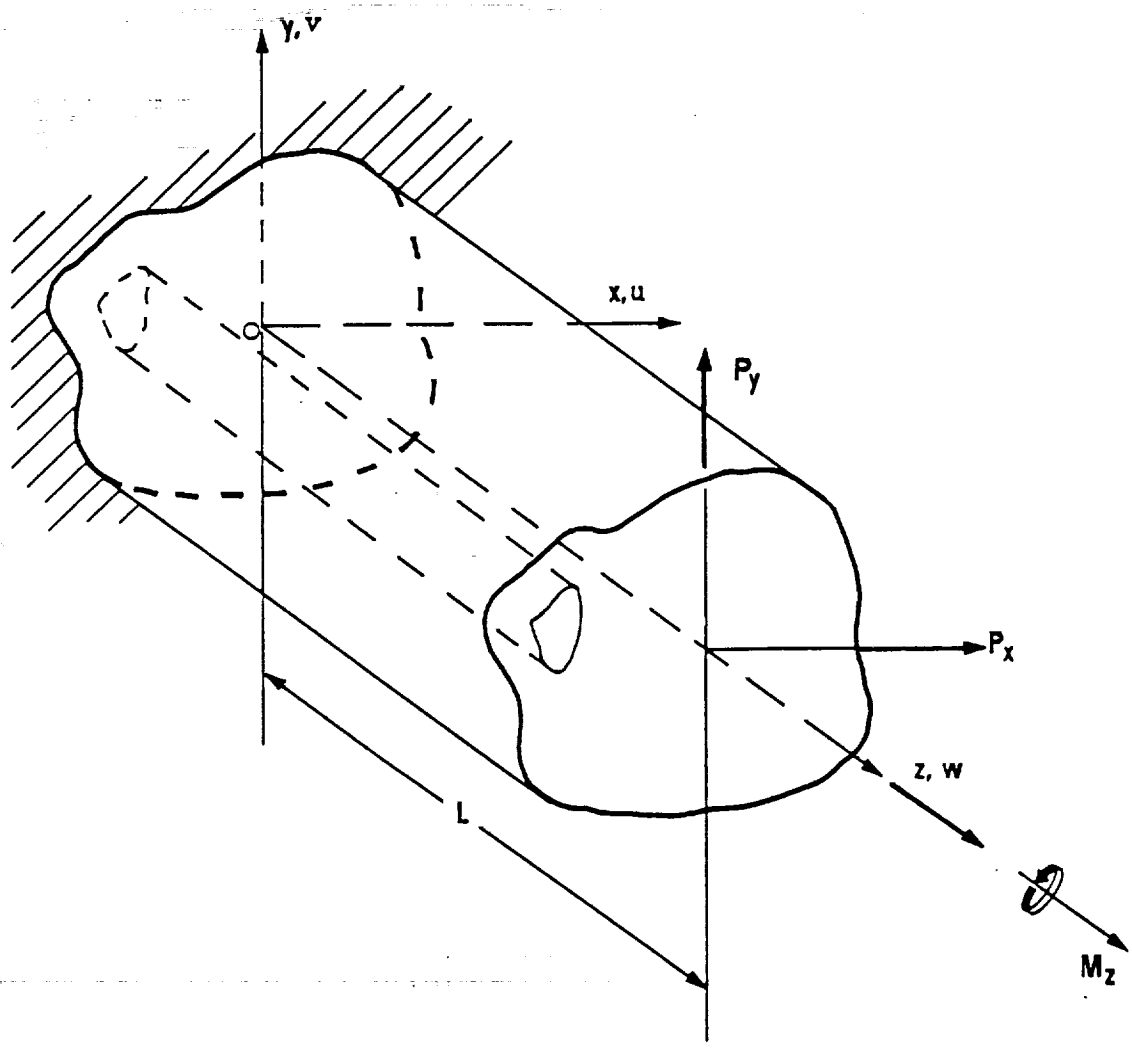

1.) Prismatic cantilever beam.

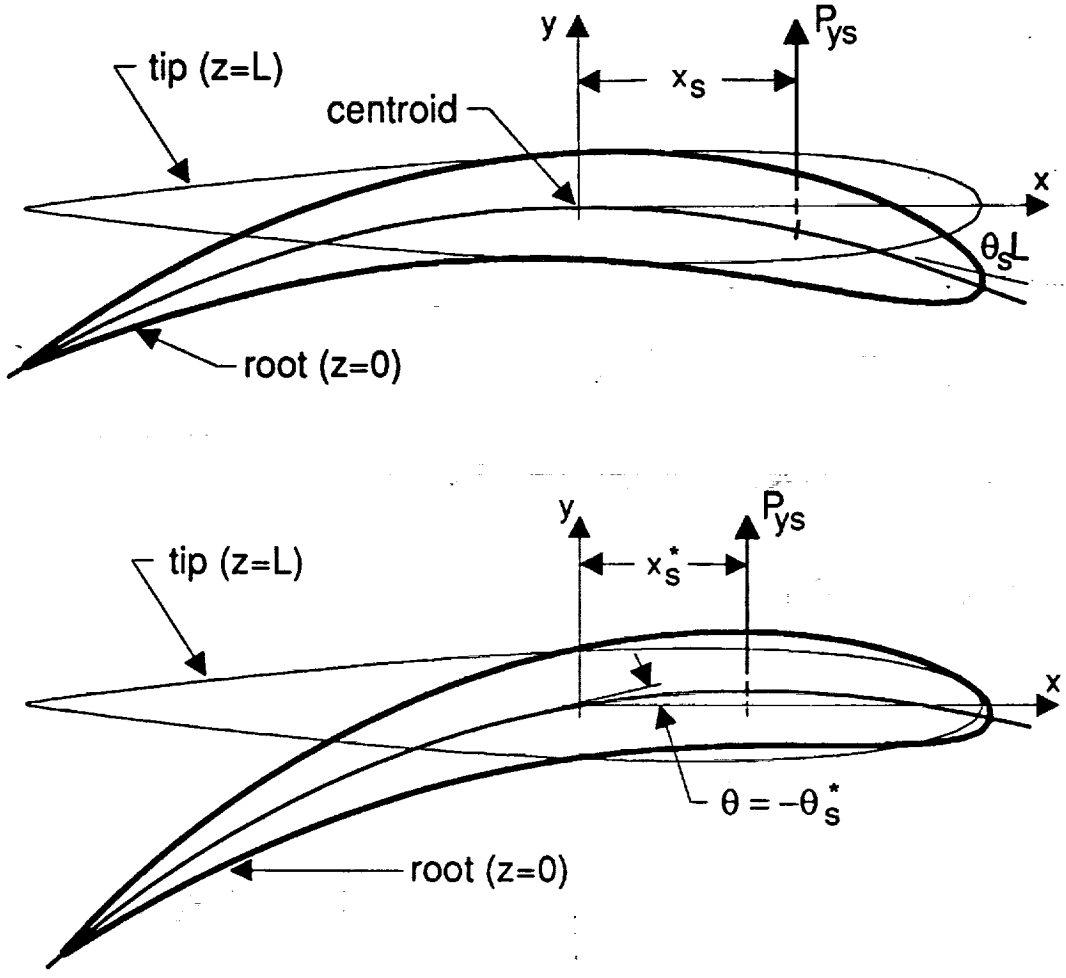

2.) Tip (—) and root (▬) cross-section planforms of a tip-loaded (P_{ys}) cantilever beam with an airfoil cross-section where (a.) zero twist about the centroidal axis and (b.) zero twist rate about the calculated line of shear centers.

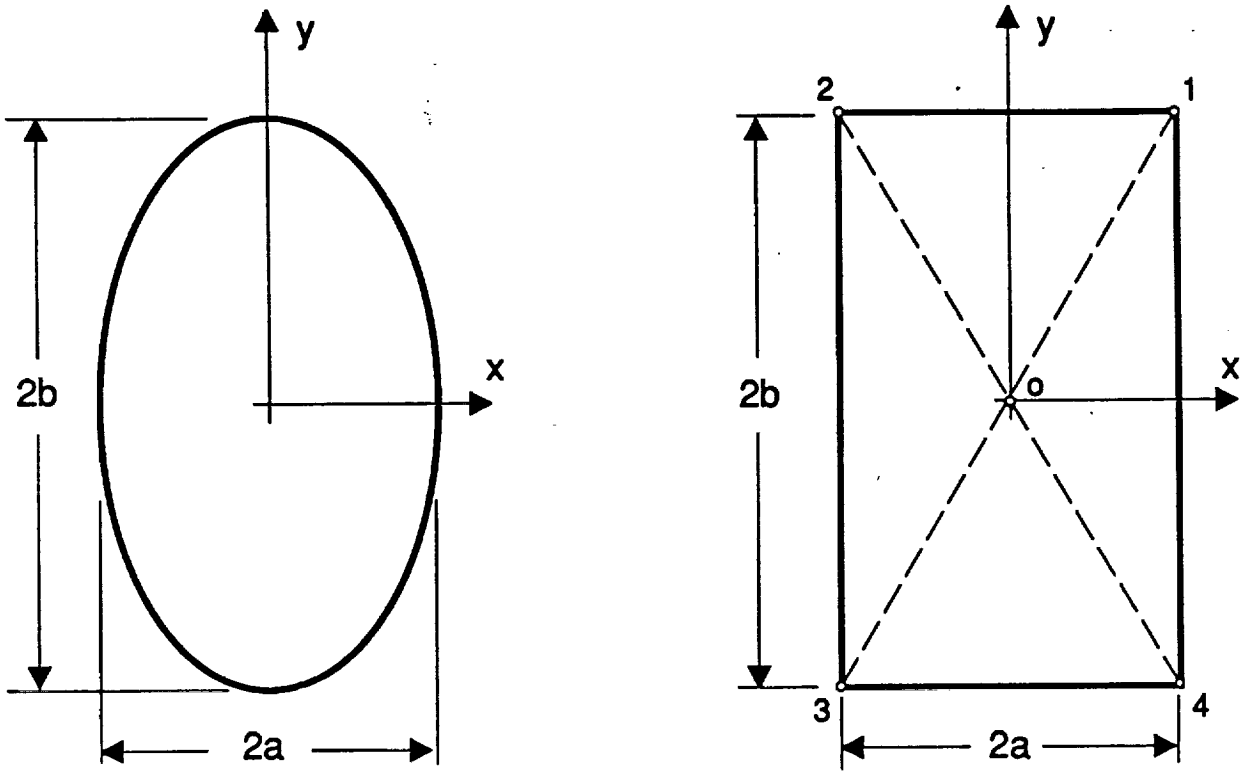

3.) Elliptical and rectangular cross-sections with aspect ratio (b/a). The rectangular cross-section reveals the four triangular subregions.

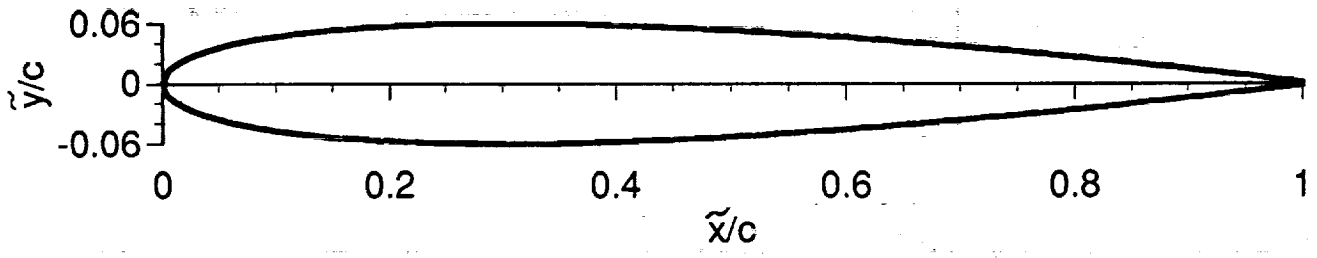

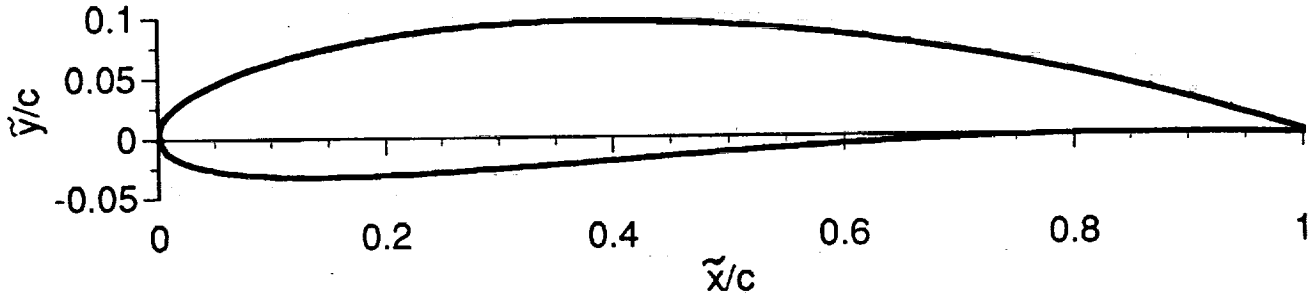

4.) (a) NACA-0012 airfoil, and (b) NACA-4512 airfoil.

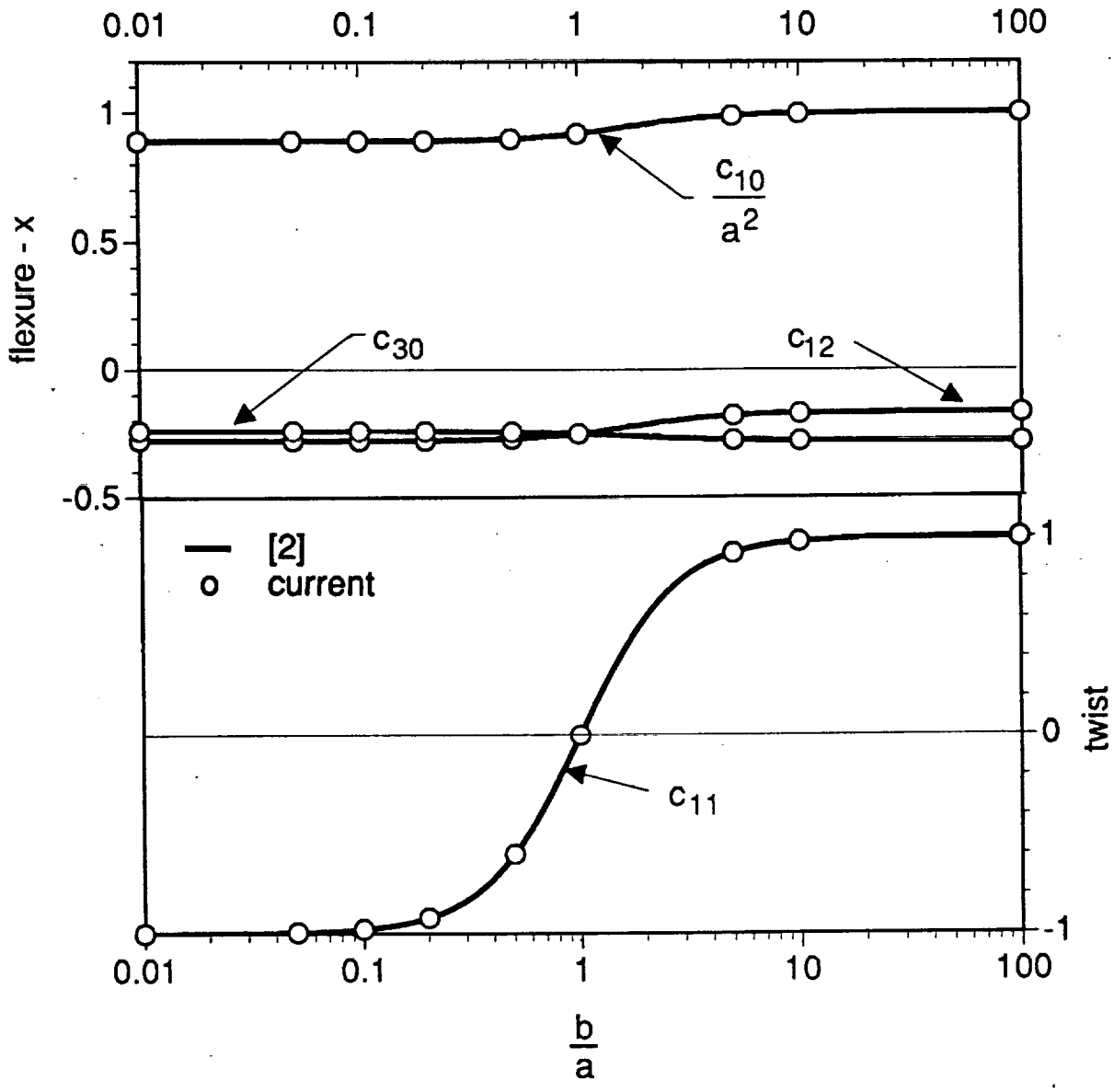

5.) Comparison of calculated flexure and twist power series coefficients with the exact results of [2] for an elliptical cross-section.

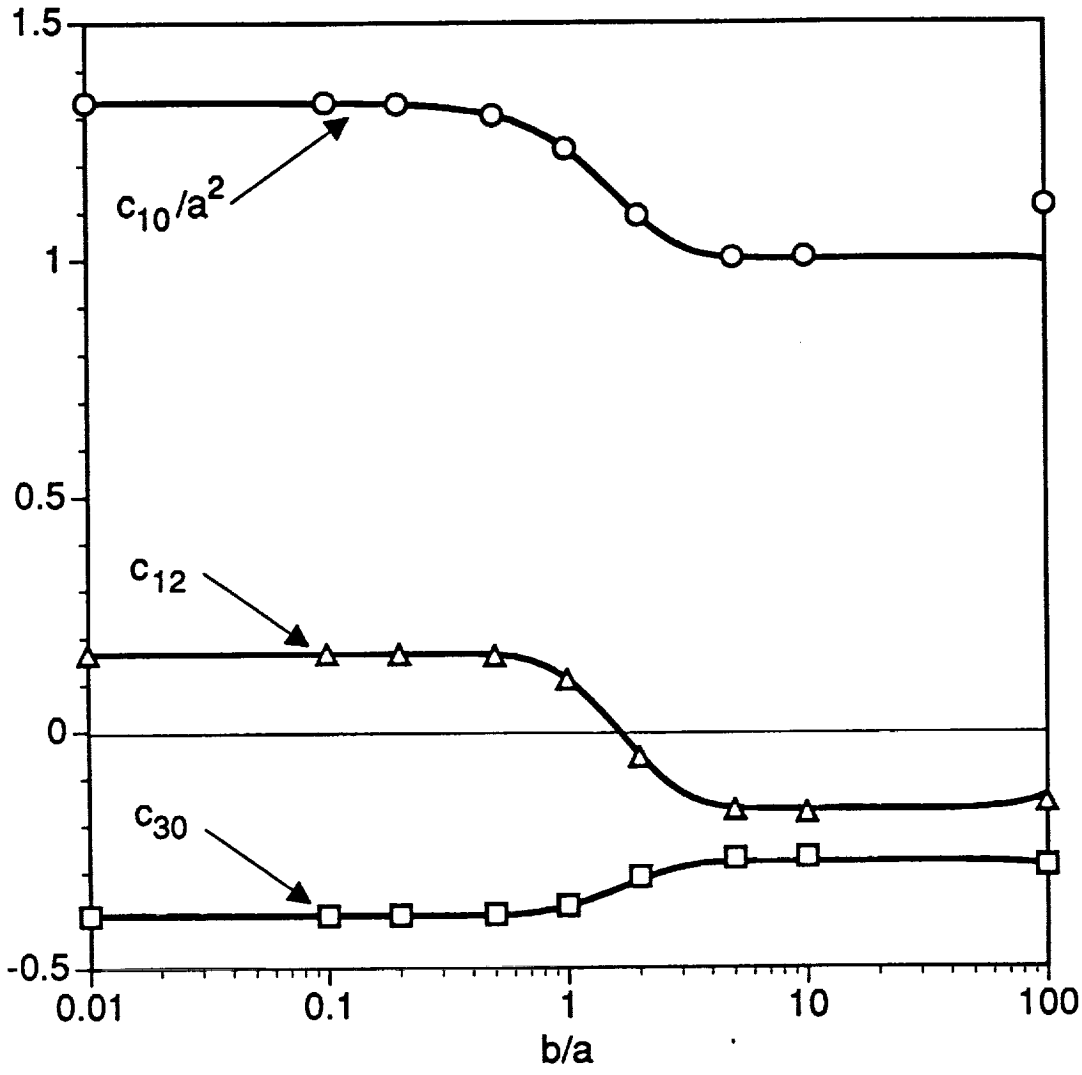

6.) Comparison of the first-three nonzero calculated flexure power series coefficients with the Taylor series expansion of the results from [2] (—) for a rectangular cross-section.

Chapter 3: A Power Series Approach for Generally Anisotropic Beams Arbitrary Cross-Sections

Abstract

The behavior of a tip-loaded anisotropic cantilever beam with an arbitrary cross-section is studied using Saint-Venant's semi-inverse method along with a power series solution for the local in-plane and out-of-plane deformation warping functions. The power series coefficients are determined by solving a set of variationally derived linear algebraic equations. Using the resulting three-dimensional displacement solutions, the shear deformation associated with applied tip loads is investigated as well as the shear center location. Both of the extended definitions reveal the linear dependency of the shear center location with beam-length. Numerical results are presented for three different cross-sections (ellipse, triangle, NACA-0012 airfoil) and two different materials (Al 6061-T6, off-angle high-strength graphite/epoxy fibers).

Introduction

Closed-form solutions for Saint-Venant's problems (tip-loaded cantilever beam) exist for only a few simple isotropic homogeneous cross-section shapes (ellipse, rectangle, equilateral triangle) (Sokolnikoff, 1956) and one anisotropic homogeneous cross-section (ellipse) (Ie and Kosmatka, 1992). For general cross-section shapes, the local deformation functions of the cross-section cannot be determined exactly and thus approximate techniques must be used. One proven approach for approximately determining these local deformations in isotropic cross-sections (Herrmann, 1965; Mason and Herrmann, 1968) and anisotropic cross-sections (Kosmatka and Dong (1991)) involves the application of the finite element method. In this approach, the general anisotropic cross-section is discretized into triangular and/or quadrilateral subregions (elements) with in-plane and out-of-plane nodal variables that represent the local in-plane deformations and out-of-plane warping. But the finite element method requires a large number of elements for complex cross-sections, which will lead to a large set of linear algebraic equations (thousands of unknowns). Moreover, the calculated array of nodal deformations provides little insight into the deformation and warping distribution over the cross-section and thus one must resort to graphical finite element post-processing techniques to understand this distribution. An alternative approach, which has been used by Mindlin (1975) for the solution of Saint-Venant's isotropic torsion problem and by Kosmatka (1992) for the isotropic flexure problem, involves assuming a double power series for the each of the local in-plane deformations

and the out-of-plane warping. The power series coefficients are determined by solving a set of linear algebraic equations, where the number of equations is equal to the number of unknown coefficients. Thus, the problem size is independent of the cross-section complexity, and only dependent on the number of terms in the power series.

The objective of this paper is to develop a method for studying the behavior of tip-loaded anisotropic beams with general cross-sections using Saint-Venant's semi-inverse method, where the local deformations of the cross-section are expressed as a double power series in terms of the cross-section coordinates. The coefficients associated with the power series terms are determined by solving a set of variationally derived linear algebraic equations, where the number of equations is equal to the number of unknown coefficients. For complex cross-sections, the calculated coefficients represent a "best-fit approximation" to the exact warping function which may be an infinite series of transcendental functions. To aid in the evaluation of the power series weighted area integrals, the cross-section is discretized into a series of triangular subregions, where the integration in each subregion is evaluated exactly using Guassian Qaudrature formulas for triangles (Dunavant, 1985). The triangle aspect ratio is not critical, as opposed to the finite element method, since the power series is a global cross-section function and not a local element function.

Numerical results are presented for three different cross-sections (ellipse, triangle, NACA-0012) and two different materials (Al 6061-T6, off-angle high-strength graphite/epoxy fibers) to first validate the approach, second prove convergence of warping related cross-section parameters (torsion constant, shear center location, shear deformation), third present important behavioral data not currently found in the literature and fourth investigate the sensitivity of the shear center location with cross-section shape, beam length, and material definition.

Theoretical Background

We begin by considering a cantilevered prismatic beam of length L with an arbitrary cross-section of area A composed of a homogeneous, rectilinearly anisotropic material. A rectangular Cartesian coordinate system (x,y,z) with corresponding displacements (u,v,w) is established with the origin at the centroid of the root end and the (x,y) axes coincide with the cross-section principal axes. See Fig. 1. The constitutive relations for the material are given by:

$$\{\sigma\} = [C]\{\varepsilon\},$$
$$\{\varepsilon\} = [S]\{\sigma\}, \qquad (1.a\text{-}c)$$
$$[C] = [S]^{-1},$$

where $[C]$ and $[S]$ are fully populated symmetric matrices with 21 distinct elements and the stress and strain arrays are given as:

$$\{\sigma\} = \{\sigma_{xx}, \sigma_{yy}, \sigma_{zz}, \tau_{yz}, \tau_{xz}, \tau_{xy}\},$$
$$\{\varepsilon\} = \{\varepsilon_{xx}, \varepsilon_{yy}, \varepsilon_{zz}, \gamma_{yz}, \gamma_{xz}, \gamma_{xy}\}. \qquad (1.d,e)$$

At the root end, the beam is fully fixed. Within the framework of the Saint-Venant problems, this condition cannot be described on a point-wise basis and the equivalent statement at the centroid (x=y=z=0) can be used:

$$u = v = w = 0,$$
$$\frac{\partial u}{\partial z} = \frac{\partial v}{\partial z} = \frac{\partial v}{\partial x} - \frac{\partial u}{\partial y} = 0. \qquad (2.a\text{-}f)$$

At the free end, tractions are applied which reduce to an equivalent force P and moment M with respect to the cross-section centroid. The force P and moment M can be decomposed into flexure components; P_x and P_y, an extensional component; P_z, bending moments; M_x and M_y, and a torsion moment; M_z. As a result of the applied tip loads, five of the stresses are independent of z and the sixth stress (σ_{zz}) has flexure components which vary linearly with z

$$\sigma_{zz} = \left\{\frac{P_x}{I_{yy}}x + \frac{P_y}{I_{xx}}y\right\}z + \sigma^o_{zz}(x,y) \qquad (3)$$

where I_{xx} and I_{yy} are the area moments of inertia about the x and y axes, respectively, and σ^o_{zz} is associated with extension, bending, and torsion. Introducing these assumptions into the stress equilibrium equations and integrating yields the following displacement and strain components (see Kosmatka, 1986; Kosmatka and Dong, 1991; for further details):

$$u = -\frac{P_x}{2EI_{yy}}\left\{\frac{z^2}{3}(z-3L)-\frac{\nu_4}{2}yz(z-2L)+\left\{\nu_1x^2-\nu_2y^2\right\}(z-L)\right\}+\frac{1}{2EI_{yy}}\left\{M_y+\frac{\nu_4}{2}M_z\right\}z^2-\theta yz$$

$$-\frac{P_y}{2EI_{xx}}\left\{\{2\nu_1x+\nu_6y\}y(z-L)+\frac{\nu_5}{2}yz(z-2L)\right\}+\psi_x(x,y) \qquad (4.a)$$

$$v = -\frac{P_y}{2EI_{xx}}\left\{\frac{z^2}{3}(z-3L)-\frac{\nu_5}{2}xz(z-2L)+\left\{\nu_2y^2-\nu_1x^2\right\}(z-L)\right\}-\frac{1}{2EI_{xx}}\left\{M_x+\frac{\nu_5}{2}M_z\right\}z^2+\theta xz$$

$$-\frac{P_x}{2EI_{yy}}\left\{\{\nu_6x+2\nu_2y\}x(z-L)+\frac{\nu_4}{2}xz(z-2L)\right\}+\psi_y(x,y) \qquad (4.b)$$

$$w = -\frac{P_x}{2EI_{yy}}\left\{\{\nu_5x+\nu_4y\}x(z-L)-xz(z-2L)\right\}-\frac{1}{EI_{yy}}\left\{M_y+\frac{\nu_4}{2}M_z\right\}xz+\frac{1}{EI_{xx}}\left\{M_x+\frac{\nu_5}{2}M_z\right\}yz$$

$$-\frac{P_y}{2EI_{xx}}\left\{\{\nu_5x+\nu_4y\}y(z-L)-yz(z-2L)\right\}-\frac{1}{EA}\left\{\frac{\nu_5}{2}P_x+\frac{\nu_4}{2}P_y-P_z\right\}z+\psi_z(x,y) \qquad (4.c)$$

and

$$\varepsilon_{xx} = -\frac{P_x\nu_1}{EI_{yy}}x(z-L)-\frac{P_y\nu_1}{EI_{xx}}y(z-L)+\frac{\partial\psi_x}{\partial x} \qquad (4.d)$$

$$\varepsilon_{yy} = -\frac{P_x\nu_2}{EI_{yy}}x(z-L)-\frac{P_y\nu_2}{EI_{xx}}y(z-L)+\frac{\partial\psi_y}{\partial y} \qquad (4.e)$$

$$\varepsilon_{zz} = -\frac{P_x}{2EI_{yy}}\{\nu_5x+\nu_4y+2(L-z)\}x-\frac{P_y}{2EI_{xx}}\{\nu_5x+\nu_4y+2(L-z)\}y$$

$$+\frac{1}{EI_{xx}}\left\{M_x+\frac{\nu_5}{2}M_z\right\}y-\frac{1}{EI_{yy}}\left\{M_y+\frac{\nu_4}{2}M_z\right\}x-\frac{1}{2EA}\{\nu_5P_x+\nu_4P_y-2P_z\} \qquad (4.f)$$

$$\gamma_{yz} = -\frac{P_x}{EI_{yy}}\left\{\frac{\nu_6}{2}x+\nu_2y+\nu_4(z-L)\right\}x+\frac{P_y}{2EI_{xx}}\left\{\nu_1x^2-\nu_2y^2-2\nu_4y(z-L)\right\}+\theta x+\frac{\partial\psi_z}{\partial y} \qquad (4.g)$$

$$\gamma_{xz} = -\frac{P_y}{EI_{xx}}\left\{\nu_1x+\frac{\nu_6}{2}y+\nu_5(z-L)\right\}y-\frac{P_x}{2EI_{yy}}\left\{\nu_1x^2-\nu_2y^2+2\nu_5x(z-L)\right\}-\theta y+\frac{\partial\psi_z}{\partial x} \qquad (4.h)$$

$$\gamma_{xy} = -\frac{P_x \nu_6}{E I_{yy}} x(z-L) - \frac{P_y \nu_6}{E I_{xx}} y(z-L) + \frac{\partial \psi_x}{\partial y} + \frac{\partial \psi_y}{\partial x} \tag{4.i}$$

where, A is the cross-section area, θ is the twist rate of the beam about the centroidal axis (z), E ($= 1/S_{33}$) is commonly called Young's modulus, and ν_i are cross-coupling coefficients defined as:

$$\nu_i = -\frac{S_{i3}}{S_{33}} . \tag{4.j}$$

Here ν_1 and ν_2, are the usual Poisson coefficients, and ν_4, ν_5, and ν_6, express the three-dimensional extension-shear coupling that can occur in a completely anisotropic body. The remaining functions (ψ_x, ψ_y, ψ_z) represent local cross-section (x,y) dependent deformations and are unique for each cross-section shape and material configuration, and are linearly proportional to the six applied loads and twist rate (see Kosmatka and Dong, 1991)

$$(\psi_x, \psi_y, \psi_z) = \sum_{i=1}^{7} \left(\psi_{x(i)}, \psi_{y(i)}, \psi_{z(i)}\right) Q_i , \tag{4.k}$$

where Q_i are the components of

$$\{Q\}^T = \{P_x, P_y, P_z, M_x, M_y, M_z, \theta\} . \tag{4.l}$$

In the current development, the "unit" local cross-section deformations ($\psi_{x(i)}$, $\psi_{y(i)}$, $\psi_{z(i)}$) are assumed to have the form of a power series:

$$\psi_{x(i)} = \sum_{m=0}^{\infty} \sum_{n=0}^{\infty} a_{mn(i)} x^m y^n ,$$

$$\psi_{y(i)} = \sum_{m=0}^{\infty} \sum_{n=0}^{\infty} b_{mn(i)} x^m y^n , \tag{5.a-c}$$

$$\psi_{z(i)} = \sum_{m=0}^{\infty} \sum_{n=0}^{\infty} c_{mn(i)} x^m y^n ,$$

where ($a_{mn(i)}, b_{mn(i)}, c_{mn(i)}$) are unknown coefficients that depend upon the cross-section shape, material properties, and load-type (Q_i), and the subscripts (m) and (n) correspond to the order of (x) and (y), respectively. The four rigid body motions of the cross-section (three translations, rotation about the z-axis) for each of the seven cases are constrained by setting ($a_{00} = b_{00} = c_{00} = 0$) and requiring that ($a_{01} = b_{10}$). Assuming that the series is finite, Eqns (4.*k*) and (5.*a-c*) are combined to form:

$$\{\psi\} = [H][\Psi]\{Q\} , \tag{6.a}$$

where

$$\{\psi\}^T = \{ \psi_x , \ \psi_y , \ \psi_z \} , \tag{6.b,c}$$

$$[H] = \begin{bmatrix} [N(x,y)] & 0 & 0 \\ 0 & [N(x,y)] & 0 \\ 0 & 0 & [N(x,y)] \end{bmatrix} ,$$

and [Ψ] is comprised of seven columns of unknown coefficients that have the form:

$$\{\Psi_{(i)}\}^T = \left\{ \{a_{(i)}\}^T , \{b_{(i)}\}^T , \{c_{(i)}\}^T , \right\} , \quad i = 1\text{-}7 . \tag{6.d}$$

For example, if a cubic polynomial was selected, then based upon Pascal's triangle, [$N(x,y)$] has 10 terms:

$$[N(x,y)] = \left\{ 1 , \quad x , \quad y , \quad x^2 , \quad xy , \quad y^2 , \quad x^3 , \quad x^2y , \quad xy^2 , \quad y^3 \right\} , \tag{7.a}$$

and $\{a_{(i)}\}$, $\{b_{(i)}\}$ and $\{c_{(i)}\}$ for the i^{th} column of [Ψ] has the form:

$$\{a_{(i)}\}^T = \{ a_{00(i)} , a_{10(i)} , a_{01(i)} , a_{20(i)} , a_{11(i)} , a_{02(i)} , a_{30(i)} , a_{21(i)} , a_{12(i)} , a_{03(i)} \} ,$$

$$\{b_{(i)}\}^T = \{ b_{00(i)} , b_{10(i)} , b_{01(i)} , b_{20(i)} , b_{11(i)} , b_{02(i)} , b_{30(i)} , b_{21(i)} , b_{12(i)} , b_{03(i)} \} , \tag{7.b-d}$$

$$\{c_{(i)}\}^T = \{ c_{00(i)} , c_{10(i)} , c_{01(i)} , c_{20(i)} , c_{11(i)} , c_{02(i)} , c_{30(i)} , c_{21(i)} , c_{12(i)} , c_{03(i)} \} ,$$

and the aforementioned three rigid body translations and one rigid body rotation are constrained using standard finite procedures after the cross-section model is fully assembled.

The strain array $\{\varepsilon\}$ of Eq. (1.*e*) can be obtained in terms of the matrix of unknown coefficients $[\Psi]$, the applied forces and moments, and the centroidal twist rate by substituting Eq. (6.*a*) into Eqns. (4.*d-i*):

$$\{\varepsilon\} = \left\{ [B][\Psi] + [\overline{F_C}] \right\} \{Q\}, \tag{8.a}$$

where

$$[B]^T = \begin{bmatrix} \frac{\partial[N(x,y)]}{\partial x} & 0 & 0 & 0 & 0 & \frac{\partial[N(x,y)]}{\partial y} \\ 0 & \frac{\partial[N(x,y)]}{\partial y} & 0 & 0 & 0 & \frac{\partial[N(x,y)]}{\partial x} \\ 0 & 0 & 0 & \frac{\partial[N(x,y)]}{\partial y} & \frac{\partial[N(x,y)]}{\partial x} & 0 \end{bmatrix} \tag{8.b}$$

and $[\overline{F_C}]$ is defined in the Appendix.

The magnitude of the unknown coefficients in $[\Psi]$ can be determined by applying the principle of minimum potential energy:

$$\delta\Pi = \delta U - \delta W_e = 0 \tag{9.a}$$

where δU is the variation of the strain energy;

$$\delta U = \int_0^L \int_A \{\delta\varepsilon\}^T [C] \{\varepsilon\} \, dA \, dz, \tag{9.b}$$

and δW_e is the variation of the work of external forces that results from the applied tractions on the beam ends;

$$\delta W_e = \int_A \{\tau_{xz}\delta\psi_x + \tau_{yz}\delta\psi_y + \sigma_{zz}\delta\psi_z\}|_{(z=L)} dA - \int_A \{\tau_{xz}\delta\psi_x + \tau_{yz}\delta\psi_y + \sigma_{zz}\delta\psi_z\}_{(z=0)} dA$$

(9.*c*)

which reduces to (Kosmatka and Dong, 1991):

$$\delta W_e = \frac{P_x L}{I_{yy}} \int_A x\, \delta\psi_z dA + \frac{P_y L}{I_{xx}} \int_A y\, \delta\psi_z dA . \tag{9.d}$$

A set of linear algebraic equations for determining the seven "unit" unknown deformation coefficients is obtained by substituting (8.*a*), (9.*b*), and (9.*d*) into (9.*a*), integrating over the beam volume, and taking the variation with respect to the unknown coefficients:

$$[K][\Psi] = \left[[F_W] - [F_C] \right], \tag{10.a}$$

where

$$[K] = L \int_A [B]^T [C][B]\, dA \tag{10.b}$$

$$[F_W] = L \begin{bmatrix} 0 & 0 & 0 & 0 & 0 & 0 & 0 \\ 0 & 0 & 0 & 0 & 0 & 0 & 0 \\ \frac{1}{I_{yy}} \int_A x[N(x,y)]\, dA & \frac{1}{I_{xx}} \int_A y[N(x,y)]\, dA & 0 & 0 & 0 & 0 & 0 \end{bmatrix} \tag{10.c}$$

and

$$[F_C] = L \int_A [B]^T [C] \left[\overline{\overline{F_c}} \right] dA . \tag{10.d}$$

with $[\overline{\overline{F_c}}]$ also being defined in the Appendix. The final form of the local cross-section deformations (Eq. (4.*k*)) are determined by solving (Eq. (10.*a*)) for $[\Psi]$ and substituting the results into Eq. (6.*a*). Similarly, the stress components (Eq. (1.*d*)) can be written in terms of $\{Q\}$, using Eqns. (1.*a*) and (8.*a*), as;

$$\{\sigma\} = [\overline{\sigma}]\{Q\}, \tag{12.a}$$

where

$$\left[\overline{\sigma}\right] = \left[C\right]\left[\left[B\right]\left[\Psi\right] + \left[\overline{FC}\right]\right] . \qquad (12.b)$$

The centroidal twist rate θ (Q_7) can now be determined in terms of the three applied forces and moments by substituting the fourth (τ_{yz}) and fifth (τ_{xz}) rows of Eq. (12.*a*) into the cross-section torsion moment equilibrium equation

$$M_z = \int_A x\,\tau_{yz} - y\,\tau_{xz}\,dA \ , \qquad (13.a)$$

integrating, and rearranging to get:

$$\theta = a_1 P_x + a_2 P_y + a_3 P_z + a_4 M_x + a_5 M_y + a_6 M_z , \qquad (13.b)$$

where

$$a_k = -\frac{\overline{a_k}}{\overline{a_7}} , \qquad (k = 1\text{-}5) \qquad (13.c)$$

$$a_6 = \frac{1 - \overline{a_6}}{\overline{a_7}} , \qquad (13.d)$$

and

$$\overline{a_k} = \int_A \left\{x\left(\overline{\sigma}_{4k}\right) - y\left(\overline{\sigma}_{5k}\right)\right\} dA \ , \qquad (k = 1,7) \ . \qquad (13.e)$$

The (i) and (j) subscripts of σ_{ij} in Eq. (13.*e*) correspond to the row and column position in $[\sigma]$ (Eq. (12.*b*)). The coefficients a_1-a_6 are all independent of the beam-length because from the original assumptions, the shear stress distribution is only a function of the cross-section coordinates (x) and (y). Moreover, the torsion stiffness is commonly defined as: $GJ = 1/a_6$ (see Kosmatka and Dong, 1991).

Lastly, the local deformations, the strain array, and the stress array can be expressed in terms of only the three applied forces and moments by combining Eq. (13.*b*) with Eqns. (6.*a*), (8.*a*), (11) and (12.*a*):

$$\begin{Bmatrix} \psi_x \\ \psi_y \\ \psi_z \end{Bmatrix} = [H][\Psi][T]\{Q^*\}, \tag{14.a}$$

$$\{\varepsilon\} = \left[[B][\Psi] + [\overline{FC}]\right][T]\{Q^*\}, \tag{14.b}$$

$$\{\sigma\} = [C]\left[[B][\Psi] + [\overline{FC}]\right][T]\{Q^*\}, \tag{14.c}$$

where

$$[T] = \begin{bmatrix} 1 & 0 & 0 & 0 & 0 & 0 \\ 0 & 1 & 0 & 0 & 0 & 0 \\ 0 & 0 & 1 & 0 & 0 & 0 \\ 0 & 0 & 0 & 1 & 0 & 0 \\ 0 & 0 & 0 & 0 & 1 & 0 \\ 0 & 0 & 0 & 0 & 0 & 1 \\ a_1 & a_2 & a_3 & a_4 & a_5 & a_6 \end{bmatrix}, \tag{14.d}$$

and

$$\{Q^*\}^T = \{P_x, P_y, P_z, M_x, M_y, M_z\}. \tag{14.e}$$

Behavior of an Anisotropic Beam

The general behavior of a cantilever anisotropic beam having an arbitrary cross section can now be studied using the displacement (4.*a-c*) and stress distributions (14.*b*) along with the calculated twist rate (13.*b*) and the cross-section deformations (14.*a*). In a previous paper, (Kosmatka and Dong, 1991), a detailed discussion was presented covering the extension, bending, torsion, and flexure behavior of anisotropic cantilever prismatic beams based upon Saint-Venant solutions. In the current paper, we will focus our discussions on two topics: shear deformation and further issues concerning the shear center location.

Shear Deformation

An examination of the transverse displacements (u,v), from Eqns. (4.*a,b*), reveals that applying either a bending moment (M_x,M_y) or a flexure force (P_x,P_y) will produce centroidal tip components (x=y=0, z=L) that agree with the standard (isotropic) strength of material solutions

$$u(x=y=0, z=L) = \frac{P_x L^3}{3 EI_{yy}} + \frac{M_y L^2}{2 EI_{yy}}, \qquad v(x=y=0, z=L) = \frac{P_y L^3}{3 EI_{xx}} - \frac{M_x L^2}{2 EI_{xx}}, \qquad (15.a,b)$$

and applying an extension force (P_z) will produce only an axial component (w). But the transverse components associated with shear deformation are not included in Eqns. (4.*a-c*) because the fixed root boundary was defined by setting the deformed centroidal axis slope to zero ($\partial u/\partial z = \partial v/\partial z = 0$). These additional transverse components can be included by simply rotating the deformed beam so that the slope of the deformed cross-section at the centroid ($x=y=0$) is coincident with the x-y plane, and thus the deformed centroidal axis will have a nonzero slope at the origin. These rotation angles are equal to the shear strains (γ_{xz}, γ_{yz}) at the centroid of the beam root and can be found evaluating the 4th and 5th equations of Eq. (14.*b*) at ($x=y=z=0$). For example the rotation angle, about the y-axis, associated with shear deformation in the x-z plane is equal (from Eqns. (4.*h*), (5.*c*), and (14.*a*)) to:

$$\gamma_{xz_{(o)}} = \gamma_{xz}\Big|_{x=y=0} = \frac{\partial \psi_z}{\partial x}\Big|_{x=y=0} = \sum_{i=1}^{6} \left(c_{10\,(i)} + a_i\, c_{10\,(7)} \right) Q_i^* \,. \qquad (16)$$

Similarly the rotation angle, about the -x-axis, associated with shear deformation in the y-z plane is equal to:

$$\gamma_{yz_{(o)}} = \frac{\partial \psi_z}{\partial y}\Big|_{x=y=0} = \sum_{i=1}^{6} \left(c_{01\,(i)} + a_i\, c_{01\,(7)} \right) Q_i^* \,. \qquad (17)$$

The final form of the displacement components including shear deformation are

$$u = -\frac{P_x}{2EI_{yy}}\left\{\frac{z^2}{3}(z-3L) - \frac{\nu_4}{2} yz(z-2L) + \left\{\nu_1 x^2 - \nu_2 y^2\right\}(z-L)\right\} + \frac{1}{2EI_{yy}}\left\{M_y + \frac{\nu_4}{2} M_z\right\} z^2 - \theta yz$$

$$-\frac{P_y}{2EI_{xx}}\left\{\left\{2\nu_1 x + \nu_6 y\right\} y(z-L) + \frac{\nu_5}{2} yz(z-2L)\right\} + \gamma_{xz_{(o)}} z + \psi_x(x,y) \qquad (18.a)$$

$$v = -\frac{P_y}{2EI_{xx}}\left\{\frac{z^2}{3}(z-3L) - \frac{\nu_5}{2}xz(z-2L) + \left\{\nu_2 y^2 - \nu_1 x^2\right\}(z-L)\right\} - \frac{1}{2EI_{xx}}\left\{M_x + \frac{\nu_5}{2}M_z\right\}z^2 + \theta xz$$

$$-\frac{P_x}{2EI_{yy}}\left\{\left\{\nu_6 x + 2\nu_2 y\right\}x(z-L) + \frac{\nu_4}{2}xz(z-2L)\right\} + \gamma_{yz_{(o)}}z + \psi_y(x,y) \qquad (18.b)$$

$$w = -\frac{P_x}{2EI_{yy}}\left\{\left\{\nu_5 x + \nu_4 y\right\}x(z-L) - xz(z-2L)\right\} - \frac{1}{EI_{yy}}\left\{M_y + \frac{\nu_4}{2}M_z\right\}xz + \frac{1}{EI_{xx}}\left\{M_x + \frac{\nu_5}{2}M_z\right\}yz$$

$$-\frac{P_y}{2EI_{xx}}\left\{\left\{\nu_5 x + \nu_4 y\right\}y(z-L) - yz(z-2L)\right\} - \frac{1}{EA}\left\{\frac{\nu_5}{2}P_x + \frac{\nu_4}{2}P_y - P_z\right\}z$$

$$-\gamma_{xz_{(o)}}x - \gamma_{yz_{(o)}}y + \psi_z(x,y) \qquad (18.c)$$

where θ, ψ_x, ψ_y, ψ_z, $\gamma_{xz_{(o)}}$, and $\gamma_{yz_{(o)}}$ are defined in Eqns. (13.*b*), (14.*a*), (16), and (17), respectively.

Shear Center Location, Line of Shear Centers

For prismatic cantilever beams that exhibit less than generally anisotropic behavior ($\nu_4, \nu_5 = 0$), the shear center is a property of the cross-section and independent of beam-length (line of shear centers is parallel to the centroidal axis). For this class of materials, a classic definition has been presented for locating the shear center (Griffith and Taylor, 1917) as '*the load point that produces a zero mean value cross-section twist rate (i.e., zero twist rate about the centroidal axis)*'. Attempting to extend this definition to a beam composed of a generally anisotropic material ($\nu_4, \nu_5 \neq 0$) leads to a shear center location that is a function of the cross-section shape, material definition, and is linearly dependent upon beam-length (Kosmatka and Dong, 1991). Thus, the line of shear centers for a generally anisotropic beam is straight, but it is not parallel to the centroidal axis.

We can study this phenomena by calculating the micromolar twist rate for a particle in the beam:

$$\frac{\partial \omega_z}{\partial z} = \frac{1}{2}\left(\frac{\partial \gamma_{yz}}{\partial x} - \frac{\partial \gamma_{xz}}{\partial y}\right) = \theta - \frac{P_x}{2EI_{yy}}\left\{\nu_6 x + 2\nu_2 y + \nu_4(z-L)\right\} + \frac{P_y}{2EI_{xx}}\left\{2\nu_1 x + \nu_6 y + \nu_5(z-L)\right\} \qquad (19)$$

where the (z) dependent terms are associated with anisotropic 'bend-twist' coupling as a result of applied flexure. The micromolar twist rate about the centroidal axis (x=y=0), to be consistent with the work of (Griffith and Taylor, 1917), is:

$$\frac{\partial \omega_z}{\partial z} = \theta - \frac{P_x v_4}{2EI_{yy}}(z - L) + \frac{P_y v_5}{2EI_{xx}}(z - L) . \tag{20}$$

Next, we apply a general tip flexural force (P_{xs}, P_{ys}) through the unknown shear center location (x_s,y_s), where the equivalent centroidal forces and moments are defined as

$$P_x = P_{xs} , \qquad P_y = P_{ys} , \qquad M_z = P_{ys}\, x_s - P_{xs}\, y_s . \tag{21.a-c}$$

Substituting Eqns. (21.*a-c*) and (13.*b*) into Eq. (20) results in

$$\frac{\partial \omega_z}{\partial z} = P_{xs}\left(a_1 - a_6 y_s - \frac{v_4}{2EI_{yy}}(z - L)\right) + P_{ys}\left(a_2 + a_6 x_s + \frac{v_5}{2EI_{xx}}(z - L)\right) . \tag{22}$$

Since the micromolar twist rate ($\partial\omega_z/\partial z$) varies linearly with ($z$) for a generally anisotropic beam, it is not possible to locate the shear center so that the twist rate about the centroidal axis is zero independent of beam axial position. Thus the Griffith and Taylor definition can not be implemented if ($v_4, v_5 \neq 0$). Instead, we recognize that since the twist rate varies linearly with (z), then the micromolar twist (ω_z) will vary quadratically with (z). Thus, the best that can be achieved is to "locate the shear center (x_s,y_s) so that there is zero micromolar twist at the beam root (z=0) and zero twist in the cross-section plane that contains the applied load (for a tip load, z=L)". This is accomplished by requiring that

$$\int_0^L \frac{\partial \omega_z}{\partial z}\, dz = 0 . \tag{23}$$

Substituting Eq. (22) into Eq. (23), carrying out the integration, and solving, produces the shear center location for the beam tip cross-section (z=L) that is independent of the magnitude of the applied loads:

$$x_s(z=L) = x_{sL} = -\frac{1}{a_6}\left(a_2 - \frac{v_5 L}{4EI_{xx}}\right) , \quad y_s(z=L) = y_{sL} = \frac{1}{a_6}\left(a_1 + \frac{v_4 L}{4EI_{yy}}\right) . \tag{24.a,b}$$

The shear center location at the root of a generally anisotropic beam (or a very short anisotropic beam ($L \approx 0$)) is equal to the classic Griffith/Taylor definition for an isotropic cross-section ($x_{so} = -a_2/a_6$, $y_{so} = a_1/a_6$). The shear center location in the beam-tip cross-section (Eq. (24.*a,b*)) is composed of two terms; one which is independent of the beam-length (i.e. the classic Griffith/Taylor definition) and one which is linearly proportional to the beam-length, the material properties (v_4, v_5), and the ratio of the torsion stiffness to the bending stiffness ($1/(a_6 EI_{xx})$, $1/(a_6 EI_{yy})$). This development and discussion is consistent with the shear center location proposed by Ie and Kosmatka (1992) for a generally anisotropic beam with an elliptical cross-section.

An alternate shear center definition has been proposed by Reissner (1989, 1991) using thin-plate theory so that "*the application of an applied flexure force will produce zero twist about the calculated line of shear centers*" and thus insure that the shear center is coincident with the center of twist. Recently, Kosmatka (1992) applied this definition to Saint-Venant's flexure and torsion problems and developed a linear relationship for calculating this new shear center location in an isotropic beam with an arbitrary cross-section:

$$x_s^* = -\frac{a_2}{a_6 + \dfrac{v}{EI_{xx}}} \quad , \qquad y_s^* = \frac{a_1}{a_6 + \dfrac{v}{EI_{yy}}} \quad , \tag{25.a,b}$$

where the difference between this definition and the classic Griffith/Taylor definition for an isotropic cross-section is an additional term in the denominator.

Now to apply this definition to a generally anisotropic beam with an arbitrary cross-section, we again apply a general flexure force (P_{xs}, P_{ys}) through an unknown shear center location (x_{sL}^*, y_{sL}^*) in the tip ($z=L$) cross-section, where the equivalent centroidal forces and moments are given in Eq. (21.*a-c*) and the micromolar twist rate about the unknown shear center location is determined by substituting Eqns. (21.*a-c*) and (13.*b*) into Eq. (19):

$$\begin{aligned} \frac{\partial \omega_z}{\partial z} = {} & P_{xs}\left(a_1 - a_6 y_{sL}^* - \frac{1}{2EI_{yy}}\left(v_6 x_{sL}^* + 2v_2 y_{sL}^* + v_4 (z - L) \right) \right) \\ & + P_{ys}\left(a_2 + a_6 x_{sL}^* + \frac{1}{2EI_{xx}}\left(2v_1 x_{sL}^* + v_6 y_{sL}^* + v_5 (z - L) \right) \right) . \end{aligned} \tag{26}$$

Once again, the micromolar twist rate ($\partial\omega_z/\partial z$) varies linearly with ($z$), and thus the best that can be attained for an anisotropic beam is to locate the shear center so that the micromolar twist (ω_z) is zero at the beam root (z=0) and beam tip (load plane, z=L) and varies quadratically between the root and tip. Substituting Eq. (26) into Eq. (23) and carrying out the integration over the beam-length, results in two coupled linear algebraic equations that are used to solve for the new shear center location in the beam-tip cross-section:

$$\begin{bmatrix} a_6 + \dfrac{v_1}{EI_{xx}} & \dfrac{v_6}{2EI_{xx}} \\ \dfrac{v_6}{2EI_{yy}} & a_6 + \dfrac{v_2}{EI_{yy}} \end{bmatrix} \begin{Bmatrix} x^*_{sL} \\ y^*_{sL} \end{Bmatrix} = \begin{Bmatrix} -a_2 + \dfrac{v_5 L}{4EI_{xx}} \\ a_1 + \dfrac{v_4 L}{4EI_{yy}} \end{Bmatrix}. \qquad (27)$$

An examination of the above equation reveals that: (1.) this new shear center location for anisotropic beams will identically reduce to the results of Eq. (25) for isotropic materials (v_4,v_5,v_6=0), (2) the form of the length-dependency effects is identical to that of Eq. (24), which was developed by extending the Griffith/Taylor definition for anisotropy, and (3.) the presence of (v_6) introduces coupling between the (x) and (y) locations. The coupling associated with (v_6) is unique in that it is not present in the extension of the Griffith/Taylor definition (Eq. (24)) and furthermore, (v_6) type material coupling can not be included by studying plate-type theories, which make use of plane stress assumptions. Finally, the shear center location (x_{so}^*, y_{so}^*) in the beam root cross-section is determined by solving Eq. (27), where (L) is set to zero. An example of the two different '*line of shear centers*' definitions are presented in Fig. 2, where it is possible that the shear center in the tip cross-section plane can be well outside of the cross-section planform.

Computer Program

A computer program was written where, first, the boundary of a general cross-section is defined using (n) coordinate points with (n) straight line segments connecting the points. Second, the cross-section is discretized into (n) triangular subregions, where one edge of a triangle is a boundary line segment and the other two edges connect the end-points of a boundary line segment with the user-defined cross-section origin. Thus all of the subregions have one corner that is defined at the origin. Third, the cross-section centroid and principal axes are calculated and then the user-defined cross-section coordinates are transformed to the cross-section principal axes. Next, the area integrals (Eqns. 10.*b-d*) for each triangle subregion are evaluated using exact Gaussian

Quadrature formulas (Dunavant, 1985), where the cross-section power series polynomial can be user-defined. Fifth, the complete cross-section stiffness and force matrices are formed by simply adding together (not finite element type assembling) all of the triangular subregion matrices and the three rigid body translations and rigid body rotation are constrained. Sixth, the coefficients for each of the seven cases of $\{Q\}$ are determined. Seventh, the calculated coefficients along with the power series polynomial definition are used to determine the shear stress distribution, the constants (a_i (i=1-7)), the cross-section properties (shear center location, torsion constant, shear deformation, etc.), and transform the seven sets of calculated power series coefficients to six sets associated with the six applied loads. Finally, the calculated values are transformed from the principal axes back to the user defined coordinate system.

This approach strongly differs from our previous finite element based approach (Kosmatka and Dong, 1991) in that the global matrix size is defined by the assumed polynomial order and not the complexity of the cross-section. Moreover, cross-section cavities can be easily treated by simply subtracting off the triangular subregions that define the cavity. The aspect ratio of a triangle subregion is not critical, since the power series is a global cross-section function and not a local subregion function (i.e., finite element method).

Numerical Results

Prismatic cantilever beams with three different cross-section types are studied to validate the current approach (ellipse), prove convergence (triangles), and illustrate interesting beam behavior not found in the literature (triangle, NACA-0012 airfoil). See Fig. 3.*a-c*. Two different materials are considered including; an isotropic material (Al 6061-T6, E=69 *GPa*, ν=0.333) and a transversely isotropic material (unidirectional high-strength graphite/epoxy fibers, (Table 1)) with $G_{23} = E_{22}/(2(1+\nu_{23}))$. Generally orthotropic or anisotropic beam behavior is introduced by orienting the material reference frame (1,2,3) associated with the graphite/epoxy fibers relative to the beam coordinate frame (x,y,z) using (α) and (β), where the angles are defined in Fig. 4 and the resulting transformation between the two orthonormal coordinate systems is given as:

$$\begin{Bmatrix} 1 \\ 2 \\ 3 \end{Bmatrix} = \begin{bmatrix} \sin(\alpha)\cos(\beta) & \sin(\alpha)\sin(\beta) & \cos(\alpha) \\ \cos(\alpha)\cos(\beta) & \cos(\alpha)\sin(\beta) & -\sin(\alpha) \\ -\sin(\beta) & \cos(\beta) & 0 \end{bmatrix} \begin{Bmatrix} x \\ y \\ z \end{Bmatrix}. \qquad (28)$$

The resulting 21 distinct flexibility coefficients (S_{ij}) are determined using standard techniques (see Lekhnitskii, 1963) and are presented in detail in a recent paper (Ie and Kosmatka, 1992; Appendix *B*). Aligning the fiber axes with the beam coordinate axes with (α=β=0) will result in transversely isotropic beam behavior with ν_4=ν_5=ν_6=0. Rotating the material axes about the (y) axis (set β=0, and vary α), will produce orthotropic beam behavior with ($\nu_5 \neq 0$) and ν_4=ν_6=0. Similarly, rotating the material axes about the (x) axis (set β=90°, and vary α), will produce ($\nu_4 \neq 0$, ν_5=ν_6=0). Finally, rotating the material fibers in the cross-section (x-y) plane (set α=90°, and vary β) results in (ν_4=ν_5=0, $\nu_6 \neq 0$).

Elliptical Cross-Section

The current approach was initially verified by calculating the local cross-section deformations associated with applied flexure (P_y) for anisotropic cantilever beams with elliptical cross-sections having three different aspect ratios (b/a = 0.1, 1.0, 10.0), see Fig. 3.*a*, and comparing with the exact results presented by Ie and Kosmatka (1992). Anisotropic behavior was introduced by rotating the graphite/epoxy fibers in the x-z plane ($0° < \alpha < 90°$, β=0°) so that ν_1, ν_2, and ν_5 are nonzero. Each elliptical cross-section was discretized using 90 points along the perimeter (i.e. divide the cross-section into 90 triangular subregions) and the local deformations of the cross-section (ψ_x, ψ_y, ψ_z) were modeled using cubic polynomials (Eq. 7.*a-d*). Thus the resulting matrix equation of (Eq. 10.*a*) had 26 unknowns. The calculated power series coefficients were found to be comprised of only nine nonzero values that have the form

$$\psi_x = P_y\left(a_{01}y + a_{21}x^2y + a_{03}y^3\right),$$

$$\psi_y = P_y\left(b_{10}x + b_{12}xy^2 + b_{30}x^3\right), \qquad (29.a\text{-}c)$$

$$\psi_z = P_y\left(c_{01}y + c_{21}x^2y + c_{03}y^3\right),$$

where these nine coefficients are expressed from Eq. (14) as:

$$a_{mn} = \left(a_{mn(2)} + a_2\, a_{mn(7)} \right) ,$$

$$b_{mn} = \left(b_{mn(2)} + a_2\, b_{mn(7)} \right) , \qquad (29.d\text{-}f)$$

$$c_{mn} = \left(c_{mn(2)} + a_2\, c_{mn(7)} \right) ,$$

and the subscripts (2) and (7) are associated with the second and seventh column of $[\Psi]$. The remaining 17 coefficients were always identically equal to zero independent of aspect ratio and orientation angle. In Figs. 5-7, the variation of the nine nonzero local deformation coefficients are presented as a function of orientation angle (α) for the three aspect ratios, where the the exact solutions (Ie and Kosmatka, (1992)) are represented by solid lines and the current approach is represented with circles. From these figures it is clear that the current approach can reproduce the exact local deformation results over a broad range of aspect ratios and orientation angles. Using these local cross-section deformation functions, the torsion constant, shear deformation, and shear center location were calculated and also found to be in complete agreement with the exact solutions. Readers interested in further discussions involving the variation of cross-section warping, stress distribution, and section properties with fiber orientation angle and elliptical cross-section aspect ratio are referred to (Ie and Kosmatka (1992)).

Triangular Cross-Section

A second set of homogeneous isotropic and anisotropic cantilever beams having triangular cross-sections were analyzed to first prove convergence of the cross-section parameters with increasing power series polynomial order and second illustrate interesting section property information not found in the literature. The triangle represents an interesting cross-section shape because even though it is geometrically simple (3 corner points, three triangular subregions), closed-form torsion and flexure solutions for the local cross-section deformations exist for only the isotropic equilateral triangle, whereas the local cross-section deformations for any other aspect ratio (*b/a*) are represented by an infinite series of transcendental functions. For these cross-sections, the current approach represents a "best-fit" to the infinite series, where almost all of the calculated coefficents will be nonzero. As the order of the power series polynomial is increased, the calculated coefficients may vary slightly, but the calculated cross-section integrals (section properties) will experience virtually no change. In this study, a 9th order power-series polynomial was used for each of the three local deformation functions (161 total unknown coefficients) and the numerical integration was performed exactly

using a 52-point Gaussian Quadrature formula (Dunavant, 1985). A second coordinate system $(\tilde{x},\tilde{y})$ is introduced in the triangle (Fig. 3.*b*), where the origin is located at the mid-length of the base (b) and $(\tilde{x})$ bisects the triangle.

To study convergence of the section properties with polynomial order, we initially analyze an isotropic (Al 6061-T6) cantilever beam with a thin triangular cross-section (L/a=10, b/a=0.1). In Table 2, the key section parameters are presented as a function of polynomial order and matrix size ($[K]$). The normalized shear center locations, $\tilde{x}_s/a$ and $\tilde{x}_s^*/a$, are presented in the $(\tilde{x},\tilde{y})$ system, where the two values are significantly different for this thin cross-section, but both approaches exhibit monotonic convergence. The torsion constant ($GJ = 1/a_3$) is also presented, where again the solutions converge quickly. Lastly, the ratios of the centroidal tip displacement associated with shear deformation to the total centroidal tip displacement for applied flexure loads (P_x) and (P_y) are presented, where the magnitudes of the ratios are given, from Eq. (18.*a-c*), as:

$$\frac{u_{shear}}{u_{total}} = \frac{\gamma_{xz_{(o)}} L}{\gamma_{xz_{(o)}} L + \frac{P_x L^3}{3EI_{yy}}}, \qquad \frac{v_{shear}}{v_{total}} = \frac{\gamma_{yz_{(o)}} L}{\gamma_{yz_{(o)}} L + \frac{P_y L^3}{3EI_{xx}}}. \qquad (30.a,b)$$

As expected, shear deformation is a much larger effect for flexure loads applied in x-direction because the effective beam-length aspect ratio is much shorter in the x-z plane (L/a = 10) compared to the y-z plane (L/b = 100). Both values exhibit monotonic convergence, where it is interesting to note that the x-direction value converges quickly using a low polynomial order (3). A second convergence study was performed using the same geometric beam dimensions, but generally anisotropic behavior was introduced by orientating unidirectional high-strength graphite/epoxy fibers with α=β=30°. The calculated section properties are presented as a function of polynomial order in Table 3. The beam root and tip shear center locations are presented using both approaches, where it is observed that: (1.) the location converges monotonically with increasing polynomial order, (2.) the root shear center locations are within the cross-section, (3.) the tip shear center locations are well outside of the cross-section, and (4.) and the result obtained by extending Reissner's approach is closer to the centroid ($\tilde{x}_s/a$=0.333), more conservative, than the result obtained by extending the Griffith/Taylor approach. The torsion constant (GJ) and the ratios of the centroidal tip displacement associated with shear deformation to the total centroidal tip displacement for applied flexure loads (P_x) and (P_y) are also presented, where again these parameters converge monotonically.

In addition to the convergence study, three studies are presented that investigate the variation of the shear center location with cross-section aspect ratio and material properties. In Fig. 8, the sensitivity of the shear center location with aspect ratio (b/a) and Poisson's ratio (ν) is presented for an isotropic cantilever beam. The bold solid line and the thin solid lines represent the shear center locations based upon extending Reissner's and Griffith/Taylor's approaches, respectively, where the shear center location based upon Griffith/Taylor's approach is clearly dependent upon (ν) for thin sections, whereas the extended Reissner-based prediction is independent of (ν). The circular symbol represents the closed form thin-plate prediction of Reissner (1989) for triangular isotropic cross-sections. These results illustrate: (1) for very low aspect ratio triangles the difference in the two approaches for locating the shear center can be profound, (2) the thin plate solutions of Reissner (1989) are valid for only a very small aspect ratio range (b/a<0.04), (3) both shear center predictions converge as the aspect ratio approaches that of an equilateral triangle (b/a= 1.155), then ($x_S = x_S^* = 0$), and (4) for large aspect ratios, both shear center predictions are nearly coincident and they converge to the cross-section mid-length ($a/2$). This occurs because for triangular cross-sections with large aspect ratios, the out-of-plane flexural warping function approaches that of a thin rectangle cross-section.

In a second study, the shear center location was determined for a slender cantilever beam (L/a=10) with a thin triangular cross-section (b/a=.01) composed of off-axis unidirectional high-strength graphite/epoxy fibers ($-90^\circ<\alpha<90^\circ$, $\beta=0^\circ$). In Fig. 9, both shear center locations are presented for the beam root and beam tip as a function of orientation angle (α). At the beam root, the extended Reissner based approach is independent of (α) whereas the extended Griffith/Taylor approach is highly dependent upon (α). This is expected, based upon the above results for an isotropic triangular section which showed that the Griffith/Taylor solution is sensitive to material cross-coupling effects for thin sections. At the beam tip, both approaches for locating the shear center produce identical results when the orientation angle is either close to 0° ($-10^\circ<\alpha<10^\circ$) or close to 90° ($-70^\circ<\alpha<-110^\circ$, $70^\circ<\alpha<110^\circ$). Outside of this range, the two approaches produce tip shear center locations that can lie well outside of the cross-section shape, where the extended Reissner approach is much more conservative.

In a third investigation, the sensitivity of the shear center location with varying (ν_6) was determined by studying a slender cantilever beam (L/a=10) with a triangular cross-section (b/a=.1) composed of off-axis unidirectional high-strength graphite/epoxy fibers ($\alpha=0^\circ$, $-90^\circ<\beta<90^\circ$). Since ($\nu_4=\nu_5=0$) the shear center location is a cross-section

property that is independent of beam-length. In Fig. 10, both shear center locations are presented as a function of orientation angle (β). In the x-direction, the Griffith-Taylor based prediction is farther from the centroid and more sensitive to (β) than the extended Reissner approach, whereas in the y-direction, the extended Reissner approach is clearly dependent upon (β) and the Griffith-Taylor based prediction is virtually zero.

NACA-0012 Cross-Section

A final study was performed to investigate the variation of the shear center location with material orientation angle (α) in typical composite general aviation aircraft wings and helicopter blades. These structures are approximated as homogeneous cantilever beams having a NACA-0012 airfoil cross-section (Fig. 3.*c*), where a second coordinate system ($\tilde{x},\tilde{y}$) is introduced with the origin at the leading edge. Two beam-lengths were considered; (L/c=3) for typical general aviation aircraft wings and (L/c=20) for long slender helicopter blades, where (c) is the cross-section chord. The airfoil cross-section is discretized using 95 points on the boundary (i.e. 95 triangular subregions), based upon the mathematical definition of (Abbott and Von Doenhoff, 1959), and the section centroid is located at (0.42067c). Each of the three local deformation functions are modeled using a 9th order power-series polynomial (161 total unknown coefficients) and the numerical integration was performed exactly using a 52-point Gaussian Quadrature formula (Dunavant, 1985).

In Fig 11, both shear center locations are presented for the beam root and beam tip (L/c=3,20) as a function of orientation angle (α). At the beam root the results are similar to the above triangular cross-section study (Fig. 9), where the extended Reissner based approach is nearly independent of (α), whereas the extended Griffith/Taylor approach is slightly more dependent upon (α). At the aircraft wing tip (Fig. 11, center region), it is observed that: (1) the two shear center definitions are in near perfect agreement when ($-5^o<\alpha<10^o$) and ($60^o<\alpha<110^o$), (2) the extended Reissner definition of the shear center can be ahead ($\tilde{x}<0$) and outside of the airfoil section if ($-8^o<\alpha<-52^o$) or behind ($\tilde{x}>c$) and outside the airfoil section if ($15^o<\alpha<42^o$), whereas the extended Griffith/Taylor definition of the shear center can be ahead ($\tilde{x}<0$) or behind ($\tilde{x}>c$) the airfoil section if ($-8^o<\alpha<-60^o$) or ($12^o<\alpha<55^o$), respectively, and (3) the maximum distance that the shear center can be located either ahead or behind the wing-tip section occurs for the extended Reissner definition at (α=-30^o, $\tilde{x}^*_{SL}$=-.5c) and (α=30^o, $\tilde{x}^*_{SL}$=1.2c), respectively, whereas the extended Griffith/Taylor definition has (α=-38^o, $\tilde{x}_{SL}$=-1.1c) and (α=36^o, $\tilde{x}_{SL}$=1.7c), respectively.

For the tip section of the helicopter blade (Fig. 11, upper region), the shape of the curves represent an amplified version of the wing section. Thus, the shear center location is well outside of the tip cross-section for most values of (α), where the maximum distance that the shear center can be located either ahead or behind the wing-tip section occurs for the extended Reissner definition at (α=-30°, $\tilde{x}^*_{sL}$=-5c) and (α=30°, $\tilde{x}^*_{sL}$=6.5c), respectively, whereas the extended Griffith/Taylor definition has (α=-38°, $\tilde{x}_{sL}$=-9c) and (α=36°, $\tilde{x}_{sL}$=9c), respectively.

Conclusions

The behavior of a tip-loaded anisotropic cantilever beam with an arbitrary cross-section is studied using Saint-Venant's semi-inverse method along with a power series solution for the local in-plane and out-of-plane deformation warping functions. The power series coefficients are determined by solving a set of variationally derived linear algebraic equations. Using the resulting three-dimensional displacement solutions, the shear deformation associated with applied tip loads is investigated as well as the shear center location. Two different definitions of the shear center are presented for anisotropic beams by extending the classic approaches of Griffith/Taylor and that of Reissner. Both of the extended definitions reveal the linear dependency of the shear center location with beam-length, where the extended-Reissner prediction is much closer to the centroid then the extended Griffith/Taylor prediction. Numerical results are presented for three different cross-sections and two different materials. For elliptical cross-sections, it was shown that the calculated power series coefficients were in exact agreement with existing elasticity solutions for anisotropic beams over a wide variety of cross-section aspect ratios. For the triangular cross-sections, it was shown that the calculated power series coefficients represent a "best-fit" to the infinite series of transcendental functions and the warping-related section properties (shear center, torsion constant, shear deformation) converge quickly with increasing power series order. Moreover, three studies were performed to illustrate the sensitivity of the shear center location with cross-section aspect ratio, material definition, fiber orientation, and beam-length. A final investigation was performed to study the length-dependency of the shear center in composite general aviation aircraft wings (L/c=3) and helicopter blades (L/c=20). At the beam root, the extended Reissner approach is nearly independent of material orientation angle, whereas the extended Griffith/Taylor approach is dependent. At the aircraft wing tip, it is observed that the two shear center definitions are in near perfect agreement over a small range of orientation angles and the shear center can be located either ahead or behind

the wing-tip section. For the helicopter blade tip section, the shear center location is well outside of the tip cross-section for most values of orientation angle.

Acknowledgements

The support of this research was provided by the NASA-Langley Research Center through grant NAG-1-1151-FDP, with R. C. Lake as project monitor.

References

Abbott, I. R., and A. E. Von Doenhoff (1959), *Theory of Wing Sections*, Dover Publications, 1st edition, 111-115.

Dunavant, D. A. (1985), High Degree Efficient Symmetrical Gaussian Quadrature Rules for Triangle, *International Journal for Numerical Methods in Engineering*, **21**, 1129-1148.

Griffith, A.A., and G. I. Taylor (1917), The Problem of Flexure and its Solution by the Soap-Film Method, *Reports and Memoranda Adv. Comm. Aeronautics*, No. 399.

Herrmann, L. R. (1965), Elastic Torsional Analysis of Irregular Shapes, *Journal of the Engineering Mechanics Division ASCE*, **91**, (EM6), 11-19.

Ie, C.A. and J. B. Kosmatka (1992), Flexure-Torsion Behavior of Prismatic Beams, Part I: Warping and Section Properties via Power Series, *International Journal of Solids and Structures,* (to appear).

Kosmatka, J. B. (1986), Structural Dynamic Modeling of Advanced Composite Propellers by the Finite Element Method, *Ph.D. Dissertation*, University of California, Los Angeles.

Kosmatka, J. B. and S. B. Dong (1991), Saint-Venant Solution for Prismatic Anisotropic Beams, *International Journal of Solids and Structures*, **28**, 917-938.

Kosmatka, J. B. (1992), Flexure-Torsion Behavior of Prismatic Beams, Part I: Warping and Section Properties via Power Series, *AIAA Journal*, (to appear).

Lekhnitskii, S. G. (1963), *Theory of Elasticity of an Anisotropic Body*, Holden-Day Inc., San Francisco.

Mason, W. E. and L. R. Herrmann (1968), Elastic Shear Analysis of General Prismatic Shaped Beams, *Journal of the Engineering Mechanics Division ASCE*, **94**, (EM4), 965-983.

Mindlin, R. D. (1975), Solution of St. Venant's Torsion Problem by Power Series, *International Journal of Solids and Structures*, **11**, 321-328.

Reissner, E. (1989) The Center of Shear as a Problem of the Theory of Plates of Variable Thickness, *Ingenieur-Archiv*, **59**, 324-332.

Reissner, E. (1991) Approximate Determinations of the Center of Shear by Use of the Saint-Venant Solution for the Flexure Problem of Plates of Variable Thickness, *Archive of Applied Mechanics-Ingenieur-Archiv*, **61**, 555-566.

Sokolnikoff, I.S. (1946), *Mathematical Theory of Elasticity*, Maple Press Company, 1st edition.

Appendix

The matrix $\left[\overline{F_c}\right]$ is defined as;

$$\left[\overline{F_C}\right]=\begin{bmatrix}
-\frac{v_1}{EI_{yy}}x\left(z-L\right) & -\frac{v_1}{EI_{xx}}y\left(z-L\right) & 0 & 0 & 0 & 0 & 0\\
-\frac{v_2}{EI_{yy}}x\left(z-L\right) & -\frac{v_2}{EI_{xx}}y\left(z-L\right) & 0 & 0 & 0 & 0 & 0\\
-\frac{1}{2EI_{yy}}\left\{v_5x+v_4y-2\left(z-L\right)\right\}x-\frac{v_5}{2EA} & -\frac{1}{2EI_{xx}}\left\{v_5x+v_4y-2\left(z-L\right)\right\}y-\frac{v_4}{2EA} & \frac{1}{EA} & \frac{1}{EI_{xx}}y & -\frac{1}{EI_{yy}}x & \frac{v_5}{2EI_{xx}}y-\frac{v_4}{2EI_{yy}}x & 0\\
-\frac{1}{EI_{yy}}\left\{\frac{v_6}{2}x+v_2y+v_4\left(z-L\right)\right\}x & \frac{1}{2EI_{xx}}\left\{\left(v_1x^2-v_2y^2\right)-2v_4y\left(z-L\right)\right\} & 0 & 0 & 0 & 0 & x\\
-\frac{1}{2EI_{yy}}\left\{\left(v_1x^2-v_2y^2\right)+2v_5x\left(z-L\right)\right\} & -\frac{1}{EI_{xx}}\left\{v_1x+\frac{v_6}{2}y+v_5\left(z-L\right)\right\}y & 0 & 0 & 0 & 0 & -y\\
-\frac{v_6}{EI_{yy}}x\left(z-L\right) & -\frac{v_6}{EI_{xx}}y\left(z-L\right) & 0 & 0 & 0 & 0 & 0
\end{bmatrix} \qquad (A.1)$$

Integrating the matrix of (*A*.1) over the beam length results in

$$\int_0^L \left[\overline{FC}\right] dz = L\left[\overline{\overline{FC}}\right] \tag{A.2}$$

where

$$\left[\overline{\overline{FC}}\right] = \begin{bmatrix}
\frac{v_1 L}{2EI_{yy}}x & \frac{v_1 L}{2EI_{xx}}y & 0 & 0 & 0 & 0 & 0 \\
\frac{v_2 L}{2EI_{yy}}x & \frac{v_2 L}{2EI_{xx}}y & 0 & 0 & 0 & 0 & 0 \\
-\frac{1}{2EI_{yy}}\left(v_5 x + v_4 y + L\right)x - \frac{v_5}{2EA} & -\frac{1}{2EI_{xx}}\left(v_5 x + v_4 y + L\right)y - \frac{v_4}{2EA} & \frac{1}{EA} & \frac{1}{EI_{xx}}y & -\frac{1}{EI_{yy}}x & \frac{v_5}{2EI_{xx}}y - \frac{v_4}{2EI_{yy}}x & 0 \\
-\frac{1}{2EI_{yy}}\left(v_6 x + 2v_2 y - v_4 L\right)x & \frac{1}{2EI_{xx}}\left(\left(v_1 x^2 - v_2 y^2\right) + v_4 L y\right) & 0 & 0 & 0 & 0 & x \\
-\frac{1}{2EI_{yy}}\left(\left(v_1 x^2 - v_2 y^2\right) - v_5 L x\right) & -\frac{1}{2EI_{xx}}\left(2v_1 x + v_6 y - v_5 L\right)y & 0 & 0 & 0 & 0 & -y \\
\frac{v_6 L}{2EI_{yy}}x & \frac{v_6 L}{2EI_{xx}}y & 0 & 0 & 0 & 0 & 0
\end{bmatrix} \tag{A.3}$$

Table 1: Material properties for unidirectional high-strength graphite/epoxy fibers.

E_{11}	145	GPa
$E_{22} = E_{33}$	10	GPa
$G_{12} = G_{13}$	4.8	GPa
$\nu_{12} = \nu_{13}$	0.250	
ν_{23}	0.400	

Table 2: Calculated section properties of an isotropic cantilever beam with a thin triangular cross-section as a function of power series order (b/a=0.1, L/a=10, ν=0.333)

Polynomial order	matrix size	$\tilde{x}_s/a$	$\tilde{x}^*_s/a$	GJ (10^{-3})	$\frac{u_{shear}}{u_{total}}$ (10^{-3})	$\frac{v_{shear}}{v_{total}}$ (10^{-5})
2	14	.2718	.2923	2.168	4.640	-24.26
3	26	.1398	.2035	2.118	5.815	4.594
4	41	.1441	.2053	2.060	5.815	5.049
5	59	.1481	.2070	2.007	5.815	4.583
6	80	.1515	.2082	1.969	5.815	4.671
7	104	.1530	.2089	1.943	5.815	4.690
8	131	.1536	.2093	1.938	5.815	4.700
9	161	.1536	.2093	1.936	5.815	4.701

Table 3: Calculated section properties of a generally anisotropic cantilever beam with a thin triangular cross-section as a function of power series order (b/a=0.1, L/a=10, α=β=30°).

Polynomial order	$\tilde{x}_{so}/a$	$\tilde{y}_{so}/b$ (10^{-2})	$\tilde{x}_{sL}/a$	$\tilde{y}_{sL}/b$	$\tilde{x}^*_{so}/a$	$\tilde{y}^*_{so}/b$ (10^{-2})	$\tilde{x}^*_{sL}/a$	$\tilde{y}^*_{sL}/b$	GJ (10^{-4})	$\frac{u_{shear}}{u_{total}}$ (10^{-3})	$\frac{v_{shear}}{v_{total}}$ (10^{-5})
2	.2724	-.1881	3.627	.1434	.2914	4.231	2.600	-2.246	5.332	5.642	-26.00
3	.1481	-2.089	3.419	.1208	.2049	11.12	2.473	-2.079	5.199	5.468	5.082
4	.1566	-1.991	3.340	.1179	.2099	10.36	2.435	-1.985	5.059	5.461	3.036
5	.1632	-1.916	3.279	.1158	.2137	9.803	2.406	-1.914	4.953	5.469	4.193
6	.1666	-1.877	3.248	.1146	.2159	9.512	2.390	-1.877	4.897	5.475	5.310
7	.1681	-1.862	3.235	.1142	.2166	9.401	2.384	-1.863	4.875	5.475	5.260
8	.1685	-1.856	3.231	.1140	.2169	9.353	2.382	-1.858	4.868	5.474	5.220
9	.1686	-1.855	3.230	.1140	.2170	9.348	2.381	-1.856	4.864	5.474	5.214

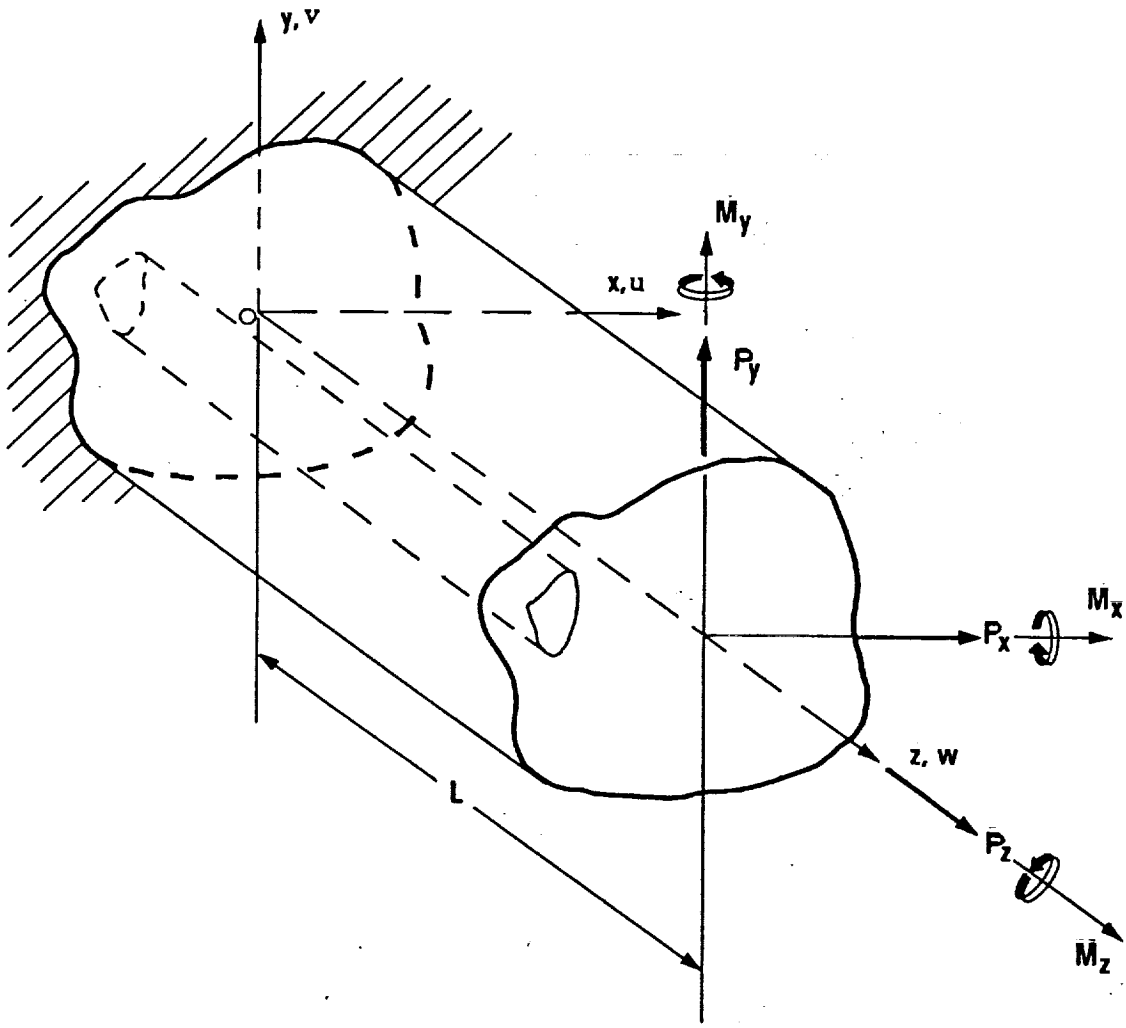

Fig. 1 Anisotropic cantilever beam.

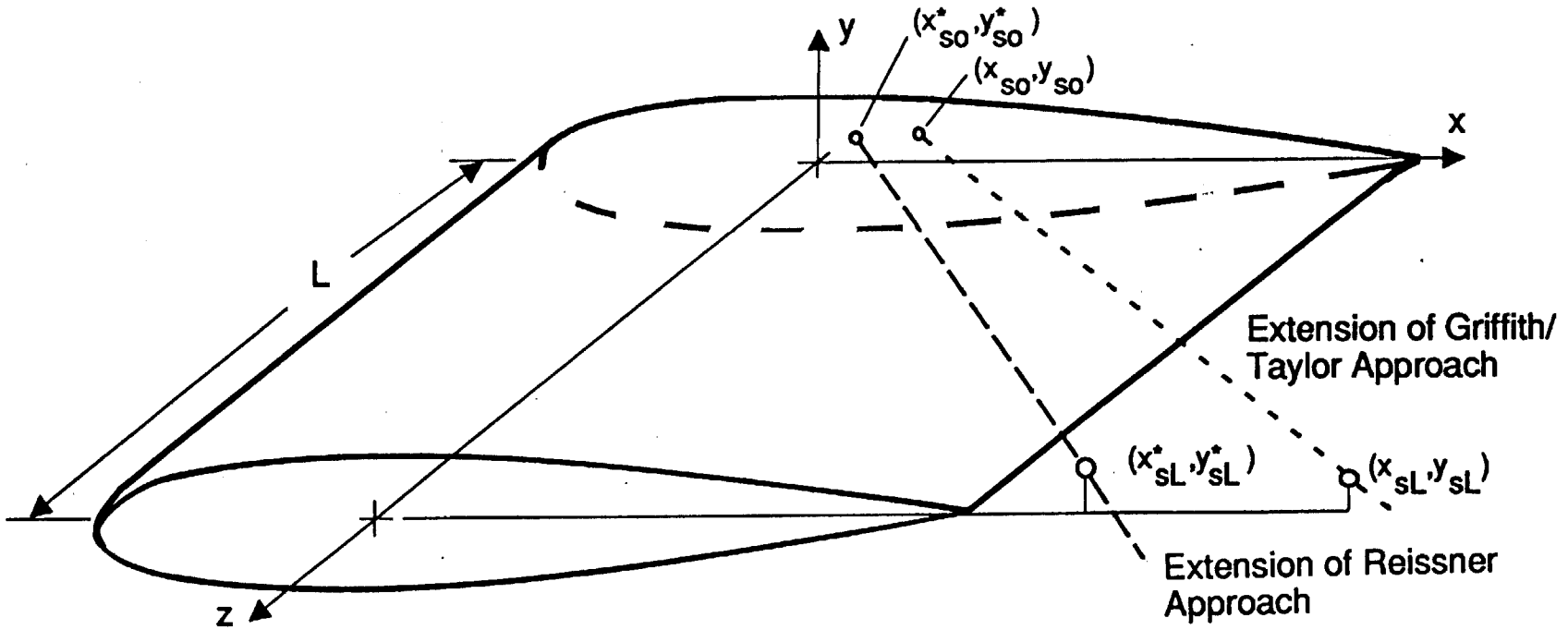

Fig. 2 Line of shear centers in an anisotropic beam.

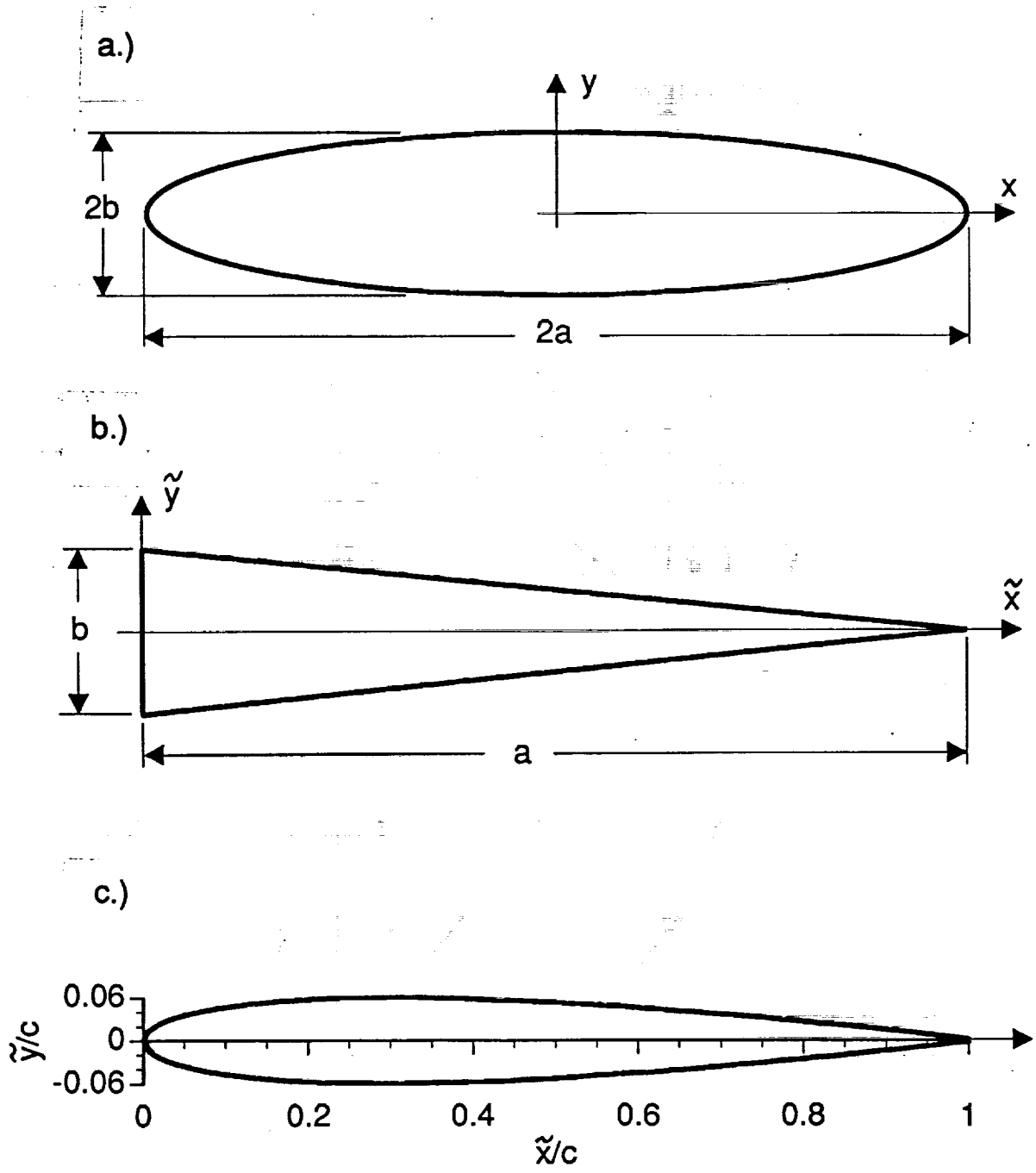

Fig. 3 a.) Elliptical, b.) triangular, and c.) NACA-0012 airfoil cross-sections.

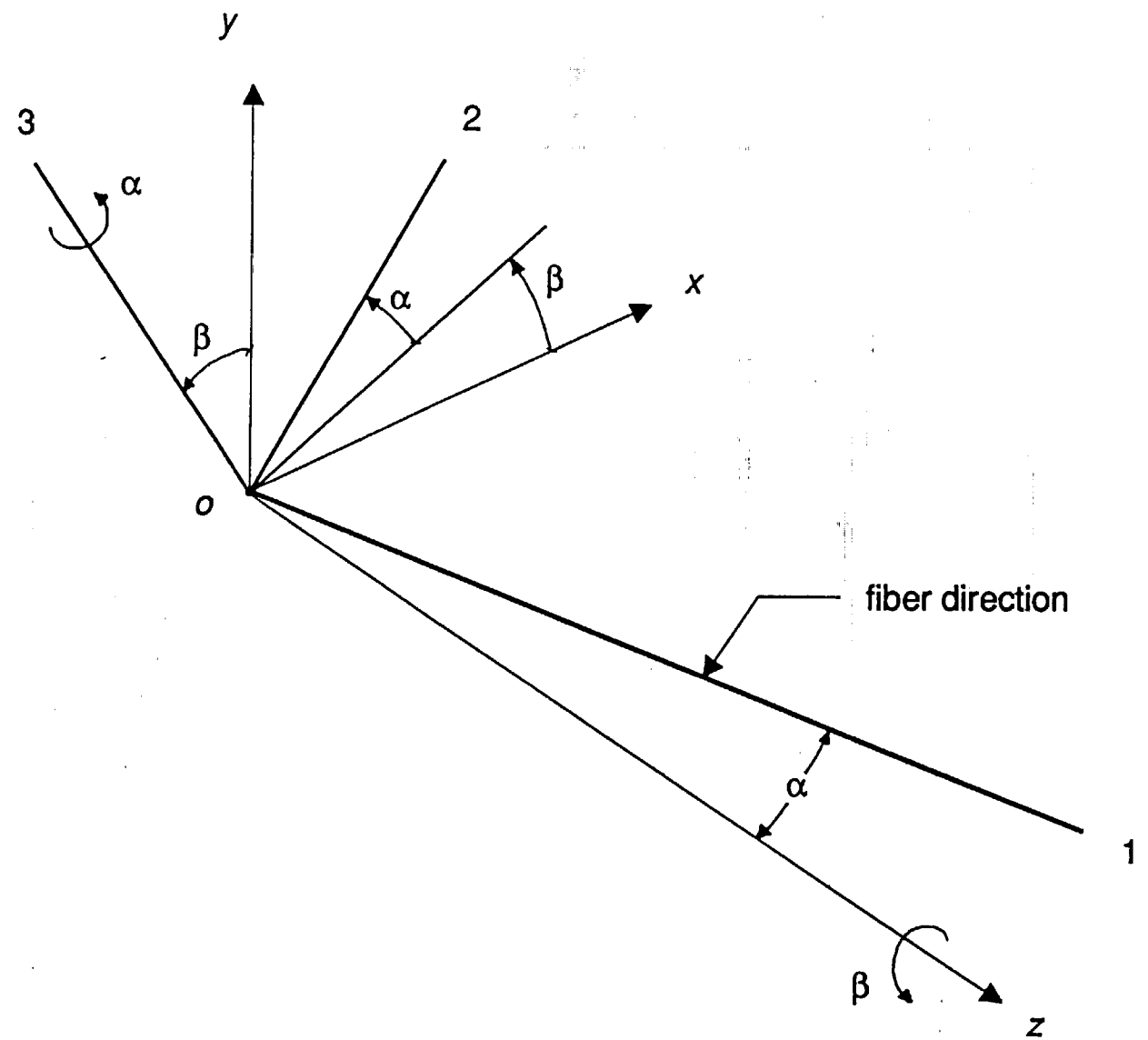

Fig. 4 Orientation of material fibers (1,2,3) relative to Cartesian frame (*x,y,z*).

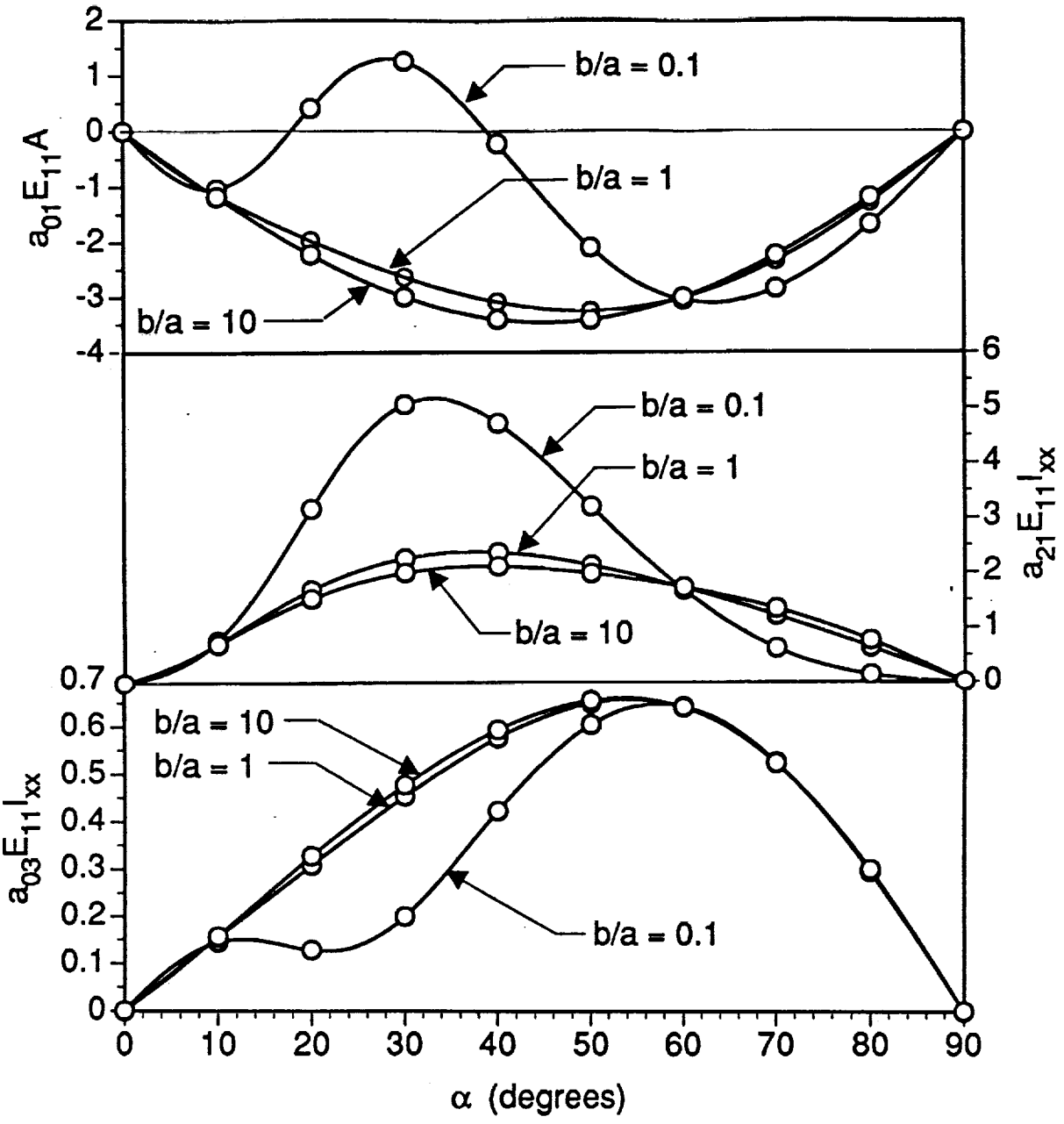

Fig. 5 Nondimensionalized in-plane coefficients (a_{01},a_{21},a_{03}) as a function of orientation angle (α), (β=0) and cross-section aspect ratio (b/a) for an elliptical cross-section (— exact, o current approach).

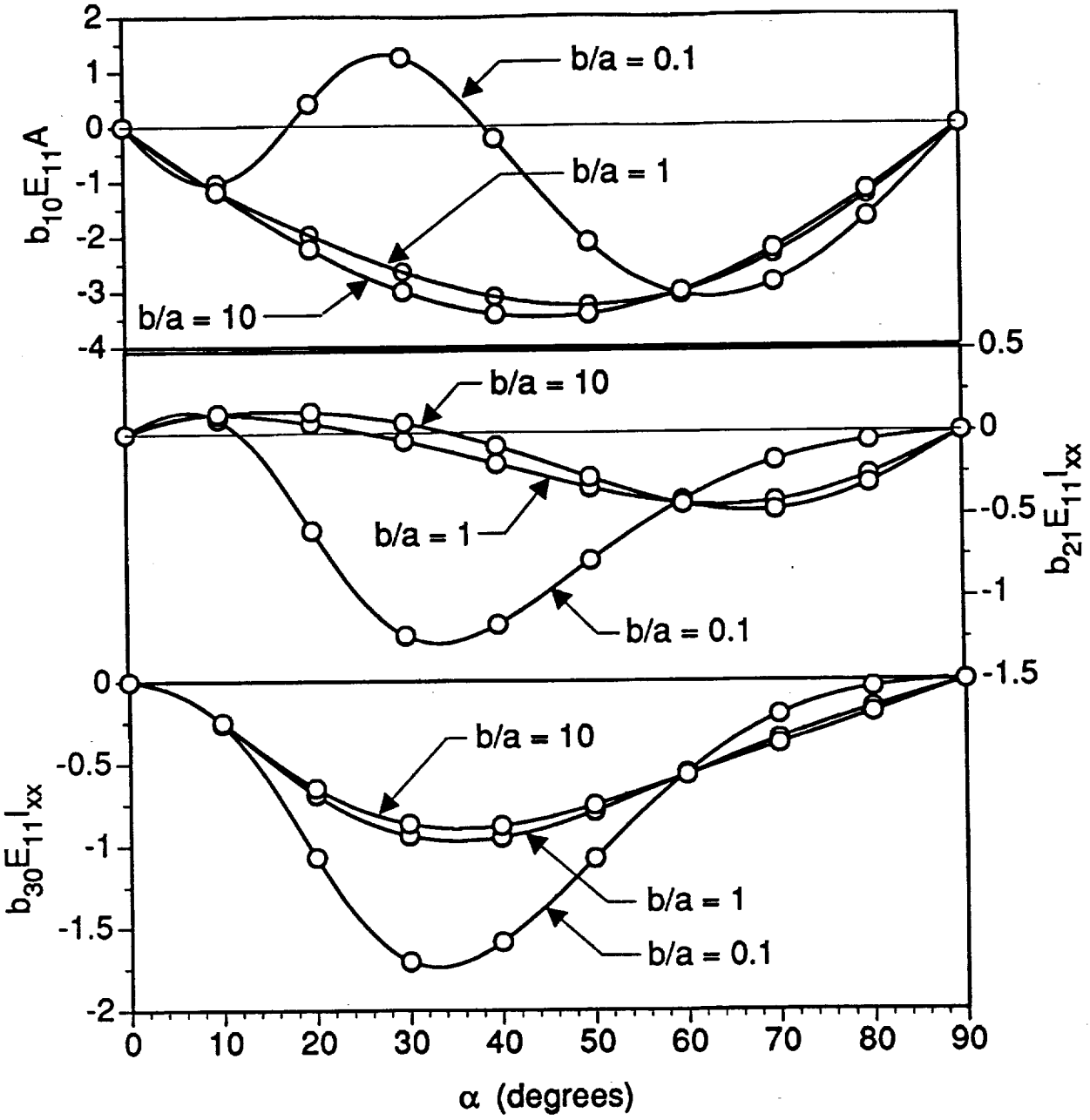

Fig. 6 Nondimensionalized in-plane coefficients (b_{10},b_{12},b_{30}) as a function of orientation angle (α), (β=0) and cross-section aspect ratio (b/a) for an elliptical cross-section (— exact, o current approach).

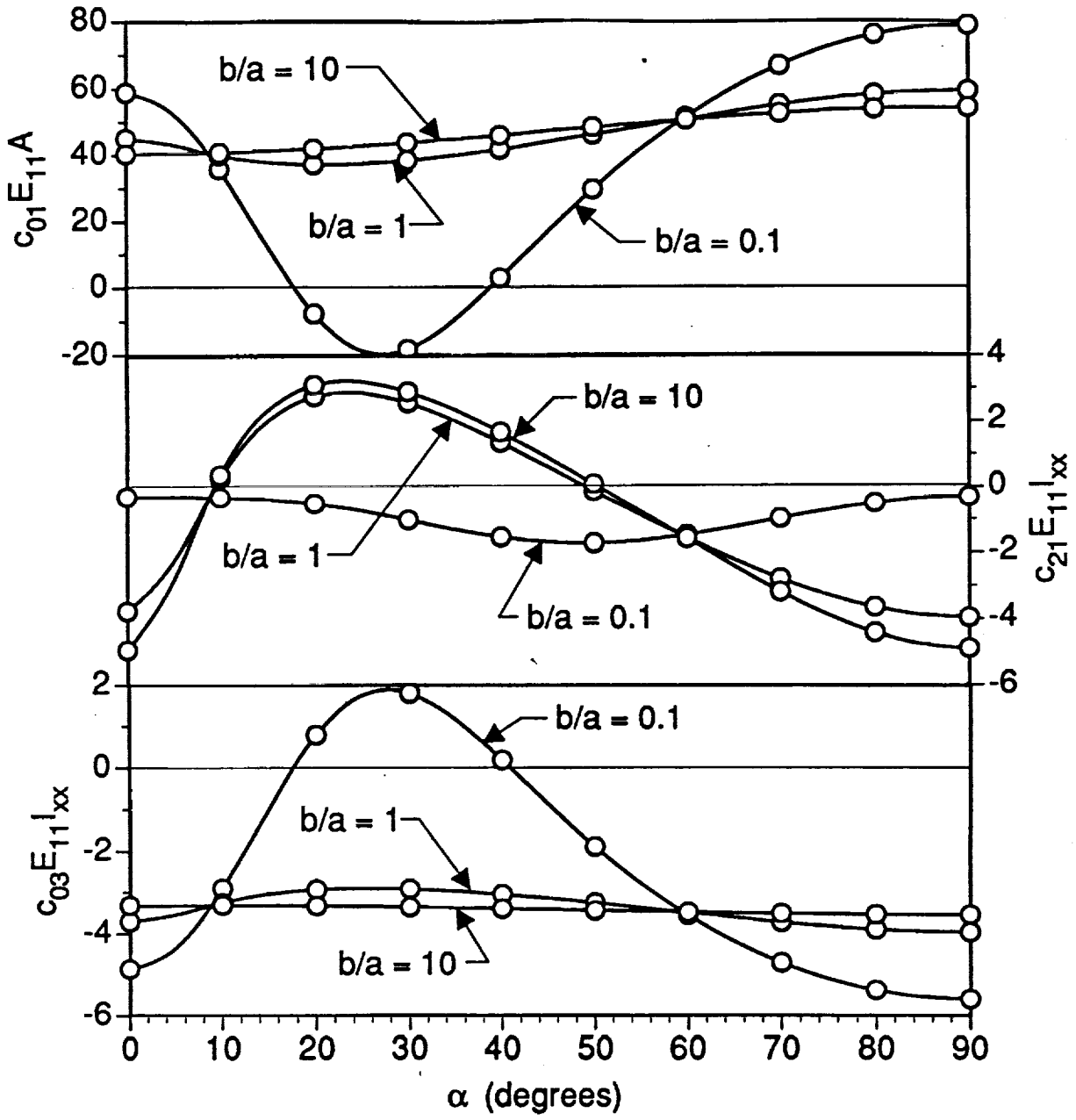

Fig. 7 Nondimensionalized in-plane coefficients (c_{01},c_{21},c_{03}) as a function of orientation angle (α), (β=0) and cross-section aspect ratio (b/a) for an elliptical cross-section (— exact, o current approach).

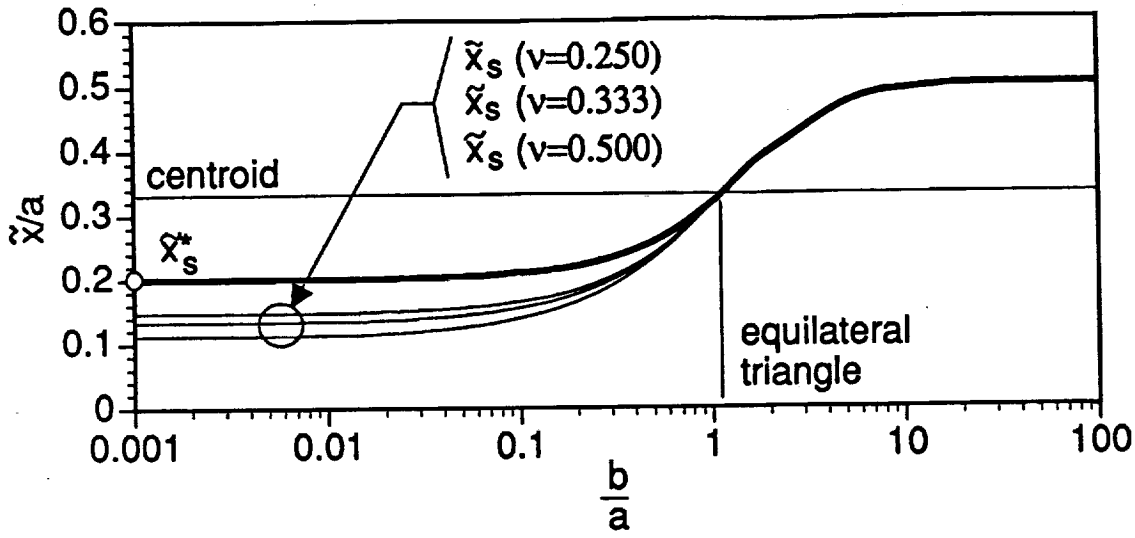

Fig. 8 Variation of the shear center location in an isotropic triangular cross-section as a function of (b/a) and (ν), (—— Griffith/Taylor approach, ▬ adaptation of Reissner approach, o Reissner prediction).

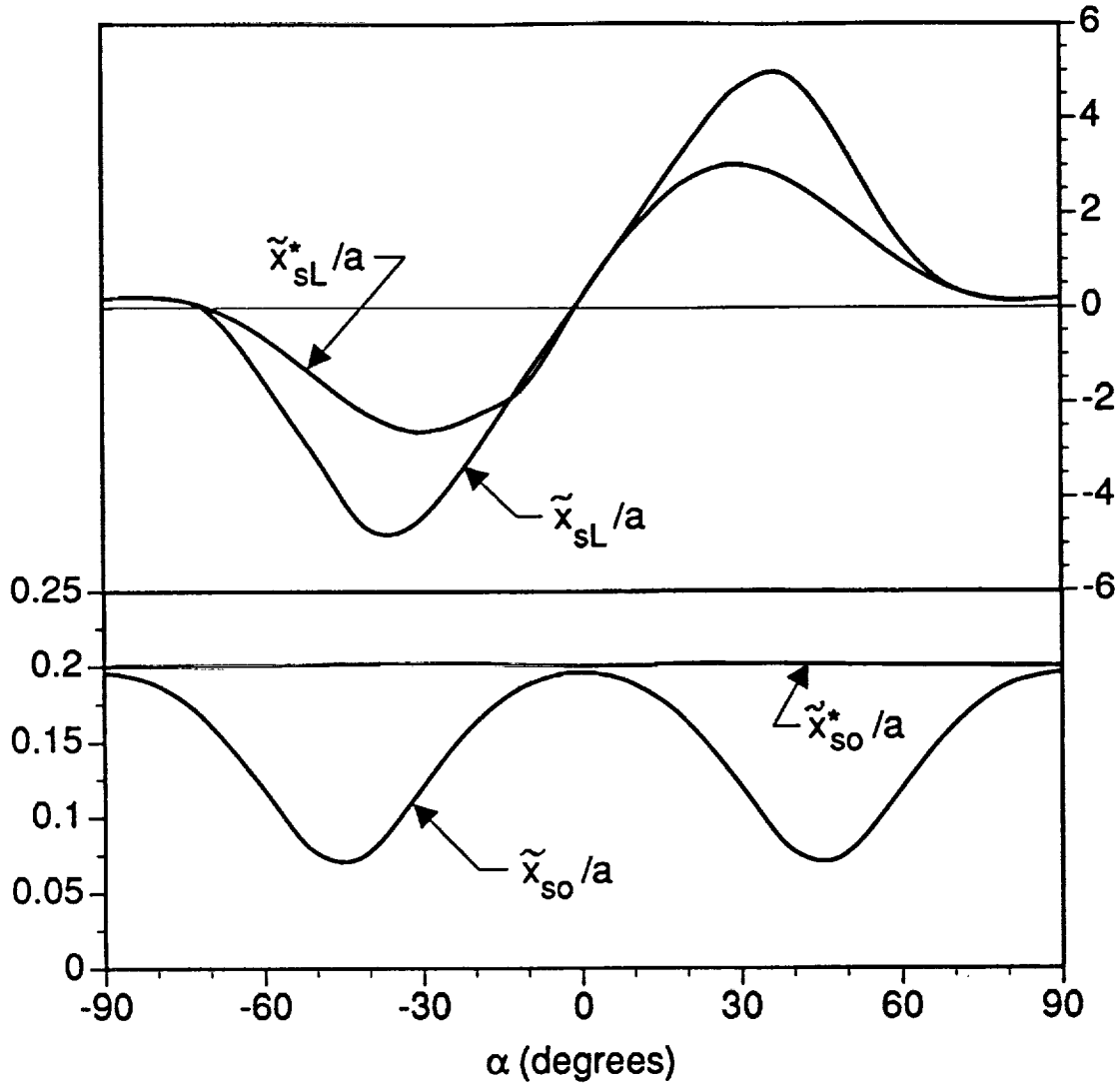

Fig. 9 Variation of the shear center locations at the beam root and beam tip of a thin composite triangular cross-section (*b/a*) as a function of orientation angle (α), (β=0°).

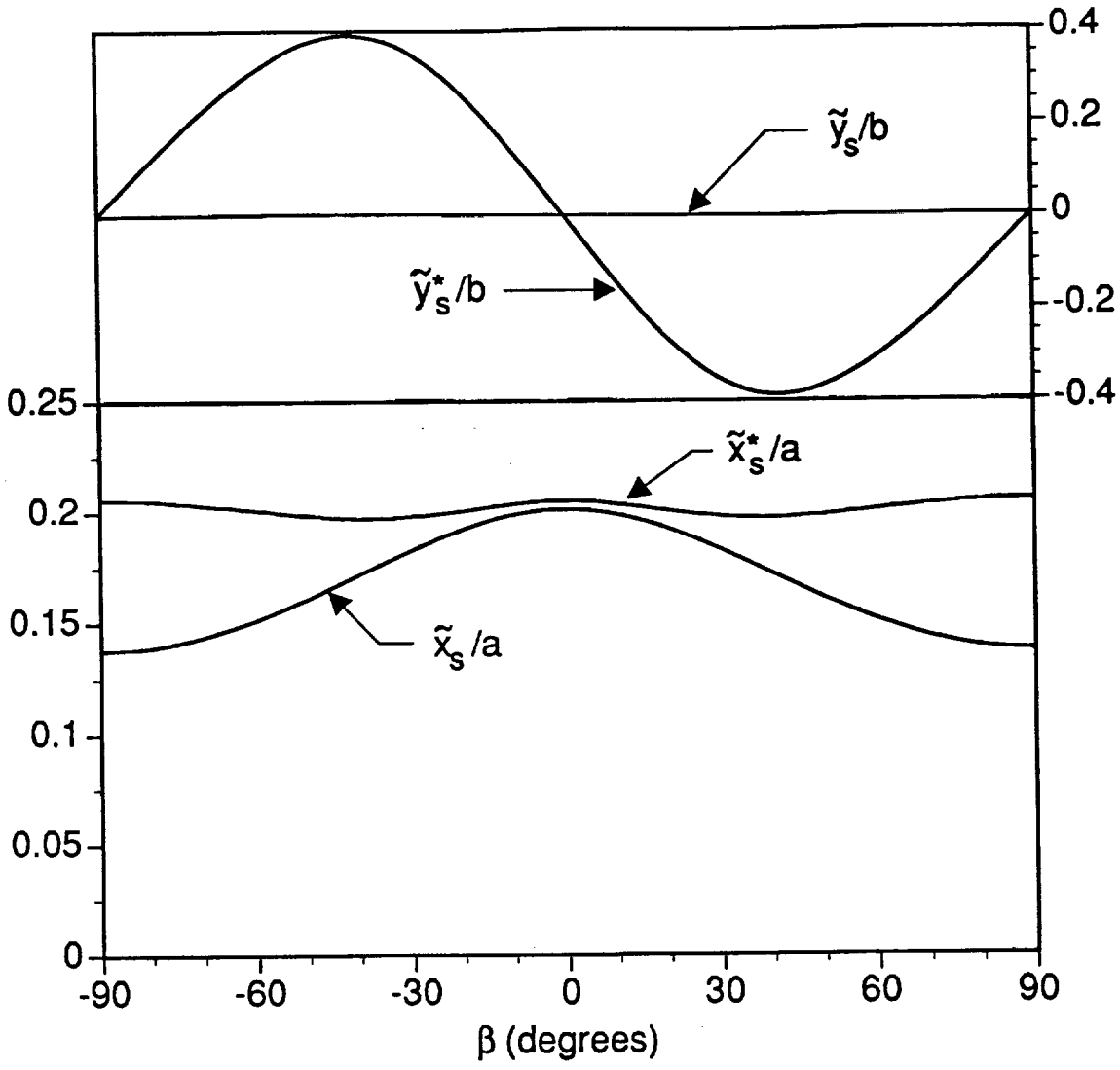

Fig. 10 Variation of the shear center locations at the beam root and beam tip of a thin composite triangular cross-section (*b/a*) as a function of orientation angle (β), (α=90°).

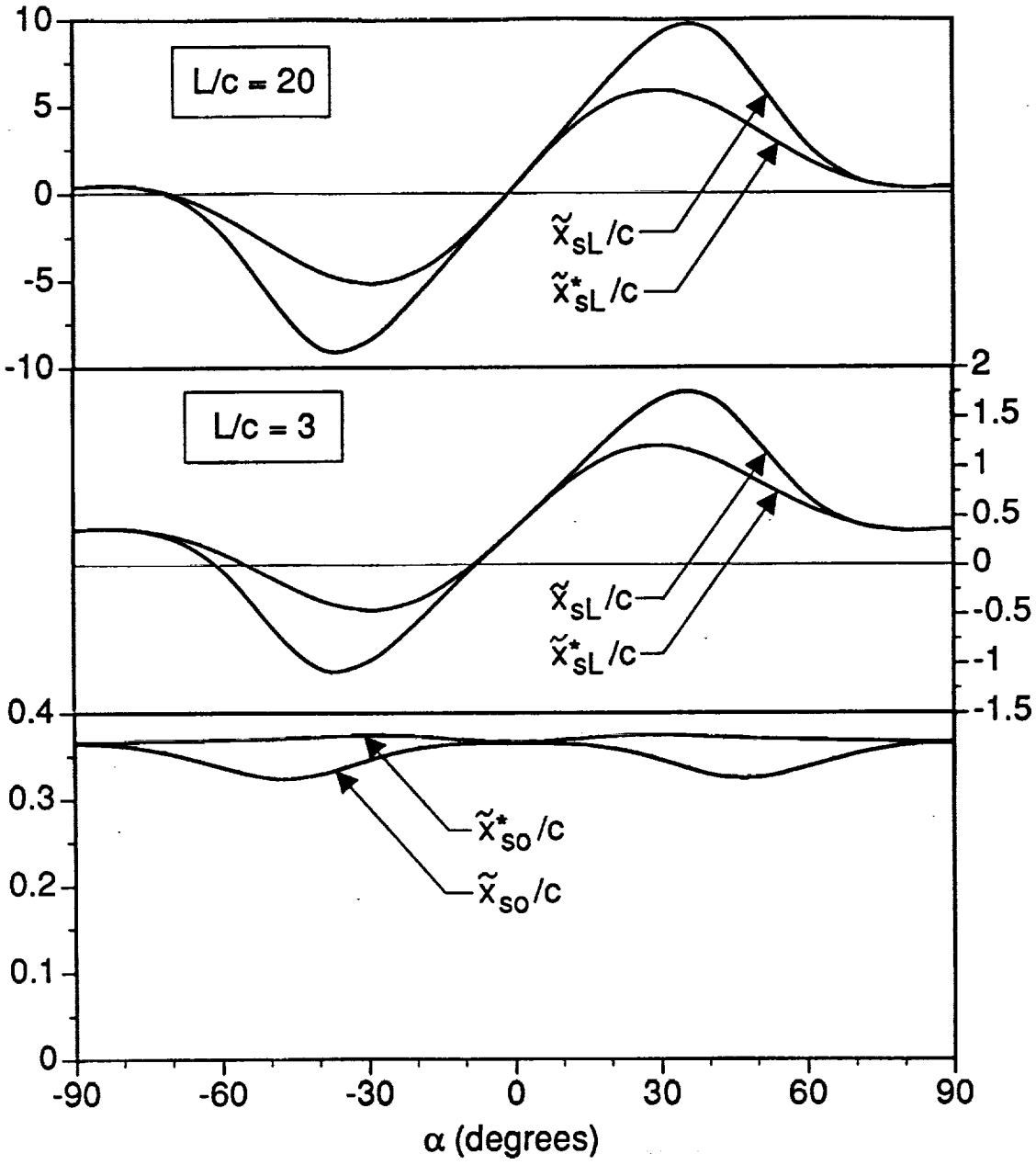

Fig. 11 Variation of the shear center locations at the beam root and beam tip of a composite aircraft (L/c=3) and a composite helicopter blade (L/c=20) as a function of orientation angle (α), (β=0°).

Chapter 4 Exact Cross-Section Warping Functions for Generally Anisotropic Beams Having Solid Elliptical Cross-Sections

by

C. A. Ie and J. B. Kosmatka
Department of Applied Mechanics and Engineering Sciences
University of California, San Diego
La Jolla, CA 92093

ABSTRACT

The St Venant displacement distributions are developed, based upon the theory of elasticity, for a tip-loaded homogeneous cantilever beam having an elliptical cross-section and rectilinear anisotropy. These distributions are found by integrating the strain distributions, where the local in-plane deformation and out-of-plane warping of the cross-section are exactly determined. A definition for the '*anisotropic shear center*' is presented by extending the classical definition for isotropic beams. The additional transverse beam displacement associated with shear deformation is determined for applied extension and flexure loads. Numerical results are presented which show (1.) the anisotropic shear center location is linearly dependent upon beam length and can be located outside the cross-section, (2.) shear deformation can actually be negative for certain beam aspect ratios and material definitions, and (3.) the local cross-section deformations and the transverse shear stress distributions bear no resemblance to their isotropic counterparts.

INTRODUCTION

The elastic stress and displacement distributions of isotropic cantilever beams subjected to tip loads (i.e., extension, bending, torsion, and flexure) has been exhaustively investigated by making use of Saint-Venant's principle in the formulation of the boundary-value problem. Closed-form displacement and stress solutions exist for simple (elliptical) cross-sections, series solutions exist for slightly more complex (rectangular, triangular) solutions, and approximate solutions based upon the application of the Ritz method exist for arbitrary cross-sections. Detailed examples of these solutions can be found in many texts covering the theory of elasticity (for example, (Sokolnikoff, 1956) or (Timoshenko and Goodier, 1970)).

---

* Ph.D. candidate

** Assistant Professor

Conversely, the study of generally anisotropic cantilever beams subjected to tip loads has received far less attention. In Lekhnitskii's monograph (1963), the stress and displacement distributions were formulated in terms of known quantities (geometric and material properties) and unknown functions which represented the local in-plane deformation and out-of-plane warping of the cross-section. A solution procedure for determining the stress distribution was presented based upon the use of Airy and Prandtl stress functions, where numerical examples include beams having an elliptical (closed-form), rectangular (series), or an arbitrary cross-section (approximate). But no results were presented for the displacement distributions. Recently Kosmatka and Dong (1991) developed an analytical (finite element based) model for determining the complete displacement and stress distributions of a homogeneous prismatic anisotropic beam with an arbitrary cross-section, by solving the two-dimensional boundary problem in terms of the local in-plane deformation and out-of-plane warping of the cross-section. Numerical results used these calculated displacement and stress distributions to study the beam behavior, determine important section constants, and show that the shear center location is linearly dependent upon beam length.

In the current paper, we will develop the complete St. Venant displacement and stress distributions, based upon the theory of elasticity, for a tip-loaded homogeneous cantilever beam having an elliptical cross-section and rectilinear anisotropy. The displacement distributions are found by integrating the strain distributions calculated by Lekhnitskii (1963), where the local in-plane deformation and out-of-plane warping of the cross-section are exactly determined. The resulting displacement solutions are used to develop a definition of the '*anisotropic shear center*' which involves extending the original work of Griffith and Taylor (1917) to homogeneous prismatic anisotropic beams. Moreover, the additional transverse beam displacement associated with shear deformation is determined for applied extension and flexure loads. It is also shown that the shear deformation is zero for applied bending and torsion of homogeneous anisotropic beams. Numerical results are presented to show how material anisotropy effects (1) the local in-plane deformation and out-of-plane warping, (2.) the shear center location, and (3.) the stress distribution.

This model will be useful to developers of refined (or higher-order) one-dimensional theories for anisotropic beams, who wish to include the local in-plane deformation and out-of-plane warping of the cross-section as part of the displacement kinematic field in order to get exact three-dimensional stress distributions.

DISPLACEMENT DISTRIBUTIONS

Consider a cantilevered beam of length (L) with an elliptical cross section of area (A) composed of an anisotropic homogeneous material (see Fig. 1). A Cartesian coordinate system (x,y,z) is defined on the beam where (x) and (y) axes are coincident with the principal (i.e., major and minor) axes of the root cross section and (z) is coincident with the line of centroids. Displacements in the (x,y,z) directions are defined as (u), (v), and (w), respectively. At the root end (z=0), the beam is constrained by fixing the displacements at the centroid and the rotations about the centroid as follows

$$u = v = w = 0, \qquad \frac{\partial u}{\partial z} = \frac{\partial v}{\partial z} = \frac{\partial v}{\partial x} - \frac{\partial u}{\partial y} = 0. \tag{1.a-f}$$

At the beam's free end, tractions are applied that are equivalent to a general force (P) with flexural (P_x, P_y) and extensional (P_z) components and a general moment (M) with bending (M_x, M_y) and a torsional (M_z) components. It is further assumed that the lateral surface of the beam is traction-free.

The stresses and strains at a point can be written in array form as:

$$\{\sigma\}^T = \{\, \sigma_{xx}, \sigma_{yy}, \sigma_{zz}, \tau_{yz}, \tau_{zx}, \tau_{xy} \,\},$$
$$\{\varepsilon\}^T = \{\, \varepsilon_{xx}, \varepsilon_{yy}, \varepsilon_{zz}, \gamma_{yz}, \gamma_{zx}, \gamma_{xy} \,\}. \tag{2.a,b}$$

where the strains are related to the displacement components by:

$$\varepsilon_{xx} = \frac{\partial u}{\partial x}, \qquad \varepsilon_{yy} = \frac{\partial v}{\partial y}, \qquad \varepsilon_{zz} = \frac{\partial w}{\partial z},$$
$$\gamma_{yz} = \frac{\partial v}{\partial z} + \frac{\partial w}{\partial y}, \qquad \gamma_{zx} = \frac{\partial w}{\partial x} + \frac{\partial u}{\partial z}, \qquad \gamma_{xy} = \frac{\partial u}{\partial y} + \frac{\partial v}{\partial x}. \tag{2.c-h}$$

and the stress and strain components are related by the constitutive relations of a linearly-anisotropic hyperelastic material:

$$\{\varepsilon\} = [S]\{\sigma\}. \tag{2.i}$$

Here $[S]$ is a fully populated symmetric matrix with 21 distinct coefficients S_{ij} (i,j=1–6).

The behavior of the beam will be studied as two independent cases. The first case, which involves generalized plane strain behavior of the beam, is associated with the extensional force (P_z), the bending moments (M_x, M_y), and the torsional moment (M_z). The second case is associated with the applied flexural forces (P_x, P_y), where it is assumed that the stress (σ_{zz}) varies linearly in the z-direction and the remaining five stress compo-

nents can be nonzero.

Case I: Generalized Plane Strain

For a homogeneous anisotropic cantilever beam with an elliptical cross-section subjected to an applied extensional force (P_z), bending moments (M_x, M_y), and/or torsional moment (M_z), the stress distributions are given (from Lekhnitskii (1963)) as:

$$\sigma_{xx} = \sigma_{yy} = \tau_{xy} = 0\,, \quad \sigma_{zz} = \frac{P_z}{A} + \frac{M_x}{I_{xx}}y - \frac{M_y}{I_{yy}}x\,, \quad \tau_{yz} = \frac{M_z}{2I_{yy}}x\,, \quad \tau_{zx} = -\frac{M_z}{2I_{xx}}y\,, \qquad (3.a\text{–}f)$$

where (a) and (b) are one-half of the major and the minor dimensions of the cross-section, respectively, (see Fig. 1), A is the cross sectional area given as (πab), and I_{xx} and I_{yy} are the area moments of inertia about the (x) and (y) axes given as ($\pi ab^3/4$) and ($\pi a^3 b/4$), respectively. These stress components, which are independent of (z), are equal to those of an identical isotropic beam.

The displacement components (u,v,w) are determined by substituting Eqns. (3.a-f) into (2.i) and integrating using the standard technique (see Sokolnikoff (1946) or Timoshenko (1970)), where the constants of integration are determined using the boundary conditions (1.a-f) at the root. Thus,

$$\begin{aligned} u = &-\frac{P_z}{EA}\left(\nu_1 x + \frac{\nu_6}{2}y\right) - \frac{M_x}{E I_{xx}}\left(\nu_1 x + \frac{\nu_6}{2}y + \frac{\nu_5}{2}z\right)y + \frac{M_y}{2E I_{yy}}(z^2 + \nu_1 x^2 - \nu_2 y^2 - \nu_4 yz) \\ &+ \frac{M_z}{2E I_{yy}}\left(\frac{\nu_4}{2}z^2\right) - \frac{M_z}{4I_{xx}}(2S_{15}x + S_{56}y + S_{55}z)y + \frac{M_z}{4I_{yy}}(S_{14}x^2 - S_{24}y^2 - S_{44}yz)\,, \end{aligned} \qquad (4.a)$$

$$\begin{aligned} v = &-\frac{P_z}{EA}\left(\frac{\nu_6}{2}x + \nu_2 y\right) + \frac{M_y}{2E I_{yy}}(\nu_6 x^2 + 2\nu_2 xy + \nu_4 xz) - \frac{M_x}{2E I_{xx}}(z^2 - \nu_1 x^2 + \nu_2 y^2 - \nu_5 xz) \\ &- \frac{M_z}{2E I_{xx}}\left(\frac{\nu_5}{2}z^2\right) + \frac{M_z}{4I_{xx}}(S_{15}x^2 - S_{25}y^2 + S_{55}xz) + \frac{M_z}{4I_{yy}}(S_{46}x + 2S_{24}y + S_{44}z)x\,, \end{aligned} \qquad (4.b)$$

$$\begin{aligned} w = &\frac{P_z}{EA}(z - \nu_5 x - \nu_4 y) - \frac{M_x}{EI_{xx}}\left(\frac{\nu_5}{2}x + \frac{\nu_4}{2}y - z\right)y + \frac{M_y}{E I_{yy}}\left(\frac{\nu_5}{2}x + \frac{\nu_4}{2}y - z\right)x \\ &- \frac{M_z}{4I_{xx}}(S_{55}x + S_{45}y + 2S_{35}z)y + \frac{M_z}{4I_{yy}}(S_{45}x + S_{44}y + 2S_{34}z)x\,, \end{aligned} \qquad (4.c)$$

in which E ($=1/S_{33}$) is Young's modulus in the z-direction and ν_i are the cross-coupling coefficients defined as $\nu_i = -S_{i3}/S_{33}$, where ν_1 and ν_2 are the usual Poisson coefficients, and ν_4, ν_5, and ν_6 express the three-dimensional extension-shear coupling in the anisotropic beam. The above displacement results are in agreement with the plane-strain

solutions developed by Lekhnitskii (1963) for an anisotropic beam. One can see that the application of an extension force (P_z) will produce beam extension, shear deformation (as a result of ν_4 and ν_5), and deformations within the cross-section plane composed of Poisson contractions (from ν_1, ν_2) and shear (ν_6). Applying a bending moment (M_x, M_y) will produce beam bending as well as beam twisting (as a result of ν_4 and ν_5), in-plane cross-section deformations which include the formation of an anticlastic surface (ν_1, ν_2) and shearing (ν_6), and out-of-plane cross-section deformation that resembles torsion-type warping (bi-linear function) as a result of anisotropic material coupling (ν_4,ν_5). Finally, applying a torsion moment (M_z), will produce beam twisting as well as beam bending (as a result of ν_4 and ν_5) and shear deformation, in-plane cross-section deformations which include shearing and the formation of an anticlastic-type surface, and out-of-plane cross-section deformation associated with torsion-warping (bi-linear function).

Case II: Applied Flexure Load

The behavior of the homogeneous anisotropic cantilever beam subjected to applied flexural load (P_y) can be studied using the following stress functions (from Lekhnitskii (1963))

$$\psi_1 = P_y B_1 \left\{1 - \left(\frac{x}{a}\right)^2 - \left(\frac{y}{b}\right)^2\right\}^2, \qquad \psi_2 = -xP_y B_2 \left\{1 - \left(\frac{x}{a}\right)^2 - \left(\frac{y}{b}\right)^2\right\} - yP_y B_3 \left\{1 - \left(\frac{x}{a}\right)^2 - \left(\frac{y}{b}\right)^2\right\}, \quad (5.a,b)$$

where the coefficients (B_i , $i=1,2,3$), which are functions of the cross-section aspect ratio and the material definition, are determined by solving a set of linear algebraic equations. These three equations are presented in the Appendix (Eqns. *A*.1-14). The stress components written in terms of the stress functions are

$$\sigma_{xx} = \frac{\partial^2 \psi_1}{\partial y^2}, \qquad \sigma_{yy} = \frac{\partial^2 \psi_1}{\partial x^2},$$

$$\sigma_{zz} = -\frac{P_y}{2I_{xx}}\left\{2y(L - z) + \nu_5 xy + \nu_4 y^2 + \nu_4 \frac{I_{xx}}{A}\right\} + \nu_1 \sigma_{xx} + \nu_2 \sigma_{yy} + \nu_4 \tau_{yz} + \nu_5 \tau_{zx} + \nu_6 \tau_{xy}, \quad (6.a\text{–}f)$$

$$\tau_{yz} = -\frac{\partial \psi_2}{\partial x} + \frac{P_y b^2}{2I_{xx}}\left(1 - \left(\frac{x}{a}\right)^2 - \left(\frac{y}{b}\right)^2\right), \qquad \tau_{zx} = \frac{\partial \psi_2}{\partial y}, \qquad \tau_{xy} = -\frac{\partial^2 \psi_1}{\partial x\, \partial y}.$$

By substituting the stress functions (Eqns. 5.*a,b*) into (6.*a-f*), one can easily sees that: (1) the in-plane stresses (σ_{xx}, σ_{yy}, τ_{xy}) are nonzero as a result of anisotropy and only functions of the cross-section coordinates, (2) the normal stress (σ_{zz}) contains the classical strength of material term ($-P_y\ (L-z)\ y\ /\ I_{xx}$) and the remaining terms of (σ_{zz}) are inde-

pendent of (z) and produce a zero resultant when integrated over the cross-section area, and (3) the shear stresses (τ_{xz}, τ_{yz}) contain the classical isotropic terms and additional terms associated with anisotropy which are both independent of (z).

The displacement components (u,v,w) are determined by first substituting Eqns. (5.*a-f*) into (6.a-f), follow by substituting the resulting stresses into (2.*i*) and then integrating the strains, where the constants of integration are determined using the boundary conditions (1.*a-f*) at the root. Thus,

$$u = -\frac{P_y}{2E\,I_{xx}}\left\{(2\nu_1 x + \nu_6 y)\,y(z-L) + \frac{\nu_5}{2}yz(z-2L)\right\}$$
$$+\ P_y\left(a_{10}\,x + a_{01}\,y + a_{30}\,x^3 + a_{21}\,x^2\,y + a_{12}\,x\,y^2 + a_{03}\,y^3\right),$$

$$v = -\frac{P_y}{2E\,I_{xx}}\left\{\frac{z^2}{3}(z-3L) - \frac{\nu_5}{2}xz(z-2L) + \left(\nu_2\,y^2 - \nu_1\,x^2\right)(z-L)\right\} \qquad (7.a\text{-}c)$$
$$+\ P_y\left(b_{10}\,x + b_{01}\,y + b_{30}\,x^3 + b_{21}\,x^2\,y + b_{12}\,x\,y^2 + b_{03}\,y^3\right),$$

$$w = -\frac{P_y}{2\,E\,I_{xx}}\left((\nu_5 x + \nu_4 y)\,y(z-L) - yz(z-2L)\right) - \frac{\nu_4\,P_y}{2\,E\,A}z$$
$$+\ P_y\left(c_{10}\,x + c_{01}\,y + c_{30}\,x^3 + c_{21}\,x^2\,y + c_{12}\,x\,y^2 + c_{03}\,y^3\right),$$

where the coefficients a_{ij}, b_{ij}, and c_j (i,j = 0-3) are presented in the Appendix (Eqns. A.15-32) and the subscripts (i) and (j) refer to the order of the polynomial ($x^i\,y^j$). The above displacement distribution exactly describes the extension, bending, and twisting of the anisotropic cantilever beam as a result of an applied flexure force (P_x, P_y), as well as local in-plane cross-section deformations (all terms associated with a_{ij} and b_{ij}) and out-of-plane cross-section warping (all terms associated with c_{ij}). These solutions are in exact agreement with the results of (Kosmatka and Dong (1991)), where their model uses the finite element method to approximately determine the local cross-section deformations for an arbitrary cross-section.

ANISOTROPIC SHEAR CENTER

The '*shear center*' for a prismatic beam composed of an isotropic material is a

property of the cross-section and independent of beam-length. It is located using the classical definition (Griffith and Taylor (1917)), '*the load point that produces a zero mean value cross-section twist (i.e., zero twist about the centroidal axis)*'. In fact for doubly-symmetric cross-sections (including the current elliptical cross-section), the shear center of an isotropic prismatic beam is located at the centroid. For a prismatic beam composed of a generally anisotropic material (v_4, $v_5 \neq 0$), the classic definition is not applicable and we will develop a more appropriate definition.

The twist about the centroidal axis ($x=y=0$) for the cantilever beam subjected to a y-direction tip flexure load (P_2) offset from the centroid by an amount (x_s) is calculated using

$$\theta = \frac{1}{2}\left(\frac{\partial v}{\partial x} - \frac{\partial u}{\partial y}\right), \tag{8.a}$$

where (u, v) are found by combining Eqns. (4.*a,b*) and (7.*a,b*) with ($P_y=P_2$) and ($M_z=P_2x_s$);

$$\theta = \frac{P_2}{4I_{xx}}\left\{\underline{S_{35}(2L - z)} + x_s\left\{\underline{\underline{S_{44}\left(\frac{b}{a}\right)^2 + S_{55}}}\right\}\right\}z \ . \tag{8.b}$$

The single-underlined term, which is associated with anisotropic 'bend-twist' coupling (Kosmatka and Dong (1991)), is a quadratic variation of the cross-section twist as a result of the applied flexure force ($P_y=P_2$), whereas the double-underlined term represents a linear variation as a result of the applied torsion moment ($M_z=P_2x_s$). Since the cross-section twist varies quadratically along the beam-length, it is not possible to achieve zero twist along the entire beam-length. Instead the best that one can achieve is zero twist at two locations: the beam root ($z=0$) and the x-y plane that contains the applied load. Thus the x-direction '*anisotropic shear center*' location for the free-end of the cantilever beam is found by substituting ($z=L$) into Eq. (8.*b*) and finding the value of (x_s) that produces a zero cross-section twist ($\theta=0$):

$$x_s = -\frac{S_{35}}{\left(S_{44}\left(\frac{b}{a}\right)^2 + S_{55}\right)}L \ , \tag{9}$$

where the location depends upon the beam-length and reduces to the classic definition (centroid) for isotropic materials. The variation of the cross-section twist over the beam-length is found by substituting Eq. (9) into (8.*b*)

$$\theta = \frac{P_2L^2S_{35}}{4I_{xx}}\left(\frac{z}{L}\right)\left\{1 - \left(\frac{z}{L}\right)\right\} \ , \tag{10}$$

where the twist is zero at the beam root and tip (load plane) and reaches a maximum at the beam mid-length (Fig.2).

The *y*-direction component of the shear center can be found in a similar fashion by applying an *x*-direction flexure force (P_1) that is offset form the centroid by an amount (y_s). Finally we formally define the '*anisotropic shear center*' as; "*the load point that produces general bending and twisting of an anisotropic beam with zero mean value twist (zero twist about the centroid) in the cross-section plane that contains the applied load.*"

SHEAR DEFORMATION

An examination of the displacement components of Eqns. (4.*a-c*) and (7.*a-c*) reveals that the deformation of the centroidal axis (x=y=0) agrees with the standard strength of materials solutions, but that the additional displacement associated with shear deformation is not included. This occurs because our original root boundary conditions (Eqns (1.*a-f*)) assume that the slope of the centroidal axis is zero ($\partial u/\partial z = \partial v/\partial z = 0$) as opposed to fixing the rotation of the root cross-section ($\partial w/\partial x = \partial w/\partial y = 0$). This additional displacement associated with shear deformation can be included by simply rotating the deformed beam so that slope of the deformed root cross-section at (x=y=0) is coincident with the *x-y* plane, and thus the deformed centroidal axis will have a nonzero root slope (see Timoshenko and Goodier (1970) for further details). These rotation angles are equal to the shear strains (γ_{xz}, γ_{yz}) at the beam root centroid (x=y=z=0). Calculating the rotational angles using Eqns. (4.*a-c*) and (7.*a-c*):

$$\phi_x = \gamma_{yz}\Big|_{x=y=z=0} = P_y(c_{01}) - P_z\left\{\frac{v_4}{EA}\right\}, \qquad \phi_y = \gamma_{xz}\Big|_{x=y=z=0} = P_y(c_{10}) - P_z\left\{\frac{v_5}{EA}\right\}, \quad (11.a,b)$$

where shear deformation for a homogeneous anisotropic beam occurs as a result of applied extension and flexure, but not applied bending or torsion. The final form of the displacements distributions that includes shear deformation is found by modifying the displacements (u,v,w) of Eqns. (4.*a-c*, 7.*a-c*) in the following manner:

$$\tilde{u} = u + z\,\phi_y, \qquad \tilde{v} = v + z\,\phi_x, \qquad \tilde{w} = w - y\,\phi_x - x\,\phi_y. \qquad (12.a\text{-}c)$$

NUMERICAL EXAMPLES

In this section, three detailed numerical examples are presented to show how material orthotropy or anisotropy effects the local in-plane deformation and warping of the cross-section, the shear center location, and the shear stress distribution. Only the behavior of the beam as a result of an applied flexure force (P_y) will be studied, since beam be-

havior as a result of extension (P_z), torsion (M_z), and bending (M_x, M_y) has been studied in detail by Lekhnitskii (1963) and Kosmatka and Dong (1991).

The beam is assumed to be composed of a single set of unidirectional high strength graphite/epoxy fibers, which is a transversely isotropic material that has five independent constants (see Table 1) with a sixth constant that is equal to $G_{23} = E_{22}/(2(1+\nu_{23}))$. To achieve orthotropic and/or anisotropic beam behavior, the material reference frame (1,2,3) is oriented relative to the beam Cartesian coordinate frame (x,y,z) using reference angles (β) and (α), which are defined as rotations about the positive z-axis and the positive material 3-axis, respectively. See Fig. 3, where the transformation relation between (1,2,3) and (x,y,z) is equal to

$$\begin{Bmatrix} 1 \\ 2 \\ 3 \end{Bmatrix} = \begin{bmatrix} \sin(\alpha)\cos(\beta) & \sin(\alpha)\sin(\beta) & \cos(\alpha) \\ \cos(\alpha)\cos(\beta) & \cos(\alpha)\sin(\beta) & -\sin(\alpha) \\ -\sin(\beta) & \cos(\beta) & 0 \end{bmatrix} \begin{Bmatrix} x \\ y \\ z \end{Bmatrix} . \qquad (13)$$

The resulting 21 unique material compliance coefficients (S_{ij}, i,j=1-6) are determined using standard transformation techniques (see Lekhnitskii, 1963).

Example 1

In this example, the local cross-section deformation and the shear center location are studied as a function of material orthotropy and cross-section aspect ratio. Material orthotropy is introduced by rotating the fiber set in the x-z plane using the reference angle (α), while holding (β=0). Note that, in this situation, $S_{i4}=S_{i6}=0$ (i=1–3,5) and $\nu_4=\nu_6=0$.

The coefficients (B_i, i = 1,2,3) are determined using Eq. (*A*.1) as $B_1 = B_3 = 0$ and

$$B_2 = \frac{1}{A}\left\{\frac{S_{35}^2 - 4S_{13}S_{33} + 2S_{33}S_{44}\left(\frac{b}{a}\right)^2}{S_{35}^2 - S_{33}S_{55} - 3S_{33}S_{44}\left(\frac{b}{a}\right)^2}\right\} . \qquad (14)$$

The local deformation within the cross-section (x-y) plane and warping out of the cross-section plane as a result of an applied flexural force (P_y) is characterized in the u, v, and w directions, using Eqns. (7.*a*-*c*), as simply

$$P_y\left(a_{01}y + a_{21}x^2y + a_{03}y^3\right), \quad P_y\left(b_{10}x + b_{12}xy^2 + b_{30}x^3\right), \quad P_y\left(c_{01}y + c_{21}x^2y + c_{03}y^3\right), \quad (15.a\text{-}c)$$

where the other deformation coefficients (a_{ij}, b_{ij}, c_{ij}) are zero for (β=0). In Figs. 4 through 11, the nonzero coefficients are presented as a function of orientation angle (α) and

aspect ratio (b/a), where they have been nondimensionalized using either ($E_{11}A$) or ($E_{11}I_{xx}$). For this material, all of the deformation coefficients are independent of aspect ratio (b/a) for α=8° and 60°. The coefficients a_{01} and b_{10}, which define the uniform in-plane cross-section shear, are presented in Fig. 4, where positive values can be obtained for thin cross-sections (b/a=0.1) with 18°<α <39°. In Figs. 5 and 6, the coefficients (a_{21} and b_{30}) which are associated with (x^2) variations in (γ_{xy}) are presented. These two coefficients, which have relatively large magnitudes and opposite signs, represent a significant amount of in-plane cross-section deformation associated with relatively low (γ_{xy}). The remaining coefficients (a_{03} and b_{12}), which are associated with (y^2) variations in (γ_{xy}), are presented in Figs. 7 and 8. Although these coefficients are generally smaller than a_{21} and b_{30}, they are associated with a larger component of (γ_{xy}). For thin cross-sections (b/a=0.1), a_{03} reaches a positive maximum at 60°, b_{12} reaches a negative maximum at approximately 33°, and the resulting component associated with (y^2) variations in (γ_{xy}) reaches a positive maximum at 60° and a negative maximum at 30°. Whereas for thicker cross-sections (b/a=1.0,10.0), the component associated with (y^2) variations in (γ_{xy}) is always positive and reaches a maximum at 45°.

The coefficient (c_{01}), which is proportional to the amount of y-direction shear deformation associated with P_y (see Eq. 11.*a*), is presented in Fig. 9, where for thin cross-sections (b/a=0.1) this term is becomes negative for 18°<α <39°. The out of plane warping constant (c_{21}), which is always negative for thin cross-sections (b/a=0.10), is presented in Fig. 10. The remaining out of plane warping constant (c_{03}) is presented in Fig. 11, where it is always negative for all but the thinnest cross-sections.

The '*anisotropic shear center location*' of the beam tip cross-section (z=L) as a result of an applied transverse tip load (P_2) can be determined by substituting the definition of the compliance coefficients with (β=0) into Eq. (9)

$$x_s = \frac{L}{2}\left\{\frac{\left(\frac{1}{E_{22}}-\frac{1}{E_{11}}\right)\sin(2\alpha)+\left(\frac{1}{G_{13}}-\frac{1}{E_{11}}(1+2\nu_{13})-\frac{1}{E_{22}}\right)\frac{\sin(4\alpha)}{2}}{\frac{\cos^2(2\alpha)}{G_{13}}+(1+\frac{E_{11}}{E_{22}}+2\nu_{13})\frac{\sin^2(2\alpha)}{E_{11}}+\left(\frac{b}{a}\right)^2\left(\frac{\cos^2(\alpha)}{G_{13}}+\frac{2(1+\nu_{23})\sin^2(\alpha)}{E_{22}}\right)}\right\}, \quad (16)$$

where the results are presented in Fig. 12 as a function of orientation angle (α), aspect ratio (b/a), and normalized to the beam length (L). For (α=0°) and (80°<α<90°) the shear center is located at the centroid (i.e. isotropic shear center). For (0°<α<80°), the anisotropic shear center is offset from the centroid, with the maximum offset occurring near (α=40°) for thin cross-sections (b/a=0.1) and approaches (30°) for circular (b/a=1) and thicker cross-sections (b/a=5). As an illustration, the anisotropic shear center of a

slender beam (L/a=10) with a thin cross-section (b/a=0.10) and (α=40°) can be found using Eq. (16) or Fig. 12 as $x_s = 4.8a$, which is well outside the cross-section. Furthermore, doubling the beam length (L/a=20), will double the offset to the shear center location (x_s=9.6a). A simplified form of the shear center location for small orientation angles (α) can be found by taking a Taylor series expansion of Eq. (16)

$$x_s = \frac{\left\{1 - 2\frac{G_{13}}{E_{11}}(1 + \nu_{13})\right\}}{1 + \left(\frac{b}{a}\right)^2} \alpha L \ . \tag{17}$$

Example 2

A second example is presented to explain why the added displacement associated with shear deformation ($c_{01}L$) can be negative for a thin (b/a=0.1) tip loaded (P_y) cantilever beam composed of off-angle unidirectional graphite/epoxy with 18°<α <39° and β=0°. See Fig. 9. Thus the inclusion of shear deformation makes the beam stiffer, as opposed to more flexible as one normally sees in plate bending. From Eqn. (*A*.28),

$$c_{01} = \beta_{44}\left(\frac{2}{A} + B_2\right), \tag{18}$$

where this unusual situation occurs whenever (B_2 < -2/A), since β_{44} which equals S_{44} for ($\alpha \neq 0$, β=0) is always greater than zero. Substituting Eqns (5.*a*,*b*) into (6.*d*), the transverse shear stress (τ_{yz}) can be written as

$$\tau_{yz} = P_y\left\{\left(\frac{2}{A} + B_2\right)\left(1 - \left(\frac{y}{b}\right)^2\right) - \left(\frac{2}{A} + 3B_2\right)\left(\frac{x}{b}\right)^2\right\}, \tag{19}$$

where the shear stress (τ_{yz}) at the centroid (x=y=0) will be negative whenever B_2 < -2/A. The transverse shear stress (τ_{yz}) distribution for two slices of a beam element (dz) is presented in Fig. 13, where the stresses are small and negative near the centroid and large and positive near the outer edges (x=±a) so that the integral of (τ_{yz}) over the cross-section will equal (P_y). This situation is typical for elliptical cross-sections and will not occur for rectangular (plate-like) cross-sections, since (τ_{yz}=0) on the upper and lower surfaces of the rectangular (plate-like) cross-section to satisfy the traction free boundary conditions.

An expression can be developed to define the bounds on this unusual condition by substituting Eq. (14) into (20) and rearranging

$$\left(\frac{b}{a}\right)^2 < \frac{3S_{35}^2 - 2S_{33}(S_{55} + 2S_{13})}{4S_{33}S_{44}} \ . \tag{20}$$

For an isotropic beam, the above expression reduces to $(b/a)^2 < -1/(2(1+\nu))$ and thus this condition will not occur. For an anisotropic beam composed of off-angle uni-directional S-glass/epoxy (E_{11} = 55 GPa, $E_{22}=E_{33}$=16 GPa, $G_{12}=G_{13}$=7.6 GPa, $\nu_{12}=\nu_{13}$=0.28), the normalized shear deformation coefficient (c_{01}) is presented in Fig. 14 for a broad range of (α) and (b/a). It can be seen that this unusual condition does not occur and thus the inclusion of shear deformation will only make the beam more flexible. This can be traced to the fact that S-glass/epoxy is closer to an isotropic material than the graphite/epoxy of example 1. It is interesting to note that for S-glass/epoxy, all of the deformation coefficients are independent of aspect ratio (b/a) for α =22° and 55° and the width between these two points is smaller than that of the graphite/epoxy. Finally, as one chooses a material that closely resembles an isotropic material ($G_{12} \approx E_{11}/(2(1+\nu_{12}))$), then these two points disappear so that all curves are independent of (α).

Example 3

In this final example, the local cross-section deformation and the shear stress distribution are studied for the case of a general anisotropic ($\alpha,\beta \neq 0$) beam composed of graphite/epoxy (Table 1) and subjected to a flexural force (P_y). For this general case, all three coefficients (B_i, i=1-3) and all eighteen deformation coefficients (a_{ij}, b_{ij}, c_{ij}, i,j=1-3) are nonzero. The local in-plane deformations and the out-of-plane warping of the cross-section are presented in Fig. 15.a,b for the case of (b/a=0.5) with orientation angles of (α=30°) and (β=60°). The local in-plane deformation (Fig. 15.*a*) is represented by a nonsymmetric shape that is dependent upon the material orientation angles (α,β). The out-of-plane warping (Fig. 15.*b*), which does not resemble the symmetric cubic-like warping of an isotropic beam (Sokolnikoff, 1956), is divided into six alternating regions of positive (solid lines) and negative (dashed lines) deformations. The effects associated with the shear deformation coefficients (c_{10}, c_{01}) are not included in Fig. (15.*b*) because they produce only a rigid cross-section rotation and no cross-section deformation.

A quantitative vectorial scaled plot of the transverse shear stresses (τ_{zx}, τ_{yz}) for (a/b=0.5) with orientation angles of (α=30°) and (β=30°) is presented in Fig. 16. From this figure, it is interesting to see that the stress distribution does not resemble that of an isotropic beam (i.e. a paraboloid with the maximum occurring at the centroid). Instead, the distribution is nonsymmetric with the maximum occurring on the outer edge.

CONCLUSION

The complete St Venant elastic displacement and stress distributions are devel-

oped, based upon the theory of elasticity, for a tip-loaded homogeneous cantilever beam having an elliptical cross-section and rectilinear anisotropy. The displacement distributions are found by integrating the strain distributions, where the local in-plane deformation and out-of-plane warping of the cross-section are exactly determined. A definition for the *'anisotropic shear center'* is presented based upon extending the classical definition for isotropic beams. The additional transverse beam displacement associated with shear deformation is determined for applied extension and flexure loads. Numerical results are presented which show for the flexural behavior of an orthotropic ($\alpha \neq 0, \beta = 0$) beam that the local in-plane deformation and out-of-plane warping are highly dependent upon fiber orientation and cross-section aspect ratio, where for two orientations the local deformations are completely independent of cross-section aspect ratio. The anisotropic shear center location is linearly dependent upon beam length and can be located outside the cross-section depending upon the fiber orientation. Moreover, the added transverse displacement associated with shear deformation can actually be negative for certain beam aspect ratios and material definitions so that the inclusion of shear deformation may actually make the beam stiffer, as opposed to more flexible. Finally, the local cross-section deformations and the transverse shear stress distributions bear no resemblance to their isotropic counterparts.

REFERENCES

Griffith, A. A. and Taylor, G. I. (1917). The Problem of Flexure and Its Solution by the Soap-Film Method, *Reports and Memoranda Adv. Comm. Aeronautics*, No. **339**, 1-13.

Kosmatka, J. B. and Dong, S. B. (1991). Saint-Venant Solutions for Prismatic Anisotropic Beams, *Int. J. Solids Structures*, **28** (7), 917-938.

Lekhnitskii, S.G. (1963). *Theory of Elasticity of an Anisotropic Elastic Body* . (Translated by P. Fern) , Holden-Day, Inc., San Francisco.

Sokolnikoff, I. S. (1956). *Mathematical Theory of Elasticity*, 2nd Edn. McGraw-Hill, New York.

Timoshenko, S. P. and Goodier, J. N. (1970). *Theory of Elasticity.* 3rd Edn. McGraw-Hill Book Co., New York.

Appendix

The constants (B_i, $i = 1,2,3$) are determined by solving

$$\begin{bmatrix} G_{11} & G_{12} & G_{13} \\ G_{21} & G_{22} & G_{23} \\ G_{31} & G_{32} & G_{33} \end{bmatrix} \begin{Bmatrix} B_1 \\ B_2 \\ B_3 \end{Bmatrix} = \begin{Bmatrix} H_1 \\ H_2 \\ H_3 \end{Bmatrix} \qquad (A.1)$$

where the coefficents of [G] and [H] are defined as:

$$G_{11} = \frac{4}{a^2}\left(3\beta_{11}\left(\frac{a}{b}\right)^2 + 3\beta_{22}\left(\frac{b}{a}\right)^2 + 2\beta_{12} + \beta_{66}\right), \quad G_{12} = -\left(3\beta_{24}\left(\frac{b}{a}\right)^2 + \beta_{14} + \beta_{56}\right),$$

$$G_{13} = \left(3\beta_{15} + (\beta_{25} + \beta_{46})\left(\frac{b}{a}\right)^2\right), \quad G_{21} = -\frac{4}{a^2}\left(\beta_{14} + 3\beta_{24}\left(\frac{b}{a}\right)^2 + \beta_{56}\right),$$

$$G_{22} = \left(3\beta_{44}\left(\frac{b}{a}\right)^2 + \beta_{55}\right), \quad G_{23} = -\left(2\beta_{45}\left(\frac{b}{a}\right)^2\right), \qquad (A.2\text{-}A.10)$$

$$G_{31} = \frac{4}{a^2}\left(\beta_{25} + \beta_{46} + 3\beta_{15}\left(\frac{a}{b}\right)^2\right), \quad G_{32} = -2\beta_{45},$$

$$G_{33} = \left(\beta_{44}\left(\frac{b}{a}\right)^2 + 3\beta_{55}\right),$$

$$H_1 = -\frac{2}{A}\left\{(S_{14} - 2\beta_{14}) - \frac{1}{2}(S_{56} - \beta_{56}) - \beta_{24}\left(\frac{b}{a}\right)^2\right\},$$

$$H_2 = -\frac{2}{A}\left\{\frac{1}{2}(S_{55} - \beta_{55}) - 2S_{13} + \beta_{44}\left(\frac{b}{a}\right)^2\right\}, \qquad (A.11\text{-}13)$$

$$H_3 = -\frac{2}{A}\left\{\frac{1}{2}(S_{45} - 3\beta_{45}) - S_{36}\right\},$$

and

$$\beta_{ij} = S_{ij} - \frac{S_{3i}\,S_{3j}}{S_{33}}. \qquad (A.14)$$

The x-direction deformation coefficients associated with an applied flexure load:

$$a_{10} = -4B_1\left\{\frac{\beta_{12}}{a^2} + \frac{\beta_{11}}{b^2}\right\} + B_2\{\beta_{14}\} - B_3\{\beta_{15}\} + \frac{\nu_1\nu_4}{2EA} + \frac{\beta_{14}b^2}{2I_{xx}},$$

$$a_{01} = -2B_1\left\{\frac{\beta_{16}}{b^2} + \frac{\beta_{26}}{a^2}\right\} + B_2\left\{\frac{\beta_{46}}{2}\right\} - B_3\left\{\frac{\beta_{56}}{2}\right\} + \frac{\nu_4\nu_6}{4EA} + \frac{\beta_{46}b^2}{4I_{xx}}, \qquad (A.15\text{-}18)$$

$$a_{30} = \frac{4B_1}{a^2}\left\{\frac{\beta_{11}}{3b^2} + \frac{\beta_{12}}{a^2}\right\} - B_2\left\{\frac{\beta_{14}}{a^2}\right\} + B_3\left\{\frac{\beta_{15}}{3a^2}\right\} - \frac{\beta_{14}}{6I_{xx}}\left(\frac{b}{a}\right)^2,$$

$$a_{21} = -B_1\left\{\frac{4\beta_{16}}{a^2b^2}\right\} + B_2\left\{\frac{\beta_{15}}{b^2}\right\} - B_3\left\{\frac{\beta_{14}}{a^2}\right\} + \frac{\nu_1\nu_5}{4EI_{xx}},$$

$$a_{12} = \frac{4B_1}{b^2}\left\{\frac{3\beta_{11}}{b^2} + \frac{\beta_{12}}{a^2}\right\} - B_2\left\{\frac{\beta_{14}}{b^2}\right\} + B_3\left\{\frac{3\beta_{15}}{b^2}\right\} + \frac{\nu_1\nu_4}{2EI_{xx}} - \frac{\beta_{14}}{2I_{xx}},$$

$$a_{03} = \frac{4B_1}{b^2}\left\{\frac{\beta_{16}}{b^2} + \frac{2\beta_{26}}{3a^2}\right\} - B_2\left\{\frac{\beta_{25}+\beta_{46}}{3b^2}\right\} + B_3\left\{\frac{\beta_{24}}{3a^2} + \frac{\beta_{56}}{b^2}\right\} + \frac{4\nu_4\nu_6 - \nu_2\nu_5}{12EI_{xx}} - \frac{S_{46}}{6I_{xx}}, \qquad (A.19\text{-}20)$$

The *y*-direction deformation coefficients associated with an applied flexure load:

$$b_{10} = -2B_1\left\{\frac{\beta_{16}}{b^2} + \frac{\beta_{26}}{a^2}\right\} + B_2\left\{\frac{\beta_{46}}{2}\right\} - B_3\left\{\frac{\beta_{56}}{2}\right\} + \frac{\nu_4\nu_6}{4EA} + \frac{\beta_{46}b^2}{4I_{xx}},$$

$$b_{01} = -4B_1\left\{\frac{\beta_{12}}{b^2} + \frac{\beta_{22}}{a^2}\right\} + B_2\{\beta_{24}\} - B_3\{\beta_{25}\} + \frac{\nu_2\nu_4}{2EA} + \frac{\beta_{24}b^2}{2I_{xx}},$$

$$b_{30} = \frac{4B_1}{a^2}\left\{\frac{2\beta_{16}}{3b^2} + \frac{\beta_{26}}{a^2}\right\} - B_2\left\{\frac{\beta_{15}}{3b^2} + \frac{\beta_{46}}{a^2}\right\} + B_3\left\{\frac{\beta_{14}+\beta_{56}}{3a^2}\right\} - \frac{\nu_1\nu_5}{12EI_{xx}} - \frac{\beta_{46}}{6I_{xx}}\left(\frac{b}{a}\right)^2,$$

$$b_{21} = \frac{4B_1}{a^2}\left\{\frac{3\beta_{22}}{a^2} + \frac{\beta_{12}}{b^2}\right\} - B_2\left\{\frac{3\beta_{24}}{a^2}\right\} + B_3\left\{\frac{\beta_{25}}{a^2}\right\} - \frac{\beta_{24}}{2I_{xx}}\left(\frac{b}{a}\right)^2, \qquad (A.21\text{-}26)$$

$$b_{12} = -B_1\left\{\frac{4\beta_{26}}{a^2b^2}\right\} + B_2\left\{\frac{\beta_{25}}{b^2}\right\} - B_3\left\{\frac{\beta_{24}}{a^2}\right\} + \frac{\nu_2\nu_5}{4EI_{xx}},$$

$$b_{03} = \frac{4B_1}{b^2}\left\{\frac{\beta_{22}}{3a^2} + \frac{\beta_{12}}{b^2}\right\} - B_2\left\{\frac{\beta_{24}}{3b^2}\right\} + B_3\left\{\frac{\beta_{25}}{b^2}\right\} + \frac{\nu_2\nu_4}{6EI_{xx}} - \frac{\beta_{24}}{6I_{xx}}.$$

The out-of-plane deformation coefficients associated with an applied flexure load:

$$c_{10} = -4B_1\left\{\frac{\beta_{15}}{b^2} + \frac{\beta_{25}}{a^2}\right\} + B_2\{\beta_{45}\} - B_3\{\beta_{55}\} + \frac{\nu_4\nu_5}{2EA} + \frac{\beta_{45}b^2}{2I_{xx}},$$

$$c_{01} = -4B_1\left\{\frac{\beta_{14}}{b^2} + \frac{\beta_{24}}{a^2}\right\} + B_2\{\beta_{44}\} - B_3\{\beta_{45}\} + \frac{(\nu_4)^2}{2EA} + \frac{\beta_{44}b^2}{2I_{xx}}, \qquad (A.27\text{-}29)$$

$$c_{30} = \frac{4B_1}{a^2}\left\{\frac{\beta_{15}}{3b^2} + \frac{\beta_{25}}{a^2}\right\} - B_2\left\{\frac{\beta_{45}}{a^2}\right\} + B_3\left\{\frac{\beta_{55}}{3a^2}\right\} - \frac{\beta_{45}}{6I_{xx}}\left(\frac{b}{a}\right)^2,$$

$$c_{21} = -B_1\left\{\frac{4\beta_{56}}{a^2b^2}\right\} + B_2\left\{\frac{\beta_{55}}{b^2}\right\} - B_3\left\{\frac{\beta_{45}}{a^2}\right\} + \frac{2\nu_1 + (\nu_5)^2}{4EI_{xx}},$$

$$c_{12} = \frac{2B_1}{b^2}\left\{\frac{3\beta_{15}}{b^2} + \frac{\beta_{25}-\beta_{46}}{a^2}\right\} - B_3\left\{\frac{\beta_{44}}{2a^2} - \frac{3\beta_{55}}{2b^2}\right\} + \frac{3\nu_4\nu_5 + 2\nu_6}{8EI_{xx}} - \frac{\beta_{45}}{4I_{xx}}, \qquad (A.30\text{-}32)$$

$$c_{03} = \frac{4B_1}{b^2}\left\{\frac{\beta_{14}}{b^2} + \frac{\beta_{24}}{3a^2}\right\} - B_2\left\{\frac{\beta_{44}}{3b^2}\right\} + B_3\left\{\frac{\beta_{45}}{b^2}\right\} + \frac{\nu_2 + (\nu_4)^2}{6EI_{xx}} - \frac{\beta_{44}}{6I_{xx}}.$$

Table 1: Typical Material Properties of High-Strength Graphite/Epoxy.

E_{11}	145.0 GPa
$E_{22} = E_{33}$	10.0 GPa
$G_{12} = G_{13}$	4.8 GPa
$\nu_{12} = \nu_{13}$	0.25
ν_{23}	0.40

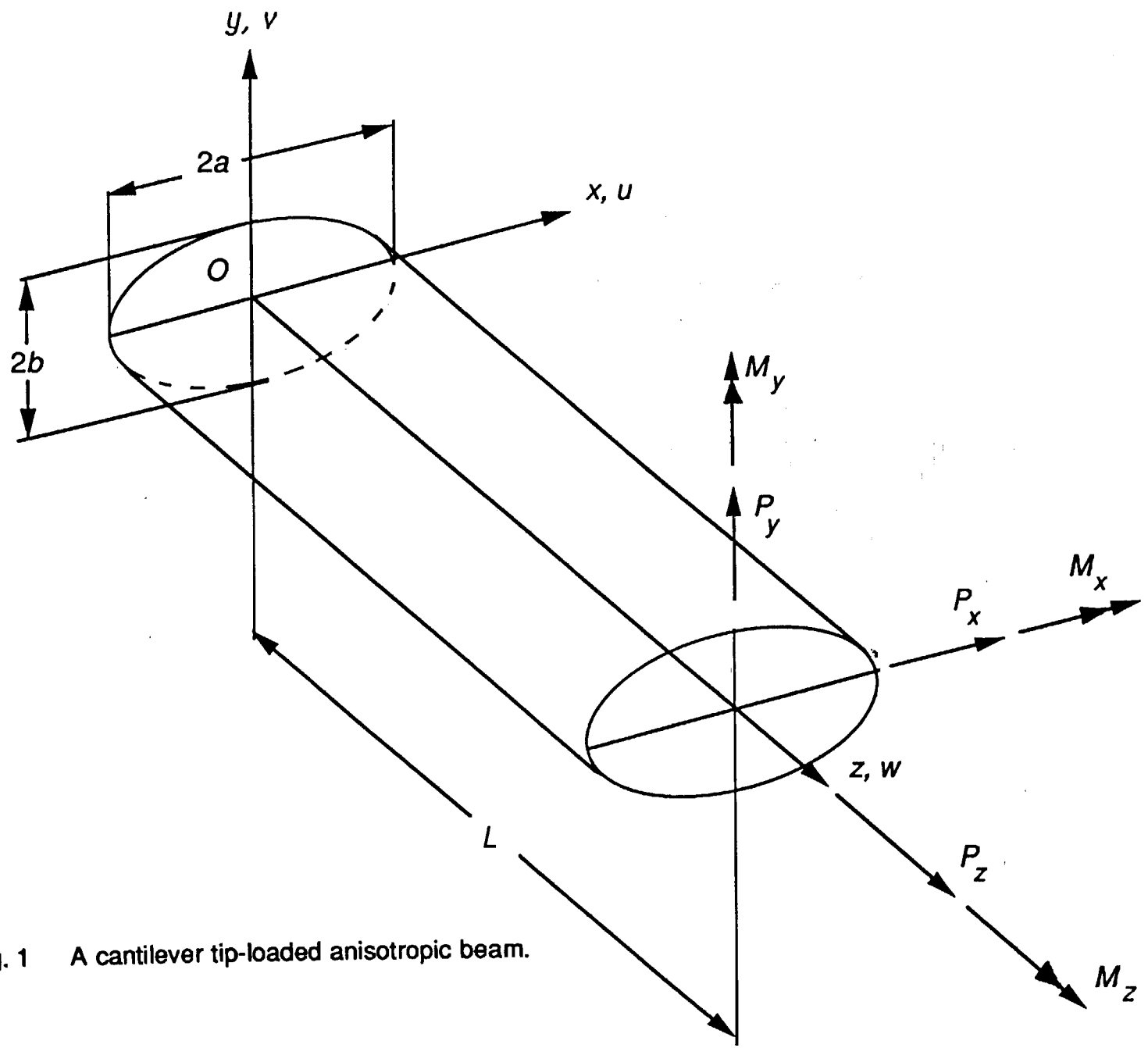

Fig. 1 A cantilever tip-loaded anisotropic beam.

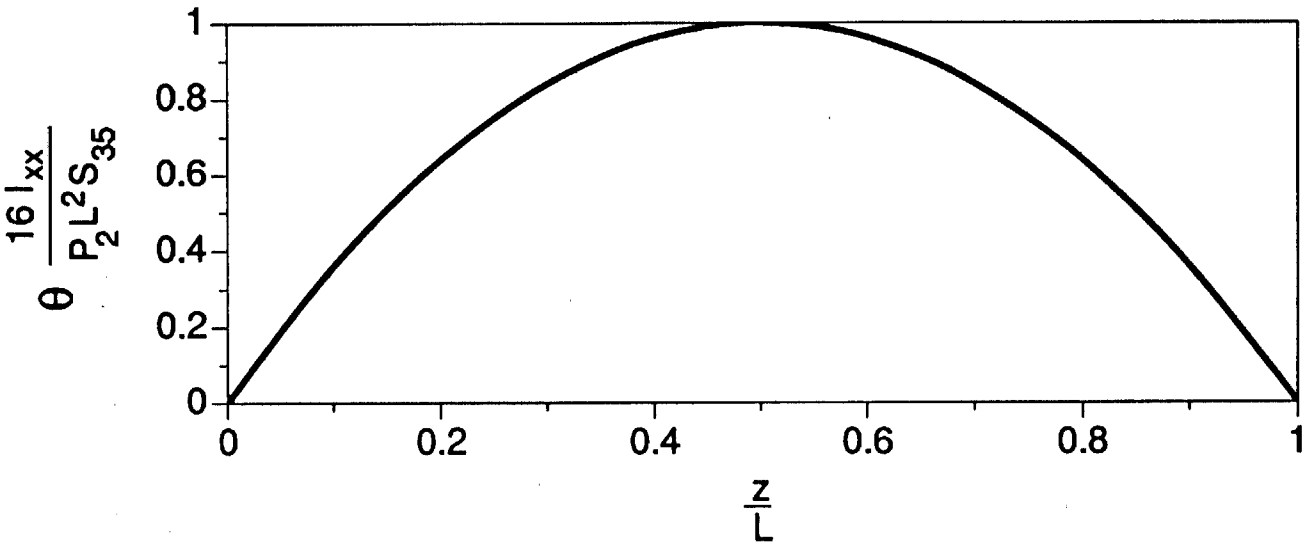

Fig. 2 Variation of beam twist (θ) with P_2 acting through the shear center of the tip (z=L) cross-section.

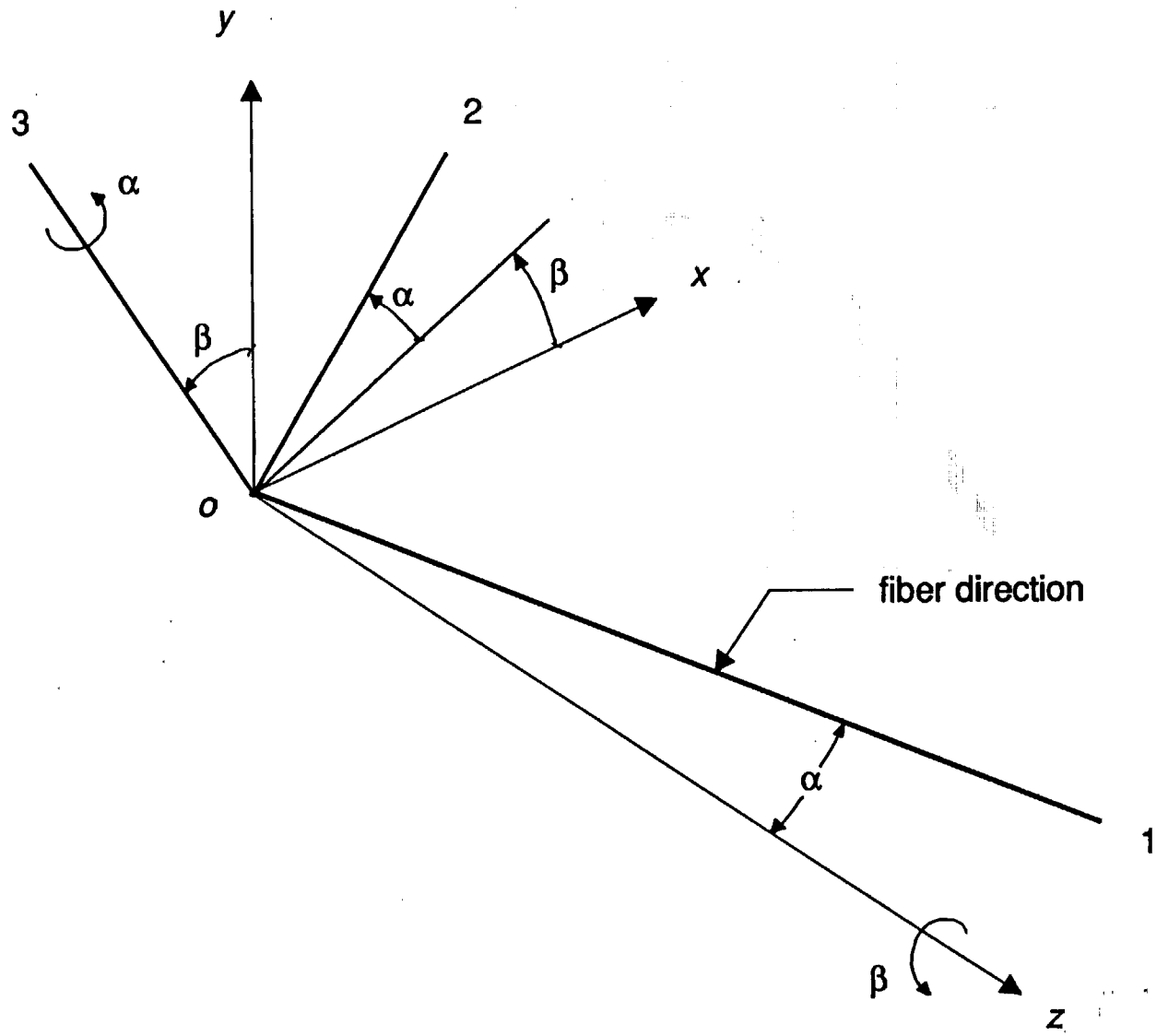

Fig. 3 Orientation of material fibers (1,2,3) relative to Cartesian frame (*x,y,z*).

Fig. 3

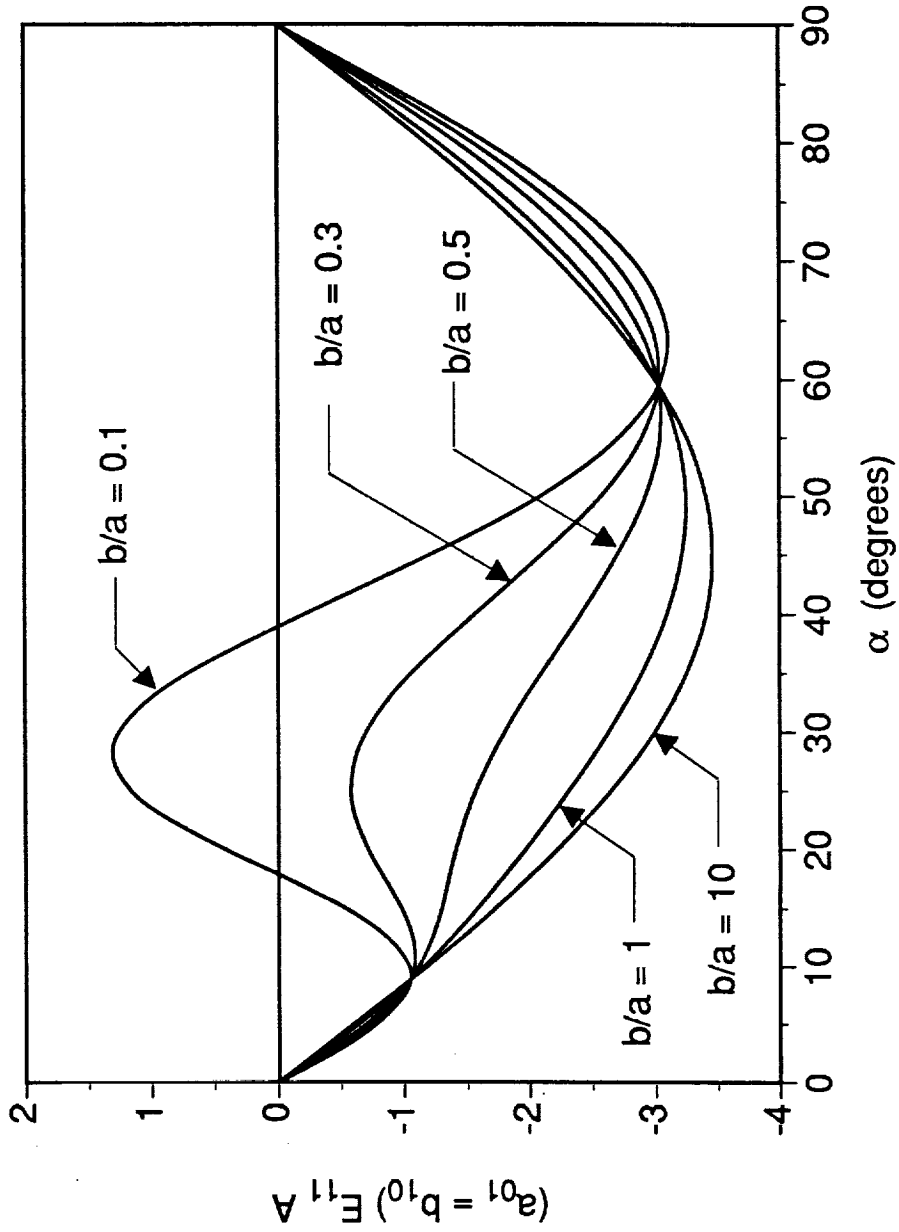

Fig. 4 Nondimensionalized in-plane coefficients (a_{01}, b_{10}) with (α), (β=0).

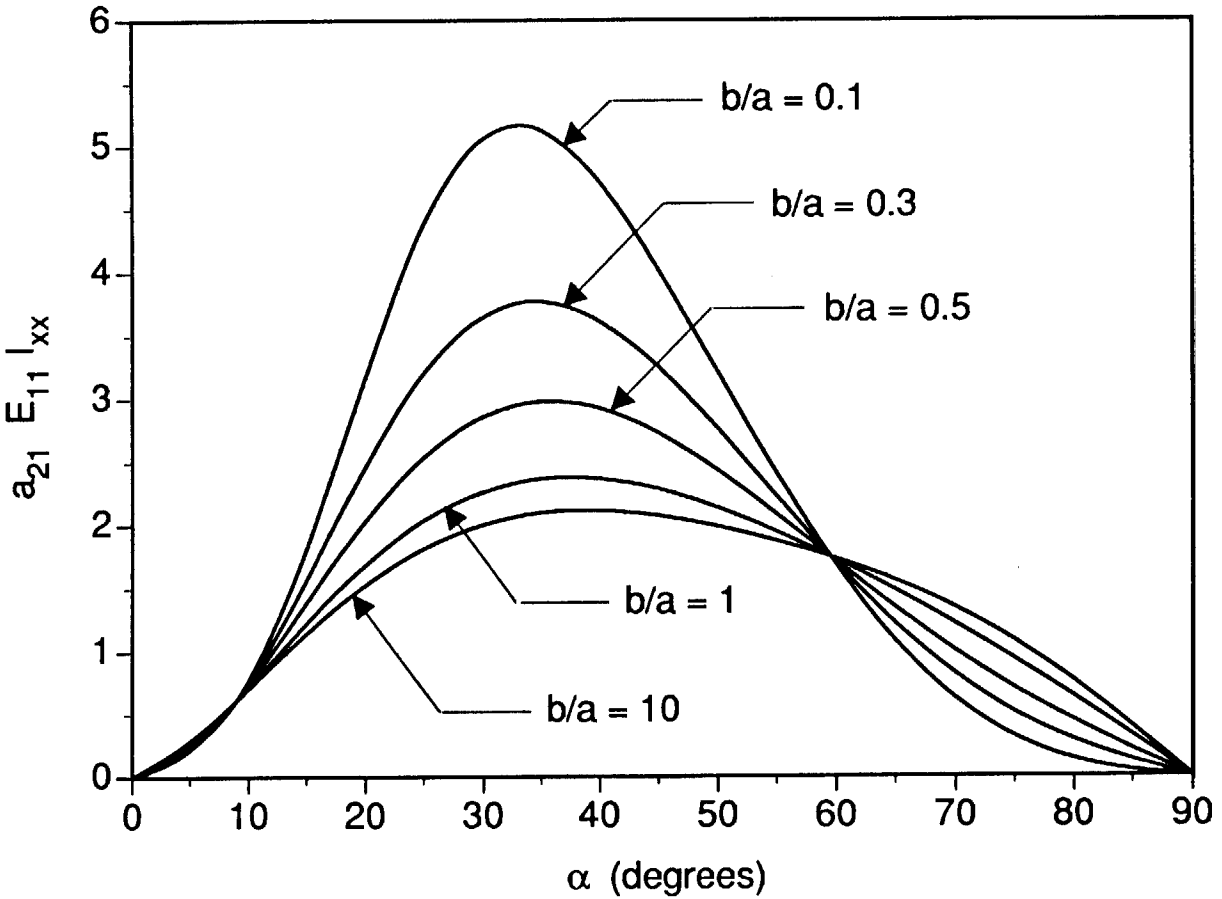

Fig. 5 Nondimensionalized in-plane coefficient (a_{21}) with (α), (β=0).

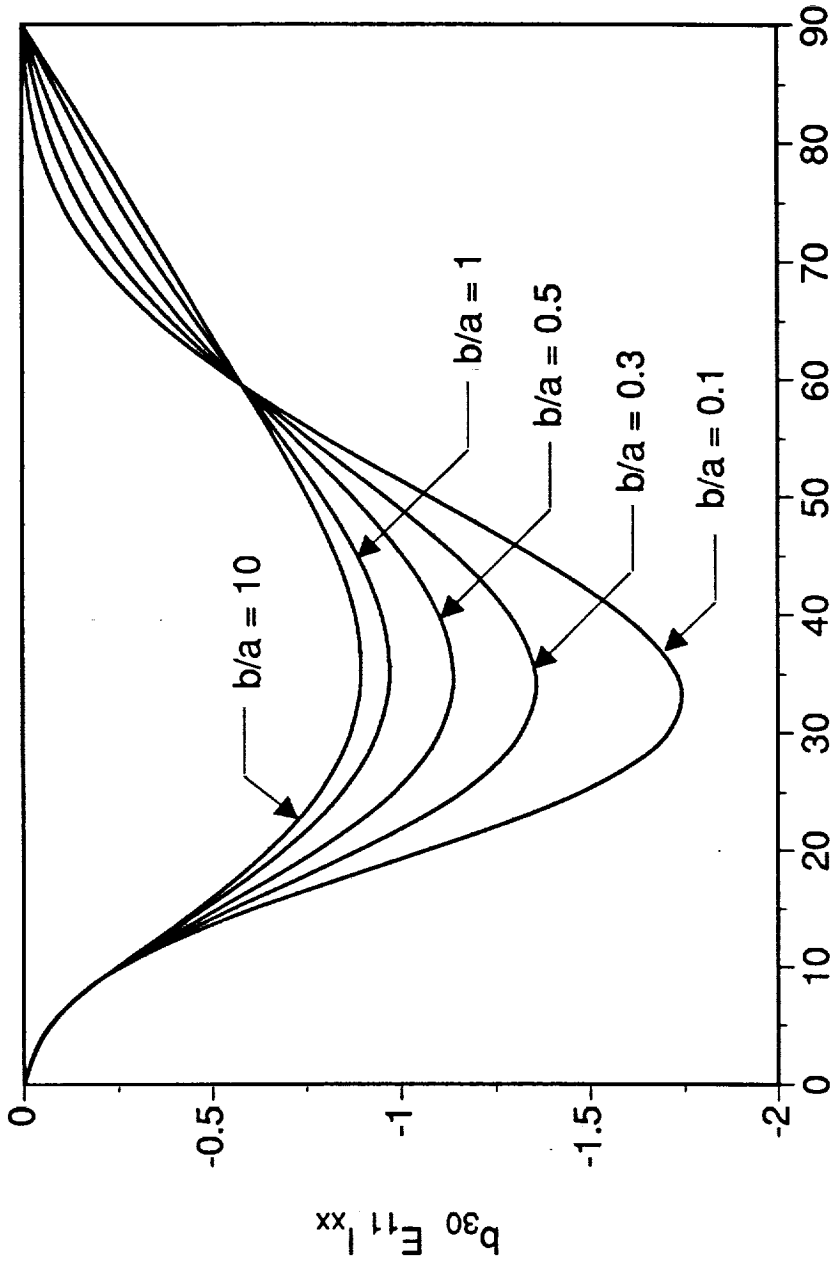

Fig. 6 Nondimensionalized in-plane coefficient (b_{30}) with (α), (β=0).

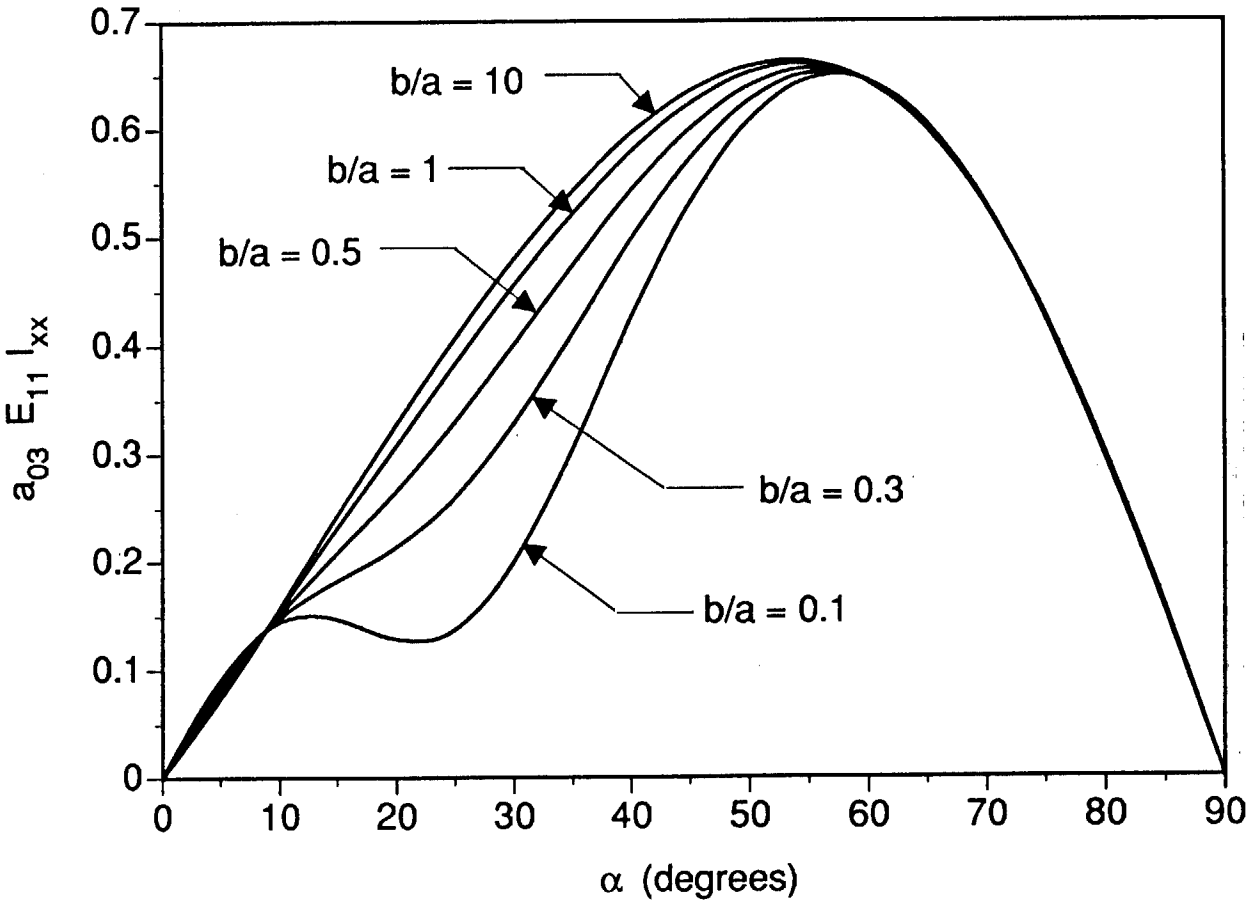

Fig. 7 Nondimensionalized in-plane coefficient (a_{03}) with (α), (β=0).

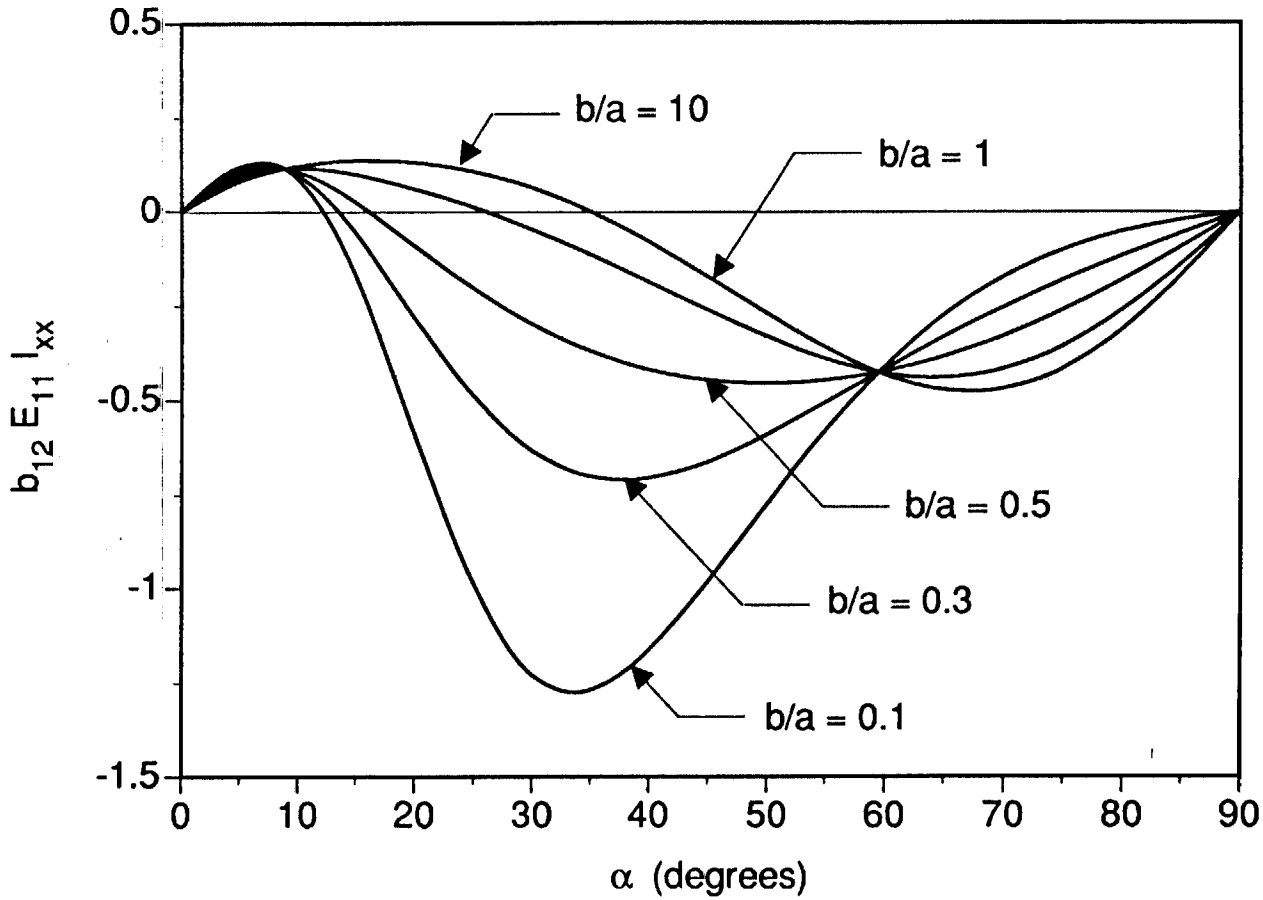

Fig. 8 Nondimensionalized in-plane coefficient (b_{12}) with (α), (β=0).

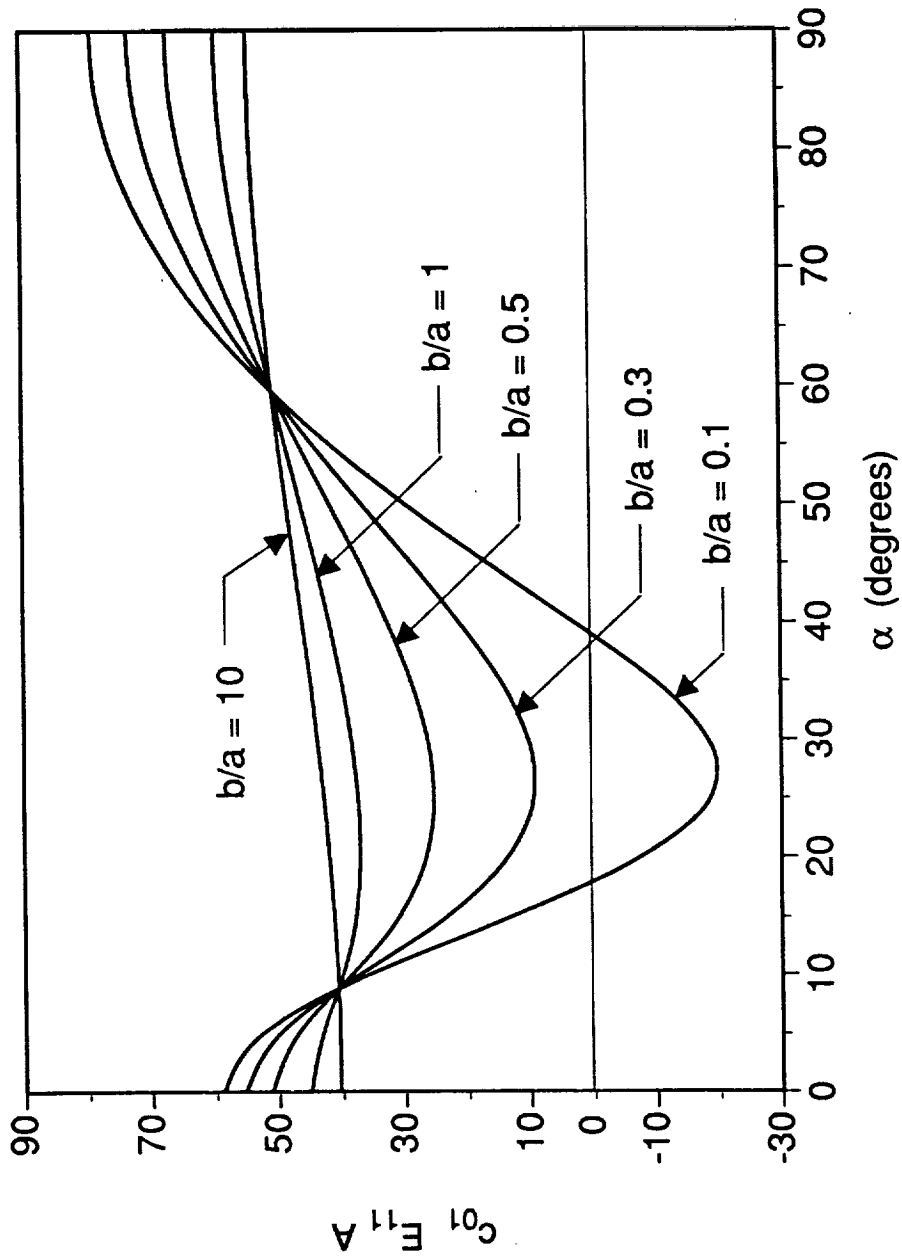

Fig. 9 Nondimensionalized shear deformation coefficient (c_{01}) with (α), (β=0).

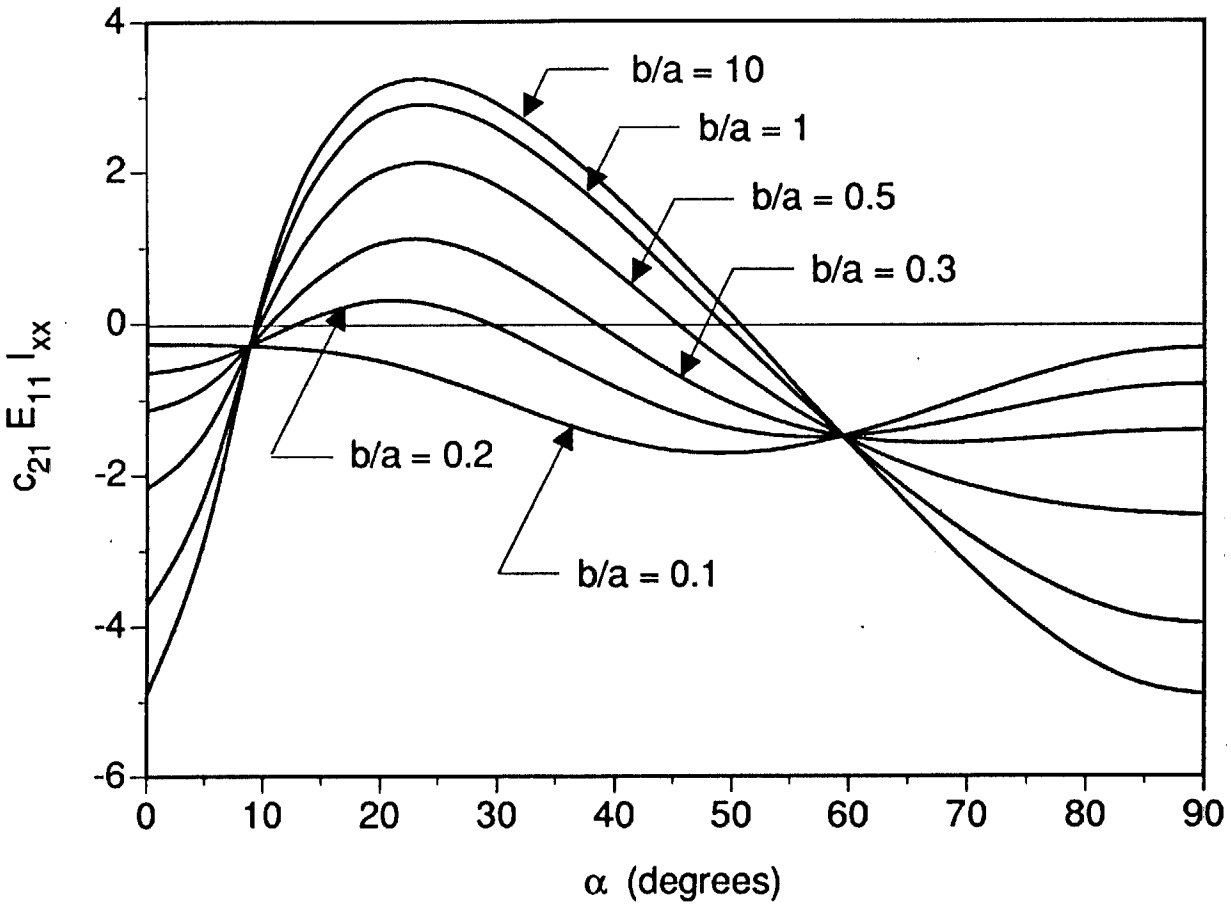

Fig. 10 Nondimensionalized out-of-plane coefficient (c_{21}) with (α), (β=0).

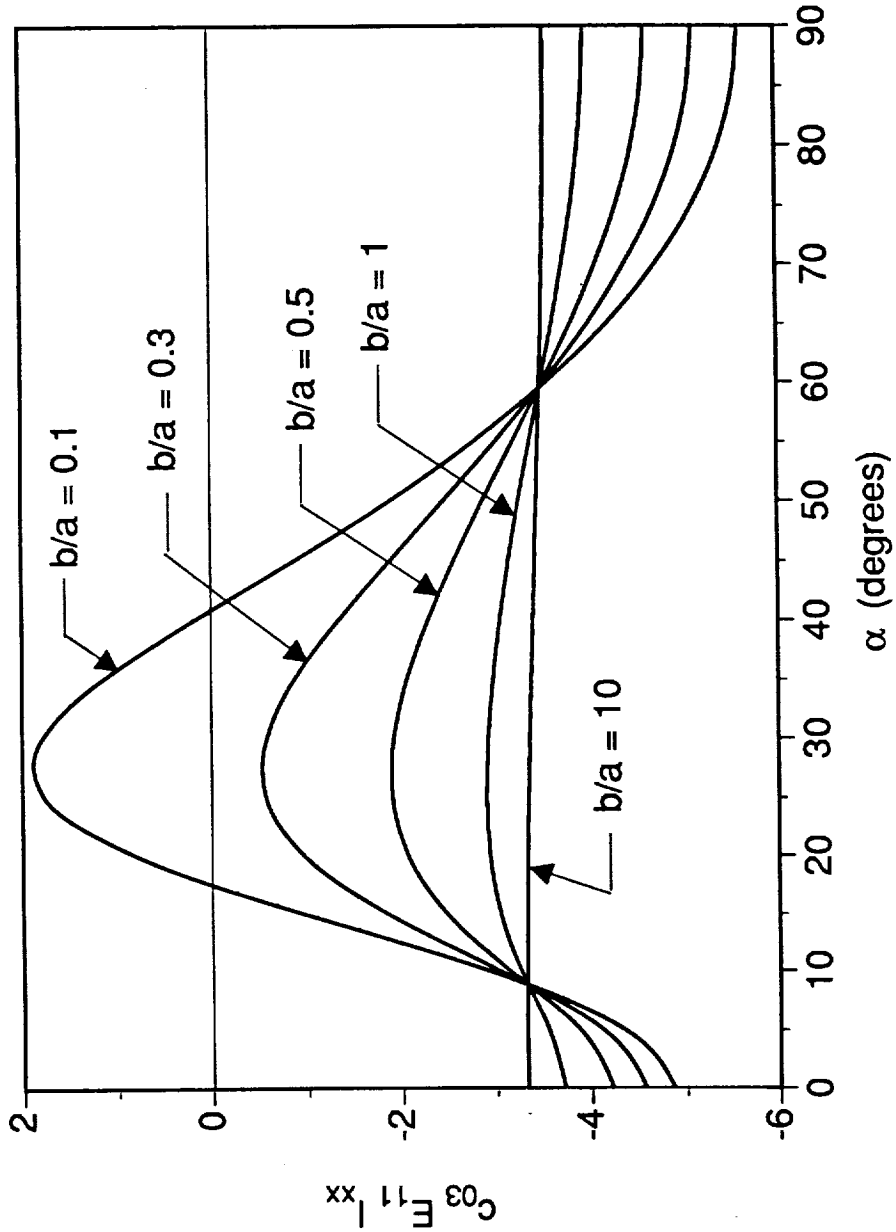

Fig. 11 Nondimensionalized out-of-plane coefficient (c_{03}) with (α), (β=0).

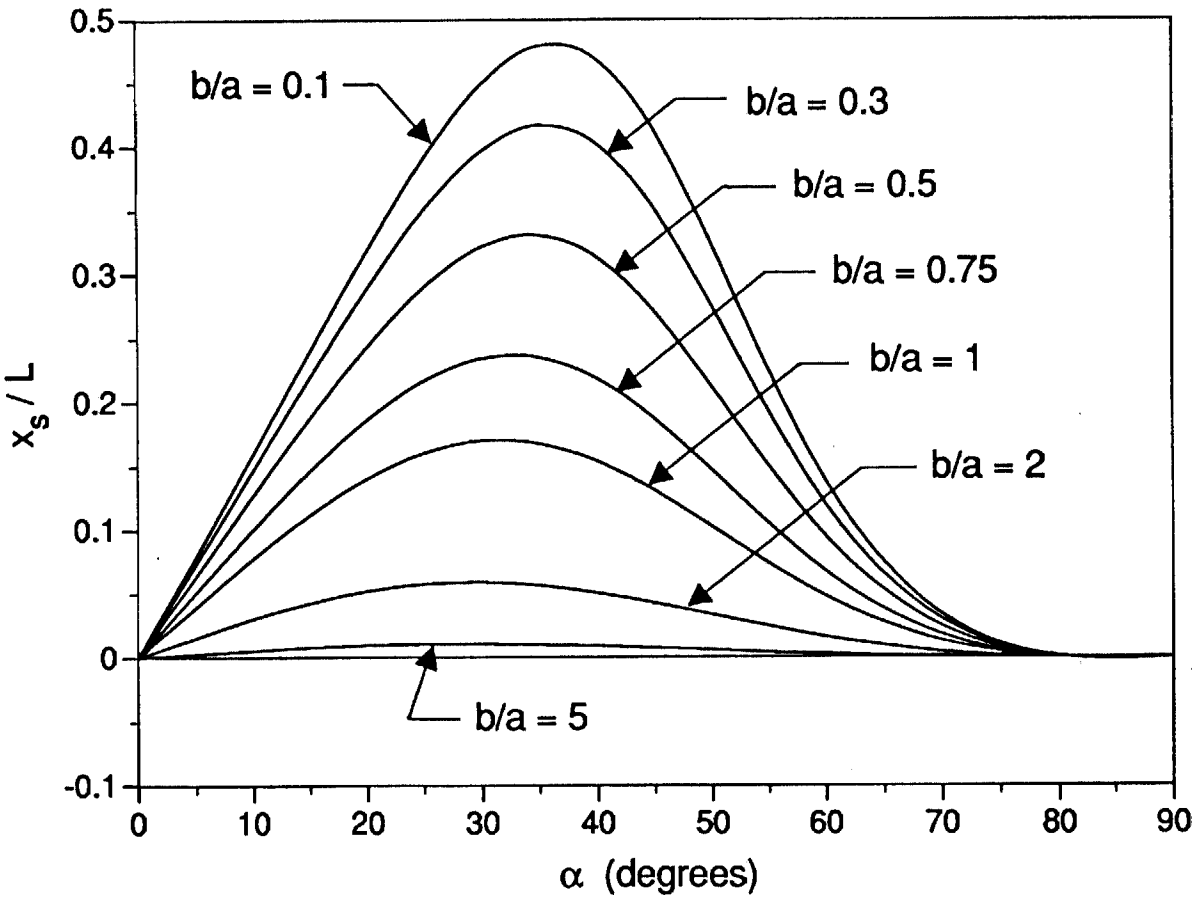

Fig. 12 Variation of normalized shear center location (x_S) with (α), (β=0).

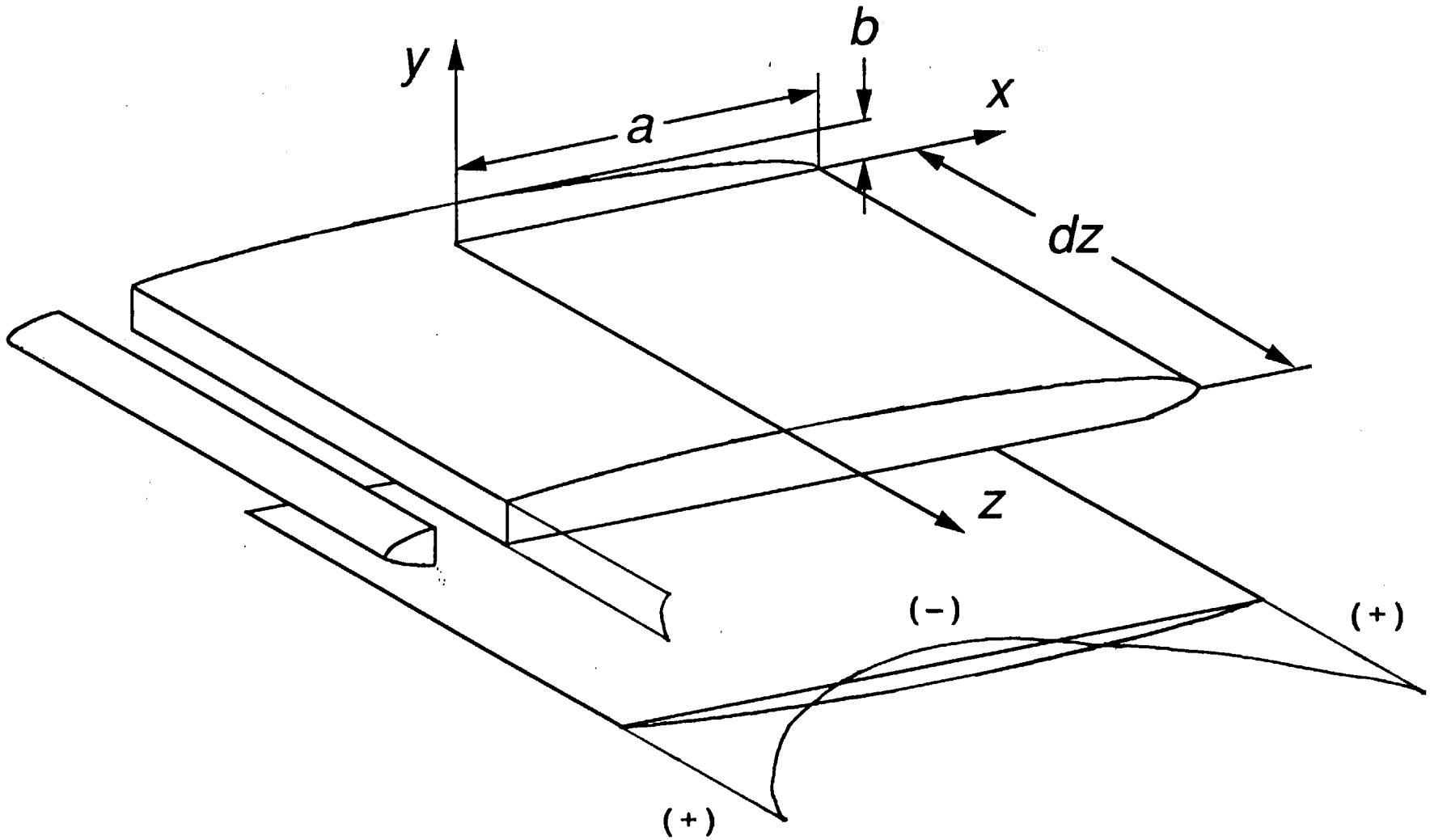

Fig. 13 Transverse shear stress distribution (τ_{yz}) on two slices of a thin cross-section beam element.

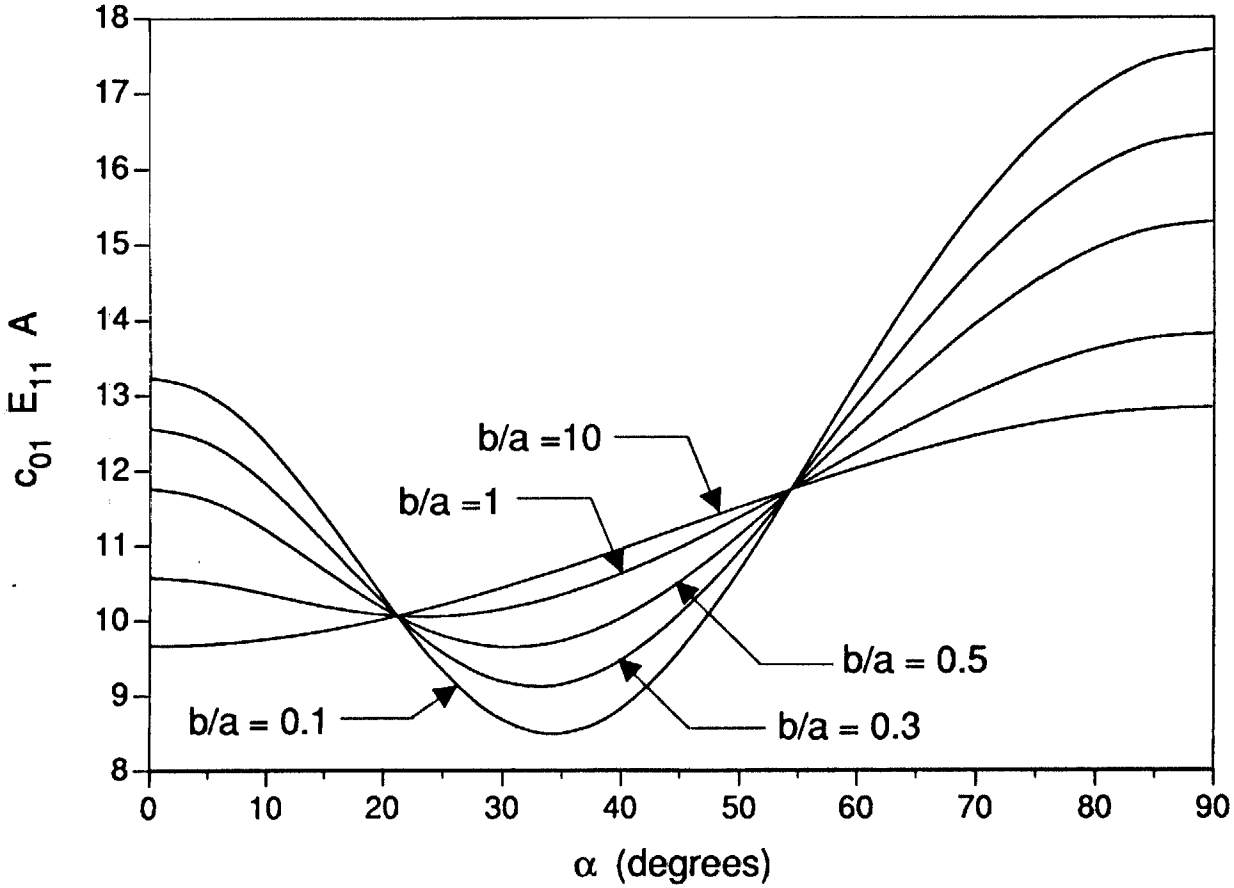

Fig. 14 Nondimensionalized shear deformation coefficient (c_{01}) with (α), (β=0) for S-glass/epoxy.

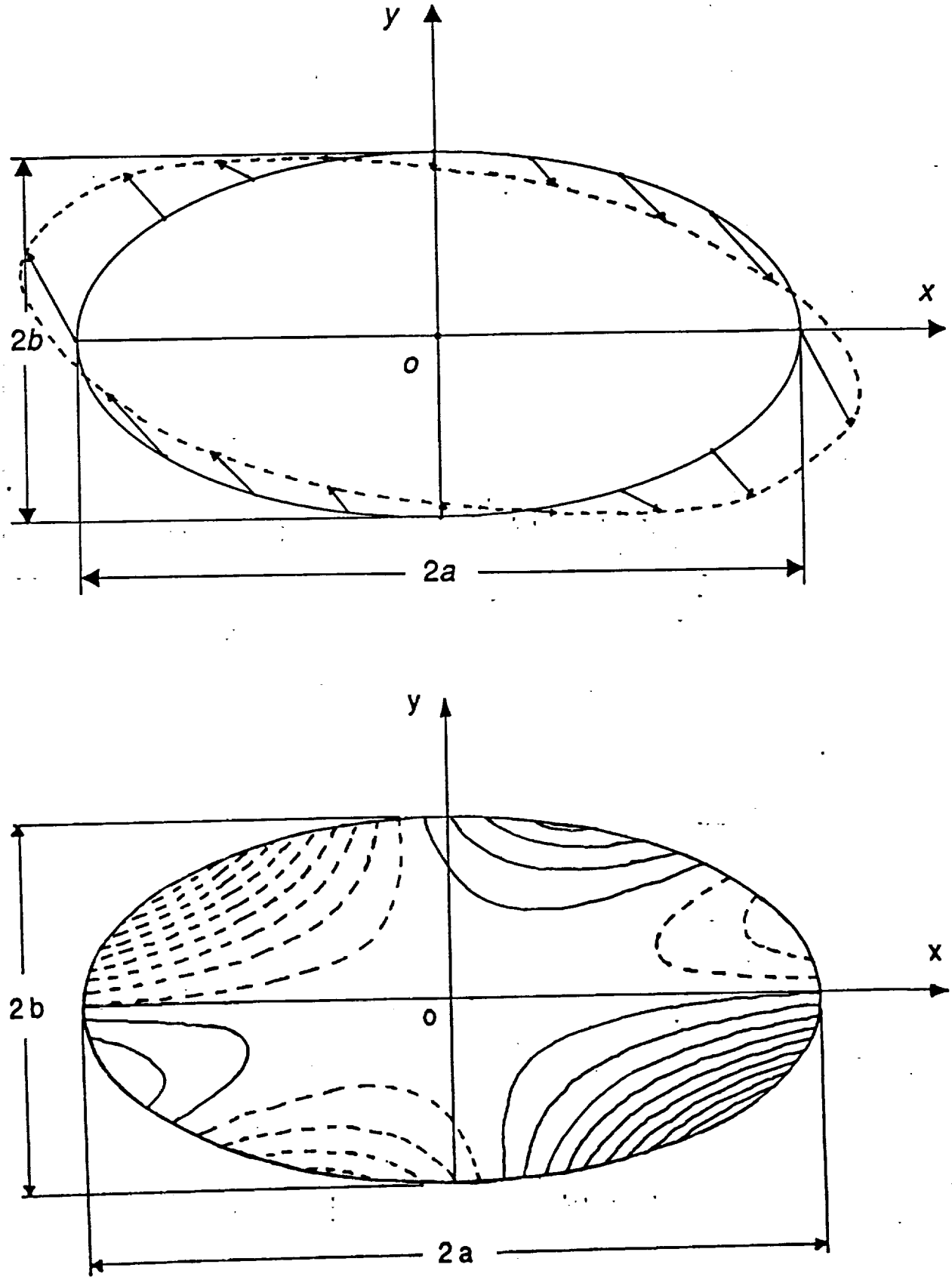

Fig. 15 a.) In-plane deformation, and b.) contour of out-of-plane warping of cross-section with (b/a=0.5, α =30°, β=60°).

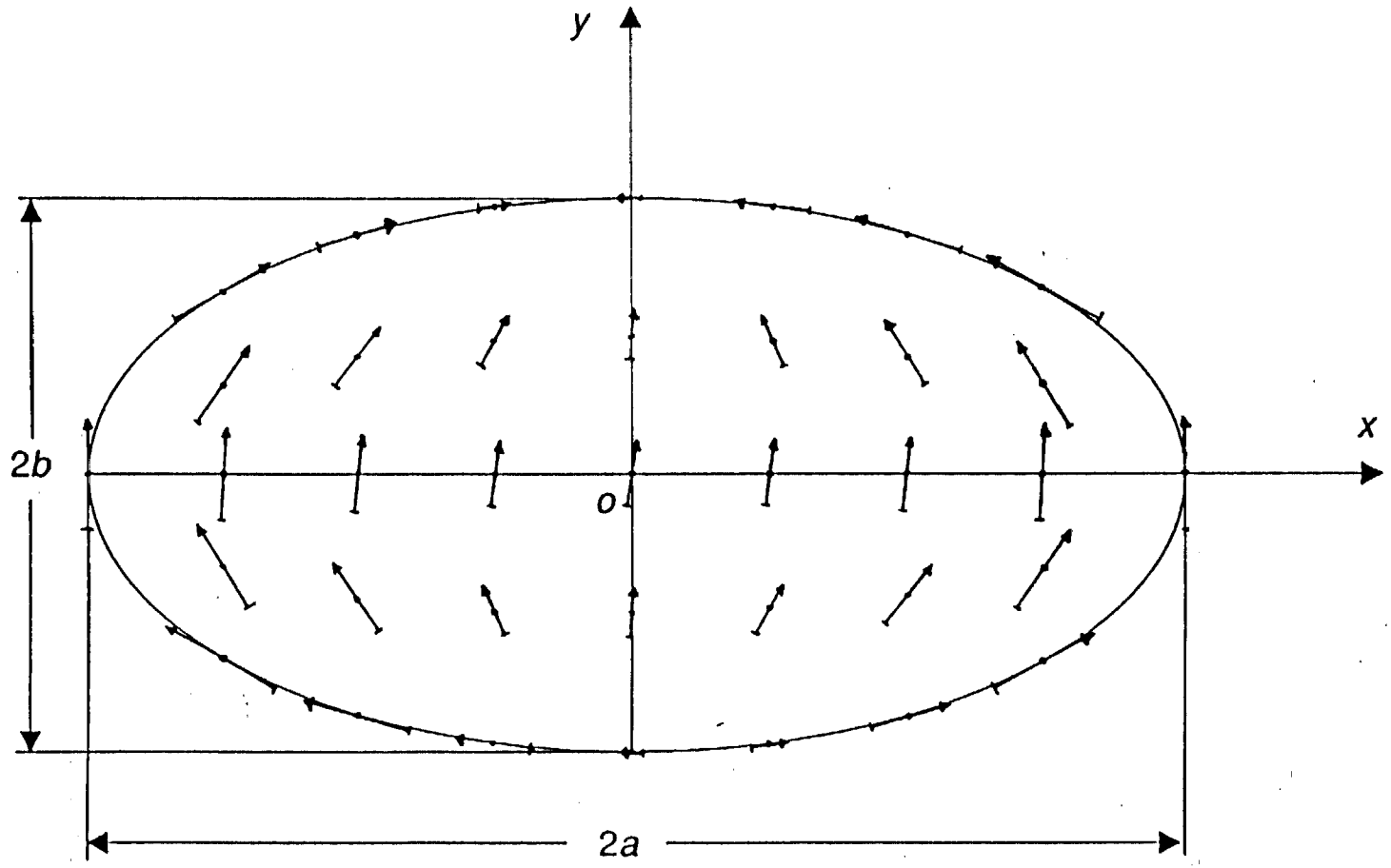

Fig. 16 Vectorial contour of transverse shear stress distribution for (b/a=0.5, $\alpha = \beta$=30°).

Chapter 5 Transverse Vibrations of Shear-Deformable Beams Using a General Higher-Order Theory

by

J. B. Kosmatka
Department of Applied Mechanics and Engineering Science
University of California
San Diego, California 92093

1. INTRODUCTION

The fundamental vibration behavior of long slender cylindrical or prismatic beams can be studied using the classical Bernoulli-Euler beam theory. Attempting to use this theory to study either short beams or higher vibrational modes can lead to a significant over-prediction of the natural frequencies since both transverse shear deformation and rotatory inertia effects have been ignored. Timoshenko [1,2] developed a theory which allows one to study the vibrational behavior of shorter beams (and/or higher vibrational modes) by approximately accounting for both transverse shear deformation and rotatory inertia, where the cross-section remains undistorted and the in-plane stresses are zero. The resulting model is characterized by two differential equations of motion encompassing two independent variables; the transverse deflection of the neutral axis, v and the rotation of the cross-section measured about the neutral axis, θ. In addition, the model requires the determination of a well-known shear-correction factor (k), which is defined as the ratio of the average shear strain within the cross-section to the shear strain at the section centroid. Other researchers [3-5] have attempted to show that the magnitude of (k) should be adjusted for studying the higher mode vibrational behavior of beams because the dynamic shear strain distribution may differ significantly from the parabolic form of the static shear strain distribution. Cowper [6] presented a conceptual modification to Timoshenko equations by assuming that the transverse displacement, v, and the rotation, θ, represent the average cross-section values instead of the point-wise values. Thus, the (k) values could be determined, based upon static three-dimensional elasticity theory along with Saint-Venant's static flexure warping function, for a wide variety of cross-section shapes and Poisson ratios. A further study by Cowper [7] has shown, by comparison to plane-stress elasticity solutions, that the (k) does not have to be adjusted for higher vibrational modes.

Goodier [8] was one of the first researchers to improve upon Timoshenko's beam theory by incorporating second-order stress effects associated with shear deformation and cross-section warping. While this model is limited to static behavior, it does provide valuable insight into beam behavior. Murthy [9] took a fresh look at the model of [1,2] by incorporating additional displacements to insure a zero in-plane stress state without the need for a correction factor (k). Stephen and Levinson [10] developed a second order model for studying beam vibrations that combines the best features of [2], [6], and [8] with two governing differential equations having two independent coefficients. The first coefficient is similar to Timoshenko's (or Cowper's) shear correction factor that depends upon Saint-Venant's static flexure warping function, while the second coefficient depends upon the transverse shear stress state.

Higher-order (or refined) shear-deformable theories [11-14] have been developed for beams with thin rectangular cross-sections that correctly account for the stress-free boundary conditions on the upper and lower surfaces as well as the parabolic shear-strain distribution through the thickness without the need for a shear correction factor (k). This is accomplished by expanding the axial displacement to include a cubic distribution through the thickness. This additional displacement is identical to the Saint-Venant's static flexure warping function for thin rectangular cross-sections, but for general cross-section shapes the correct expansion should be an infinite series of transcendental functions. These theories further assume that the in-plane cross-section stresses are negligible and that the cross-section does not deform in it's own plane. Thus, the possibility of dynamic deformation within the cross-section plane that occurs as a result of Poisson coupling with the out-of-plane cross-section stress distribution (anticlastic-type surface) is not included. The wave (or vibrational) behavior of a general prismatic bar with an arbitrary cross-section was studied by Aalami [15] using a Rayleigh-Ritz energy approach to the general three-dimensional problem. His numerical and graphical results clearly illustrate the presence and importance of both the out-of-plane shear deformation and in-plane (anticlastic) deformation for extremely short wave (high vibrational) modes ($2b/L = 3$). Recently, Ie and Kosmatka [16] developed a static theory for a general cylindrical or prismatic beam that incorporates both out-of-plane shear and in-plane (anticlastic-type) deformation functions, where these functions are assumed known. In actuality, these functions can be determined exactly for simple cross-sections (rectangle, ellipse) by solving Saint-Venant's bending and flexure problems and approximately for an arbitrary cross-section by applying either a two-dimensional finite element approach [17] or a power series approach [18]. Numerical results show that the

calculated displacements and stresses are indistinguishable from elasticity solutions for a wide variety of beam loadings, boundary conditions, and cross-section shapes.

The purpose of the current study is to develop a general higher order theory to study the static and vibrational behavior of beam structures having an arbitrary cross-section that utilizes both out-of-plane shear-dependent warping and in-plane (anticlastic) deformations. The equations of motion are derived via Hamilton's principle, where the full three-dimensional constitutive relations are used. In addition, a simplified version of the general higher-order theory is also presented for beams having an arbitrary cross-section that includes out-of-plane shear-deformation, but assumes that stresses within the cross-section and in-plane deformations are negligible. This simplified model, which is accurate for long to moderately short wave-lengths, offers substantial improvements over existing higher-order theories [11-14] that are limited to beams with thin rectangular cross-sections. Furthermore, the current approach will be very useful in the study of thin-wall closed-cell beams (for example, airfoil-type sections), where the magnitude of shear related cross-section warping is significant.

A series of numerical results are presented that fully validate the current model with existing one-dimensional models as well as with appropriate elasticity solutions where available. The vibrational behavior of a simply-supported beam having either a rectangular or an elliptical cross-section is studied using the Ritz method for a wide variety of cross-section aspect ratios and beam (wave) lengths. Moreover, this problem contains a second (higher) spectrum of shear-dominant frequencies [19-22] and thus, the interaction of the current theory having dynamic in-plane deformations with the second frequency spectrum will also be investigated.

2. GENERAL HIGHER-ORDER THEORY

Consider a cylindrical or prismatic isotropic beam, of length L, having a general homogeneous cross section of area A. See Fig. 1. A Cartesian coordinate system (x,y,z) is defined on the beam where x and y are coincident with the principal axes of the beam root cross-section and z is coincident with the centroidal axis. To eliminate complications associated with torsional vibrations, it is assumed that the centroidal axis and the elastic axis are coincident. The current development is further restricted to the study of vibrational behavior in the y-z plane only and the displacement relations are defined as;

$$\tilde{u}(x,y,z,t) = M(z,t)\, U_o(x,y)\,,$$

$$\tilde{v}(x,y,z,t) = v(z,t) + M(z,t)\, V_o(x,y)\,, \qquad (1.a\text{-}c)$$

$$\tilde{w}(x,y,z,t) = y\,\theta(z,t) + Q(z,t)\, W_o(x,y)\,,$$

where the components are defined in three groups. The first group contains the classical (or first-order) terms (v, $y\theta$), where $v(z,t)$ represents the time-dependent y-direction displacement and $\theta(z,t)$ the time-dependent rotation about x axis. The second group includes the out-of-plane warping of the cross-section that is linearly proportional to the local time-dependent shear resultant (Q). The third group represents the in-plane deformation of the cross-section that forms an anticlastic surface and is linearly proportional to the local time-dependent moment resultant (M). The three functions (U_o, V_o, W_o), which are assumed to be known, can be determined exactly for simple cross-sections (rectangle, ellipse) by solving Saint Venant's bending and flexure problems [23], or approximately for arbitrary cross-sections using either a two-dimensional finite element (Ritz) approach [17] or a power series approach [18].

The time-dependent strain displacement relationships of the beam are defined as

$$\begin{aligned} \varepsilon_{xx} &= \tilde{u}_{,x}\,, & \gamma_{yz} &= \tilde{v}_{,z} + \tilde{w}_{,y}\,, \\ \varepsilon_{yy} &= \tilde{v}_{,y}\,; & \gamma_{xz} &= \tilde{w}_{,x} + \tilde{u}_{,z}\,, \\ \varepsilon_{zz} &= \tilde{w}_{,z}\,, & \gamma_{xy} &= \tilde{u}_{,y} + \tilde{v}_{,x}\,, \end{aligned} \qquad (2.a\text{-}f)$$

where ε_{xx}, ε_{yy}, and ε_{zz} are the normal strains in the x, y, and z directions, respectively, and γ_{yz}, γ_{xz}, and γ_{xy} are the shear strains. The notation $(\ )_{,x}$ and $(\ )_{,y}$ refer to partial derivatives with respect to the x and y coordinates respectively. The general constitutive relations are given as

$$\{\sigma\} = [C]\{\varepsilon\}\,, \qquad (3.a)$$

where the stress and strain arrays are defined as

$$\{\sigma\}^T = \{\, \sigma_{xx},\ \sigma_{yy},\ \sigma_{zz},\ \tau_{yz},\ \tau_{xz},\ \tau_{xy} \,\}\,,$$

$$\{\varepsilon\}^T = \{\, \varepsilon_{xx},\ \varepsilon_{yy},\varepsilon_{zz},\ \gamma_{yz},\ \gamma_{xz},\ \gamma_{xy} \,\}\,, \qquad (3.b,c)$$

and the nonzero coefficients of the material stiffness matrix are given as

$$C_{11} = C_{22} = C_{33} = (\lambda + 2G),$$
$$C_{12} = C_{13} = C_{23} = \lambda, \qquad (3.d)$$
$$C_{44} = C_{55} = C_{66} = G,$$

Here, λ and G are defined as Lame's constants.

At this point, we assume that ($Q(z,t)_{,z} = 0$), so that the displacement field of Eqns (1.a-c) can be expressed in terms of the kinematic variables (v,θ) only, instead of with a mixed form (v,θ,Q,M). Clearly, for extremely short wave-length (higher vibrational) modes the current assumption that the warping deformation is only dependent upon the local bending moment and shear resultants, may lead to minor inaccuracies. For these types of modes, where the characteristic length is much less than the cross-section dimensions, one could further assume that the warping deformation is proportional not only to the local bending moment and shear resultants but also to their (first, second, etc.) derivatives as well.

The local bending moment can be expressed in terms of the kinematic variables by making use of the cross-section equilibrium equation with

$$M(z,t) = \int_A y\sigma_{zz} dA = \tilde{E} I_{xx}\, \theta(z,t)_{,z}, \qquad (4.a)$$

where

$$\tilde{E} = \frac{(\lambda + 2G)}{1 - \lambda H_1}, \qquad H_1 = \int_A y\,(U_{o,x} + V_{o,y})\, dA, \qquad (4.b,c)$$

and A and I_{xx} are the area and area moment of inertia about the x axis, respectively. Similarly, the local shear resultant can be expressed as

$$Q(z,t) = \int_A \tau_{yz} dA = k_o G\, A(v_{,z} + \theta), \qquad (5.a)$$

where, $M_{,z} = Q$,

$$k_o = \frac{1}{(1 - G H_2)} \qquad (5.b)$$

and

$$H_2 = \int_A (V_o + W_{o,y}) \, dA \, . \tag{5.c}$$

Substituting Eqns. (4.*a*) and (5.*a*) into Eqn. (1) results in the final form of the displacement relations defined in terms of the kinematic variables (v and θ) only;

$$\begin{aligned} \tilde{u}(x,y,z,t) &= \theta(z,t)_{,z} \, \psi_x(x,y), \\ \tilde{v}(x,y,z,t) &= v(z,t) + \theta(z,t)_{,z} \psi_y(x,y), \\ \tilde{w}(x,y,z,t) &= y \, \theta(z,t) + \left(v(z,t)_{,z} + \theta(z,t)\right)\psi_z(x,y) \end{aligned} \tag{6.a-c}$$

where

$$\begin{aligned} \psi_x(x,y) &= \tilde{E}I \; U_o \, (x,y) \, , \\ \psi_y(x,y) &= \tilde{E}I \; V_o(x,y) \, , \\ \psi_z(x,y) &= k_o \, G \, A \, W_o(x,y) \, . \end{aligned} \tag{6.d-f}$$

The six strain components can be written by substituting Eqns. (6.a-c) into (2.a-f);

$$\begin{aligned} \varepsilon_{xx} &= \theta_{,z} \, \psi_{x,x} \, , \\ \varepsilon_{yy} &= \theta_{,z} \, \psi_{y,y} \, , \\ \varepsilon_{zz} &= y\theta_{,z} + \left(v_{,z} + \theta\right)_{,z} \psi_z \, , \\ \gamma_{yz} &= \left(v_{,z} + \theta\right)\left(1 + \psi_{z,y}\right) + \theta_{,zz} \, \psi_y \, , \\ \gamma_{xz} &= \left(v_{,z} + \theta\right)\left(\psi_{z,x}\right) + \theta_{,zz} \, \psi_x \, , \\ \gamma_{xy} &= \theta_{,z}\left(\psi_{x,y} + \psi_{y,x}\right) . \end{aligned} \tag{7.a-f}$$

The equations of motion are derived via Hamilton's principle

$$\delta \Pi = \int_{t_1}^{t_2} (\delta U - \delta T - \delta W_e) dt = 0 \tag{8}$$

where δU, δT, and δW_e are the variations of the strain energy, the kinetic energy, and the work of external forces, respectively. The variation of the strain energy, which can be written in two parts, is given as;

$$\delta U = \int_0^L \int_A \{\delta\sigma\}^T\{\varepsilon\}\, dA\, dz = \delta U_B + \delta U_S \tag{9.a}$$

where the first portion represents the strain energy variation associated with bending;

$$\delta U_B = \int_0^L \begin{Bmatrix} \delta\theta_{,z} \\ \delta v_{,zz} \end{Bmatrix}^T \begin{bmatrix} D_{11} & D_{12} \\ D_{12} & D_{22} \end{bmatrix} \begin{Bmatrix} \theta_{,z} \\ v_{,zz} \end{Bmatrix} dz, \tag{9.b}$$

the second portion is associated with shear;

$$\delta U_S = \int_0^L \begin{Bmatrix} \delta v_{,z} + \delta\theta \\ \delta\theta_{,zz} \end{Bmatrix}^T \begin{bmatrix} A_{11} & A_{12} \\ A_{12} & A_{22} \end{bmatrix} \begin{Bmatrix} v_{,z} + \theta \\ \theta_{,zz} \end{Bmatrix} dz, \tag{9.c}$$

and the coefficients A_{ij} and D_{ij} (i,j=1,2) are defined in the Appendix (*A*.1-6). The constants A_{12} and A_{22} represent additional shear deformation as a result of in-plane cross-section deformation. The variation of the kinetic energy is given as

$$\delta T = \int_0^L \int_A \rho\left(\delta\dot{\vec{u}}\cdot\dot{\vec{u}} + \delta\dot{\vec{v}}\cdot\dot{\vec{v}} + \delta\dot{\vec{w}}\cdot\dot{\vec{w}}\right) dA\, dz \tag{10}$$

where ρ is the mass density and $\dot{(\,)}$ represents a derivative with respect to time; *t*. Substituting Eqns. (6.*a-c*) into (10), taking the appropriate derivatives with respect to time; *t*, and then integrating over the cross-section; *A*, the resulting kinetic energy variation is equal to;

$$\delta T = \int_0^L \begin{Bmatrix} \delta\dot{v} \\ \delta\dot{v}_{,z} \\ \delta\dot{\theta} \\ \delta\dot{\theta}_{,z} \end{Bmatrix}^T \begin{bmatrix} m & 0 & 0 & J_1 \\ 0 & J_z & J_2 & 0 \\ 0 & J_2 & I_p & 0 \\ J_1 & 0 & 0 & J_p \end{bmatrix} \begin{Bmatrix} \dot{v} \\ \dot{v}_{,z} \\ \dot{\theta} \\ \dot{\theta}_{,z} \end{Bmatrix} dz \tag{11}$$

and the nonzero matrix coefficients are defined in the Appendix (A.7-12). The constants J_1, and J_p represent the additional kinetic energy associated with in-plane cross-section deformation. The variation of the work of external forces is given as;

$$\delta W_e = \int_0^L p(z,t)\delta v_a dz \,, \tag{12}$$

where v_a represents the displacement on the surface of the beam at the point of the applied load ($\tilde{v}(x=0, y=\bar{y}, z, t)$).

The two differential equations of motion and associated boundary conditions are obtained by substituting Eqns. (9.a-c), (10), and (12) into (8) and integrating by parts;

$$\left\{A_{11}(v_{,z} + \theta) + A_{12}\theta_{,zz}\right\}_{,z} - \left\{D_{22}v_{,zz} + D_{12}\theta_{,z}\right\}_{,zz} = m\ddot{v} + J_1\ddot{\theta}_{,z} - \left\{J_z\ddot{v}_{,z} + J_2\ddot{\theta}\right\}_{,z} - p \,, \tag{13.a}$$

$$\begin{aligned} &\left\{A_{11}(v_{,z} + \theta) + A_{12}\theta_{,zz}\right\} - \left\{D_{11}\theta_{,z} + D_{12}v_{,zz}\right\}_{,z} + \left\{A_{22}\theta_{,zz} + A_{12}(v_{,z} + \theta)\right\}_{,zz} \\ &\quad = -I_p\ddot{\theta} - J_2\ddot{v}_{,z} + \left\{J_1\ddot{v} + J_p\ddot{\theta}_{,z}\right\}_{,z} - p_{,z}\overline{\psi_y} \,, \end{aligned} \tag{13.b}$$

where $\overline{\psi_y}$ is the magnitude of the warping displacement at the point of the applied load given as

$$\overline{\psi_y} = \psi_y(x=0, y=\bar{y}) \,. \tag{13.c}$$

There are four sets of boundary conditions that must be specified at the beam ends (x=0,L). First, define either the transverse displacement (v) or the effective shear force

$$\begin{aligned} Q = &\left\{A_{11}(v_{,z} + \theta) + A_{12}\theta_{,zz}\right\} - \left\{D_{22}v_{,zz} + D_{12}\theta_{,z}\right\}_{,z} \\ &+ J_z\ddot{v}_{,z} + J_2\ddot{\theta} \,. \end{aligned} \tag{14.a}$$

Second, specify either the rotation of the cross section (θ) or the effective cross-section moment;

$$M = \left(D_{11}\theta_{,z} + D_{12}v_{,zz}\right)_{,z} + J_1\ddot{v} + J_p\ddot{\theta}_{,z}$$
$$- \left(A_{22}\theta_{,zz} + A_{12}(v_{,z} + \theta)\right)_{,z} - p\overline{\psi}_y \ . \qquad (14.b)$$

Third, define either the derivative of the transverse displacement ($v_{,z}$) or the generalized moment;

$$\widetilde{M} = D_{22}v_{,zz} + D_{12}\theta_{,z}. \qquad (14.c)$$

Finally, specify either the derivative of the rotation ($\theta_{,z}$) or;

$$R = A_{22}\theta_{,zz} + A_{12}(v_{,z} + \theta) \ . \qquad (14.d)$$

3. SIMPLIFIED GENERAL HIGHER-ORDER THEORY

A simplified version of the general higher-order theory can be developed by assuming that the cross-section is rigid within it's own plane (i.e., the third displacement group of Eq. (1) is zero (U_0, V_0=0)) and that the stresses within the arbitrary cross-section are negligible ($\sigma_{xx}, \sigma_{yy}, \tau_{xy}$=0). This model represents a logical extension to existing higher-order theories [11-14], which are limited to thin rectangular cross-sections. The displacement field will have the form;

$$\widetilde{u}(x,y,z,t) = 0 \ ,$$
$$\widetilde{v}(x,y,z,t) = v(z,t) \ , \qquad (15.a\text{-}c)$$
$$\widetilde{w}(x,y,z,t) = y\,\theta(z,t) + \left(v(z,t)_{,z} + \theta(z,t)\right)\psi_z(x,y)$$

where

$$\psi_z(x,y) = k_o\, G\, A\, W_o(x,y) \ , \qquad (15.d)$$

and

$$k_o = \left[1 - G\int_A W_{o,y}\,dA\right]^{-1} \ . \qquad (15.e)$$

The resulting three nonzero strain components have the form;

$$\varepsilon_{zz} = y\theta_{,z} + (v_{,z} + \theta)_{,z}\,\psi_z\,,$$

$$\gamma_{yz} = (v_{,z} + \theta)(1 + \psi_{z,y})\,, \qquad (16.a\text{-}c)$$

$$\gamma_{xz} = (v_{,z} + \theta)(\psi_{z,x})\,.$$

The one-dimensional constitutive relations are developed by assuming that the stresses within the cross-section are zero ($\sigma_{xx}, \sigma_{yy}, \tau_{xy}$=0) in Eq. (3.a), then a static condensation approach is used to solve for the remaining three stresses in terms of the corresponding three strains;

$$\begin{Bmatrix} \sigma_{zz} \\ \tau_{yz} \\ \tau_{xz} \end{Bmatrix} = \begin{bmatrix} E & 0 & 0 \\ 0 & G & 0 \\ 0 & 0 & G \end{bmatrix} \begin{Bmatrix} \varepsilon_{zz} \\ \gamma_{yz} \\ \gamma_{xz} \end{Bmatrix}. \qquad (16.d)$$

where E and G are Young's modulus and the shear modulus, respectively.

The equations of motion are again derived via Hamilton's principle (Eq. (8)), where the simplified form of the strain energy variation is expressed as;

$$\delta U = \int_0^L \begin{Bmatrix} \delta\theta_{,z} \\ \delta v_{,zz} \end{Bmatrix}^T \begin{bmatrix} D_{11} & D_{12} \\ D_{12} & D_{22} \end{bmatrix} \begin{Bmatrix} \theta_{,z} \\ v_{,zz} \end{Bmatrix} + (\delta v_{,z} + \delta\theta)^T A_{11}(v_{,z} + \theta)dz\,, \qquad (17.a)$$

the simplified form of the kinetic energy is given as;

$$\delta T = \int_0^L \begin{Bmatrix} \delta\dot{v} \\ \delta\dot{v}_{,z} \\ \delta\dot{\theta} \end{Bmatrix}^T \begin{bmatrix} m & 0 & 0 \\ 0 & J_z & J_2 \\ 0 & J_2 & I_p \end{bmatrix} \begin{Bmatrix} \dot{v} \\ \dot{v}_{,z} \\ \dot{\theta} \end{Bmatrix} dz \qquad (17.b)$$

the simplified form of the work of external forces is defined as;

$$\delta W_e = \int_0^L p(z,t)\delta v dz\,, \qquad (17.c)$$

and the associated section constants are given in the Appendix (A.13-20).

The resulting differential equations of motion have the form;

$$\{A_{11}(v_{,z} + \theta)\}_{,z} - \{D_{22}v_{,zz} + D_{12}\theta_{,z}\}_{,zz} = m\ddot{v} - \left\{J_z\ddot{v}_{,z} + J_2\ddot{\theta}\right\}_{,z} - p\,, \tag{18.a}$$

$$A_{11}(v_{,z} + \theta) - \{D_{11}\theta_{,z} + D_{12}v_{,zz}\}_{,z} = -I_p\ddot{\theta} - J_2\ddot{v}_{,z}\,, \tag{18.b}$$

where the three geometric and natural boundary conditions that must be specified at the beam ends (x=0,L) include;

Geometric	Natural	
v	$Q = A_{11}(v_{,z} + \theta) - \{D_{22}v_{,zz} + D_{12}\theta_{,z}\}_{,z} + J_z\ddot{v}_{,z} + J_2\ddot{\theta}$	
$v_{,z}$	$\widetilde{M} = D_{22}v_{,zz} + D_{12}\theta_{,z}$	(18.c)
θ	$M = D_{11}\theta_{,z} + D_{12}v_{,zz}$	

4. MODEL VERIFICATION

The differential equations of motion for the general higher-order theory (Eqns. 13.*a*,*b*) and the simplified general higher-order theory (Eqns. 18.*a*,*b*) reduce identically to the linear form of the higher-order theory for beams, developed by Heyliger and Reddy [14], if one assumes a rigid in-plane cross-section ($\psi_x = \psi_y = 0$), negligible in-plane stresses ($\sigma_{xx}, \sigma_{yy}, \tau_{xy} \approx 0$), and a cross-section that is an extremely thin (plane stress) rectangle so that the out-of-plane shear-dependent warping can be described from Saint-Venant's static flexure warping function [23] as;

$$\psi_z = -\frac{4}{3}\left(\frac{y^3}{(2b)^2}\right), \tag{19.a}$$

where (2b) is the overall height of the cross-section (Fig. 2) and the remaining eight section constants are determined by making use of Eqns. (*A*.13-20);

$$
\begin{aligned}
A_{11} &= \frac{8}{15}GA\,, \qquad m = \rho A\,,\\
D_{11} &= \frac{68}{105}EI_{xx}\,, \quad I_p = \frac{68}{105}\rho I_{xx}\,,\\
D_{12} &= \frac{-16}{105}EI_{xx}\,, \quad J_2 = \frac{-16}{105}\rho I_{xx}\,,\\
D_{22} &= \frac{1}{21}EI_{xx}\,, \quad J_z = \frac{1}{21}\rho I_{xx}\,.
\end{aligned}
\tag{19.b-i}
$$

Furthermore, the current equations will reduce to the well-known Timoshenko equations of motion [1,2] by neglecting both in-plane deformation ($\psi_x = \psi_y = 0$) and out-of-plane warping ($\psi_z = 0$) effects;

$$
\{A_{11}(v_{,z} + \theta)\}_{,z} = mv - p\,, \tag{20.a}
$$

$$
\{A_{11}(v_{,z} + \theta)\} - \{D_{11}\theta_{,z}\}_{,z} = -I_p\ddot{\theta}\,, \tag{20.b}
$$

where the four section constant are equal to:

$$
\begin{aligned}
A_{11} &= kGA\,, \qquad m = \rho A\,,\\
D_{11} &= EI_{xx}\,, \quad I_p = \rho I_{xx}\,,
\end{aligned}
\tag{20.c-f}
$$

with k being a shear coefficient that is dependent upon the geometry and material definition of the cross-section [1-7].

5. FREE VIBRATION OF A SIMPLY-SUPPORTED BEAM

The natural frequencies of a simply-supported beam can be obtained by applying the Ritz method where the following displacement functions satisfy both the geometric and natural boundary conditions;

$$
v(z,t) = Q_1 \sin\left(n\pi\frac{x}{L}\right)\sin(\omega t), \quad \theta(z,t) = Q_2 \cos\left(n\pi\frac{x}{L}\right)\sin(\omega t), \tag{21.a,b}
$$

where n is equal to the mode number, ω is the corresponding natural frequency, and Q_1 and Q_2 are unkown generalized coordinates. Alternatively, this solution represents the motion of a standing wave in an infinitely long beam where n=1 and L is taken as the wavelength. Clearly, as L becomes small (or n becomes very large), the effects of local in-plane deformation and out-of-plane warping (shear-deformation) will become

significant. Substituting the assumed displacement field (21.*a*,*b*) into the strain energy (9.*a*-*c*) and kinetic energy variations (11), integrate over the length; *L*, and substituting the results into Hamilton's principle (8), will lead to the following 2 by 2 matrix form of the algebraic eigenvalue equation;

$$\left\{[K] - \omega^2[M]\right\}\{Q\} = \{0\} \tag{22.a}$$

where, the coefficients of [*K*] are given as

$$K_{11} = \frac{L}{2}\left\{A_{11}\left(\frac{n\pi}{L}\right)^2 + D_{22}\left(\frac{n\pi}{L}\right)^4\right\}$$

$$K_{12} = K_{21} = \frac{L}{2}\left\{A_{11}\left(\frac{n\pi}{L}\right) + (D_{12} - A_{12})\left(\frac{n\pi}{L}\right)^3\right\} \tag{22.b}$$

$$K_{22} = \frac{L}{2}\left\{A_{11} + (D_{11} - 2A_{12})\left(\frac{n\pi}{L}\right)^2 + A_{22}\left(\frac{n\pi}{L}\right)^4\right\}$$

with

$$[M] = \frac{L}{2}\begin{bmatrix} m + J_2\left(\frac{n\pi}{L}\right)^2 & (J_2 - J_1)\left(\frac{n\pi}{L}\right) \\ (J_2 - J_1)\left(\frac{n\pi}{L}\right) & I_p + J_p\left(\frac{n\pi}{L}\right)^2 \end{bmatrix}, \tag{22.c}$$

and

$$\{Q\}^T = \{Q_1,\ Q_2\}\ . \tag{22.d}$$

The coefficients of the stiffness and mass matrices for the simplified model can be obtained by setting (A_{12}, A_{22}, J_1, J_p) equal to zero in (Eqns. 21.*b*,*c*) and calculating the remaining eight section constants using (Eqns. *A*.13-20).

6. NUMERICAL EXAMPLES

Two sets of numerical examples are presented. First, the general higher-order theory (GHOT) and the simplified higher-order theory (SGHOT) are validated with previously published solutions over a broad range of beam (or wave) lengths. Second,

the vibration behavior of a simply-supported beam is studied for a wide range of rectangular and elliptical cross-section aspect ratios (b/a). See Fig. 2.*a,b*. Comparisons with existing models are made so that the features of the current development can be assessed. The required section constants for the rectangular and elliptical cross-sections are presented in tables 1 and 2, respectively, where the in-plane deformation functions (ψ_x, ψ_y) and out-of-plane warping function (ψ_z) were developed from Sokolnikoff's full three-dimensional elasticity solutions [23], assuming that the Poisson's ratio (ν) is equal 0.333 and $b = 1$. For example, the force-dependent warping functions for a rectangular cross-section have the form

$$U_o(x,y) = -\frac{\nu}{E\, I_{xx}}\, x\, y\,, \tag{23.a}$$

$$V_o(x,y) = -\frac{\nu}{2\, E\, I_{xx}}\,(y^2 - x^2)\,, \tag{23.b}$$

$$W_o(x,y) = \frac{-1}{E\, I_{xx}}\left\{\frac{2+\nu}{6}\, y^3 - \frac{\nu}{2}\, y\, x^2 + \frac{4\nu\, a^2}{\pi^3}\sum_{n=1}^{\infty}\frac{(-1)^n}{n^3}\,\frac{\left(a\,\sinh\left(\frac{n\pi y}{a}\right)\cos\left(\frac{n\pi x}{a}\right) - n\pi y\right)}{\cosh\left(\frac{n\pi b}{a}\right)}\right\}, \tag{23.c}$$

and the constant (k_o) is calculated using Eq. (5.b) as;

$$k_o = \left[1 + \frac{1}{2\,(1+\nu)}\left\{1+\nu\left(1-\left(\frac{a}{b}\right)^2\right) - \frac{12\,\nu}{\pi^2}\left(\frac{a}{b}\right)^2\sum_{n=1}^{\infty}\frac{(-1)^n}{n^2}\,\frac{1}{\cosh\left(n\pi\left(\frac{b}{a}\right)\right)}\right\}\right]^{-1}. \tag{23.d}$$

This coefficient (k_o) will approach 2/3 for very thin rectangular cross sections ($a/b \to 0$). The desired form of the warping functions (ψ_x, ψ_y, ψ_z) can be determined by substituting Eqns. (23.*a-d*) into (6.*d-f*). Thus,

$$\psi_x = -\nu\, x\, y\,, \tag{24.a}$$

$$\psi_y = \frac{-\nu}{2}\,(y^2 - x^2)\,, \tag{24.b}$$

and ψ_z is found using Eq. (6.*f*), where W_o and k_o are given in Eqns. (23.*c,d*).

In the following figures, the two calculated frequencies (ω_1, ω_2) are normalized with respect to ω_0 (= $n\pi(\sqrt{E/\rho})/L$) and plotted versus ($2nb/L$). For extremely long slender beams ($2nb/L$≈0), the lower frequency, ω_1, is just the Bernoulli-Euler prediction with ($Q_1 \neq 0$, $Q_2=0$) , while the upper frequency,ω_2, will equal the "thickness-shear" frequency, ω_{ts} (=$\sqrt{A_{11}/I\rho}$), where the beam experiences pure shearing through the cross-section ($Q_2 \neq 0$) with no beam bending ($Q_1=0$). As ($2nb/L$) increases, the modes become coupled, where the lower natural frequency, ω_1, is predominantly beam bending with some shear deformation, whereas the upper frequency, ω_2, is predominantly beam shear with some beam bending. A second (lower) x-axis, is included in the figures, that represents the corresponding mode number assuming a characteristic long slender beam ($2b/L$=0.1).

6.1 VALIDATION STUDIES

The current theories; (GHOT) and (SGHOT), were validated by comparing the calculated natural frequencies of a simply-supported beam having a thin rectangular (b/a=1000) cross-section with numerous existing solutions over a broad range of beam lengths (Fig. 3) and by comparing the calculated "thickness-shear" frequencies (Table 3) with previously published results [24]. The lower frequency ω_1, has four distinct lines which represent; (1) the Bernoulli-Euler solution, (2) the current (GHOT) solution, (3) a plane-stress elasticity solution [7], and (4) the Timoshenko solution with k=2/3 [1,2]. The line which contains the plane stress elasticity solution also represents the current (SGHOT) model, a higher-order theory [14], and the Timoshenko solution with k=.8551 [6]. All of the shear-deformable models are in complete agreement with the Bernoulli-Euler solution when the beam is long and slender, but as the beam (or wave) length gets shorter, the Timoshenko beam theory with k=2/3 is more flexible than the remaining beam theories, and for extremely short beam lengths (2b>L) the current (GHOT) model predicts a natural frequency that is slightly higher than existing one-dimensional beam theories. This difference is clearly a result of including in-plane deformations in both the strain and kinetic energies.

The shear-dominant frequency ω_2, has only two distinct lines which represent; (1) the Timoshenko solution with k=2/3 [1,2], and (2) the Timoshenko solution with k=.8551 [6]. The second line also represents a higher-order theory [14], and the current (GHOT) and (SGHOT) models. The Timoshenko solution with k=2/3 is measurably more flexible when the beam is long and slender, but converges to the other beam solutions when the beam (or wave) length becomes very short.

A comparison of the predicted "thickness-shear" mode frequency (Table 3) with an elasticity solution [24] shows that the current (SGHOT) model and the model of [11] is in near exact agreement, while the Timoshenko-based predictions are somewhat deficient. The current (GHOT) model differs slightly as a result of including the kinetic energy associated with in-plane deformations, which was ignored in [24].

6.2 VARYING CROSS-SECTION ASPECT

In the second study, the vibration behavior of a simply-supported beam was analyzed for a wide range of rectangular and elliptical cross-section aspect ratios (b/a). In Fig. 4, the two calculated natural frequencies using the current (GHOT) model are presented as a function of rectangular cross-section aspect ratio (b/a). It can be seen that (b/a) has very little effect on ω_1, even for extremely short beam (or wave) lengths, but it can have a measurable effect on ω_2 for moderate and shorter beam lengths. In Table 4, a comparison of the lower and higher frequencies is given as a function of b/a for an extremely short beam length ($2b=L$) and one can see that b/a has a minimal effect on the bending frequency, whereas the effect on the shear-dominant frequency can be significant.

As a further validation of the current model, Aalami [15] predicted that $\omega_1=0.4724\omega_0$ for an extremely short beam ($2b=L$) having a square cross-section ($b/a=1$) using a Rayleigh-Ritz energy approach on the full three-dimensional problem, which is within 0.4% of the current (GHOT) solution. The "thickness-shear" mode frequency is also presented in Table 4, where it is seen that the frequency increases with a reduction in the aspect ratio (wider cross-section). The results from the Bernoulli-Euler solution, the Timoshenko solutions [1,2,6], and the higher-order models [11-14] were not included in either Fig. 4 or Table 4 because these solutions do not depend upon aspect-ratio for rectangular cross-sections and are equal to the results given in Fig. 3 and Table 3, respectively.

In Figs. 5-7, the two calculated natural frequencies are presented as a function of elliptical cross-section aspect ratio (b/a) for the Timoshenko model and the current (GHOT) and (SGHOT) models. The shear correction factor (k) used in the Timoshenko model was taken from [6], where the magnitude varies with aspect ratio. The results from the Timoshenko solution (Fig. 5) show that ω_1 and ω_2 become slightly more flexible with

decreasing aspect ratio (b/a), where a large unrealistic reduction occurs when $b/a<0.50$. This reduction is apparent in short wave-lengths for the bending-dominant frequency (ω_1) and in the long wave-lengths for the shear-dominant frequency (ω_2). Alternatively, the frequency results using the current (GHOT) model (Fig. 6) show very little change in ω_1 with b/a except for extremely short beams ($2b>L$), whereas the change in ω_2 can be significant over the broad range of wave-lengths. It is interesting to note that aspect ratio has a negligible effect on both the calculated frequencies for a wide range of cross-section shapes ($1<b/a<1000$), but as the cross-section becomes wide ($b/a<1.0$) the variation in the calculated frequencies, especially ω_2, can be important. Finally, the frequencies as a function of beam-length and aspect ratio b/a using the current (SGHOT) model are presented in Fig. 7, where the bending dominant frequency (ω_1) will undergo a slight increase for extremely short beams ($2b/L>2$), while the shear dominant frequency (ω_2) experiences a small decrease for long slender beams.

In Tables 5.*a*,*b*, ω_1 and ω_2 for an extremely short ($2b=L$) simply-supported beam with an elliptical cross-section are compared using the three different solution approaches for a variety of aspect ratios. It is clear that decreasing b/a (wide section) will decrease both ω_1 and ω_2 based upon either the Timoshenko results or the (SGHOT) model, but the results using the (GHOT) model show that the ω_1 may actually increase for wide cross-sections (low b/a), which is in agreement with the three-dimensional results using Aalami's model [15]. From Fig. 6, it is apparent that as the beam wave-length is much smaller than the cross-section dimensions ($2b$), then (ω_1) will decrease. Finally, in Table 5.*c* the "thickness-shear" mode frequency is presented using the three different methods and compared to an elasticity solution of Jeffreys [25]. Both the (GHOT) and the (SGHOT) models are in near perfect agreement with the exact results for a wide variety of cross-section aspect ratios, whereas the Timoshenko based solutions [6] slightly over predict the results.

7. CONCLUSIONS

A new one-dimensional theory has been developed to study the vibrational behavior of prismatic beam-type structures that utilizes both out-of-plane shear-dependent warping and in-plane (anticlastic) deformations. The two equations of motion were derived using Hamilton's principle, where the full three-dimensional constitutive equations are used and it is assumed that the cross-section deformation functions are

known. A simplified form of the current general higher-order theory was also presented which includes out-of-plane shear-deformation but neglects in-plane deformations by assuming that the stresses within the cross-section were negligible. It was shown that the current model reduces identically to existing higher-order models of beams having a thin rectangular cross-section, when in-plane deformations are not included. Furthermore, the current model reduces to the Timoshenko equations when out-of-plane shear-dependent warping is neglected. Results from a numerical validation study of a simply-supported beam with a thin-rectangular (b/a=1000) proved that the current model is in near exact agreement with existing approaches over a broad range of beam (or wave) lengths for the bending-dominant, shear-dominant, and thickness-shear frequencies. It was shown that including the in-plane cross-section deformations and the three-dimensional constitutive model will slightly increase the bending-dominant frequency and greatly reduce the shear-dominant frequency for extremely short wavelengths. Results from a second numerical study showed that the cross-section aspect ratio has only a minimal effect on the bending-dominant frequency even for short wavelengths, but the effect on the shear-dominant frequency can be significant for long slender beams with either rectangular and elliptical cross-sections. Moreover, the "thickness-shear" mode frequency was found to increase slightly with decreasing aspect ratio for the rectangular cross-section, whereas the frequency associated with this mode was found to decrease for the elliptical cross-section and be in near exact agreement with existing published solutions.

ACKNOWLEDGEMENTS

The support of this research by the National Science Foundation through Grant MSM-9909132 and NASA Langley Research Center through Grant NAG 1-1151-FDP is greatly appreciated.

REFERENCES

1. S. P. TIMOSHENKO 1921 *Philosophical Magazine* **41**, 744-746. On the Correction for Shear of the Differential Equation for Transverse Vibrations of Prismatic Beams

2. S. P. TIMOSHENKO 1922 *Philosophical Magazine* **43**, 125-131. On the Transverse Vibration of Bars with Uniform Cross-Section.

3. R. D. MINDLIN and H. DERESIEWICZ 1954 *Proceedings of the Second U. S. National Congress on Applied Mechanics* **1**, 175-178. Timoshenko's Shear Coefficient for Flexural Vibrations of Beams.

4. L. E. GOODMAN, discussion of paper; R. A. ANDERSON 1954 *ASME Journal of Applied Mechanics* **21**, 202-204. Flexural Vibrations in Uniform Beams According to the Timoshenko Theory.

5. L. E. GOODMAN and J. G. SUTHERLAND, discussion of paper; A. S. AYRE and L. S. JACOBSEN 1951 *ASME Journal of Applied Mechanics* **18**, 217-218. Natural Frequencies of Continuous Beams of Uniform Span Length.

6. G. R. COWPER 1966 *ASME Journal of Applied Mechanics* **33**, 335-340. The Shear Coefficient in Timoshenko's Beam Theory.

7. G. R. COWPER 1968 *ASCE Journal of the Engineering Mechanics Division* **EM6** 1447-1453. On the Accuracy of Timoshenko's Beam Theory.

8. J. N. GOODIER 1938 *Transactions of the Royal Society of Canada* **32**, 65-88. On the Problems of the Beam and Plate in the Theory of Elasticity.

9. A. V. MURTHY 1970 *AIAA Journal* **8**, 34-38 Vibrations of Short Beams.

10. N. G. STEPHEN and M. LEVINSON 1979 *Journal of Sound and Vibrations* **67** (3), 293-305. A Second Order Beam Theory.

11. M. LEVINSON 1981 *Journal of Sound and Vibration* **74** 81-87. A New Rectangular Beam Theory.

12. W. B. BICKFORD 1982 *Developments in Theoretical and Applied Mechanics* **11**, 137-150. A Consistent High-Order Beam Theory.

13. A. V. K. MURTY 1985 *Journal of Sound and Vibration* **101**, 1-12. On the Shear Deformation Theory for Dynamic Analysis of Beams.

14. P. R. HEYLIGER and J. N. REDDY 1987 *Journal of Sound and Vibration*, **126**, 309-326. A Higher Order Beam Element for Bending and Vibration Problems.

15. B. AALAMI 1973 *ASME Journal of Applied Mechanics* **40** 1067-1072. Waves in Prismatic Guides of Arbitrary Cross-Section.

16. C. IE and J. B. KOSMATKA (to appear) *The International Journal of Solids and Structures*. On the Analysis of Prismatic Beams Using First-Order Warping Functions.

17. W. E. MASON and L. R. HERRMANN 1968 *ASCE Journal of the Engineering Mechanics Division*, **94**, 965-983. Elastic Shear Analysis of General Prismatic Beams.

18. J. B. KOSMATKA (to appear) *AIAA Journal* , Flexure-Torsion Behavior of Prismatic Beams, Part I: Warping and Section Properties via Power Series.

19. B. DOWNS 1976 *ASME Journal of Applied Mechanics*, **43**, 671-674. Transverse Vibration of a Uniform, Simply-Supported Timoshenko Beam without Transverse Deflection.

20. B. A. ABBAS and J. THOMAS 1977 *Journal of Sound and Vibration* **51**, 123-137. The Second Frequency Spectrum of Timoshenko Beams.

21. G. R. BHASHYAM and G. PRATHAP 1981 *Journal of Sound and Vibration* **76**, 407-420. The Second Frequency Spectrum of Timoshenko Beams.

22. M. LEVINSON and D. W. COOKE 1982 *Journal of Sound and Vibration* **84**, 319-326. On the Second Frequency Spectra of Timoshenko Beams.

23. I. S. SOKOLNIKOFF 1956 *Mathematical Theory of Elasticity*, McGraw-Hill Book Company, New York, Second Edition.

24. H. LAMB 1945 *Hydrodynamics*, Dover Publications, New York, Sixth Edition, 282-290.

25. H. JEFFREYS 1924 *Proceedings of the London Mathematical Society* **23**, 455-476. The Free Oscillations of Water in an Elliptical Lake.

APPENDIX

The bending and shear related cross-section constants for the current general higher-order theory (GHOT) are defined as

$$D_{11} = \int_A (\lambda+2G)\left\{(y+\psi_z)^2+\psi_{x,x}^2+\psi_{y,y}^2\right\}+2\lambda\left\{(y+\psi_z)\left\{\psi_{x,x}+\psi_{y,y}\right\}+\psi_{x,x}\psi_{y,y}\right\}+G\left\{\psi_{x,y}+\psi_{y,x}\right\}^2 dA \tag{A.1}$$

$$D_{12} = \int_A \left\{(\lambda + 2G)(y + \psi_z) + \lambda\left\{\psi_{x,x} + \psi_{y,y}\right\}\right\}\psi_z \, dA \tag{A.2}$$

$$D_{22} = \int_A (\lambda + 2G)\, \psi_z^2 \, dA \tag{A.3}$$

$$A_{11} = \int_A G\left\{\left\{1 + \psi_{z,y}\right\}^2 + \psi_{z,x}^2\right\} dA \tag{A.4}$$

$$A_{12} = \int_A G\left\{\left\{1 + \psi_{z,y}\right\}\psi_y + \psi_{z,x}\psi_x\right\} dA \tag{A.5}$$

and

$$A_{22} = \int_A G\left\{\psi_x^2 + \psi_y^2\right\} dA \; . \tag{A.6}$$

The mass related cross-section constants for the general higher-order theory (GHOT) are defined as

$$I_p = \int_A \rho\,(y + \psi_z)^2 \, dA \tag{A.8}$$

$$J_1 = \int_A \rho\psi_y \, dA \tag{A.9}$$

$$J_p = \int_A \rho\left(\psi_x^2 + \psi_y^2\right) dA \tag{A.10}$$

$$J_z = \int_A \rho\psi_z^2 \, dA \tag{A.11}$$

and

$$J_2 = \int_A \rho(y + \psi_z)\psi_z \, dA \, . \tag{A.12}$$

The following eight nonzero section constants are used in the simplified general higher-order theory (SGHOT)

$$D_{11} = \int_A E(y + \psi_z)^2 dA \tag{A.13}$$

$$D_{12} = \int_A E(y + \psi_z)\psi_z \, dA \tag{A.14}$$

$$D_{22} = \int_A E\,\psi_z^2 \, dA \tag{A.15}$$

$$A_{11} = \int_A G\left\{\left(1 + \psi_{z,y}\right)^2 + \psi_{z,x}^2\right\} dA \tag{A.16}$$

$$m = \int_A \rho \, dA \tag{A.17}$$

$$I_p = \int_A \rho\,(y + \psi_z)^2 \, dA \tag{A.18}$$

$$J_z = \int_A \rho \psi_z^2 \, dA \tag{A.19}$$

and

$$J_2 = \int_A \rho(y + \psi_z)\psi_z \, dA \, . \tag{A.20}$$

Table 1 Nondimensionalized section constants for rectangular cross-sections (b/a) with $\nu = 0.333$.

b/a	0.50	1	2	10	100	1000
A_{11}/GA	.55373	.60373	.58046	.57019	.56977	.56976
A_{12}/GAb^2	.10788	.0075697	−.018517	−.026057	−.026356	−.026359
A_{22}/GAb^4	.11890	.017249	.0074311	.0056066	.0055451	.0055445
D_{11}/EI_{xx}	.67878	.73949	.71522	.70501	.70460	.70459
D_{12}/EI_{xx}	−.12390	−.10703	−.11659	−.12024	−.12039	−.12039
D_{22}/EI_{xx}	.07343	.046448	.051600	.054504	.054630	.054631
$m/(\rho A)$	1.	1.	1.	1.	1.	1.
$I_p/(\rho I_{xx})$	.65436	.72405	.69806	.68689	.68643	.68643
$J_1/(\rho I_{xx})$	.49950	0	−.12488	−.16484	−.16648	−.16650
$J_2/(\rho I_{xx})$	−.14831	−.12248	−.13375	−.13837	−.13855	−.13855
$J_z/(\rho I_{xx})$	.049015	.031004	.034443	.036381	.036465	.036466
$J_p/(\rho I_{xx}b^2)$	.35669	.051748	.022293	.016820	.016635	.016633

Table 2 Nondimensionalized section constants for elliptical cross-sections (b/a) with $\nu = 0.333$ for (a.) the general higher-order theory, and (b.) the simplified general higher-order theory (where $A_{12} = A_{22} = J_1 = J_p = 0.0$).

b/a	0.50	1	2	10	100	1000
A_{11}/GA	.41945	.57846	.64773	.67502	.67622	.67654
A_{12}/GAb^2	.075454	.015139	−.013469	−.024242	−.024707	−.024712
A_{22}/GAb^4	.068151	.0092408	.0042599	.0034887	.0034655	.0034653
D_{11}/EI_{xx}	.58259	.69203	.74236	.76257	.76345	.76346
D_{12}/EI_{xx}	−.12992	−.12612	−.10940	−.10146	−.10109	−.10109
D_{22}/EI_{xx}	.15757	.055736	.038845	.034518	.034354	.034352
$m/(\rho A)$	1.	1.	1.	1.	1.	1.
$I_p/(\rho I_{xx})$	.53020	.67350	.72944	.75109	.75203	.75204
$J_1/(\rho I_{xx})$	.49950	0.0	−.12488	−.16483	−.16648	−.16650
$J_2/(\rho I_{xx})$	−.18231	−.14465	−.12231	−.11293	−.11251	−.11251
$J_z/(\rho I_{xx})$	.10518	.037204	.025929	.023041	.022931	.022930
$J_p/(\rho I_{xx}b^2)$	.27260	.036963	.017038	.013955	.013862	.013861

b/a	0.50	1	2	10	100	1000
A_{11}/GA	.42130	.51852	.58848	.62334	.62498	.62531
D_{11}/EI_{xx}	.53472	.61111	.66975	.69994	.70137	.70138
D_{12}/EI_{xx}	−.18750	−.16667	−.14506	−.13257	−.13195	−.13195
D_{22}/EI_{xx}	.090278	.055555	.040123	.034931	.034724	.034722
$m/(\rho A)$	1.	1.	1.	1.	1.	1.
$I_p/(\rho I_{xx})$	.53472	.61111	.66975	.69994	.70137	.70138
$J_2/(\rho I_{xx})$	−.18750	−.16667	−.14506	−.13257	−.13195	−.13195
$J_z/(\rho I_{xx})$	.090278	.055555	.040123	.034931	.034724	.034722

Table 3 Natural frequencies of a short ($2b/L = 1$) simply-supported beam with a thin rectangular cross-section ($b/a = 1000$) including thickness-shear mode frequency (ω_{ts}).

	elasticity	Bernoulli-Euler	Timoshenko [1,2] k = 2/3	Timoshenko [1,2] k = .8511	Refined [11]	Current (GHOT)	Current (SGHOT)
ω_1/ω_o	.4666 [7]	.9069	.4269	.4623	.4628	.4763	.4628
ω_2/ω_o	-	-	.1712	1.2222	1.2138	1.2010	1.2138
ω_{ts}/ω_s	.9069 [20]	-	.8166	.9226	.9076	.9111	.9076

with $\omega_o = \frac{n\pi}{L}\sqrt{\frac{E}{\rho}}$, and $\omega_s = \sqrt{\frac{G}{\rho r}}$.

Table 4 Natural frequencies of a simply-supported beam ($2b/L = 1$) for various rectangular cross-section aspect ratios.

	$b/a = 1/2$	$b/a = 1$	$b/a = 2$	$b/a = 1000$
ω_1/ω_o	.4786	.4744	.4756	.4763
ω_2/ω_o	.9762	1.1486	1.1890	1.201
ω_{1s}/ω_s	.9200	.9132	.9120	.9111

with $\omega_o = \frac{n\pi}{L}\sqrt{\frac{E}{\rho}}$, and $\omega_s = \sqrt{\frac{G}{\rho r}}$.

Table 5 Natural frequencies of a simply-supported beam ($2b/L = 1$) for various elliptical cross-section aspect ratios for (a.) the bending dominant frequency (ω_1/ω_0), (b.) the shear-dominant frequency (ω_2/ω_0), and (c.) the thickness-shear frequency (ω_{1s}/ω_s).

	Bernoulli-Euler	Timoshenko [6]	Current (GHOT)	Current (SGHOT)
$b/a = 0.50$	.7854	.4377	.4636	.4394
$b/a = 1$	.7854	.4462	.4563	.4436
$b/a = 2$	.7854	.4489	.4564	.4474
$b/a = 1000$	.7854	.4499	.4566	.4495

	Timoshenko [6]	Current (GHOT)	Current (SGHOT)
b/a = 0.50	1.274	1.014	1.259
b/a = 1	1.294	1.209	1.280
b/a = 2	1.301	1.264	1.290
b/a = 1000	1.304	1.282	1.294

	elasticity [3,21]	Timoshenko [6]	Current (GHOT)	Current (SGHOT)
b/a = 0.50	1.257	1.289	1.257	1.255
b/a = 1	1.303	1.333	1.305	1.303
b/a = 2	1.328	1.349	1.331	1.335
b/a = 1000	1.339	1.354	1.342	1.336

with $\omega_o = \frac{n\pi}{L}\sqrt{\frac{E}{\rho}}$, and $\omega_s = \sqrt{\frac{G}{\rho r}}$.

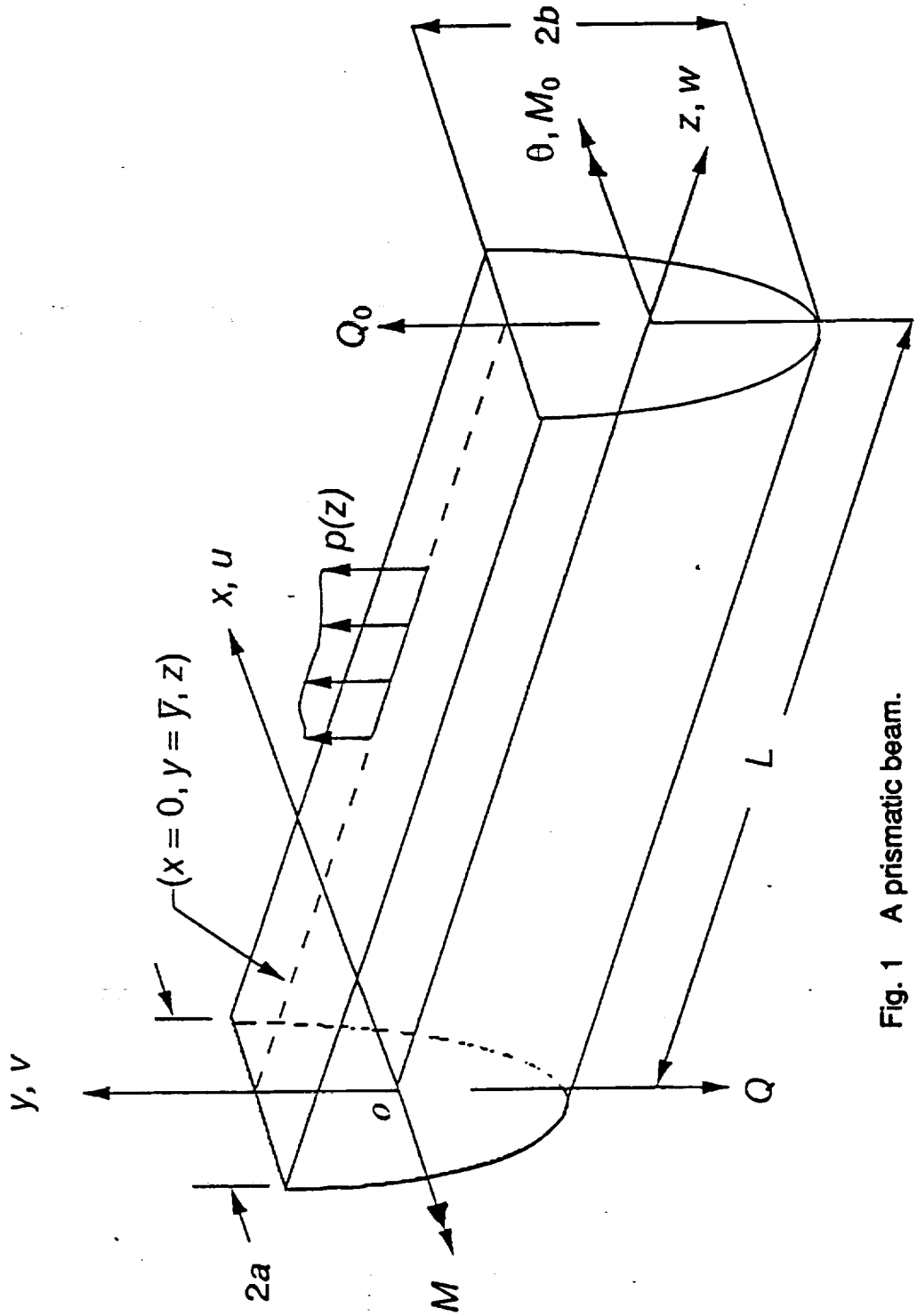

Fig. 1 A prismatic beam.

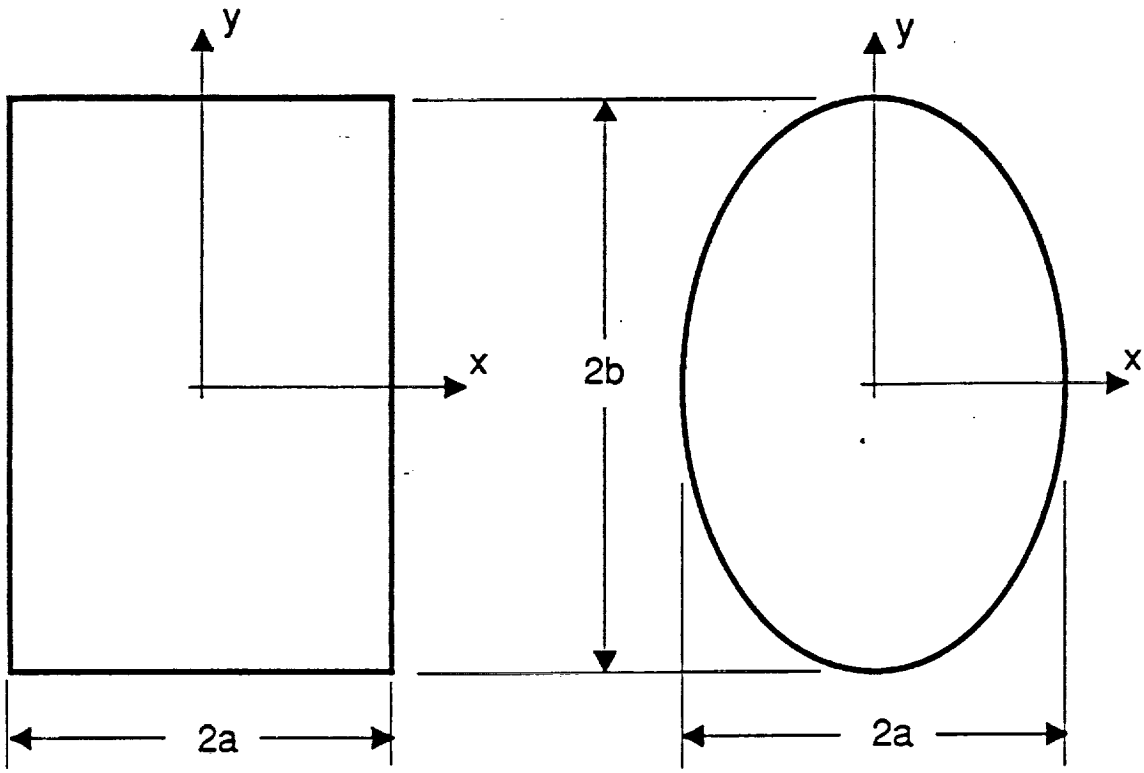

Fig. 2 A rectangular and an elliptical cross-section.

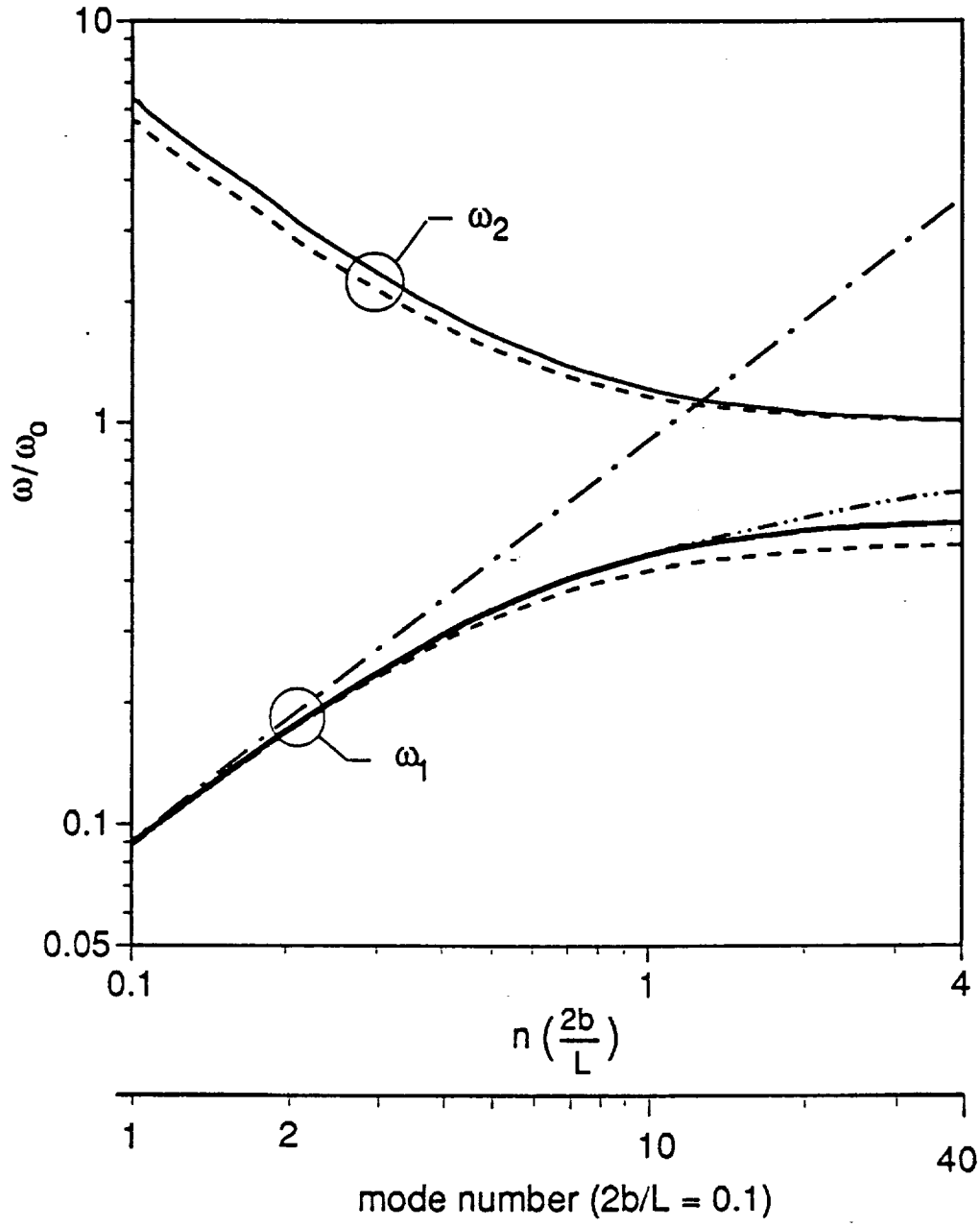

Fig. 3 Natural frequencies of a simply-supported beam with a thin rectangular cross-section (b/a=1000) (——— [6,7,11] and SGHOT, — - - - GHOT, — — — [1,2], — · — Bernoulli-Euler).

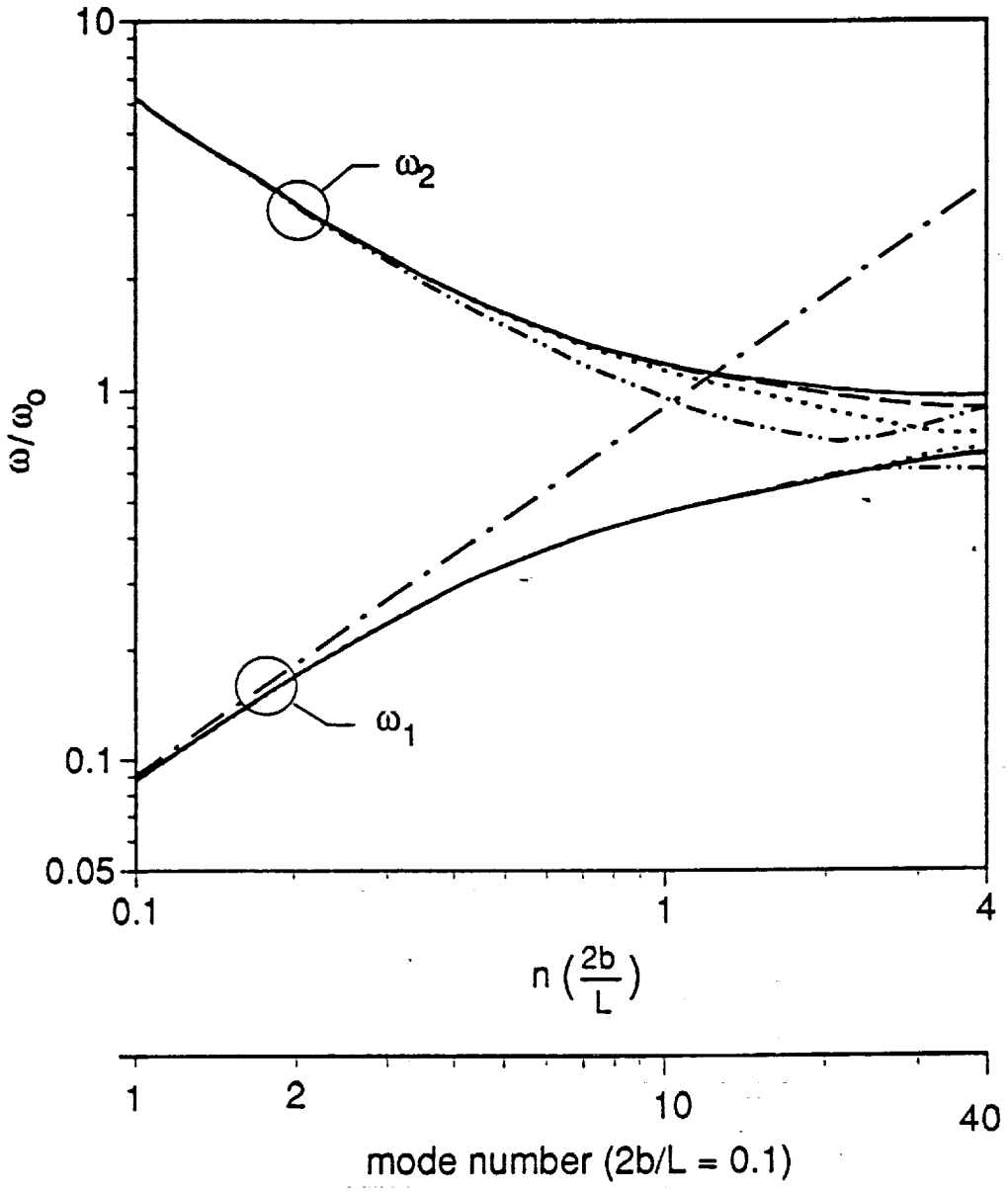

Fig. 4 Natural frequencies of a simply-supported beam with a rectangular cross-section using the general higher-order theory (GHOT), (——— *b/a*=10-1000, — — *b/a*=2, - - - - *b/a*=1, — - - — *b/a*=0.5, — - — Bernoulli-Euler).

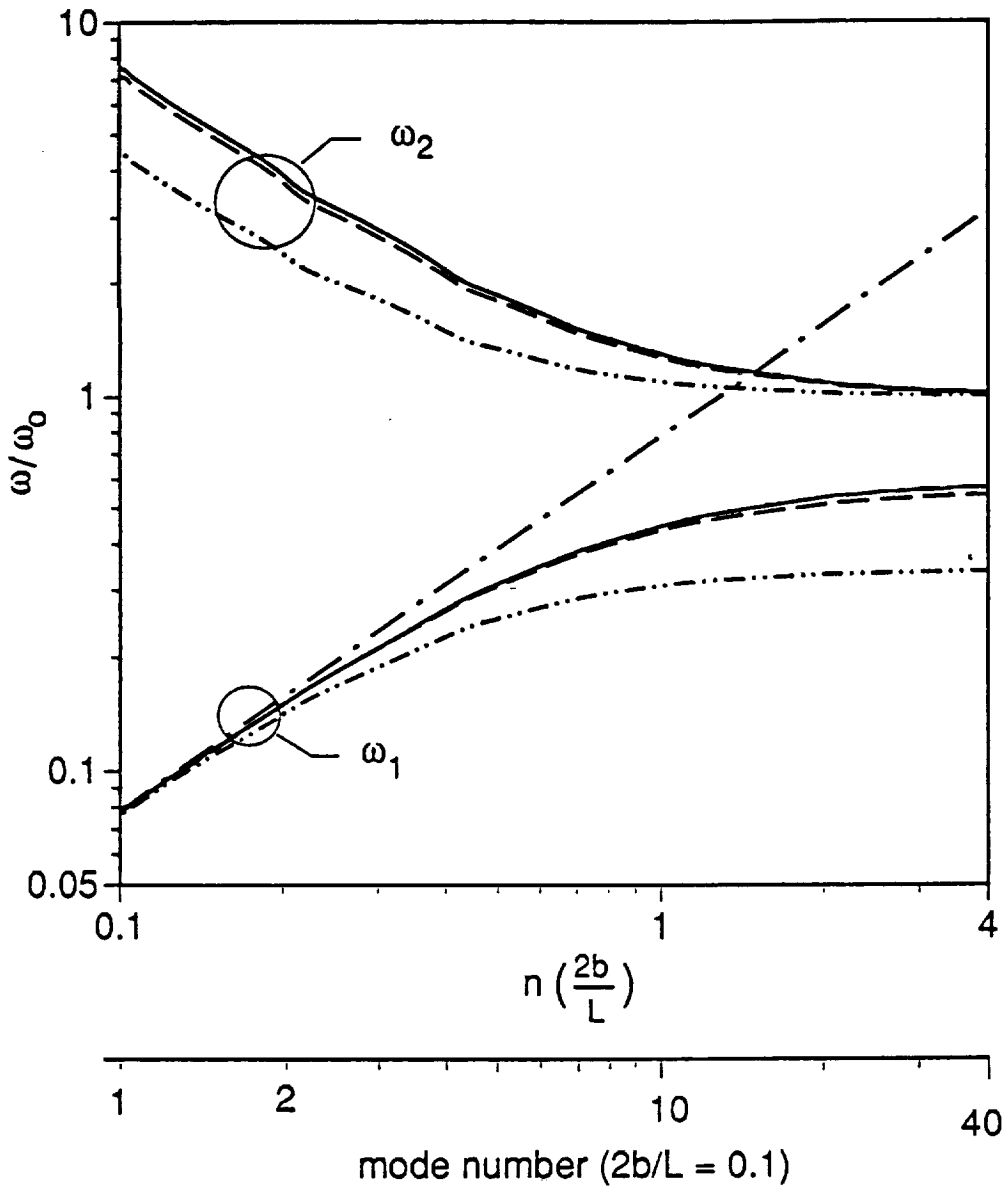

Fig. 5 Natural frequencies of a simply-supported beam with an elliptical cross-section using the Cowper's version of the Timoshenko theory [6] (——— *b/a*=1000 (k=0.91718), —— —— *b/a*=.5 (*k*=0.8296), —— - - —— *b/a*=0.1 (*k*=0.3040), —— - —— Bernoulli-Euler).

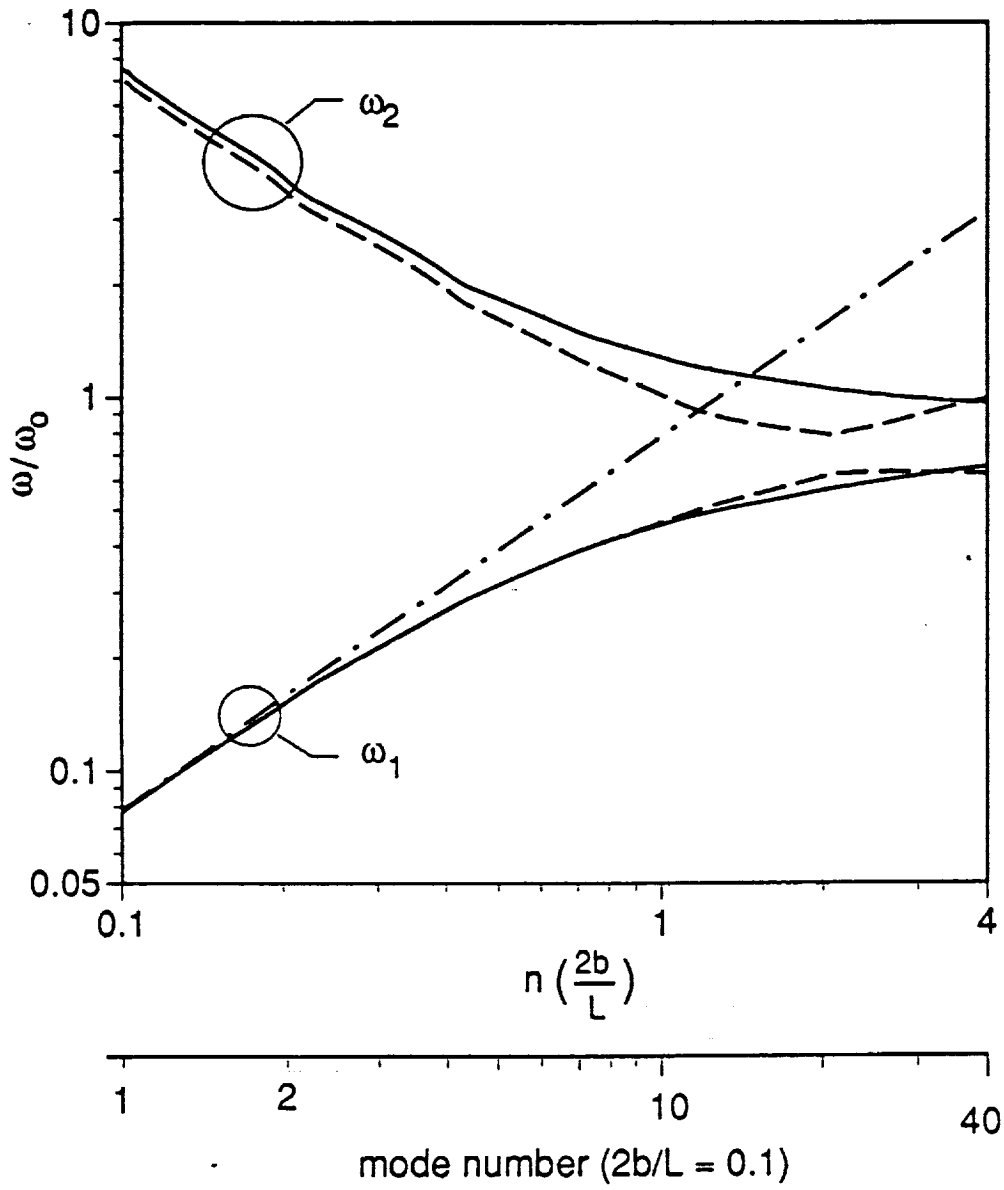

Fig. 6 Natural frequencies of a simply-supported beam with an elliptical cross-section using the general higher-order theory (GHOT), (——— *b/a*=1-1000, —— —— *b/a*=.5, —— - ——Bernoulli-Euler).

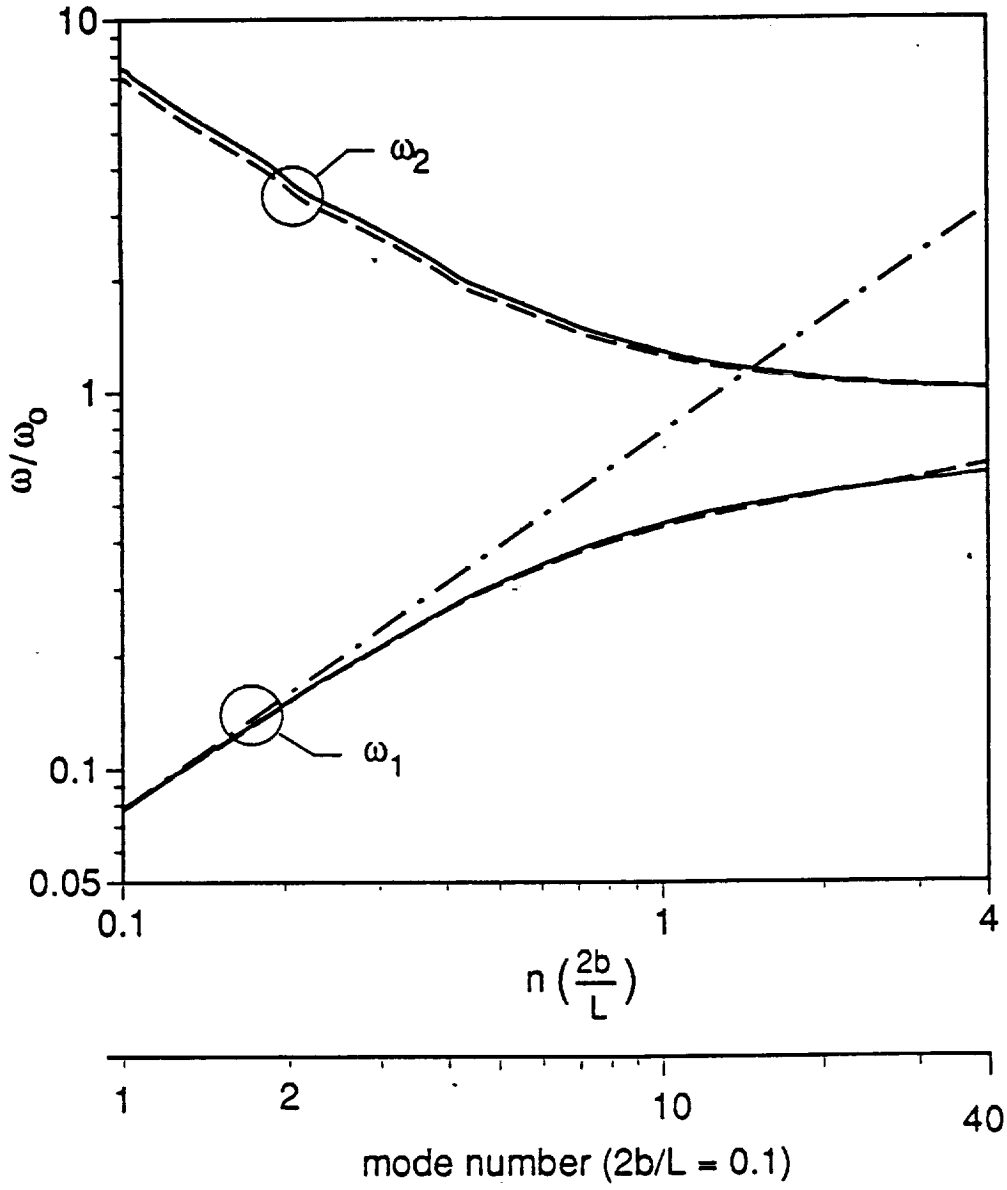

Fig. 7 Natural frequencies of a simply-supported beam with an elliptical cross-section using the simplified general higher-order theory (SGHOT), (——— *b/a*=1-1000, — — *b/a*=.5, — - — Bernoulli-Euler).

Chapter 6

FORMULATION OF A NONLINEAR THEORY FOR SPINNING ANISOTROPIC BEAMS

BY

C.A. Ie and J.B. Kosmatka

Department of Applied Mechanics and Engineering Sciences
University of California, San Diego
La Jolla, CA 92093

ABSTRACT

A geometrically nonlinear theory is developed for spinning anisotropic beams having arbitrary cross-sections. An assumed displacement field is developed using the standard three-dimensional kinematic relations to describe the global beam behavior supplemented with an additional field that represents the local deformation within the cross section and warping out of the cross section plane. It is assumed that the magnitude of this additional field is directly proportional to the local stress resultants.Using a developed ordering scheme, the nonlinear strains are calculated to the third order. Through Hamilton's principle, the six governing equations are obtained.The finite element model is developed using the weak form variational formulation. Numerical results for a static case show that the model agrees with the elasticity solution up to the stress level. Results on the free vibration cases show that the behavior of anisotropic beams are indeed more complex compared to the isotropic counterpart, i.e. complete coupling (bending torsion shear and extension) exists for these type of beams.

INTRODUCTION

Consider a prismatic beam of length (L) composed of an arbitrary anisotropic material having a general cross-section (see Fig.1). For solely the purpose of simplicity of formulation, but without loss of generality, let us assume that the material is homogeneous through out the entire body. Cartesian coordinate systems (X, Y, Z) and (x, y, z) are defined on the beam where y and z are coincident with the principle axes of the root cross-section and x is coincident with the line of centroids. The beam is located (H_X, H_Y, H_Z) with respect to the coordinate system (X, Y, Z) and spins about the coordinate Z with a constant angular velocity Ω. The beam is subjected to distributed loads p_x, p_y, and p_z, which are assumed to act on the coordinate line x.

Existing beam theories have been developed by neglecting the in-plane stresses, i.e., σ_{yy}, σ_{zz} and σ_{yz}, (Love, 1927). Classical beam theory further assumes that plane sections perpendicular to the undeformed x axis remains planes (first assumption) and perpendicular (second assumption) to the the deformed x axis. As a consequent, the shear strains will automatically vanish. To take into account the shear strain energy, Timoshenko (1921, 1922) developed a theory that abundant the

second assumption. Due to the fact that these theories were developed for isotropic materials, they assume uncoupled global material behavior.

Beams theories that were developed by abandoning both constraints exist. Levinson (1981), Heyliger and Reddy (1988) and Kant and Gupta (1988) developed theories that more accurately represent the kinematical relations by introducing shear related warping function which is proportional to the intensity of the shear strains at the centroid. These theories were developed exclusively for isotropic material with a thin rectangular cross section. Vlasov (1961) developed a theory that also include the out-of-plane warping for thin-walled isotropic beams having simple cross-sections. Bauchau (1985) extended this approach for thin-wall composite beams where eigen-warping functions were used to model the out-of-plane shear-dependent warping. Recently, Ie and Kosmatka (1992.a) developed a beam theory for isotropic general cross-sections using first-order warping functions that can predict not only the global behaviors but also the local behaviors (strains and stresses).

This paper extends the development by Ie and Kosmatka (1992.a) to a more complex material definition, i.e. anisotropic materials. For the sake of simplicity and clarity, but without loss of generality, this theory is developed for the case of beams having homogeneous material through out the body. A set of numerical examples is presented for beams having elliptical cross sections. Exact warping functions for this cross section can be found in a paper by Ie and Kosmatka (1992.b). For beams having general cross-sections and material definitions, the warping functions can be found using a model developed by Kosmatka and Dong (1991).

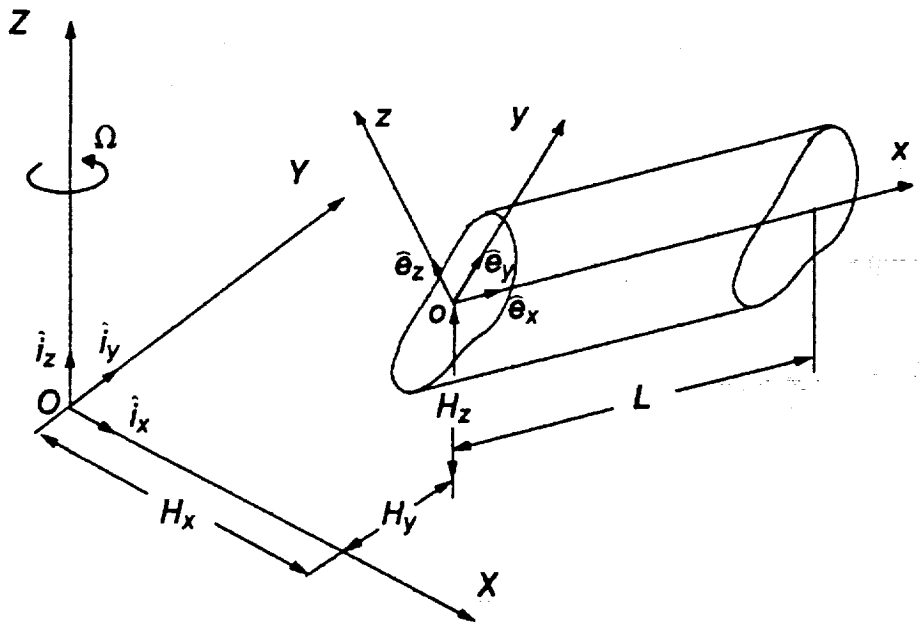

Fig. 1 A spinning anisotropic beam.

THEORETICAL DEVELOPMENT

Assumed Displacement Field, Mixed Formulation

Through out the body, the displacement distributions in the x -, y- and z -directions are defined as

$$\tilde{u}(x,y,z,t)=u(x,t)+z\,\theta_y(x,t)-y\,\theta_z(x,t)+W_1(x,y,z,t)\ ,$$
$$\tilde{v}\ (x,y,z,t)=v(x,t)-z\,\theta_x(x,t)+W_2(x,y,z,t)\ , \qquad (1.a\text{–}c)$$
$$\tilde{w}\ (x,y,z,t)=w(x,t)+y\,\theta_x(x,t)+W_3(x,y,z,t)\ ,$$

where u, v, and w represent the displacements in the directions of the coordinate axes x-, y-, and z- respectively and θ_x, θ_y and θ_z represent the rotations about the coordinate axes x-, y-, and z- respectively. W_1, W_2 and W_3, represent the total local warping functions (displacements) of the cross sections in the directions of the coordinate axes x-, y-, and z- respectively . These functions are assumed to have the following form

$$W_1\ (x,y,z,t)=\sum_{i=1}^{6} F_i\,(x,t)\ \ w_{1i}\,(y,z)\ ,$$
$$W_2\ (x,y,z,t)=\sum_{i=1}^{6} F_i\,(x,t)\ \ w_{2i}\,(y,z)\ , \qquad (2.a\text{–}c)$$
$$W_3\ (x,y,z,t)=\sum_{i=1}^{6} F_i\,(x,t)\ \ w_{3i}\,(y,z)\ ,$$

where

$$F_1(x,t)=\int_A \sigma_{xx}\,dA\ , \qquad F_2(x,t)=\int_A \sigma_{xy}\,dA\ ,$$
$$F_3(x,t)=\int_A \sigma_{zx}\,dA\ , \qquad F_4(x,t)=\int_A (y\,\sigma_{zx}-z\,\sigma_{xy})\,dA\ , \qquad (3.a\text{–}f)$$
$$F_5(x,t)=\int_A z\,\sigma_{xx}\,dA\ , \qquad F_6(x,t)=-\int_A y\,\sigma_{xx}\,dA\ ,$$

in which A is the area of the cross section, σ_{xx}, σ_{yy} and σ_{zz} are the normal stress components and σ_{yz}, σ_{zx} and σ_{xy} are the shear stress components. F_1, F_2 and F_3, are the local stress resultants (forces) in the x-, y-, and z- directions respectively and F_4, F_5 and F_6, are the local stress resultants (moments) about the coordinate axes x, y, and z respectively. Further, w_{1i} , w_{2i} and w_{3i} (named as beam warping functions) are the warpings of the cross section with a thickness dx (zero thickness) due to individual stress resultant F_i provided that the area dA is fixed against translational displacements and rotations. Solving the boundary value problem given in Fig. 2 , in which the only nonzero stress resultant is F_3, the warping functions w_{13} , w_{23} and w_{33} will be obtained. The others fifteen warping functions can be obtained in a similar way.

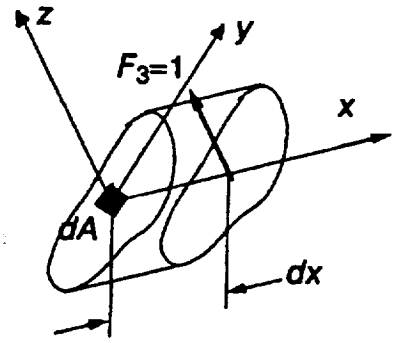

Fig. 2 A procedure to obtain warping functions.

The general constitutive relations are given as

$$\{\sigma\} = [C]\{\varepsilon\}, \tag{4}$$

where the stress and strain arrays are defined as

$$\begin{aligned} \{\sigma\}^T &= \{\ \sigma_{xx},\ \sigma_{yy},\ \sigma_{zz},\ \sigma_{yz},\ \sigma_{zx},\ \sigma_{xy}\ \}, \\ \{\varepsilon\}^T &= \{\ \varepsilon_{xx},\ \varepsilon_{yy},\varepsilon_{zz},\ \gamma_{yz},\ \gamma_{zx},\ \gamma_{xy}\ \}, \end{aligned} \tag{5.a,b}$$

and $[C]$ is the material stiffness matrix which may have twenty one distinct stiffness constants.

Assumed Displacement Field, Purely Kinematic Formulation

It is necessary to transform the assumed displacement field in eqns (1.*a-c*) to a purely kinematic field counterpart before further formulations can be furnished. For this purpose, a linear strain-displacement relationship is being adopted, i.e.

$$\begin{aligned} \varepsilon_{xx} &= \frac{\partial \tilde{u}}{\partial x}, & \varepsilon_{yy} &= \frac{\partial \tilde{v}}{\partial y}, & \varepsilon_{zz} &= \frac{\partial \tilde{w}}{\partial z}, \\ \gamma_{yz} &= \frac{\partial \tilde{w}}{\partial y}+\frac{\partial \tilde{v}}{\partial z}, & \gamma_{zx} &= \frac{\partial \tilde{u}}{\partial z}+\frac{\partial \tilde{w}}{\partial x}, & \gamma_{xy} &= \frac{\partial \tilde{v}}{\partial x}+\frac{\partial \tilde{u}}{\partial y}. \end{aligned} \tag{6.a-f}$$

On the basis of beam elemental equilibrium, the following assumptions are being made

$$\begin{aligned} F_1' &= -p_x = 0, & F_2' &= -p_y = 0, \\ F_3' &= -p_z = 0, & F_4' &= 0. \end{aligned} \tag{7.a-d}$$

Also note that

$$F_5' = F_3, \qquad F_6' = -F_2. \tag{7.e,f}$$

Using the above assumptions, the local stress resultants can be expressed in terms of u, v, w, θ_x, θ_y and θ_z (and their derivatives) by first calculating the strains using eqn (6.*a-f*) and eqn (1.*a-c*), then using this strains to get the stresses through eqn (4), and finally substituting the calculated stresses into eqns (3.*a-f*) to get the following result

$$\{F\} = [H]\{e\}, \tag{8}$$

where $\{F\}$ is an array

$$\{F\}^T = \{\ F_1,\ F_2,\ F_3,\ F_4,\ F_5,\ F_6\ \}, \tag{9}$$

$[H]$ is a six by six matrix which depends on the geometry of the cross section, material properties and warping functions, and $\{e\}$ is an array

$$\begin{aligned} \{e\}^T &= \{\ e_1,\ e_2,\ e_3,\ e_4,\ e_5,\ e_6\ \} \\ &= \{u',\ v'-\theta_z,\ w'+\theta_y,\ \theta_x',\ \theta_y',\ \theta_z'\}. \end{aligned} \tag{10}$$

Finally, the desired form of the assumed displacement field is obtained by substituting eqn (8) into eqn (1) through eqn (2), resulting in the following formulation

$$\tilde{u}(x,y,z,t) = u(x,t)+z\,\theta_y(x,t)-y\,\theta_z(x,t)+\psi_1(x,y,z,t)\ ,$$
$$\tilde{v}(,y,z,t) = v(x,t)-z\,\theta_x(x,t)+\psi_2(x,y,z,t)\ , \qquad (11.a\text{–}c)$$
$$\tilde{w}(,y,z,t) = w(x,t)+y\,\theta_x(x,t)+\psi_3(x,y,z,t)\ ,$$

where

$$\psi_i(x,y,z,t) = \sum_{k=1}^{6} e_k(x,t)\ \varphi_{ik}(y,z), \qquad i = 1\text{–}3\ , \qquad (12.a,b)$$
$$\varphi_{ij} = \sum_{k=1}^{6} H_{kj}\, w_{ik}\ , \qquad i = 1\text{–}3, \qquad j = 1\text{–}6\ .$$

This displacement field will be used as the basis for the remaining development, where no limiting assumptions are made corresponding to load type.

Ordering Scheme

To identify and delete higher order terms which are produced during the derivation of the governing equations, it is necessary to define an ordering scheme. First of all, let assume that the beam is relatively long and slender such that the geometric ratios of the cross section to the length (y/L, z/L) are in the order of e which is defined to be equal to 0.2. Since x is the centroidal axis of the beam, (x/L, $L\,\partial(\ )/\partial x$) are in the order of one. To assign the orders of others terms, a study of the deflection patterns of a tip loaded anisotropic cantilever beam composed of material properties of High-Strength Graphite/Epoxy (see Table 1) has been performed using the exact results obtained by Ie and Kosmatka (1992.b). Due to the fact that the beam spins, the order of u/L has been increased up to ε^2.

Table 1: Typical Material Properties of High-Strength Graphite/Epoxy.

E_{11}	145.0	GPa
$E_{22} = E_{33}$	10.0	GPa
$G_{12} = G_{13}$	4.8	GPa
$\nu_{12} = \nu_{13}$	0.25	
ν_{23}	0.40	
ρ	1580	kg/m^3

Taking only up to the third order of ε, an ordering scheme will be obtained in the following manner

Order 1 :

$$\frac{x}{L}, \qquad L\,\frac{\partial(\ )}{\partial x}\ . \qquad (13.a)$$

Order ε :

$$\frac{y}{L}, \qquad \frac{z}{L}, \qquad \frac{v}{L}, \qquad \frac{w}{L}, \quad \theta_x, \quad \theta_y, \quad \theta_z . \tag{13.b}$$

Order ε^2 :

$$\frac{u}{L}, \qquad \frac{\partial(\psi_1, \psi_2, \psi_3)}{\partial y}, \qquad \frac{\partial(\psi_1, \psi_2, \psi_3)}{\partial z} . \tag{13.c}$$

Order ε^3 :

$$\frac{(\psi_1, \psi_2, \psi_3)}{L}, \qquad \frac{\partial(\psi_1, \psi_2, \psi_3)}{\partial x} . \tag{13.d}$$

Nonlinear Strain-Displacement Relations

A geometrically nonlinear strain-displacement relationship is being adopted as follows

$$\varepsilon_{xx} = \frac{\partial \tilde{u}}{\partial x} + \frac{1}{2}\left[\left(\frac{\partial \tilde{u}}{\partial x}\right)^2 + \left(\frac{\partial \tilde{v}}{\partial x}\right)^2 + \left(\frac{\partial \tilde{w}}{\partial x}\right)^2\right], \qquad \varepsilon_{yy} = \frac{\partial \tilde{v}}{\partial y} + \frac{1}{2}\left[\left(\frac{\partial \tilde{u}}{\partial y}\right)^2 + \left(\frac{\partial \tilde{v}}{\partial y}\right)^2 + \left(\frac{\partial \tilde{w}}{\partial y}\right)^2\right],$$

$$\varepsilon_{zz} = \frac{\partial \tilde{w}}{\partial z} + \frac{1}{2}\left[\left(\frac{\partial \tilde{u}}{\partial z}\right)^2 + \left(\frac{\partial \tilde{v}}{\partial z}\right)^2 + \left(\frac{\partial \tilde{w}}{\partial z}\right)^2\right], \qquad \gamma_{yz} = \frac{\partial \tilde{w}}{\partial y} + \frac{\partial \tilde{v}}{\partial z} + \frac{\partial \tilde{u}}{\partial y}\frac{\partial \tilde{u}}{\partial z} + \frac{\partial \tilde{v}}{\partial y}\frac{\partial \tilde{v}}{\partial z} + \frac{\partial \tilde{w}}{\partial y}\frac{\partial \tilde{w}}{\partial z}, \tag{14.a-f}$$

$$\gamma_{zx} = \frac{\partial \tilde{u}}{\partial z} + \frac{\partial \tilde{w}}{\partial x} + \frac{\partial \tilde{u}}{\partial z}\frac{\partial \tilde{u}}{\partial x} + \frac{\partial \tilde{v}}{\partial z}\frac{\partial \tilde{v}}{\partial x} + \frac{\partial \tilde{w}}{\partial z}\frac{\partial \tilde{w}}{\partial x}, \qquad \gamma_{xy} = \frac{\partial \tilde{v}}{\partial x} + \frac{\partial \tilde{u}}{\partial y} + \frac{\partial \tilde{u}}{\partial x}\frac{\partial \tilde{u}}{\partial y} + \frac{\partial \tilde{v}}{\partial x}\frac{\partial \tilde{v}}{\partial y} + \frac{\partial \tilde{w}}{\partial x}\frac{\partial \tilde{w}}{\partial y}.$$

Substituting eqns (1.*a-c*) into the above equations and applying the ordering scheme as shown in eqns (13.*a-d*), the strain array can written as follows

$$\{\varepsilon\} = [X]\{\epsilon\}, \tag{15}$$

where the matrix $[X]$ only depends upon cross sectional dependent functions and $\{\epsilon\}$ is an array of macroscopic strain measures which depends on the six variables u, v, w, θ_x, θ_y and θ_z . $[X]$ and $\{\epsilon\}$ can be decomposed into linear and nonlinear parts as follows

$$[X] = [\,[X_l]\ [X_{nl}^2]\ [X_{nl}^3]\,], \tag{16}$$

$$\{\epsilon\} = \{\epsilon_l\} + \{\epsilon_{nl}^2\} + \{\epsilon_{nl}^3\}. \tag{17}$$

See the Appendix for detailed expressions of $[X]$ and $\{\epsilon\}$.

Strain Energy

The strain energy is defined as follows

$$U = \frac{1}{2}\int_0^L \int_A \{\varepsilon\}^T [C]\{\varepsilon\} dA\, dx . \tag{18}$$

Substituting eqn (15) into eqn (18), the strain energy can be written as follows

$$U = \frac{1}{2}\int_0^L \{\epsilon\}^T [Se] \{\epsilon\} dx \ , \tag{19}$$

where the matrix $[Se]$ is called section constant and is defined as follows

$$[Se] = \int_A [X]^T [C] [X] dA \ . \tag{20}$$

Furthermore, substituting eqn (17) into eqn (19), the following will be obtained

$$U = \frac{1}{2}\int_0^L \left(\left\{\epsilon_{nl}^3\right\}^T + \left\{\epsilon_{nl}^2\right\}^T + \left\{\epsilon_l\right\}^T\right) [Se] \left(\left\{\epsilon_l\right\} + \left\{\epsilon_{nl}^2\right\} + \left\{\epsilon_{nl}^3\right\}\right) dx \ . \tag{21}$$

Finally, carry out the multiplication, neglecting the term associated with multiplication between the third order strain measures, the following expression for the strain energy will be obtained

$$\begin{aligned} U = \frac{1}{2}\int_0^L & \left(\left\{\epsilon_l\right\}^T [Se] \left\{\epsilon_l\right\} + 2\left\{\epsilon_l\right\}^T [Se] \left\{\epsilon_{nl}^2\right\} + 2\left\{\epsilon_l\right\}^T [Se] \left\{\epsilon_{nl}^3\right\}\right. \\ & \left. + \left\{\epsilon_{nl}^2\right\}^T [Se] \left\{\epsilon_{nl}^2\right\} + 2\left\{\epsilon_{nl}^2\right\}^T [Se] \left\{\epsilon_{nl}^3\right\}\right) dx \ . \end{aligned} \tag{22}$$

Kinetic Energy

The kinetic energy of the beam is defined as follows

$$T = \frac{1}{2}\int_0^L \int_A \rho \ \bar{V} . \bar{V} \ dA \ dx \ , \tag{23}$$

where ρ is the mass density and $\bar{V}$ is the velocity vector which is equal to

$$\bar{V} = \frac{\partial \bar{r}}{\partial t} + \Omega \hat{i}_z \times \bar{r} \ , \tag{24}$$

in which $\bar{r}$ is the position vector defined as

$$\bar{r} = (H_x, H_y, H_z) \begin{Bmatrix} \hat{i}_x \\ \hat{i}_y \\ \hat{i}_z \end{Bmatrix} + (x+\tilde{u}, y+\tilde{v}, z+\tilde{w}) \begin{Bmatrix} \hat{e}_x \\ \hat{e}_y \\ \hat{e}_z \end{Bmatrix} \tag{25}$$

Transforming into the beam coordinate system, the position vector can be written as follows

$$\bar{r} = (h_x+x+\tilde{u}, h_y+y+\tilde{v}, h_z+z+\tilde{w}) \begin{Bmatrix} \hat{e}_x \\ \hat{e}_y \\ \hat{e}_z \end{Bmatrix} , \tag{26}$$

where $(h_x, h_y, h_z) = (H_x, H_y, H_z)\ [B]^T$, and $[B]$ is a transformation matrix between the two sets of the coordinate systems by rotating through Euler angles $\beta_3, \beta_2, \beta_1$ in which $[B] = [B_1]\ [B_2]\ [B_3]$.

$$B_1=\begin{pmatrix} 1 & 0 & 0 \\ 0 & \cos\beta_1 & \sin\beta_1 \\ 0 & -\sin\beta_1 & \cos\beta_1 \end{pmatrix},\quad B_2=\begin{pmatrix} \cos\beta_2 & 0 & -\sin\beta_2 \\ 0 & 1 & 0 \\ \sin\beta_2 & 0 & \cos\beta_2 \end{pmatrix},\quad B_3=\begin{pmatrix} \cos\beta_3 & \sin\beta_3 & 0 \\ -\sin\beta_3 & \cos\beta_3 & 0 \\ 0 & 0 & 1 \end{pmatrix}. \quad (27.a\text{-}c)$$

Substituting eqn (26) into eqn (24) and making use of eqns (27.a-c), the velocity vector becomes

$$\begin{aligned}\overline{V}=&\left(\dot{\tilde{u}}+\Omega_y(h_z+z+\tilde{w})-\Omega_z(h_y+y+\tilde{v})\right)\hat{e}_x+\left(\dot{\tilde{v}}-\Omega_x(h_z+z+\tilde{w})+\Omega_z(h_x+x+\tilde{u})\right)\hat{e}_y+\\&\left(\dot{\tilde{w}}+\Omega_x(h_y+y+\tilde{v})-\Omega_y(h_x+x+\tilde{u})\right)\hat{e}_z\ ,\end{aligned} \quad (28)$$

in which $(\Omega_x, \Omega_y, \Omega_z) = (0, 0, \Omega)\ [B]^T$.

The Governing Equations (Equations of Motion)

The six governing equations for the beam are determined by applying the Hamilton's principle as follows

$$\delta\int_{t_1}^{t_2}(-U+T+W_e)\,dt=0\ , \quad (29)$$

where U, T and W_e are the strain energy, kinetic energy and work done by external forces, respectively.
The variation of the strain energy can be written as follows

$$\delta U=\int_0^L\int_A\{\sigma\}^T\{\delta\epsilon\}dA\,dx\ . \quad (30)$$

Substituting the expression for the strain array from eqns (15) and (17) into the above equation, the following result will be obtained

$$\delta U=\int_0^L\{R\}^T\left(\{\delta\epsilon_l\}+\{\delta\epsilon^2_{nl}\}+\{\delta\epsilon^3_{nl}\}\right)dx\ , \quad (31)$$

where $\{R\}$ is an array of stress resultants with forty eight elements defined as follows

$$\{R\}=\int_A[X]^T\{\sigma\}\,dA\ . \quad (32)$$

The variation of the kinetic energy as shown in eqn (23) can be decomposed into three parts as follows

$$\int_{t_1}^{t_2}\delta T\,dt=\int_{t_1}^{t_2}\left(\delta T_2+\delta T_1+\delta T_0\right)dt\ , \quad (33)$$

where

$$\int_{t_1}^{t_2} \delta T_2 dt = \int_{t_1}^{t_2} \int_0^L \{\delta \dot{q}\}^T [m] \{\dot{q}\}\, dx\ dt\,,$$

$$\int_{t_1}^{t_2} \delta T_1 dt = \int_{t_1}^{t_2} \int_0^L \left(\{\delta q\}^T [m_c] \{\dot{q}\} + \{\delta \dot{q}\}^T [m_c]^T \{q\} + \{\delta \dot{q}\}^T \{f_{co}\} \right) dx\, dt\,, \qquad (34.a\text{-}c)$$

$$\int_{t_1}^{t_2} \delta T_0 dt = -\int_{t_1}^{t_2} \int_0^L \left(\{\delta q\}^T (-[\bar{k}_s]) \{q\} - \{\delta q\}^T \{f_{cf}\} \right) dx\ dt\ .$$

The above equations are associated with inertia, Coriolis and centrifugal forces, respectively. Note that $\{\cdot\}$ indicates the derivatives with respect to time. The array $\{q\}$ is defined as follows

$$\{q\}^T = \left(u,\ v,\ w,\ \theta_x,\ \theta_y,\ \theta_z,\ u',\ v',\ w',\ \theta_x',\ \theta_y',\ \theta_z'\right). \qquad (35)$$

Matrix $[m]$, $[m_C]$ and $[\bar{k}_S]$ are the mass, Coriolis, and centrifugal softening -type matrices, respectively. Arrays $\{f_{CO}\}$ and $\{f_{Cf}\}$ are the Coriolis and centrifugal force-type arrays, respectively. Due to the fact that Ω is constant, the array $\{f_{CO}\}$ will not contribute to the governing equations. The details of the expressions can be found in the Appendix. Integrating by parts the expressions in eqns (34.*a-c*) with respect to time, the following results will be obtained

$$\int_{t_1}^{t_2} \delta T_2 dt = -\int_{t_1}^{t_2} \int_0^L \{\delta q\}^T \{Z\}\, dx\ dt\,,$$

$$\int_{t_1}^{t_2} \delta T_1 dt = -\int_{t_1}^{t_2} \int_0^L \{\delta q\}^T \{\bar{Z}\}\, dx\, dt\,, \qquad (36.a\text{-}c)$$

$$\int_{t_1}^{t_2} \delta T_0 dt = -\int_{t_1}^{t_2} \int_0^L \{\delta q\}^T \left(\{\hat{Z}\} - \{f\}\right) dx\ dt\ ,$$

where

$$\{Z\} = [m]\{\ddot{q}\}\,, \quad \{\bar{Z}\} = [\bar{m}_{co}]\{\dot{q}\}, \quad \{\hat{Z}\} = -[\bar{k}_s]\{q\}\,. \qquad (37.a\text{-}c)$$

in which $[\bar{m}_{CO}] = -2\,[m_{CO}]$.

The variation of the external work done is as follows

$$\delta W_e = \int_0^L (p_x\, \delta u + p_y\, \delta v + p_z\, \delta w)\, dx\,. \qquad (38)$$

Substituting eqn (31), eqns (36.*a-c*) and eqn (38) into eqn (29) and taking any necessary integration by parts, the boundary conditions and the six governing equations will be obtained as follows

Boundary Conditions :

Specify u or N_u which is equal to

$$N_u = R_1 - R_7' + R_{19}v' + R_{25}w' + R_{31}\theta_x + R_{37}\theta_y - R_{43}\theta_z + Z_7 + \overline{Z}_7 + \hat{Z}_7 - f_7 . \qquad (39.a)$$

Specify v or N_v which is equal to

$$N_v = R_2 - R_8' + R_{19}u' + (R_{13}+2R_{20})v' + (R_{21}+R_{26})w' + (R_{17}+R_{32})\theta_x + (R_{21}+R_{38})\theta_y - (R_{20}+R_{44})\theta_z + R_{22}\theta_x' + R_{23}\theta_y' + R_{24}\theta_z' + Z_8 + \overline{Z}_8 + \hat{Z}_8 - f_8 . \qquad (39.b)$$

Specify w or N_w which is equal to

$$N_w = R_3 - R_9' + R_{25}u' + (R_{21}+R_{26})v' + (R_{13}+2R_{27})w' + (R_{18}+R_{33})\theta_x + (R_{27}+R_{39})\theta_y - (R_{26}+R_{45})\theta_z + R_{28}\theta_x' + R_{29}\theta_y' + R_{30}\theta_z' + Z_9 + \overline{Z}_9 + \hat{Z}_9 - f_9 . \qquad (39.c)$$

Specify θ_x or M_x which is equal to

$$M_x = R_4 - R_{10}' + R_{22}v' + R_{28}w' + R_{34}\theta_x + R_{40}\theta_y - R_{46}\theta_z + Z_{10} + \overline{Z}_{10} + \hat{Z}_{10} - f_{10} . \qquad (39.d)$$

Specify θ_y or M_y which is equal to

$$M_y = R_5 + R_9 - R_{11}' + R_{23}v' + R_{29}w' + R_{35}\theta_x + R_{41}\theta_y - R_{47}\theta_z + Z_{11} + \overline{Z}_{11} + \hat{Z}_{11} - f_{11} . \qquad (39.e)$$

Specify θ_z or M_z which is equal to

$$M_z = R_6 - R_8 - R_{12}' + R_{24}v' + R_{30}w' + R_{36}\theta_x + R_{42}\theta_y - R_{48}\theta_z + Z_{12} + \overline{Z}_{12} + \hat{Z}_{12} - f_{12} . \qquad (39.f)$$

Specify u', v', w', θ'_x, θ'_y, and θ'_z or M_u , M_v , M_w, R_x , R_y , and R_z , respectively , which are defined as follows

$$M_u = R_7 , \quad M_v = R_8 , \quad M_w = R_9 , \quad R_x = R_{10} , \quad R_y = R_{11} , \quad R_z = R_{12} . \qquad (40.a\text{-}f)$$

The six governing equations :

$$\frac{\partial N_u}{\partial x} - (Z_1 + \overline{Z}_1 + \hat{Z}_1 - f_1) + p_x = 0 , \quad \frac{\partial N_v}{\partial x} - (Z_2 + \overline{Z}_2 + \hat{Z}_2 - f_2) + p_y = 0 , \quad \frac{\partial N_w}{\partial x} - (Z_3 + \overline{Z}_3 + \hat{Z}_3 - f_3) + p_z = 0 , \qquad (41.a\text{-}f)$$

$$\frac{\partial M_x}{\partial x} + \overline{N}(Z_4 + \overline{Z}_4 + \hat{Z}_4 - f_4) = 0 , \quad \frac{\partial M_y}{\partial x} - \overline{N}_w(Z_5 + \overline{Z}_5 + \hat{Z}_5 - f_5) = 0 , \quad \frac{\partial M_z}{\partial x} + \overline{N}_v(Z_6 + \overline{Z}_6 + \hat{Z}_6 - f_6) = 0 ,$$

where

$$\overline{N} = -R_{31}u' - (R_{17}+R_{32})v' - (R_{18}+R_{33})w' - (R_{14}+R_{15})\theta_x - R_{33}\theta_y + R_{32}\theta_z + R_{35}\theta_y' - R_{36}\theta_z' ,$$

$$\overline{N}_v = R_2 + R_{43}u' + (R_{20}+R_{44})v' + (R_{26}+R_{45})w' + R_{32}\theta_x + (R_{16}+R_{38}+R_{45})\theta_y - (R_{14}+2R_{44})\theta_z + R_{46}\theta_x' + R_{47}\theta_y' , \qquad (42.a\text{-}c)$$

$$\overline{N}_w = R_3 + R_{37}u' + (R_{21}+R_{38})v' + (R_{27}+R_{39})w' + R_{33}\theta_x + (R_{15}+2R_{39})\theta_y - (R_{16}+R_{38}+R_{45})\theta_z + R_{40}\theta_x' + R_{42}\theta_z' .$$

FINITE ELEMENT MODEL

The finite element model is developed using the weak form formulation. The six variables u, v,w ,θ_x, θ_y and θ_z are interpolated using the expressions of the form

$$u = \sum_{i=1}^{4} u_i \phi_i^u , \qquad v = \sum_{i=1}^{5} v_i \phi_i^v , \qquad w = \sum_{i=1}^{5} w_i \phi_i^w ,$$
$$\theta_x = \sum_{i=1}^{4} \theta_i^x \phi_i^x , \qquad \theta_y = \sum_{i=1}^{4} \theta_i^y \phi_i^y , \qquad \theta_z = \sum_{i=1}^{4} \theta_i^z \phi_i^z , \tag{43.a-f}$$

where the variables u,θ_x, θ_y and θ_z are interpolated using four-node Hermite polynomials and v and w are interpolated the same way as u except that one additional node being added in the mid-length of the elements. Substituting the above equations into eqn (29), the associated governing equations (the equations of motion) related to the nodal displacement $\{Q\}$ can be written as follows

$$[M]\{\ddot{Q}\}+[\overline{C}]\{\dot{Q}\}+([K_l] + [K_{nl}]-[K_{cf}])\{Q\} = \{F_e\}+\{F_{cf}\} , \tag{44}$$

where

$$\{Q\}^T = \{ (u_1, u_2, u_3, u_4), (v_1, v_2, v_3, v_4, v_5), (w_1, w_2, w_3, w_4, w_5), \\ (\theta_1^x, \theta_2^x, \theta_3^x, \theta_4^x), (\theta_1^y, \theta_2^y, \theta_3^y, \theta_4^y), (\theta_1^z, \theta_2^z, \theta_3^z, \theta_4^z) \}, \tag{45}$$

$[M]$ is the mass matrix, $[\overline{C}]$ the gyroscopic matrix, $[K_l]$ the linear stiffness matrix, $[Knl]$ the nonlinear stiffness matrix, $[K_{cf}]$ the centrifugal stiffness matrix, $\{F_e\}$ and $\{F_{cf}\}$ the force vectors related to the external and centrifugal loads, respectively.

NUMERICAL EXAMPLES

In this section, numerical examples are presented for beams with elliptical cross section composed of an anisotropic homogeneous material (see Fig. 3.*a*) where (*a*) and (*b*) are one-half of the major and minor dimensions of the cross section, respectively. Through out these examples, a value of (*b*/*a*) equal to one half has been chosen. Furthermore, the beam is assumed to be composed of a single set of unidirectional high strength graphite/epoxy fibers, which is a transversely isotropic material that has five independent constants (see Table 1)

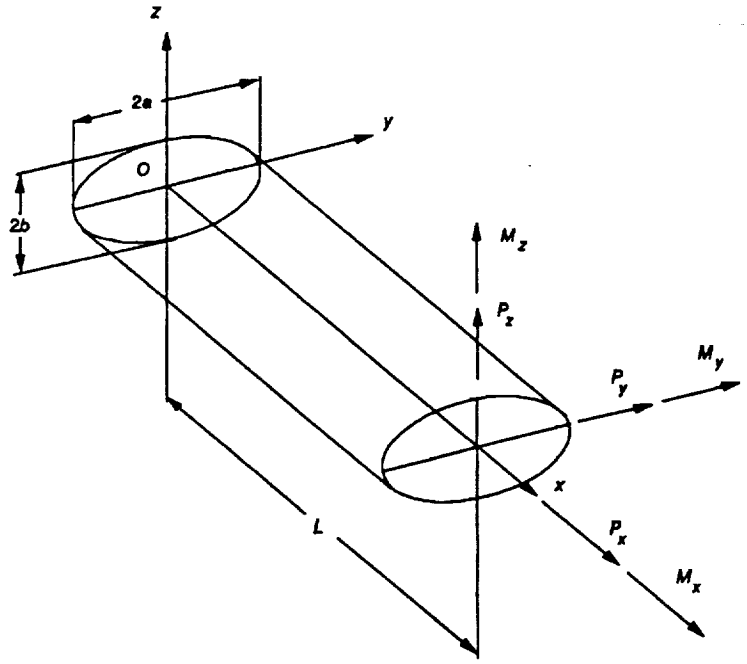

Fig. 3.a A tip-loaded cantilever beam

To achieve orthotropic and/or anisotropic beam behavior, the material reference frame (1,2,3) is oriented relative to the beam Cartesian coordinate frame (x,y,z) using reference angles (β) and (α), which are defined as rotations about the positive x-axis and the positive material 3-axis, respectively. See Fig. 3.b, where the transformation relation between (1,2,3) and (x,y,z) is equal to

$$\begin{Bmatrix} 1 \\ 2 \\ 3 \end{Bmatrix} = \begin{bmatrix} cos(\alpha) & sin(\alpha)\,cos(\beta) & sin(\alpha)\,sin(\beta) \\ -sin(\alpha) & cos(\alpha)\,cos(\beta) & cos(\alpha)\,sin(\beta) \\ 0 & -sin(\beta) & cos(\beta) \end{bmatrix} \begin{Bmatrix} x \\ y \\ z \end{Bmatrix} . \qquad (46)$$

The resulting 21 unique material compliance coefficients (S_{ij}, i,j=1-6) are determined using standard transformation techniques (Lekhnitskii, 1963). Numerical examples for static and free vibration cases are presented for the case of $\alpha = \beta = 30$ degrees, $L/(2a) = 10$. The model predicts the coupled displacements and stresses exactly.

Example 1 : Static, Nonspinning

Consider a cantilever beam fixed at the root with a single tip load P_z (see Fig. *3.a*). Unlike the isotropic counterpart, results show that all six stress components are present. Fig. 4.a-j show the countour plots of these stresses.

Normal Stress σ_{xx} :

Fig. 4.a-d show the changes of σ_{xx} distributions in the cross sections at different values of x. Dotted lines show negative stresses. At the tip (Fig. 4.a), unlike the isotropic counterpart (in which this stress is equal to zero), σ_{xx} distributes in a such a way such that the resultant is equal to zero. This stress will gradually becomes less dominant as the value of (L-x) increases (for cross sections closer to the root). Fig.4.b shows the stress distribution for a value of (L-x)= b, Fig.4.c for (L-x)= $2b$, and Fig.4.d for (L-x)=L (at the root) where the stress distribution is dominated by the "classical" normal stress distribution.

In-Plane Stresses σ_{yy} , σ_{zz} and σ_{yz} :

Due to the anisotropy of the material, these stresses exist. Because the shear forces through out the length are constant, these stress distributions do not change with respect to x . As they have to be, σ_{yy} and σ_{zz} (see Fig. 4.e,f, respectively) vanish at two locations, i.e. at $y = \pm a$, $z = 0$ for σ_{yy} and at $y = 0$, $z = \pm b$ for σ_{zz} . Likewise, σ_{yz} vanishes at four locations, i.e. at $y = \pm a$, $z = 0$ and at $y = 0$, $z = \pm b$ (see Fig.4.g).

Transverse Shear Stresses σ_{zx} and σ_{xy} :

Fig. 4.h,i show the countour plots of transverse shear stresses σ_{zx} and σ_{xy} , respectively. Fig.4.j shows a qualitative vectorial scaled plot of the resultants between these two stresses. From this figure, it is interesting to see that the stress distribution clearly does not resemble that of an isotropic counterpart (i.e. a paraboloid with a maximum occurring at the centroid). Instead, the distribution is nonsymmetric with a maximum occurring on the outer edge.

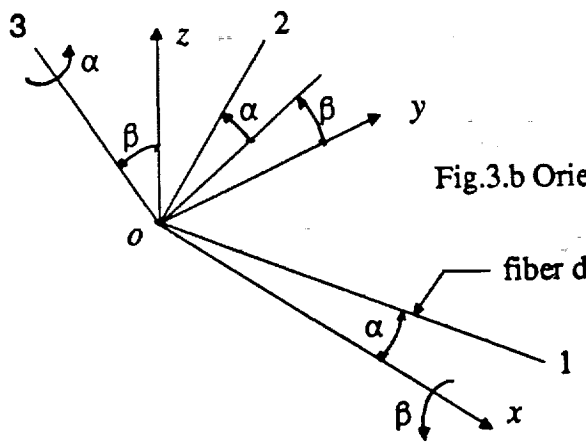

Fig.3.b Orientation of material fibers (1,2,3) relative to (x,y,z).

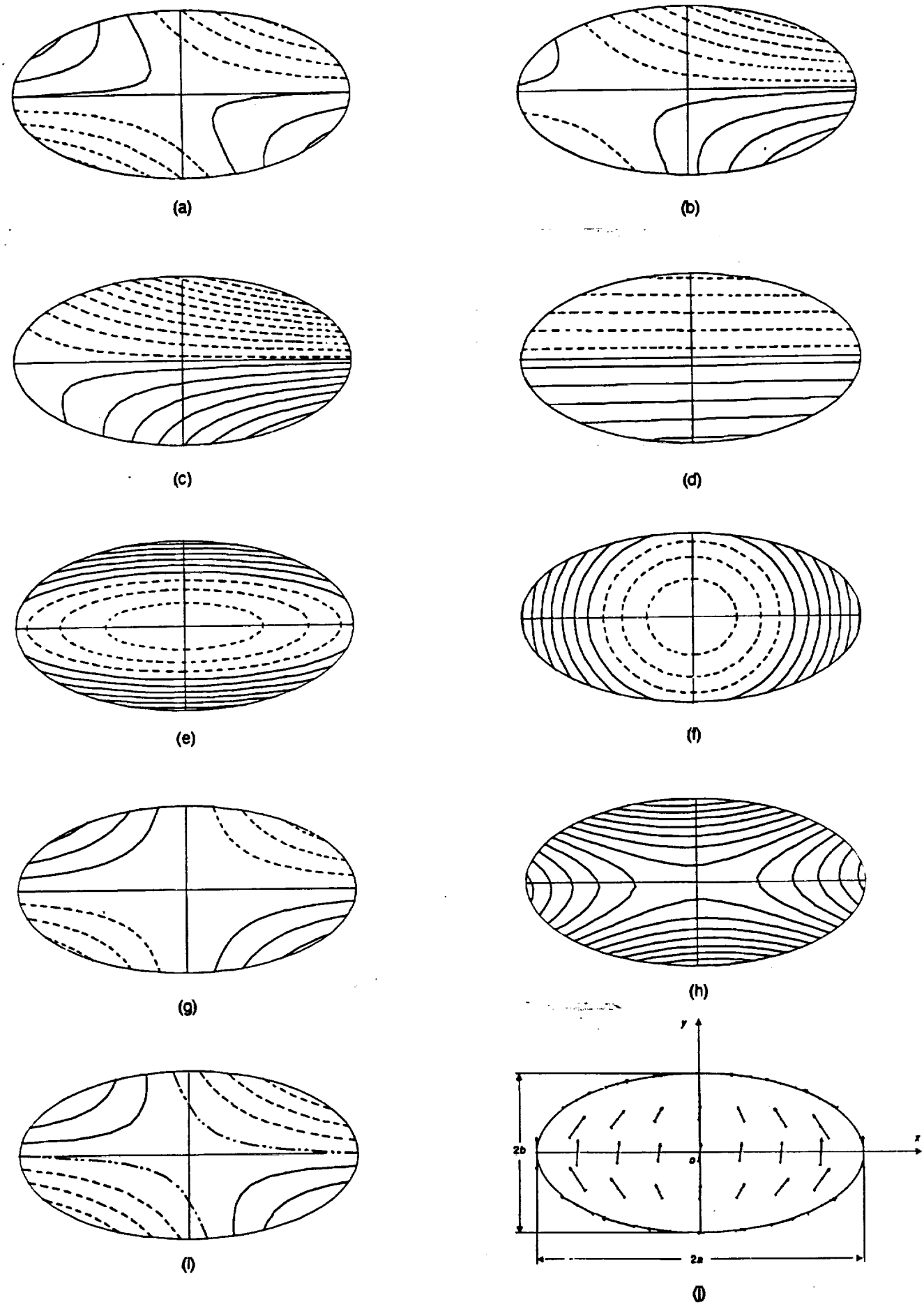

Fig. 4 Stress distributions of a tip-loaded cantilever beam.

Example 2 : Free Vibration, Nonspinning

For free vibration analysis, consider the same beam as in example 1 but with free-free boundary condition. Table 2 shows the mode number, the values of λ_i (no dimension) and information about the mode shapes, where

$$f_i = \frac{\lambda_i}{2\pi L^2}\sqrt{\frac{E_{11} I_{yy}}{\rho A}}\ , \tag{47}$$

f_i is the i-th frequencies (in hertz), and I_{yy} is the moment of inertia with respect to the y axis. As expected, the first six modes represent rigid body modes. For lower frequencies, couplings exist mainly between bending and torsion. Complete couplings (bending, torsion, shear, and extension) exist for higher frequencies.

Table 2 :

Mode Number	λ_i	Information about the mode shapes
1 to 6	0	Rigid body motions
7	8.33	First bending in the *x-o-z*--plane with little torsion
8	16.42	First bending in the *x-o-y*--plane with little torsion
9	22.66	Second bending in the *x-o-z*--plane with little torsion
10	42.93	Third bending in the *x-o-z*--plane with some torsion
11	43.40	Second bending in the *x-o-y*--plane with some torsion
12	49.99	First torsion with some third bending in the *x-o-z*--plane
13	69.80	Fourth bending in the *x-o-z*--plane with some torsion and little extension
14	80.69	Third bending in the *x-o-y*--plane with some torsion
15	94.53	First extension with some torsion and little bending in the *x-o-y*--plane
16	99.45	Second torsion with little bendings in both planes
17	101.58	Fifth bending in the *x-o-z*--plane with some torsion
18	125.76	Fourth bending in the *x-o-y*--plane with some torsion, little extension and little fourth bending in the *x-o-z*--plane

CONCLUSION

A formulation of a nonlinear theory for spinning anisotropic beams having arbitrary cross-sections has been developed. The displacement field is assumed to compose two parts, i.e. the standard kinematic relations (expanded for a three-dimensional case) to describe the global beam behavior and a supplementary additional field that represents the local warpings within and out-of the cross-section plane. It has been shown that, in the most general case, these beam warping functions may be as many as eighteen. Furthermore, it was assumed that the magnitude of this additional field is directly proportional to the local six stress resultants.

Using a weak form finite element based numerical technique, preliminary numerical results for a static and a free vibration cases have been obtained. These numerical examples show that the model can predict the displacements and the stresses exactly for a shear tip loaded cantilever beam. Due to the anisotropy of the material, stress distributions do not resemble the isotropic counterpart for all six stress components. Numerical results on the free vibration case (a free-free beam) show the coupled mode shapes of bending, torsion, shear and extension, especially for higher frequencies.

ACKNOWLEDGEMENTS

The authors wish to acknowledge to the support of this research by the NASA -Langley Research Center with R. C. Lake as the contract monitor.

REFERENCES

Bauchau, O. A., 1985, "A beam theory for anisotropic materials," *J. Appl. Mech.*, Vol. 52, pp. 416-422.

Heyliger, P. R., and Reddy, J. N., 1988, "A higher order beam finite element for bending and vibration problems," *J. Sound and Vibr.*, Vol. 126 (2), pp. 309-326.

Ie, C.A. and Kosmatka, J.B., 1992.a, "On the Analysis of Prismatic Beams Using First-Order Warping Functions,"*International Journal of Solids and Structures*, Vol. 29, No.7, pp. 879–891.

Ie, C.A. and Kosmatka, J.B., 1992.b, "Elasticity Solutions, Shear Center Location, and Shear Deformation of a Tip-Loaded Anisotropic Cantilevered Beam With an Elliptical Section," *International Journal of Solids and Structures*, submitted.

Kant, T. and Gupta, A., 1988, "A finite element model for a higher-order shear-deformable beam theory," *J. Sound Vibr.*, Vol. 125 (2), pp. 193-202.

Kosmatka, J. B. and Dong, S. B., 1991, "Saint-Venant Solutions for Prismatic Anisotropic Beams," *Int. J. Solids Structures*, Vol. 28 (7), pp. 917-938.

Lekhnitskii, S.G., 1963, "*Theory of Elasticity of an Anisotropic Elastic Body*," (Translated by P. Fern), Holden-Day, Inc., San Francisco.

Levinson, M., 1981, "A new rectangular beam theory," *J. Sound Vibr.*, Vol. 74(1), pp. 81-87.

Love, A. E. H., 1927, "*A Treatise on the Mathematical Theory of Elasticity*," Cambridge University Press, Cambridge, England.

Timoshenko, S. P., 1921, "On the correction for shear of the differential equation for transverse vibrations of prismatic bars," *Phil. Mag.*, Vol. 41, pp. 744-746.

Timoshenko, S. P., 1922, "On the Transverse Vibrations of Bars of Uniform Cross-Section," *Phil. Mag.*, Vol. 43, pp. 125-131.

Vlasov, V. Z., 1961, "*Thin-Walled Elastic Beams*," Israel Program for Scientific Translations Ltd., Jerusalem.

APPENDIX

The matrix $[X]$ is decomposed into three parts as follows

$$[X_I]^T=\begin{bmatrix} 1 & \varphi_{21,2} & \varphi_{31,3} & \varphi_{21,3}+\varphi_{31,2} & \varphi_{11,3} & \varphi_{11,2} \\ - & \varphi_{22,2} & \varphi_{32,3} & \varphi_{22,3}+\varphi_{32,2} & \varphi_{12,3} & 1+\varphi_{12,2} \\ - & \varphi_{23,2} & \varphi_{33,3} & \varphi_{23,3}+\varphi_{33,2} & 1+\varphi_{13,3} & \varphi_{13,2} \\ - & \varphi_{24,2} & \varphi_{34,3} & \varphi_{24,3}+\varphi_{34,2} & y+\varphi_{14,3} & -z+\varphi_{14,2} \\ z & \varphi_{25,2} & \varphi_{35,3} & \varphi_{25,3}+\varphi_{35,2} & \varphi_{15,3} & \varphi_{15,2} \\ -y & \varphi_{26,2} & \varphi_{36,3} & \varphi_{26,3}+\varphi_{36,2} & \varphi_{16,3} & \varphi_{16,2} \\ \varphi_{11} & - & - & - & \varphi_{31} & \varphi_{21} \\ \varphi_{12} & - & - & - & \varphi_{32} & \varphi_{22} \\ \varphi_{13} & - & - & - & \varphi_{33} & \varphi_{23} \\ \varphi_{14} & - & - & - & \varphi_{34} & \varphi_{24} \\ \varphi_{15} & - & - & - & \varphi_{35} & \varphi_{25} \\ \varphi_{16} & - & - & - & \varphi_{36} & \varphi_{26} \end{bmatrix}, \quad [X^2_{nl}]^T=\begin{bmatrix} 1 & - & - & - & - & - \\ - & 1 & - & - & - & - \\ - & - & 1 & - & - & - \\ - & - & - & 1 & - & - \\ - & - & - & - & -1 & - \\ - & - & - & - & - & 1 \end{bmatrix}, \tag{A.1.a,b}$$

$$
[X^3_{nl}]^T=\left[\begin{array}{cccccc}
- & - & - & - & \varphi_{21,3} & \varphi_{21,2} \\
- & - & - & - & \varphi_{22,3} & \varphi_{22,2} \\
- & - & - & - & \varphi_{23,3} & \varphi_{23,2} \\
-z & - & - & - & \varphi_{24,3} & \varphi_{24,2} \\
- & - & - & - & \varphi_{25,3} & \varphi_{25,2} \\
- & - & - & - & \varphi_{26,3} & \varphi_{26,2} \\
- & - & - & - & \varphi_{31,3} & \varphi_{31,2} \\
- & - & - & - & \varphi_{32,3} & \varphi_{32,2} \\
- & - & - & - & \varphi_{33,3} & \varphi_{33,2} \\
y & - & - & - & \varphi_{34,3} & \varphi_{34,2} \\
- & - & - & - & \varphi_{35,3} & \varphi_{35,2} \\
- & - & - & - & \varphi_{36,3} & \varphi_{36,2} \\
- & \varphi_{31,2} & -\varphi_{21,3} & \varphi_{31,3}-\varphi_{21,2} & - & - \\
- & \varphi_{32,2} & -\varphi_{22,3} & \varphi_{32,3}-\varphi_{22,2} & - & - \\
- & \varphi_{33,2} & -\varphi_{23,3} & \varphi_{33,3}-\varphi_{23,2} & - & - \\
- & \varphi_{34,2} & -\varphi_{24,3} & \varphi_{34,3}-\varphi_{24,2} & z & y \\
- & \varphi_{35,2} & -\varphi_{25,3} & \varphi_{35,3}-\varphi_{25,2} & - & - \\
- & \varphi_{36,2} & -\varphi_{26,3} & \varphi_{36,3}-\varphi_{26,2} & - & - \\
- & - & \varphi_{11,3} & \varphi_{11,2} & 1 & - \\
- & - & \varphi_{12,3} & \varphi_{12,2} & - & - \\
- & - & \varphi_{13,3} & \varphi_{13,2} & - & - \\
- & - & \varphi_{14,3} & \varphi_{14,2} & - & - \\
- & - & \varphi_{15,3} & \varphi_{15,2} & z & - \\
- & - & \varphi_{16,3} & \varphi_{16,2} & -y & - \\
- & \varphi_{11,2} & - & \varphi_{11,3} & - & 1 \\
- & \varphi_{12,2} & - & \varphi_{12,3} & - & - \\
- & \varphi_{13,2} & - & \varphi_{13,3} & - & - \\
- & \varphi_{14,2} & - & \varphi_{14,3} & - & - \\
- & \varphi_{15,2} & - & \varphi_{15,3} & - & z \\
- & \varphi_{16,2} & - & \varphi_{16,3} & - & -y
\end{array}\right], \qquad (A.1.c)
$$

where $(\ )_{,2}$ and $(\ )_{,3}$ indicate partial derivatives with respect to the coordinate axes y and z, respectively. Similarly, the array $\{\epsilon\}$ is also decomposed into three parts as follows

$$
\{\epsilon_l\}^T=(u',\ v'-\theta_z,\ w'+\theta_y,\theta_x',\theta_y',\theta_z',\ u'',\ v''-\theta_z',\ w''+\theta_y',\theta_x'',\theta_y'',\theta_z'',0,0,0,0,0,0,0,0,0,
\\ 0,0,0,0,0,0,0,0,0,0,0,0,0,0,0,0,0,0,0,0,0,0,0,0,0,0,0)\ , \qquad (A.2.a)
$$

$$
\{\epsilon^2_{nl}\}^T=(0,0,0,0,0,0,0,0,0,0,0,0,0.5\left[(v')^2+(w')^2\right],\ 0.5\left[(\theta_x)^2+(\theta_z)^2\right],
\\ 0.5\left[(\theta_x)^2+(\theta_y)^2\right],\ -\theta_y\,\theta_z,\ v'\,\theta_x,\ w'\,\theta_x,\ 0,0,0,0,0,0,0,0,0,0,0,
\\ 0,0,0,0,0,0,0,0,0,0,0,0,0,0,0,0,0,0)\ , \qquad (A.2.b)
$$

$$
\{\epsilon^3_{nl}\}^T=(0,0,0,0,0,0,0,0,0,0,0,0,0,0,0,0,0,0,\quad v'u',\ v'(v'-\theta_z),
\\ v'(w'+\theta_y),\ v'\theta_x',\ v'\theta_y',\ v'\theta_z',w'u',\ w'(v'-\theta_z),\ w'(w'+\theta_y),
\\ w'\theta_x',\ w'\theta_y',\ w'\theta_z',\ \theta_x u',\ \theta_x(v'-\theta_z),\ \theta_x(w'+\theta_y),\ \theta_x\theta_x',
\\ \theta_x\theta_y',\ \theta_x\theta_z',\theta_y u',\ \theta_y(v'-\theta_z),\ \theta_y(w'+\theta_y),\ \theta_y\theta_x',\ \theta_y\theta_y',\ \theta_y\theta_z',
\\ -\theta_z u',\ -\theta_z(v'-\theta_z),\ -\theta_z(w'+\theta_y),\ -\theta_z\theta_x',\ -\theta_z\theta_y',\ -\theta_z\theta_z')\ . \qquad (A.2.c)
$$

Matrices $[m]$ and $[m_C]$ are defined as follows

$$[m]=\int_A \rho\left(\{m_1\}\{m_1\}^T+\{m_2\}\{m_2\}^T+\{m_3\}\{m_3\}^T\right) dA\,, \tag{A.3.a}$$

$$[m_c]=\int_A \rho\ \{\Omega_x(\{m_2\}\{m_3\}^T-\{m_3\}\{m_2\}^T)+\Omega_y(\{m_3\}\{m_1\}^T-\{m_1\}\{m_3\}^T)+ \Omega_z(\{m_1\}\{m_2\}^T-\{m_2\}\{m_1\}^T)\}\ dA\,, \tag{A.3.b}$$

where

$$\begin{aligned}\{m_1\}^T&=(1,0,0,0,z+\varphi_{13},-y-\varphi_{12},\varphi_{11},\varphi_{12},\varphi_{13},\varphi_{14},\varphi_{15},\varphi_{16})\,,\\ \{m_2\}^T&=(0,1,0,-z,\varphi_{23},-\varphi_{22},\varphi_{21},\varphi_{22},\varphi_{23},\varphi_{24},\varphi_{25},\varphi_{26})\,,\\ \{m_3\}^T&=(0,0,1,y,\varphi_{33},-\varphi_{32},\varphi_{31},\varphi_{32},\varphi_{33},\varphi_{34},\varphi_{35},\varphi_{36})\,.\end{aligned} \tag{A.4.a-c}$$

Matrix $[k_S]$ is defined as follows

$$[\bar{k}_s]=\frac{1}{2}\left([k_s]+[k_s]^T\right)\,, \tag{A.5.a}$$

where

$$[k_s]=\int_A \rho\ \{\left(\Omega_y^2+\Omega_z^2\right)\{m_1\}\{m_1\}^T+\left(\Omega_x^2+\Omega_z^2\right)\{m_2\}\{m_2\}^T+\left(\Omega_x^2+\Omega_y^2\right)\{m_3\}\{m_3\}^T -2\Omega_y\Omega_z\{m_2\}\{m_3\}^T-2\Omega_x\Omega_z\{m_1\}\{m_3\}^T-2\Omega_x\Omega_y\{m_1\}\{m_2\}^T\}\ dA\,. \tag{A.5.b}$$

The array $\{f_{Cf}\}$ is defined as follows

$$\{f_{cf}\}=\int_A \rho\ \{\left(\Omega_y^2+\Omega_z^2\right)(h_x+x)\{m_1\}+\left(\Omega_x^2+\Omega_z^2\right)(h_y+y)\{m_2\}+\left(\Omega_x^2+\Omega_y^2\right)(h_z+z)\{m_3\}- \Omega_x\left(\Omega_z(h_z+z)+\Omega_y(h_y+y)\right)\{m_1\}-\Omega_y\left(\Omega_z(h_z+z)+\Omega_x(h_x+x)\right)\{m_2\}- \Omega_z\left(\Omega_x(h_x+x)+\Omega_y(h_y+y)\right)\{m_3\}\}\ dA\,. \tag{A.6}$$

Chapter 7

Extension-Bend-Twist Coupling Behavior of Thin-Walled Advanced Composite Beams with Initial Twist

by

J. B. Kosmatka*
Department of Applied Mechanics and Engineering Science
University of California, San Diego
La Jolla, California 92093

Abstract

An analytical model is developed for assessing the extension-bend-twist coupling behavior of nonhomogeneous anisotropic beams with initial twist. The model is formulated as a coupled two-dimensional boundary value problem, where the displacement solutions are defined with pretwist-dependent functions that represent the extension, bending, and torsion, and unknown functions that represent local in-plane deformations and out-of-plane cross-section warping. The unknown deformation functions are determined by applying the principle of minimum potential energy to a discretized representation of the cross section. Numerical results are presented that fully verify this approach and illustrate the strong extension-twist coupling behavior present in pretwisted beams with thin-wall laminated composite cross sections as a function of ply angle, initial twist level, and initial twist axis location . Cross-sections analyzed include; thin laminated rectangles with either asymmetric or symmetric ply stacking sequences and a thin-wall single cell D-section composed of a graphite/epoxy woven cloth.

Introduction

From tilt-rotor aircraft to jet turbines, rotor blade manufacturers are incorporating fibrous composite materials into their current designs as a means of reducing weight and costs, and controlling deformations. In a general sense, a laminated composite rotor blade can be described as an elastic beam that exhibits generally anisotropic behavior, where it's shape is generated by rotating a nonhomogeneous airfoil (irregular) section about an initial twist axis. The beam can have a helical line of centroids, since the section centroid is not required to lie on the initial twist axis. Thus, the application of a simple extension load will result in elongation, bending, and twisting of the beam. This coupled behavior is dependent not only upon the material property definition of the laminated section, but also upon the initial twist axis location and the initial twist level.

Exact analytical solutions to this type of problem do not exist and are generally intractable. Fundamental studies [1,2] derived the governing two-dimensional coupled equations for the extension-torsion behavior of pretwisted and spiral (helical) isotropic bars. Closed-form solutions for the extension-torsion behavior of helical isotropic bars with simple (off-centered circle and ellipse) cross sections were developed in [3] using a displacement formulation. Numerical results clearly illustrate the interaction between pretwist and local cross-section deformations. A recent study [4] developed an analytical model for pretwisted isotropic beams with an arbitrary cross section, where the Ritz method is applied to determine the pretwist dependent in-plane deformations and out-of-plane warping of the cross-section before studying the extension-bend-twist coupling behavior. Numerical results demonstrated the pronounced effects that pretwist and initial twist axis location have on the section deformations, extension-torsion coupling behavior, and section properties of solid and thin-wall multi-cell airfoil sections. Investigators have developed other isotropic models based upon either thin shell theory [5] or approximate technical beam theories (for example, [6-10]).

Pure bending of pretwisted isotropic bars with simple homogeneous sections has also been addressed by investigators. Maunder and Reissner [11] developed approximate solutions using a thin shell theory for narrow rectangular cross sections. Goodier and Griffin [12], using a stress formulation, developed an elasticity model assuming that the solution can be represented by a pretwist dependent power series. Results using the first few terms of the series for a thin elliptical cross section show that curvature will increase significantly for the stiff plane of the cross section, but the curvature in the soft plane remains virtually unchanged.

Independent of the above research on pretwisted isotropic beams, investigators have developed solutions for the behavior of prismatic anisotropic beams with a nonhomogeneous irregular cross section. Initially, a mathematical formulation

* Assistant Professor, member AIAA, ASME, AHS.

with an existence proof was derived based upon an assumed displacement field, but no numerical results were given [13]. Approximate solutions, which involve solving a coupled two-dimensional elasticity model via the Ritz method, have been developed [14-16]. In [14], the solutions are determined by uncoupling the local cross-section deformations from the global beam deformations and solving both simultaneously, whereas in [15,16], the global beam solutions are derived first using Saint-Venant's inverse method and then only the local in-plane and out-of-plane section deformations require calculation.

The objective of this paper is to develop an analytical model for studying the extension-bend-twist coupling behavior of nonhomogeneous anisotropic beams with initial twist. The model is formulated as a coupled two-dimensional boundary value problem, where the displacement solutions are defined in their most general form including: (1) pretwist-dependent functions that represent the extension, bending, and torsion, and (2) unknown functions that represent the local in-plane deformations and out-of-plane warping of the cross section. The unknown deformation functions, which are assumed to be proportional to the local axial strain, bending curvatures, and torsion twist rate, are determined by applying the principle of minimum potential energy to a discretized representation of the cross section (Ritz method). Finally, the extension-bend-twist coupling behavior is studied using the equilibrium equations of the cross section. This model has direct applications to both highly pretwisted aviation propellers and jet turbine (turbofan) blades, which have thin built-up solid laminate sections, and composite tilt-rotor blades, which have thin-wall closed-cell laminate sections.

Three sets of numerical results are presented. Initially, the extension-twist behavior of a flat (untwisted) laminated plate with an asymmetric (angle ply) lay-up is analyzed to verify that the current approach reduces to classical laminated plate theory. Second, the extension-bend-twist behavior of a thin solid laminated strip with initial twist is studied for different ply angle orientations and stacking sequences (asymmetric, symmetric), pretwist levels, and initial twist axis locations. Finally, a pretwisted beam having a thin-wall D-section composed of a graphite/epoxy woven cloth, similar to the effective structural section of a tilt-rotor blade, is analyzed to illustrate how ply orientation and initial twist can be combined to produce either maximum or minimum extension-twist coupling behavior.

Theoretical Derivation

Consider a long elastic beam, of length l, where the lateral surface is generated by rotating an arbitrary nonhomogeneous cross section about an initial twist axis (z-axis). This cross section is defined using (n) triangular and/or quadrilateral subregions, where each subregion can have a unique homogeneous anisotropic material definition. See Fig. 1. The beam may have a helical line of centroids since the modulus weighted section centroid is not required to lie on the initial twist axis. A space-fixed orthonormal vector set (x,y,z) and a curvilinear coordinate system (ξ,η,z) are used to analyze the beam, where ξ and η align with the x and y axes at the beam root (z=0), but rotate with the section about the initial twist axis. Thus, both the section geometry and the material properties are functions of ξ and η only. The two coordinate systems are related using

$$\begin{Bmatrix} \xi \\ \eta \end{Bmatrix} = \begin{bmatrix} \cos(\alpha z) & \sin(\alpha z) \\ -\sin(\alpha z) & \cos(\alpha z) \end{bmatrix} \begin{Bmatrix} x \\ y \end{Bmatrix}, \qquad (1)$$

where α is the initial twist per unit length. The constitutive relations for the i^{th} subregion of the cross section, are given as

$$\begin{Bmatrix} \sigma^{(i)} \end{Bmatrix} = \begin{bmatrix} C^{(i)} \end{bmatrix} \begin{Bmatrix} \varepsilon^{(i)} \end{Bmatrix}, \qquad \begin{Bmatrix} \varepsilon^{(i)} \end{Bmatrix} = \begin{bmatrix} S^{(i)} \end{bmatrix} \begin{Bmatrix} \sigma^{(i)} \end{Bmatrix}, \qquad (2.a\text{-}b)$$

where the i^{th} stress and strain vectors are given as,

$$\begin{Bmatrix} \sigma^{(i)} \end{Bmatrix}^T = \qquad (2.c)$$

$$\left\{ \sigma_{\xi\xi}^{(i)},\ \sigma_{\eta\eta}^{(i)},\ \sigma_{zz}^{(i)},\ \tau_{\eta z}^{(i)},\ \tau_{\xi z}^{(i)},\ \tau_{\xi\eta}^{(i)} \right\}$$

$$\begin{Bmatrix} \varepsilon^{(i)} \end{Bmatrix}^T = \qquad (2.d)$$

$$\left\{ \varepsilon_{\xi\xi}^{(i)},\ \varepsilon_{\eta\eta}^{(i)},\ \varepsilon_{zz}^{(i)},\ \gamma_{\eta z}^{(i)},\ \gamma_{\xi z}^{(i)},\ \gamma_{\xi\eta}^{(i)} \right\}$$

and the material stiffness $[C^{(i)}]$ and compliance $[S^{(i)}]$ matrices for each of the subregions in the curvilinear frame (ξ,η,z) must obey $[C^{(i)}] = [S^{(i)}]^{-1}$. These matrices will be fully populated with up to 21 distinct coefficients when the subregion material classification is either anisotropic or the subregion is composed of fiberous composite materials, where

the principle fiber directions do not align with any of the curvilinear coordinates.

The applied stress distribution on the ends of the beam (z=0,l) is statically equivalent to an applied extension force P that acts along the initial twist axis and a general moment M that can be decomposed into components M_x, M_y, and M_z about the x, y, and z axes, respectively. Furthermore, the ends of the beam are free to warp so that the twist is uniform along the length. A general moment is required for two reasons; (1) P does not act through the centroid and thus effective bending moments are produced, and (2) the solutions to the bending and torsion problems are coupled for generally anisotropic beams due to the presence of the C_{34} and C_{35} terms in the material stiffness matrix. Assuming that the body forces are negligible and a stress free condition exists along the lateral surface, then the stresses within the cross section must satisfy the following equations of equilibrium:

$$\sum_{i=1}^{n} \int_{A^{(i)}} \sigma_{zz}^{(i)}\, dA^{(i)} = P\,,$$

$$\sum_{i=1}^{n} \int_{A^{(i)}} \eta\sigma_{zz}^{(i)}\, dA^{(i)} = M_\xi\,,$$

$$\sum_{i=1}^{n} \int_{A^{(i)}} \xi\sigma_{zz}^{(i)}\, dA^{(i)} = -M_\eta\,, \qquad (3.a\text{-}d)$$

$$\sum_{i=1}^{n} \int_{A^{(i)}} \left(\xi\tau_{\eta z}^{(i)} - \eta\tau_{\xi z}^{(i)}\right) dA^{(i)} = M_z\,,$$

where, $A^{(i)}$ is the area of the i^{th} subregion and M_ξ and M_η are components of the applied moment about the ξ and η axes that satisfy

$$\begin{Bmatrix} M_\xi \\ M_\eta \end{Bmatrix} = \begin{bmatrix} \cos(\alpha z) & \sin(\alpha z) \\ -\sin(\alpha z) & \cos(\alpha z) \end{bmatrix} \begin{Bmatrix} M_x \\ M_y \end{Bmatrix}. \qquad (4)$$

The displacement distribution for each subregion can be written in its most general form as global functions that represent extending, bending, and twisting of the beam and local functions that represent warping of the nonhomogeneous cross section;

$$u^{(i)} = u_o(z) - \eta\theta_o(z) + \psi_1^{(i)}\,,$$

$$v^{(i)} = v_o(z) + \xi\theta_o(z) + \psi_2^{(i)}\,, \qquad (5.a\text{-}c)$$

$$w^{(i)} = w_o(z) - \xi\phi_\eta(z) + \eta\phi_\xi(z) + \psi_3^{(i)}\,,$$

where u_o, v_o, w_o represent z-dependent displacements in the ξ, η, and z directions, respectively, ϕ_ξ, ϕ_η, and θ_o are rotations of the cross section plane about the ξ, η, and z axes, respectively, ψ_1 and ψ_2 are deformations in the section plane (including Poisson contractions), and ψ_3 describes warping out of the section plane. These functions ($\psi_1^{(i)}$, $\psi_2^{(i)}$,$\psi_3^{(i)}$) are assumed to; (1) be directly proportional to the axial strain, bending curvatures, and twist rate within the cross section, (2) be uniform in the curvilinear coordinate frame (function of ξ and η only), and (3) have first-order continuity across the subregion boundaries.

Assuming a two-dimensional strain state, one can derive the final form of the z-dependent functions as

$$u_o(z) = \frac{\kappa_\eta}{\alpha^2}\left\{(\alpha z)\cos(\alpha z) - \sin(\alpha z)\right\} - \frac{\kappa_\xi}{\alpha^2}\left\{1 - \cos(\alpha z) - (\alpha z)\sin(\alpha z)\right\},$$

$$v_o(z) = \frac{\kappa_\xi}{\alpha^2}\left\{(\alpha z)\cos(\alpha z) - \sin(\alpha z)\right\} + \frac{\kappa_\eta}{\alpha^2}\left\{1 - \cos(\alpha z) - (\alpha z)\sin(\alpha z)\right\}, \qquad (6.a\text{-}f)$$

$$w_o(z) = e\,z\,,$$

$$\phi_\xi(z) = \frac{\kappa_\xi}{\alpha}\left\{1 - \cos(\alpha z)\right\} + \frac{\kappa_\eta}{\alpha}\left\{\sin(\alpha z)\right\},$$

$$\phi_\eta(z) = -\frac{\kappa_\eta}{\alpha}\left\{1 - \cos(\alpha z)\right\} + \frac{\kappa_\xi}{\alpha}\left\{\sin(\alpha z)\right\},$$

$$\theta_o(z) = \theta\,z\,,$$

where, e, κ_ξ, κ_η, and θ represent the extension strain, the bending curvatures of the beam in the ξ-z and η-z planes, and the elastic twist per unit length,

respectively. The current approach reduces to the models in [3, 4, 12] for isotropic materials.

The i^{th} strain components are found using the displacement relations from (5.*a-c*) and (6.*a-f*)

$$\varepsilon_{\xi\xi}^{(i)} = \psi_{1,\xi}^{(i)}, \qquad \varepsilon_{\eta\eta}^{(i)} = \psi_{2,\eta}^{(i)},$$

$$\varepsilon_{zz}^{(i)} = e - \xi\kappa_\xi + \eta\kappa_\eta + \alpha D\psi_3^{(i)},$$

$$\gamma_{\eta z}^{(i)} = \theta\,\xi + \psi_{3,\eta}^{(i)} + \alpha(\psi_1^{(i)} + D\psi_2^{(i)}), \quad (7.a\text{-}f)$$

$$\gamma_{\xi z}^{(i)} = -\theta\,\xi + \psi_{3,\xi}^{(i)} - \alpha(\psi_2^{(i)} - D\psi_1^{(i)}),$$

$$\gamma_{\xi\eta}^{(i)} = \psi_{1,\eta}^{(i)} + \psi_{2,\xi}^{(i)},$$

where, the symbol D is an operator defined as

$$D = \eta\frac{\delta}{\delta\xi} - \xi\frac{\delta}{\delta\eta}. \qquad (7.g)$$

Determination of the Local Cross Section Deformations

The local deformation functions for an arbitrary nonhomogeneous anisotropic cross-section are determined based upon the principle of minimum potential energy along with a discretized representation (finite element modeling) of the cross section. Although the displacement field is fully three-dimensional (Eq. 5.*a-c*), it is explicit in the z direction, thus only the two-dimensional cross section needs to analyzed. This approach has been applied successfully to such problems as torsion and flexure of prismatic isotropic [17], monoclinic [18], and anisotropic beams [15,16], and the extension-torsion coupling behavior of pretwisted isotropic beams [4].

The local deformations must be determined for each of the four cases (viz. extension, bending curvatures in the ξ-z and η-z planes, and the elastic twist rate). Standard isoparametric finite element methodology is employed so that most of the details can be omitted. Each material of the cross section is approximated using either quadrilateral or triangular subregions where the local deformations are represented as

$$\psi_1^{(i)} = \left[N^{(i)}(\xi,\eta)\right]\left\{\Psi_1^{(i)}\right\},$$

$$\psi_2^{(i)} = \left[N^{(i)}(\xi,\eta)\right]\left\{\Psi_2^{(i)}\right\}, \qquad (8.a\text{-}c)$$

$$\psi_3^{(i)} = \left[N^{(i)}(\xi,\eta)\right]\left\{\Psi_3^{(i)}\right\},$$

where $[N^{(i)}(\xi,\eta)]$ is a bi-quadratic isoparametric interpolation function and $\{\Psi_1^{(i)}\}$, $\{\Psi_2^{(i)}\}$, and $\{\Psi_3^{(i)}\}$ are nodal displacements on the i^{th} subregion boundary in the ξ, η, and z directions, respectively. The strain vector (Eq. 2.*d*) of the i^{th} subregion can be written in matrix form in terms of the unknown local deformations and the extension strain, bending curvatures, and elastic twist rate by substituting the interpolation functions (Eqns. 8.*a-c*) into (Eqns. 7.*a-f*):

$$\left\{\varepsilon^{(i)}\right\} = \left[B^{(i)}\right]\left\{\Psi^{(i)}\right\} + \left[f_b\right]\left\{b\right\} \qquad (9)$$

where

$$\left[B^{(i)}\right] = \begin{bmatrix} N^{(i)}(\xi,\eta)_{,\xi} & 0 & 0 \\ 0 & N^{(i)}(\xi,\eta)_{,\eta} & 0 \\ 0 & 0 & \alpha D N^{(i)}(\xi,\eta) \\ \alpha N^{(i)}(\xi,\eta) & \alpha D N^{(i)}(\xi,\eta) & N^{(i)}(\xi,\eta)_{,\eta} \\ \alpha D N^{(i)}(\xi,\eta) & -\alpha N^{(i)}(\xi,\eta) & N^{(i)}(\xi,\eta)_{,\xi} \\ N^{(i)}(\xi,\eta)_{,\eta} & N^{(i)}(\xi,\eta)_{,\xi} & 0 \end{bmatrix}. \qquad (10.a)$$

$$\left\{\Psi^{(i)}\right\}^T = \left\{\left\{\Psi_1^{(i)}\right\}, \left\{\Psi_2^{(i)}\right\}, \left\{\Psi_3^{(i)}\right\}\right\} \qquad (10.b)$$

$$\left[f_b\right] = \begin{bmatrix} 0 & 0 & 0 & 0 \\ 0 & 0 & 0 & 0 \\ 1 & -\xi & \eta & 0 \\ 0 & 0 & 0 & \xi \\ 0 & 0 & 0 & -\eta \\ 0 & 0 & 0 & 0 \end{bmatrix}, \qquad (10.c)$$

and

$$\{b\}^T = \{e,\ \kappa_\xi,\ \kappa_\eta,\ \theta\}\ . \qquad (10.d)$$

Similarly, the displacements (Eqns. 5.*a-c*) could also be written in matrix form in terms of the local cross section deformations and the vector $\{b\}$.

The principle of minimum potential energy is given as

$$\delta\Pi = \sum_{i=1}^{n} \delta U^{(i)} - \delta W_e^{(i)} = 0 \qquad (11)$$

where n is the number of subregions, $\delta U^{(i)}$ is the variation of the strain energy with respect to the unknown local deformations of the i^{th} subregion given by

$$\delta U^{(i)} = \int_0^L \int_{A^{(i)}} \left\{\delta\varepsilon^{(i)}\right\}^T \left[C^{(i)}\right] \left\{\varepsilon^{(i)}\right\} dA^{(i)} dz\ , \qquad (12.a)$$

and $\delta W_e^{(i)}$ is the variation of the work of external forces of the i^{th} subregion that results from the applied tractions on the beam ends;

$$\delta W_e^{(i)} = \int_{A^{(i)}} \left\{\tau_{\xi z}^{(i)}\delta\psi_1^{(i)} + \tau_{\eta z}^{(i)}\delta\psi_2^{(i)} + \sigma_{zz}^{(i)}\delta\psi_3^{(i)}\right\}\Big|_{(z=L)} dA^{(i)} \qquad (12.b)$$

$$- \int_{A^{(i)}} \left\{\tau_{\xi z}^{(i)}\delta\psi_1^{(i)} + \tau_{\eta z}^{(i)}\delta\psi_2^{(i)} + \sigma_{zz}^{(i)}\delta\psi_3^{(i)}\right\}\Big|_{(z=0)} dA^{(i)}\ .$$

The virtual work expression will reduce to zero since both the stresses and the local cross section deformations are assumed to be independent of the axial coordinate (z). A set of linear algebraic equations for determining the local cross section deformations in terms of $\{b\}$ is obtained by substituting Eqns. (9) and (12.*a*) into Eq. (11) and carrying out the integration over the beam volume. Writing this set of equations for the i^{th} subregion;

$$\left[K^{(i)}\right]\left\{\Psi^{(i)}\right\} + \left[F_b^{(i)}\right]\{b\} = \{0\} \qquad (13)$$

where the stiffness matrix is defined as

$$\left[K^{(i)}\right] = L\int_{A^{(i)}} \left[B^{(i)}\right]^T \left[C^{(i)}\right]\left[B^{(i)}\right] dA^{(i)} \qquad (14.a)$$

and the force matrix is presented as

$$\left[F_b^{(i)}\right] = L\int_{A^{(i)}} \left[B^{(i)}\right]^T \left[C^{(i)}\right]\left[f_b\right] dA^{(i)}. \qquad (14.b)$$

Since both the stiffness matrix ($[K^{(i)}]$) and the force matrix ($[F_b^{(i)}]$) are linearly dependent upon the beam length (L), then the calculated local deformations functions are length independent and (L) can be dropped from the above equations.

The matrix equations of Eq. (13) are assembled into a complete model of the cross section using standard finite element procedures. Unit solutions for the local deformations (Ψ_1, Ψ_2, Ψ_3) can be calculated for each of the four cases of $\{b\}$ by setting the appropriate value in the array $\{b\}$ equal to unity and the remaining three to zero. Thus, the calculated deformation functions can be written in matrix form as

$$\left\{\Psi^{(i)}\right\} = \left[\overline{\Psi^{(i)}}\right]\{b\}\ . \qquad (15)$$

where each of the four columns of $[\Psi^{(i)}]$ are the unit local deformations associated with the four cases of $\{b\}$. Thus, the calculated functions for the first case represent the local deformations as a result of applied unit axial strain (e) with dimensional units of length per unit axial strain. Similarly, the second and third cases define the local deformation associated with applied bending curvatures (κ_ξ, κ_η) with dimensional units of length per unit bending curvature. Finally the fourth case describes the local deformation from applied twist rate (θ) with dimensional units of length per unit twist rate. Similarly, the stress components of the i^{th} subregion can be expressed in terms of a set of unit stresses and $\{b\}$ by substituting Eqns. (15) and (9) into (2.a)

$$\left\{\sigma^{(i)}\right\} = \left[\overline{\sigma^{(i)}}\right]\{b\}\ , \qquad (16)$$

where

$$\left[\overline{\sigma^{(i)}}\right] = \left[C^{(i)}\right]\left[B^{(i)}\right]\left[\overline{\psi^{(i)}}\right] + \left[f_b\right] \quad . \qquad (17)$$

Relations could also be easily developed for the displacements ($u^{(i)}$, $v^{(i)}$, $w^{(i)}$) in terms of a matrix of unit displacements and {b}.

A two-dimensional finite element program was written where the cross section is discretized using 8-node quadrilateral elements and 6-node triangular elements. The cross section is defined in a local element coordinate system (ξ_e, η_e) that can be arbitrarily positioned relative to the initial twist (z) axis of the curvilinear reference frame (ξ,η,z) using offsets (ξ_i, η_i). The discretization of thin rectangular cross-section (c/t=10) using 40 quadrilateral elements is presented in Fig. 2.

Behavior of the Pretwisted Beam

The general behavior of the pretwisted beam can be studied by making use of the calculated stress distributions (Eq. (16)) and the equilibrium equations of the cross section (Eqns. (3.a-d)). Thus,

$$\begin{bmatrix} k_{11} & k_{12} & k_{13} & k_{14} \\ k_{12} & k_{22} & k_{23} & k_{24} \\ k_{13} & k_{23} & k_{33} & k_{34} \\ k_{14} & k_{24} & k_{34} & k_{44} \end{bmatrix} \begin{Bmatrix} e \\ \kappa_\xi \\ \kappa_\eta \\ \theta \end{Bmatrix} = \begin{Bmatrix} P \\ M_\eta \\ M_\xi \\ M_z \end{Bmatrix} \qquad (18)$$

where the matrix [k] is symmetric based upon reciprocity. For an untwisted isotropic beam, the twist rate is independent of axial strain and bending curvatures (k_{14}=k_{24}=k_{34}=0), the diagonal terms equal the nominal extensional stiffness (k_{11}=EA_o), bending stiffnesses (k_{22}=$EI_{\eta\eta o}$, k_{33}=$EI_{\xi\xi o}$), and torsion stiffness (k_{44}=GJ_o). The remaining off-diagonal terms, which couple extension and bending, are the first and second moments of inertia that result when the local axes (ξ,η) are not coincident with the principal axes of the section (k_{13}=$EA_{\eta o}$, k_{12}=-$EA_{\xi o}$, k_{23}=-$EI_{\xi\eta o}$). These last three terms can be used to locate the centroid and principal axes of the section. For beams exhibiting generally anisotropic behavior as a result of material definition or from the presence of initial beam twist, the matrix relation of Eq. (18) will be fully populated.

The behavior of a "constrained" nonhomogeneous anisotropic beam with initial twist can be studied by using Eq. (18) directly, where forces and/or moments are applied to restrict global beam behavior, but not cross section deformation. For example, to place a beam in pure torsion with no axial strain or bending ($\theta \neq 0$, $e = \kappa_\xi = \kappa_\eta = 0$), one must apply an axial force and a general moment with bending moment components that satisfy

$$\frac{P}{M_z} = \frac{k_{14}}{k_{44}}, \quad \frac{M_\xi}{M_z} = \frac{k_{34}}{k_{44}}, \quad \frac{M_\eta}{M_z} = \frac{k_{24}}{k_{44}} \, . \qquad (19.a\text{-}c)$$

Positive (negative) ratios of (19.a) are associated with the application of an extension force to keep the beam from contracting (extending), whereas nonzero terms of (19.b,c) signify that the general moment is acting about a vector that is skew (not perpendicular) to the cross section. Similarly, to place a beam in pure extension with no bending or twisting ($e \neq 0$, $\theta = \kappa_\xi = \kappa_\eta = 0$), one must also apply a general moment with components that satisfy

$$\frac{M_\xi}{P} = \frac{k_{13}}{k_{11}}, \quad \frac{M_\eta}{P} = \frac{k_{12}}{k_{11}}, \quad \frac{M_z}{P} = \frac{k_{14}}{k_{11}} \, . \qquad (20.a\text{-}c)$$

These ratios agree with the equations developed by Lekhnitskii [19] for untwisted generally anisotropic beams.

The behavior of an "unconstrained" anisotropic beam with initial twist can be studied by multiplying Eq. (18) by the inverse of [k], which results in a flexibility relationship. For example, applying an axial force (P) produces extension as well as bending and twisting that satisfies the following ratios

$$\frac{\kappa_\xi}{e} = \frac{a_{12}}{a_{11}}, \quad \frac{\kappa_\eta}{e} = \frac{a_{13}}{a_{11}}, \quad \frac{\theta}{e} = \frac{a_{14}}{a_{11}} \, , \qquad (21.a\text{-}c)$$

where a_{ij} are the components of the flexibility matrix [a] (=[k]$^{-1}$). Similarly, applying a torsion moment (M_z) results in extension and bending ratios of the form

$$\frac{e}{\theta} = \frac{a_{14}}{a_{44}}, \quad \frac{\kappa_\xi}{\theta} = \frac{a_{24}}{a_{44}}, \quad \frac{\kappa_\eta}{\theta} = \frac{a_{34}}{a_{44}} \, , \qquad (22.a\text{-}c)$$

Negative (or positive) ratios of (21.c) and (22.a) correspond to untwisting (or further twisting) of the beam as a result of an applied extension, and contraction (or extension) from an applied twist moment, respectively.

Results and Discussion

Three sets of numerical results are presented to illustrate the capabilities of the current analytical model and how the interaction of material and pretwist definitions effect the extension-twist be-

havior of thin-wall composite beams. Initially, a validation study is performed. Second, the extension-twist coupling behavior of a pretwisted graphite/epoxy strip, which is geometrically similar to a jet turbo-fan blade, is studied for an asymmetric $[\pm\phi]$ and symmetric $([\pm\phi]_S)$ stacking sequence. Finally, a pretwisted beam with a thin-wall D-section composed of a graphite/epoxy woven fabric is analyzed for different ply orientations and pretwist definitions. This beam is geometrically similar to blades used on tilt-rotor aircraft (NASA XV-15).

Verification Studies

Since published results do not currently exist for the behavior of pretwisted thin-wall advanced composite beams, the current model was validated using published results for pretwisted isotropic beams and flat (untwisted) laminated composite plates. Because the current approach will reduce identically to the elasticity model of ref. [4] for pretwisted isotropic beams, it is not necessary in this limited space to show that the current model is in exact agreement with the isotropic models of Refs. [3-9,12] for helical beams having a thin elliptical cross-section. Interested readers should refer to [4] for a detailed discussion and numerical results that include the variation of section and extension-twist coupling properties with pretwist definition (initial twist level, initial twist axis location).

The extension-twist coupling behavior of an axially-loaded flat laminated plate (α=0, ξ_i=η_i=0) with an asymmetric stacking sequence $[\pm\phi]$ was analyzed and the results were compared to classical lamination plate theory predictions [20]. The thin plate cross section (c/t=10) is composed of two plies of unidirectional graphite/epoxy fibers, where each ply is defined using 20 quadrilateral elements (see Fig. 2). The properties of the fiber system (Table 1) are defined relative to an orthogonal reference frame (1,2,3) where the 1-axis is coincident with the fiber direction. The 1-2 plane of the fiber system is parallel to the z-ξ plane of the plate cross section and the 3 axis is coincident with the η axis. A ply angle (ϕ) is used to locate the fiber direction (1-axis) relative to the (z) axis, where a positive angle is defined as a counterclockwise rotation about the η axis for the upper ply and a counterclockwise rotation about the $-\eta$ axis for the lower ply. If ϕ=0, then the fibers of both the upper and lower plies are parallel to the z-axis

The nondimensionalized ratio of the plate untwist (θ) for a given extensional strain (e) as a result of an applied force (P) can be expressed (from Eq. 21.c) as;

$$\frac{\theta}{e}c = \frac{a_{14}}{a_{11}}c. \qquad (23.a)$$

A similar relationship can be developed from classical laminated plate theory by making use of the inverse of the laminate stiffness matrix (commonly called the "*A-B-D*" matrix);

$$\frac{\theta}{e}c = \frac{\left(\kappa_{xy}/2\right)}{\left(\varepsilon_{xx}\right)}c = \frac{\left(B_{16}^{*}N_x/2\right)}{\left(A_{11}^{*}N_x\right)}c = \frac{B_{16}^{*}}{2A_{11}^{*}}c \qquad (23.b)$$

where A_{11}^{*} and B_{16}^{*} are the coefficients from the inverse of the laminate stiffness matrix that are associated with the amount of extension strain and twist curvature from an applied in-plane force (N_x), respectively. In Fig. 3, the variation of this twist/extension ratio as a function of ply angle (ϕ) is presented for the current approach and for classical laminated plate theory. These results illustrate that the current approach is in exact agreement with the classical laminated plate theory and that the maximum amount of positive (θ>0) or negative (θ<0) plate twisting for a minimum amount of extension strain (e) occurs when (ϕ) is equal to 12° or -12°, respectively. Furthermore, orientating the fibers at either 0° or 90° will produce plate extension only (θ=0).

Pretwisted Laminated Composite Strip

The extension-twist coupling behavior of a pretwisted graphite/epoxy strip, which is geometrically similar to aviation propeller and jet turbo-fan blades ($0.1\leq\alpha c<0.2$), is studied for an asymmetric $[\pm\phi]$ and symmetric $([\pm\phi]_S)$ stacking sequence. The thin 2-ply asymmetric cross-section of the verification study (see Fig. 2) will again be analyzed except now the strip has initial twist defined about the centroidal axis (ξ_i=η_i=0). In Fig. 4, the nondimensionalized extension/twist flexibility coefficient ($a_{14}E_{11}c^3$) is presented as a function of ply angle (ϕ) and nondimensionalized pretwist (αc). For low pretwist levels ($\alpha c\leq 0.01$), the ($a_{14}E_{11}c^3$) curve undergoes a slight downward shift. This shift is a result of untwisting of the axially loaded pretwisted beam and thus the flexibility coefficient becomes more negative for negative ply angles, less positive for positive ply angles, and the zero coefficient value shifts to a positive ply angle. For moderate pretwist levels ($\alpha c\approx 0.10$), the downward shift of the curve is substantial, where the initial twist related coupling values are of the same order as the material related coupling effects and the ply angles for maximum coupling have increased by 4°. Furthermore, the ply angles for zero coupling has shifted from 0° and -90° to 11° and 60°. Finally,

for large pretwist levels (αc=0.20, 0.30), the downward shift of the curve can be large enough that eventually no positive or zero coupling exists and thus an axially loaded pretwisted strip will always untwist independent of ply angle definition.

The variation in the extension stiffness as a function of fiber angle and pretwist level is presented in Fig. 5, where EA_0 ($=1/a_{11_0}$) is defined as the extension stiffness of a unidirectional flat strip ($\alpha=\phi=0$). The downward shift of the curves for moderate to highly pretwisted strips was expected, since it is well known that adding initial twist to an isotropic beam will lower the extension stiffness (see [4]). The shift of the relative maximum from (ϕ=0) to a small positive ply angle is a result of using the material coupling to counteract the twist/extension coupling associated with beam initial twist. The ply angles for maximum extension stiffness are equal to, for small initial twist levels, the zero values of twist/extension flexibility (from Fig. 4). In Fig. 6, the twist/extension ratio ($\theta c/e$) is presented, where the maximum untwisting (negative) for minimum extension strain generally occurs for ply angles between 0° and -12°. The ratios for maximum (positive) twisting undergo a significant reduction and the ply angle definitions for zero coupling are highly dependent upon the initial twist level. Finally, for small to moderate pretwist levels, the slopes of the curves can be extremely steep and thus small ply angle changes will cause large changes in the resulting ratios.

The torsion stiffness is presented in Fig. 7, where GJ_0 ($=1/a_{44_0}$) is the nominal torsion stiffness of a unidirectional flat strip ($\alpha=\phi=0$). For strips with small initial twist ($\alpha c \leq 0.01$), the variation in the torsion stiffness is nearly identical to a flat strip, where the relative maximums occur at $\phi=\pm 45°$. For moderate to large pretwist levels, the torsion stiffness will increase (as expected), where the largest increase occurs for small ply angles (near zero) with the magnitude of the increase tapering off near $\phi=\pm 45°$. These results are most interesting in that ply angles less than ±45° undergo the largest percentage increase.

A contour plot of the twist/extension ratio ($\theta c/e$) as a function of ply angle (ϕ) and initial twist axis offset along the chord ($\xi_i \neq 0$, $\eta_i = 0$) for the 2-ply asymmetric strip with initial twist (αc=0.10) is presented in Fig. 8. The dashed contour lines represent a mid-level between the solid contour lines. The maximum negative ratios (-35) occur when ξ_i=0 and ϕ=-5°, whereas a local maximum positive ratio (+15) can be found at ξ_i=0 and ϕ=20° but a global positive maximum will occur at large values of ξ_i/c. Thus, an initially negative ratio can always be made zero or positive by shifting the initial twist axis outward from the centroid. Finally, a region exists (ϕ=45°) where the twist/extension ratio is independent of initial twist axis location.

This thin rectangular graphite/epoxy cross-section (c/t=10) was also studied using a 4-ply symmetric ($[\pm\phi]_S$) stacking sequence, where each ply is defined using 20 quadrilateral elements (80 elements total).and a positive ply angle (ϕ) on the top and bottom plies is defined as a counterclockwise rotation about the η axis and on the two inner plies as a counterclockwise rotation about the -η axis. Initially, the initial twist is defined to act through the section centroid ($\xi_i=\eta_i=0$). The twist/extension ratio ($\theta c/e$) is presented in Fig. 9, where extension-torsion behavior occurs as a result of initial twist, since a flat strip with a symmetric ply lay-up will always have zero coupling. It is apparent that maximum untwisting occurs with a 0° ply angle and for nonzero ply configurations the amount of untwist is greatly reduced. Comparing Figs. 6 and 9, both cross-sections have the same magnitudes for ϕ=0°, but the asymmetric ply definition provides greater freedom for controlling (optimizing) twist/extension coupling.

The variation in the extension (EA/EA_0) and torsion stiffnesses (GJ/GJ_0) are presented in Figs. 10 and 11, respectively, where the curves are symmetric with respect to ϕ=0°. Comparing the variation of the extension stiffness with the 2-ply asymmetric results (Fig. 5), it is readily apparent that both results agree for ϕ=0° and the symmetric lay-up results are nearly constant for small ply angles ($-10° \leq \phi \leq 10°$), whereas the asymmetric results are extremely sensitive to small ply angles. Similarly, the increase in the torsion stiffness agrees with the asymmetric ply lay-up results (Fig. 6) for ϕ=0°, ϕ>45°, and ϕ<-45°, but the asymmetric ply lay-up can have a much greater torsion stiffness for $0° < \phi < 45°$.

A contour plot of the twist/extension ratio ($\theta c/e$) as a function of ply angle (ϕ) and initial twist axis offset along the chord ($\xi_i \neq 0$, $\eta_i = 0$) with initial twist (αc=0.10) is presented in Fig. 12. Again, the dashed contour lines represent a mid-level between the solid contour lines. The maximum negative (-32) extension/twist ratios occur with ξ_i=0 and ϕ=0°, where changing the ply angle or initial twist axis location will only increase the ratio. The values for zero coupling are independent of ply angle and thus negative coupling will always exist as long as ($-0.28 \leq \xi_i/c \leq 0.28$), but this coupling can be small for large ply angles.

Pretwisted Laminated Composite D-Section

The extension-twist coupling behavior of a pretwisted beam with a thin-wall D-section composed of a constant thickness graphite/epoxy woven fabric is analyzed for different ply [ϕ] orientations and pretwist definitions. This beam is geometrically similar to the structural box beam used in tilt-rotor aircraft blades ($0.01<\alpha c\leq 0.10$). The D-section geometry is presented in Fig. 13, where 150 quadrilateral elements are used to define the single-cell planform. The material properties of the graphite/epoxy woven cloth are given in Table 1 and a positive ply angle ϕ is defined as a counterclockwise rotation about a outward normal (n) that is perpendicular section surface. Thus, the ply angle is defined relative to the local element coordinate system to simulate the wrapping of the woven cloth. Even though the wall laminate properties are symmetric, as a result of treating the woven cloth as a single ply, the resulting beam will experience twist/extension coupling because the effective cross-section has an asymmetric material definition.

The twist/extension ratio ($\theta c/e$) is presented in Fig. 14, where the complete behavioral range can be described over a 90^{o} ply angle period, instead of the 180^{o} period typical of uniaxial fibers. The flat ($\alpha=0$) beam section obviously behaves in a fashion similar to the asymmetric ply definition (Fig. 6) with positive and negative coupling for positive ($0\leq\phi\leq 45^{o}$) and negative ($-45^{o}\leq\phi\leq 0$) ply angles, respectively. Adding initial twist, about the cross-section centroid ($\xi/c=0.523$, $\eta/c=0$), shifts the curves downward with the largest changes in the magnitude occurring with ($-15^{o}\leq\phi\leq 15^{o}$). Finally, the magnitudes are significantly less than the magnitudes associated with the uniaxial fiberous material (asymmetric; Fig. 6, symmetric; Fig. 9) because the woven material has a lower extension stiffness to shear stiffness (E/G) ratio. A contour plot of the twist/extension ratio ($\theta c/e$) as a function of ply angle (ϕ) and initial twist axis offset ($0<\xi/c<1$, $\eta/c=0$) for ($\alpha c=0.10$) is presented in Fig. 15. This plot has many of the same features of Fig. 8, with maximum positive and negative regions occurring with the initial twist axis acting through the cross-section centroid. The zero coupling, which encircles the negative coupling, can be approximated as a series of parallel (vertical) lines, as opposed to the two horizontal parallel lines for the symmetric strip (Fig. 12). Thus, the zero coupling is nearly independent of the initial twist axis location for most the chord length.

Acknowledgements

The support of this research was provided by the National Science Foundation through grant MSM-8809132 and the NASA-Langley Research Center through grant NAG-1-1151-FDP, with R. C. Lake as project monitor. The advice, assistance, and encouragement provided by R.C. Lake and M. Nixon of NASA-Langley Research Center is gratefully acknowledged.

References

1.) Okubo, H., "The Torsion and Stretching of Spiral Rods I," Quarterly of Applied Mathematics, Vol. 9, 1951, pp. 263-272.

2.) Okubo, H., "The Torsion and Stretching of Spiral Rods II," Quarterly of Applied Mathematics, Vol. 11, 1954, pp. 488-495.

3.) Shield, R. T., "Extension and Torsion of Elastic Bars with Initial Twist," ASME Journal of Applied Mechanics, Vol. 49, 1982, pp. 779-786.

4.) Kosmatka, J. B., "On the Behavior of Pretwisted Beams with Irregular Cross Sections, " (to appear: ASME Journal of Applied Mechanics, 1991).

5.) Reissner, E. and F. Y. M. Wan, "On Axial Extension and Torsion of Helicoidal Shells," Journal of Mathematics and Physics, Vol. 47, 1968, pp. 1-31.

6.) Chu, C., "The Effect of Initial Twist on the Torsional Rigidity of Thin Prismatical Bars and Tubular Members," Proceedings of the First U.S. National Congress on Applied Mechanics, Chicago, Ill., 1951, pp. 265-269.

7.) Downs, B., "The Effect of Substantial Pretwist on the Stiffness Properties of Thin Beams of Cambered Section,", ASME Journal of Applied Mechanics, Vol. 46, 1979, pp. 341-344.

8.) Hodges, D. H., "Torsion of Pretwisted Beams Due to Axial Loading," ASME Journal of Applied Mechanics, Vol. 47, 1980, pp. 393-397.

9.) Rosen, A., "The Effect of Initial Twist on the Torsional Rigidity of Beams - Another Point of View," ASME Journal of Applied Mechanics, Vol. 47, 1980, pp. 389-392.

10.) Krenk, S., "A Linear Theory for Pretwisted Elastic Beams," ASME Journal of Applied Mechanics, Vol. 50, 1983, pp. 137-142,.

11.) Maunder, L., and E. Reissner, "Pure Bending of Pretwisted Rectangular Plates," J. Mech. Phys. Solids, Vol. 5, 1958, pp. 261-266.

12.) Goodier, J. N. and D. S. Griffin, "Elastic Bending of Pretwisted Bars," International Journal of Solids and Structures, Vol. 5, 1969, pp. 1231-1245.

13.) Iesan, D., "Saint-Venant's Problem for Inhomogeneous and Anisotropic Elastic Bodies," Journal of Elasticity, Vol. 6, 1976, pp. 277-294.

14.) Giavotto, V., M. Borri, P. Mantegazza, and G. Ghiringhelli, "Anisotropic Beam Theory and Applications," Computers and Structures, Vol. 6, No. 1-4, 1983, pp. 403-413.

15.) Kosmatka, J. B., "Structural Dynamic Modeling of Advanced Composite Propellers by the Finite Element Method," Ph.D. Dissertation, University of California, Los Angeles, 1986.

16.) Kosmatka, J. B. and S. B. Dong; "Saint-Venant Solutions for Prismatic Anisotropic Beams, " (to appear: International Journal of Solids and Structures, 1991).

17.) Mason, W. E. and L. R. Herrmann; "Elastic Shear Analysis of General Prismatic Shaped Beams", Journal of the Engineering Mechanics Division ASCE, Vol. 94, No. EM4, August, 1968, pp. 965-983.

18.) Worndle, R.; "Calculation of the Cross Section Properties and the Shear Stresses of Composite Rotor Blades", Vertica, Vol. 6, 1982, pp. 111-129.

19.) Lekhnitskii, S. G., Theory of Elasticity of an Anisotropic Body, Holden-Day Inc., San Francisco, 1963, pp. 175-204.

20.) Jones, R. M.; Mechanics of Composite Materials, Hemisphere Publishing Company, New York, N. Y., 1975, pp. 19-36.

Table 1: Material properties of T300/5208 graphite/epoxy unidirectional fibers and woven cloth.

	unidirectional fibers	woven cloth
E_{11}	132.2 GPa	80.32 GPa
E_{22}	10.75 GPa	80.32 GPa
E_{33}	10.75 GPa	10.75 GPa
$G_{12} = G_{13} = G_{23}$	5.65 GPa	5.65 GPa
ν_{12}	0.239	0.050
ν_{13}	0.239	0.239
ν_{23}	0.400	0.239

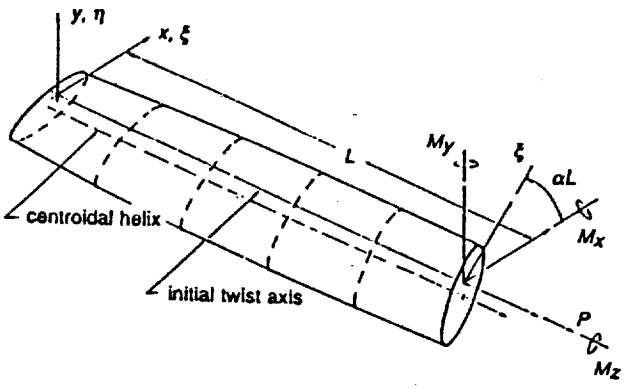

Fig. 1 Nonhomogeneous anisotropic beam with initial twist.

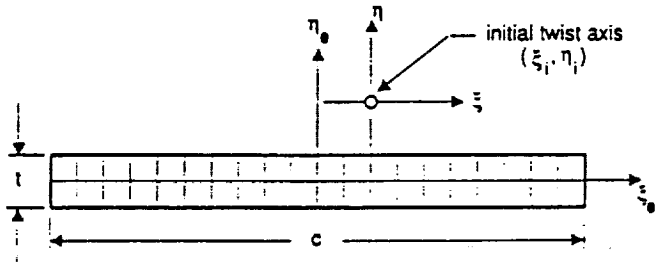

Fig. 2 Finite element discretization of a thin rectangular cross section (c/t=10).

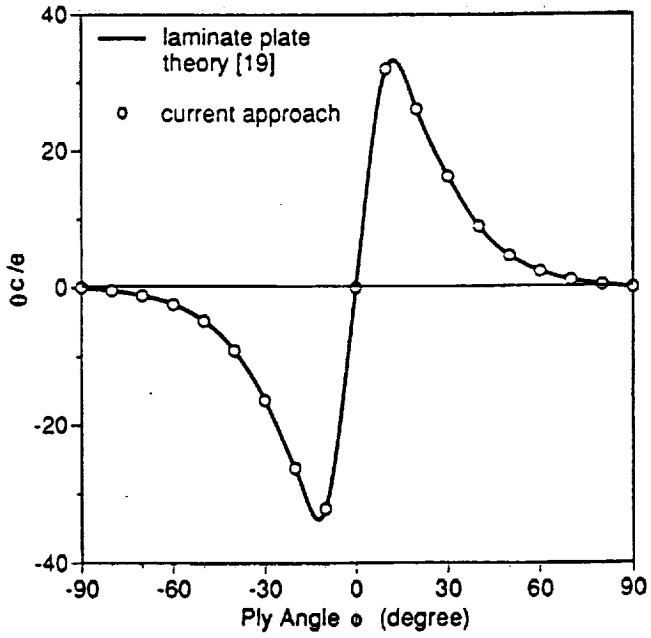

Fig. 3 Twist/extension ratio for a 2-ply asymmetric [±φ] graphite/epoxy untwisted strip.

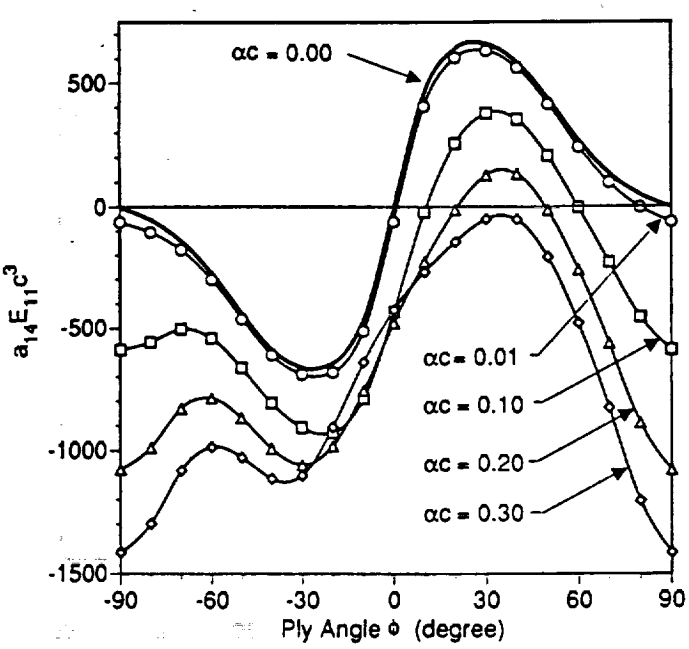

Fig. 4 Nondimensionalized extension/twist coefficient of a 2-ply asymmetric [±φ] graphite/epoxy strip with initial twist about the centroidal axis ($\xi_i=\eta_i=0$).

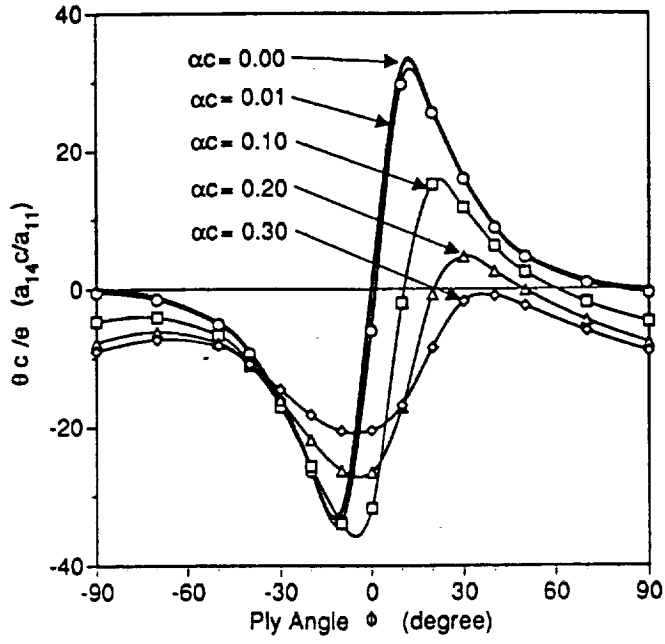

Fig. 6 Twist/extension ratio for a 2-ply asymmetric [±φ] graphite/epoxy strip with initial twist about the centroidal axis ($\xi_i=\eta_i=0$).

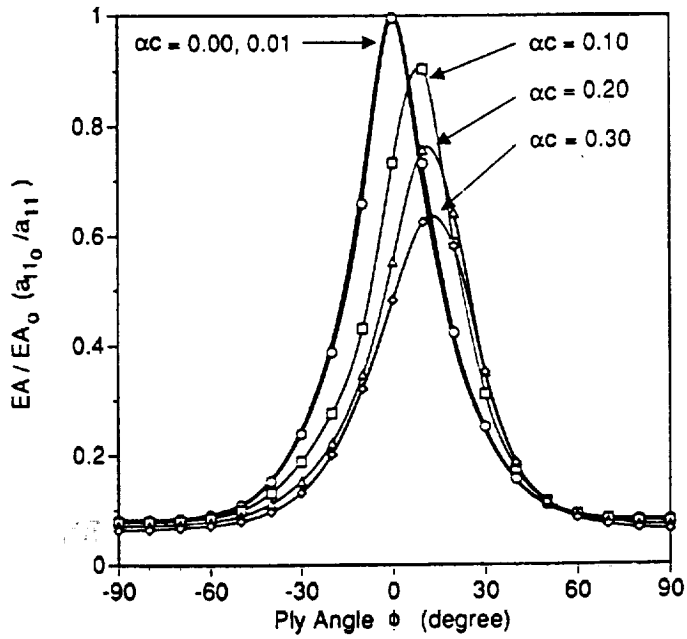

Fig. 5 Axial stiffness of a 2-ply asymmetric [±φ] graphite/epoxy strip with initial twist about the centroidal axis ($\xi_i=\eta_i=0$).

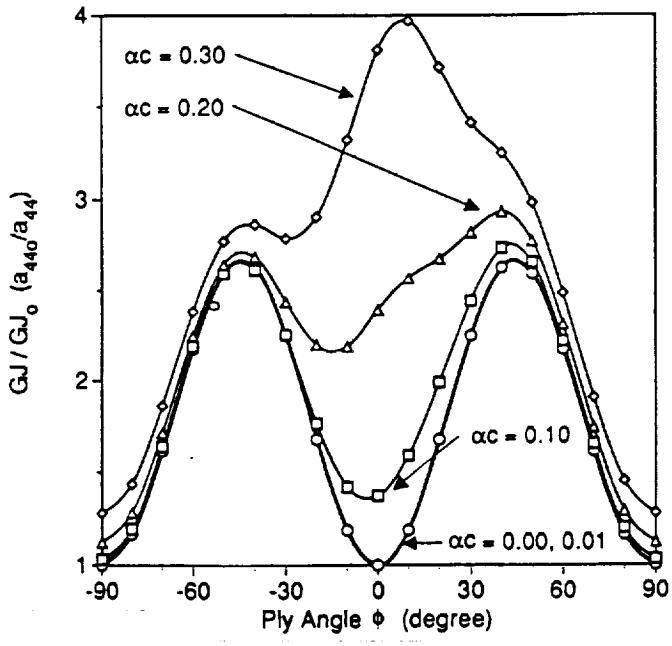

Fig. 7 Torsion stiffness of a 2-ply asymmetric [±φ] graphite/epoxy strip with initial twist about the centroidal axis ($\xi_i=\eta_i=0$).

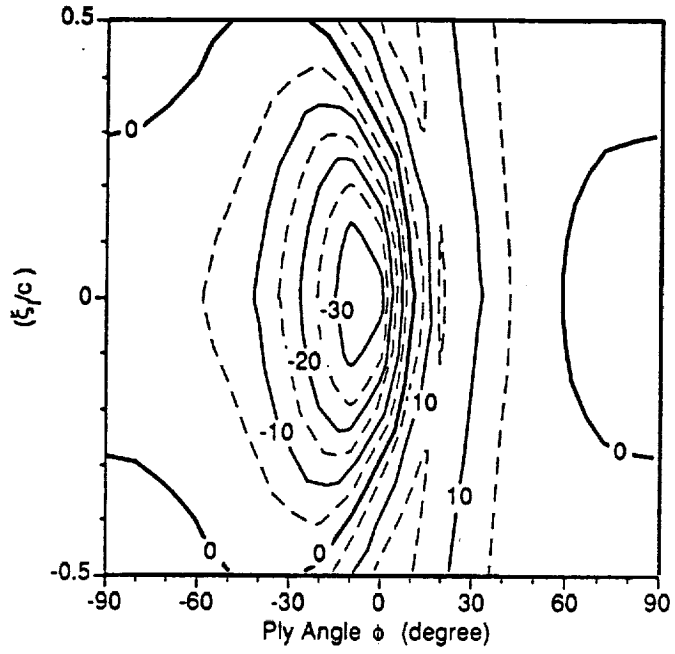

Fig. 8 Contour plot of the twist/extension ratio for a 2-ply asymmetric $[\pm\phi]$ graphite/epoxy pretwisted strip (αc=0.10).

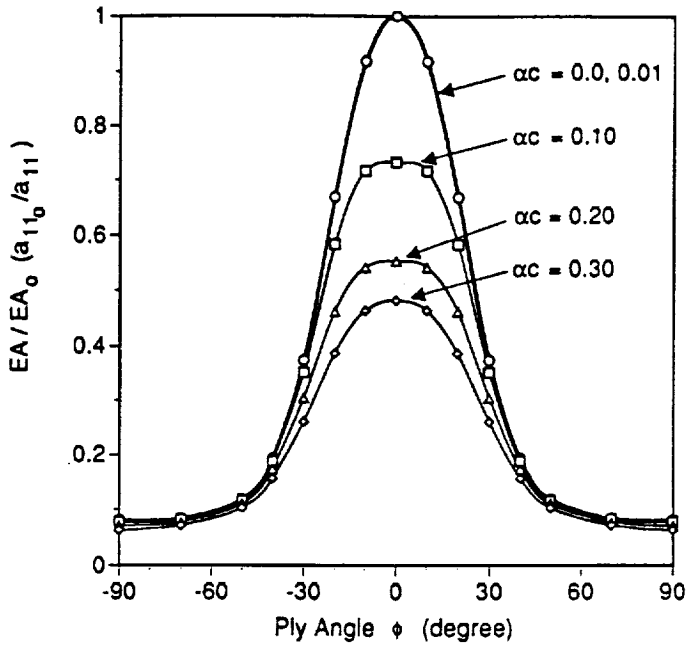

Fig. 10 Axial stiffness of a 4-ply symmetric $[\pm\phi]_S$ graphite/epoxy strip with initial twist about the centroidal axis ($\xi=\eta=0$).

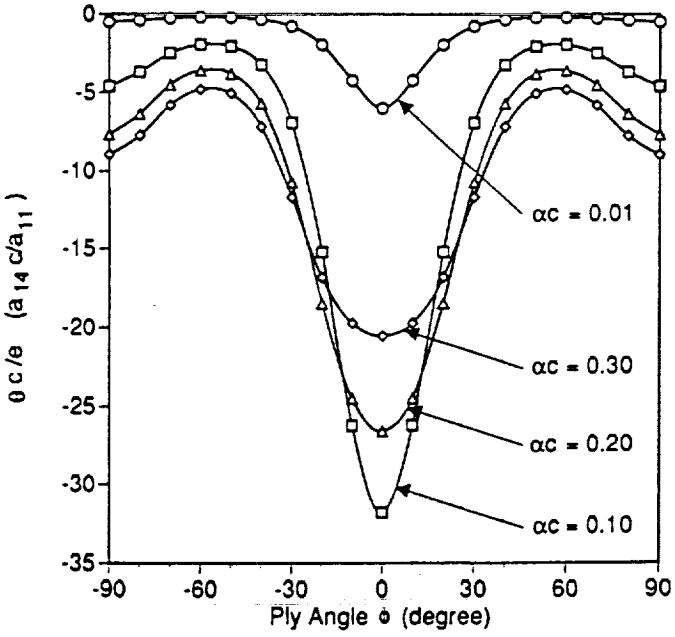

Fig. 9 Twist/extension ratio for a 4-ply symmetric $[\pm\phi]_S$ graphite/epoxy strip with initial twist about the centroidal axis ($\xi=\eta=0$).

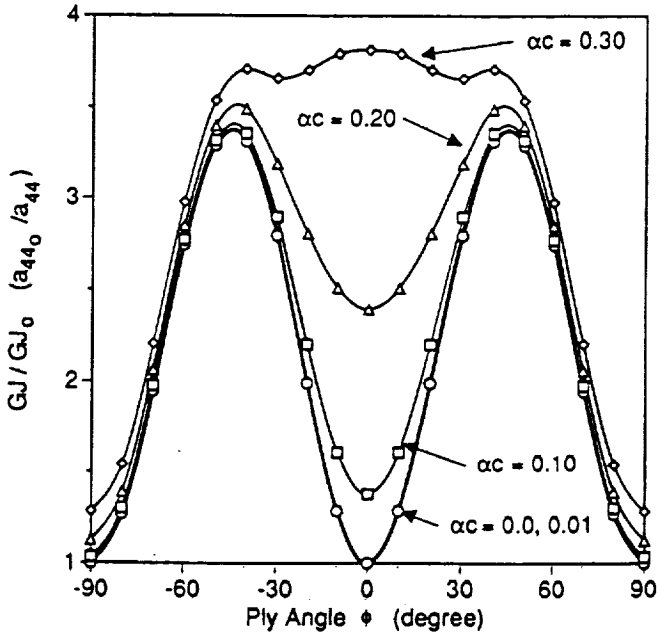

Fig. 11 Torsion stiffness of a 4-ply symmetric $[\pm\phi]_S$ graphite/epoxy strip with initial twist about the centroidal axis ($\xi=\eta=0$).

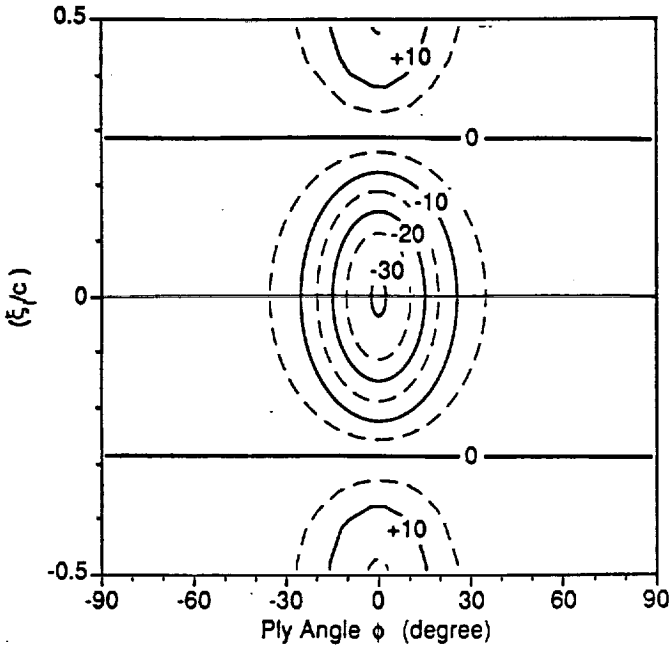

Fig. 12 Contour plot of twist/extension ratio for a 4-ply symmetric $[\pm\phi]_S$ graphite/epoxy pretwisted strip (αc=0.10).

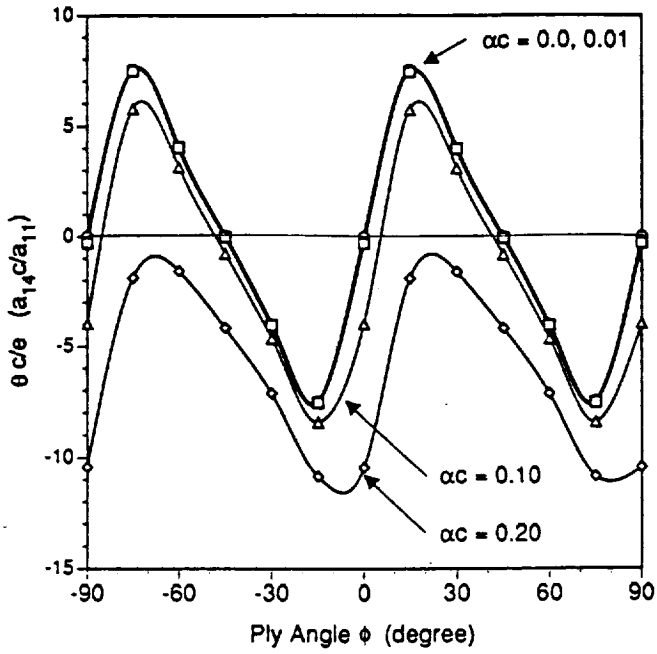

Fig. 14 Twist/extension ratio for a woven graphite/epoxy D-section with initial twist about the centroidal axis (ξ_i=0.523c, η_i=0).

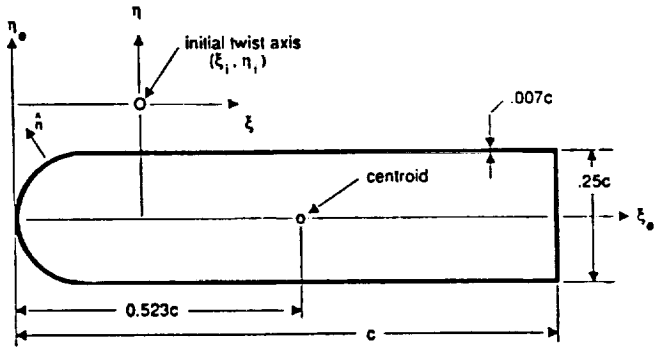

Fig. 13 Thin wall D-section composed of a single layer [ϕ] of graphite/epoxy woven cloth.

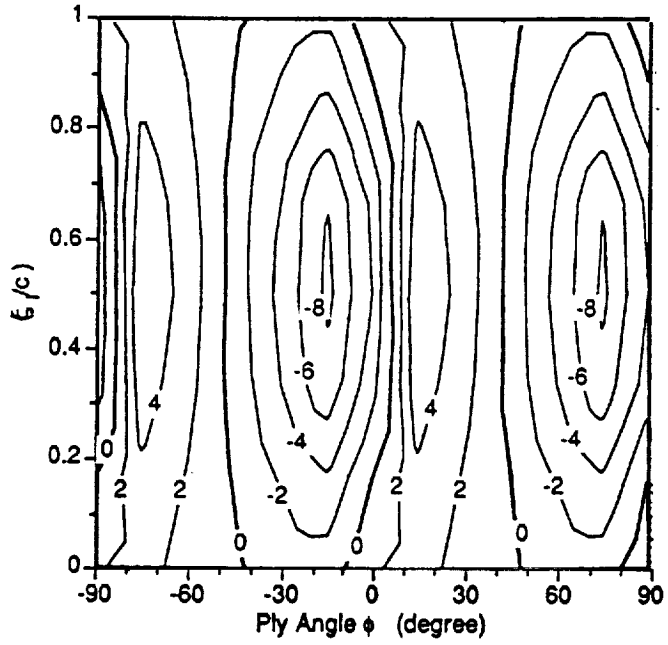

Fig. 15 Contour plot of twist/extension ratio for a woven graphite/epoxy D-section with (αc=0.10).